

UCLA

UCLA Electronic Theses and Dissertations

Title

Kinetics, Mechanism, and Specificity of Photo-induced Denitrogenation Reactions in D2-1,2,3-Triazolines and 2-Azidobiphenyls in Solution and in the Solid-State

Permalink

<https://escholarship.org/uc/item/0st1n3fc>

Author

Chung, Tim SJ

Publication Date

2017

Peer reviewed|Thesis/dissertation

UNIVERSITY OF CALIFORNIA

Los Angeles

Kinetics, Mechanism, and Specificity of Photo-induced
Denitrogenation Reactions in Δ^2 -1,2,3-Triazolines and 2-Azidobiphenyls in
Solution and in the Solid-State

A dissertation submitted in partial satisfaction of the
requirements for the degree Doctor of Philosophy
in Chemistry

by

Tim SJ Chung

2017

© Copyright by

Tim SJ Chung

2017

ABSTRACT OF THE DISSERTATION

Kinetics, Mechanism, and Specificity of Photo-induced
Denitrogenation Reactions in Δ^2 -1,2,3-Triazolines and 2-Azidobiphenyls in
Solution and in the Solid-State

by

Tim SJ Chung

Doctor of Philosophy in Chemistry

University of California, Los Angeles, 2017

Professor Miguel A. Garcia-Garibay, Chair

The development of solid-state photochemistry has been sluggish compared to solution-state photochemistry due to the lack of readily accessible analytical tools necessary to probe and understand solid-state reactions. Although significant progress towards understanding mechanistic solid-state photochemistry has been achieved through comparing X-Ray crystal structures of reactants and products and various other pulsed-laser techniques, a more efficient and operationally simple method to perform mechanistic solid-state photochemistry is vital for further development. To meet these ends, the Garcia-Garibay group has implemented the use of nanocrystalline suspensions in water to overcome the challenges of high optical densities, strong light scattering, and the potential interference by the accumulation of photoproducts in solid-state

photochemistry. This dissertation is dedicated to expanding the frontiers of solid-state photochemistry by studying the specificity, scope and mechanism of Δ^2 -1,2,3-triazolines to form the corresponding aziridines as well as probing the kinetics and mechanism of carbazole formation from selected 2-azidobiphenyls in the solid-state.

Chapter 1 provides an introduction and overview of solid-state photochemistry. It will highlight the history, current efforts, and limitation of observing mechanism of solid-state photochemical reactions.

Chapter 2 addresses the stereospecificity of photochemically forming aziridines from Δ^2 -1,2,3-triazolines both in solution and in the solid-state. We have found that the in solution, the photochemistry has modest stereospecificity and we observe high to quantitative stereospecificity in the solid-state. The computational data to support the regioselectivity of a 1,3-dipolar cycloaddition to synthesize Δ^2 -1,2,3-triazolines was a collaborative work with the Houk lab at UCLA. This work was published in *Org. Lett.* in 2015 (**DOI:** 10.1021/acs.orglett.5b02290).

Chapter 3 expands on the scope, specificity and selectivity of Δ^2 -1,2,3-triazoline photochemistry as well as probing mechanism of this reaction as a function of temperature and solvent polarity. This work is currently in the final stages in preparing for a manuscript and will be submitted shortly.

Chapter 4 is work on detecting kinetics and mechanism of the triplet 1,3-biradical as a result of irradiating Δ^2 -1,2,3-triazoline with an internal triplet sensitizer by taking advantage of transient pump-probe spectroscopy. We have found that Δ^2 -1,2,3-triazoline indeed proceeds via the 1,3-alkyl, aminyl biradical intermediate and verified this fact by observing the aryl aminyl radical formation through laser flash photolysis and product analysis. This work is currently being turned into a manuscript for submission.

Chapter 5 is work on probing the mechanism of solid-state photochemistry of 2-azidobiphenyls forming the corresponding carbazoles by a photo-induced denitrogenation reaction. We have found that the solid-state photochemical reaction is quantitative to the carbazole product compared to the reaction in solution, where many side products are formed. We observed simplified kinetics in the solid-state and high selectivity of the singlet nitrene insertion to form the carbazole product. This work was published in 2017 in *J. Phys. Chem. Lett.* (DOI: 10.1021/acs.jpcllett.7b00499).

The dissertation of Tim SJ Chung is approved.

Andrea M. Kasko

Yi Tang

Miguel A. Garcia-Garibay, Committee Chair

University of California, Los Angeles

2017

To my friends, family, and especially my parents for their sacrifice

TABLE OF CONTENTS

CHAPTER 1. Background and Introduction: Solid-state Photochemistry and Nanocrystalline Suspensions	1
1.1 Overview and Purpose.....	2
1.2 Origin of Solid-state Photochemistry: Topochemical Postulate	2
1.3 Direct Observation of Reactive Intermediates in Crystals.....	5
1.4 Nanocrystalline Suspensions in Water	6
1.5 Conclusions.....	8
1.6 References.....	9
CHAPTER 2. Stereospecific Synthesis of Substituted Aziridines by a Crystal-to-Crystal Photodenitrogenation of Δ^2-1,2,3-Triazolines	11
2.1 Introduction.....	12
2.2 Results and Discussion.....	13
2.2.1 Synthesis and Characterization.....	13
2.2.2 Computational Analysis.....	15
2.2.3 Photochemistry of Triazolines.....	17
2.3 Conclusions.....	19
2.4 Experimental.....	20
2.5 Appendix.....	26
2.5.1 General Information.....	27
2.5.2 Compound Spectra (^1H NMR, ^{13}C NMR, 2D NMR, UV-Vis).....	28

2.5.3	Crystal Pictures.....	58
2.5.4	Thermal Analysis.....	59
2.5.5	PXRD Analysis.....	62
2.5.6	Computational Supplemental Information.....	64
2.6	References.....	72
CHAPTER 3. Stereospecific Photochemistry of Δ^2-1,2,3-Triazolines in Solution and in the Solid-State: Scope and Mechanistic Studies.		
74		
3.1	Introduction.....	75
3.2	Results and Discussion.....	76
3.2.1	Synthesis and Characterization.....	76
3.2.2	Photochemical Studies.....	79
3.2.3	Mechanistic Analysis.....	83
3.3	Conclusions.....	85
3.4	Experimental.....	86
3.5	Appendix.....	97
3.5.1	Compound Spectra (^1H NMR, ^{13}C NMR, UV-Vis).....	98
3.5.2	Computational Data.....	156
3.6	References.....	157

CHAPTER 4. Kinetics and Mechanism of Photochemistry of Δ^2-1,2,3-Triazolines to form Aziridines in Solution and in Solid-State: Observation of 1,3-Biradical Intermediate by Pump-Probe Spectroscopy.	159
4.1 Introduction.....	160
4.2 Results and Discussion.....	162
4.2.1 Synthesis and Characterization.....	162
4.2.2 Laser Flash Photolysis.....	164
4.3 Conclusions.....	169
4.4 Experimental.....	170
4.5 Appendix.....	172
4.5.1 Compound Spectra (^1H NMR, ^{13}C NMR, UV-Vis).....	173
4.5.2 Dynamic Light Scattering.....	181
4.5.3 Laser Flash Photolysis.....	182
4.6 References.....	184
CHAPTER 5. Photochemistry and Transmission Pump-Probe Spectroscopy of 2-Azidobiphenyls in Aqueous Nanocrystalline Suspensions: Simplified Kinetics in Crystalline Solids.	186
5.1 Introduction.....	187
5.2 Results and Discussion.....	190
5.2.1 Synthesis and Characterization.....	190
5.2.2 Laser Flash Photolysis.....	193
5.3 Conclusions.....	198

5.4 Experimental.....	199
5.5 Appendix.....	208
5.5.1 General Methods.....	209
5.5.2 Compound Spectra (¹ H NMR, ¹³ C NMR, UV-Vis).....	211
5.5.3 Thermal Analysis.....	254
5.5.4 PXRD Analysis.....	256
5.5.5 Laser Flash Photolysis.....	259
5.6 References.....	270

List of Schemes

Scheme 1.1.....	3
Scheme 1.2.....	4
Scheme 2.1.....	13
Scheme 2.2.....	14
Scheme 3.1.1.....	76
Scheme 3.2.1.....	77
Scheme 4.1.1.....	161
Scheme 4.2.1.....	162
Scheme 4.2.2.....	167
Scheme 4.2.3.....	169
Scheme 5.1.1.....	188
Scheme 5.1.2.....	189

List of Figures

- Figure 1.1.** Powder X-Ray Diffraction (PXRD) patterns of bulk powder and nanocrystals of 2-azidobiphenyl.....7
- Figure 2.2.1.** X-Ray determined molecular structures of triazolines *trans-4* (top) and *trans-8* (bottom) in with 30% probability ellipsoids, illustrating the *trans* relationship between the ester and trifluoromethyl groups.15
- Figure 2.2.2.** Transition structures for the DMU-catalyzed (3+2) cycloaddition of PhN₃ and *trans-3*. Bond lengths are reported in Å and energies in kcal mol⁻¹.16
- Figure 3.2.1.** Differential Scanning Calorimetry (DSC) of triazoline *trans-3D*. Sharp peak at 131°C indicates melting and broad peak at 171°C shows denitrogenation of triazoline to form aziridine.79
- Figure 3.2.2.** Plausible biradical intermediate versus zwitterionic intermediate to form aziridines.....84
- Figure 4.2.1** UV-Vis absorption spectra of triazoline *trans-5* in acetonitrile (black solid line) and in nanocrystalline suspension (blue dotted line).163
- Figure 4.2.2** Powder X-Ray Diffraction (PXRD) patterns of bulk powder (black line) and nanocrystals (blue line) of triazoline *trans-5*.164
- Figure 4.2.3** a) Transient absorption spectrum of triazoline *trans-5* sliced at various time points in acetonitrile, c) transient decay of triazoline *trans-5* in acetonitrile detected at 550 nm, c) transient absorption spectrum of triazoline *trans-5* sliced at various time points in nanocrystalline

suspension, d) transient decay of triazoline *trans*-5 in nanocrystalline suspension detected at 530 nm.166

Figure 4.2.4 End-of-pulse transient absorption spectrum of 4-aminyyl benzophenone radical 4 by performing LFP studies with 4-amino benzophenone 3 in the presence of di-tertbutyl peroxide (DTBP).168

Figure 5.2.1. UV-Vis absorption spectra of 2-azidobiphenyl in pentane (blue dotted line) and in nanocrystalline suspension (black solid line).191

Figure 5.2.2. Powder X-Ray Diffraction (PXRD) patterns of bulk powder and nanocrystals of 2-azidobiphenyl (**1A**).192

Figure 5.2.3. Powder X-Ray Diffraction (PXRD) patterns of starting azide **1B** (in bottom red), as formed carbazole **2B** (middle blue), and recrystallized carbazole product **2B** (top green).....193

Figure 5.2.4. a) Transient absorption spectrum of azide **1B** sliced at various time points in pentane, b) transient absorption spectrum of azide **1B** sliced at various time points in nanocrystalline suspension c) LFP decays in both pentane and in NC suspensions of azide **1B** at 430 nm and 460 nm, respectively.195

List of Tables

Table 2.2.1 Ratio of <i>cis</i> - and <i>trans</i> -aziridines from photoreactions in solution and in the solid-state.	18
Table 3.2.1. Isolated Yields of aryl azides (2A-E) and aryl triazolines (<i>trans</i> - 3A-E and <i>cis</i> - 3A-E)	77
Table 3.2.2. Ratios of <i>cis</i> - and <i>trans</i> -aziridines from triazolines in solution and solid-state.....	82
Table 3.2.3. Solution-state photochemistry of triazoline <i>trans</i> - 3C in solvents with different polarity.	84
Table 5.1.1. Various substituents on 2-azidobiphenyl derivatives listed with their corresponding melting points and particle sizes.	189
Table 5.2.1. Transient decay lifetimes of various isocarbazoles to form carbazoles of various 2-azidobiphenyl derivatives with substituents in the 4'-biphenyl position.	196
Table 5.2.2. Transient decay lifetimes of isocarbazoles to carbazoles from 3',5'-disubstituted 2-azidobiphenyls.	197

List of Abbreviations

Ar	aryl
ca	approximately
CDCl ₃	deuterated chloroform
d	doublet (NMR)
<i>d</i>	deuterium
dd	doublet of doublets (NMR)
dq	doublet of quartet
DSC	differential scanning calorimetry
eq.	equivalent
<i>et al.</i>	<i>et alia</i>
FTIR	Fourier transformed infrared spectroscopy
g	gram
Hz	hertz
hr	hour
ISC	intersystem crossing
K	Kelvin
kcal	kilocalories
m	multiplet
MHz	megahertz
min	minute
mL	milliliter
mol	mole

m.p.	melting point
m/z	mass to charge ratio
NMR	nuclear magnetic resonance
ns	nanosecond
Ph	phenyl
PXRD	powder X-ray diffraction
ppm	parts per million
R	general alkyl group substituent
rt	room temperature
s	singlet (NMR)
sec	second
T	temperature
THF	tetrahydrofuran
TLC	thin layer chromatography
t	triplet (NMR)
t	time
UV-Vis	ultraviolet-visible spectroscopy
Å	angstrom
μs	microsecond

Acknowledgements

I would like to thank Prof. Miguel A. Garcia-Garibay, who has taught and guided me throughout the past 5 years and this dissertation would not be possible without Miguel's mentorship. Miguel's intelligence, creativity, curiosity and work-ethic has been truly inspirational and has shaped me into the scientist I am today. I would also like to thank my committee members, Professors Yi Tang, Andrea Kasko, and Neil Garg for their unwavering support and advice throughout my doctoral studies at UCLA. Additionally, I would like to thank my undergraduate research advisor, Prof. Jerry Yang who has provided me with endless support and encouragement to pursue a doctoral degree in Chemistry. I was fortunate enough to take an advanced spectroscopy and kinetics class with Prof. Charlie Perrin at UCSD, which has been an absolute game-changer and made me see the beauty and elegance of organic chemistry.

I would like to thank my family members in Korea and especially parents, Chris and Elin, my brother, Josh, and my cousins, Peter and Justin, who have always supported me from the beginning. This dissertation and graduate school would not have been possible without their advocacy. It has been a true pleasure to meet and befriend the members of the Garcia-Garibay group and at UCLA, including Dr. Braulio Rodriguez-Molina, D-Bloke, Dr. Denisse De Leora, Dr. Ira Staehle, Dr. Pat Commins, Dr. Xing Jiang, Dr. Geeta Vadehra, Dr. Woogie, Dr. Juneyoung Lee, X'avia, Taylor, V-Dog, Jin, Morgan, Jordan, Marcus, Vince, Trevor, Edris, Iris, Vato, Austin, Janice and Terry. Special thanks to my friends from San Diego, Leibniz, Kevin, Sylvia, and Emily, who have always been there for me. Unfortunately, Leibniz still hasn't taken a set off of me in tennis but I presume that day will come in the near future. Finally, I would also like to acknowledge Cornel West, Bob Marley, and Roger Federer, all of whom I've never had a

chance to meet, but their craft, passion, and excellence in their respective professions have influenced me greatly and made me into a more mature person.

VITA

2007-2011	B.S. General Biology, University of California, San Diego
2011	Chemistry Intern, BASF SE, Ludwigshafen, Germany
2011-2012	M.S. Chemistry, University of California, San Diego
2012-2017	Teaching Assistant, University of California, Los Angeles
2012-2017	Research Assistant, University of California, Los Angeles

Publications and Presentations

Publications

- 1) Chung, T. S.; Ayitou, A. J.-L.; Park, J.; Breslin, V. M.; Garcia-Garibay, M.A. "Photochemistry and Transmission Pump-Probe Spectroscopy of 2-Azidobiphenyls in Aqueous Nanocrystalline Suspensions: Simplified Kinetics in Crystalline Solids" *J. Phys. Chem. Lett.*, **2017**, *8*, 1845–1850.
- 2) Cifelli, J. L.; Chung, T. S.; Liu, H.; Prangko, P.; Mayer, M.; Yang, J. "Benzothiazole Amphiphiles Ameliorate Amyloid-beta Related Cell Toxicity and Oxidative Stress" *ACS Chem. Neurosci.*, **2016**, *6*, 682-688.
- 3) Cifelli, J. L.; Dozier, L.; Chung, T. S.; Patrick, G. N.; Yang, J. "Benzothiazole Amphiphiles Promote the Formation of Dendritic Spines in Primary Hippocampal Neurons" *J. Biol. Chem.*, **2016**, *291*, 11981-11992.
- 4) Staehle, I.O.; Chung, T.S.; Stopin, A.; Vadehra, G.S.; Hsieh, S.I.; Gibson, J.H.; Garcia-Garibay, M.A. "An Approach to Enhance the Safety Culture of an Academic Research Laboratory by Addressing Behavioral Factors." *J. Chem. Educ.*, **2016**, *93*, 217–222.

- 5) Chung, T.S.; Lopez, S.A.; Houk, K.N.; Garcia-Garibay, M.A. “Stereospecific Synthesis of Substituted Aziridines by a Crystal-to-Crystal Photodenitrogenation of Δ^2 -1,2,3-Triazolines.” *Org. Lett.*, **2015**, *17*,4568–4571.

Oral Presentations

- 1) “Photochemistry and Transmission Pump-Probe Spectroscopy of 2-Azidobiphenyls in Aqueous Nanocrystalline Suspensions: Simplified Kinetics in Crystalline Solids” Chung T.S. *253th ACS National Meeting*, San Francisco, CA, April 2017
- 2) “An Approach to Enhance the Safety Culture of an Academic Research Laboratory by Addressing Behavioral Factors” Chung, T.S. *Caltech Safety Day*, Pasadena, CA, November 2016.
- 3) “Supramolecular Photocatalysis” Chung, T.S. *Inter-American Photochemical Society Workshop*, Santiago, Chile, May 2016.
- 4) “Solid-State Photochemistry and Kinetics of Δ^2 -1,2,3-Triazolines to form Aziridines” Chung, T.S. *UC Symposium for Chemical Sciences*, Lake Arrowhead, CA, March 2016.
- 5) “Stereospecific Synthesis of Substituted Aziridines by a Crystal-to-Crystal Photodenitrogenation of Δ^2 -1,2,3-Triazolines” Chung, T.S. *250th ACS National Meeting*, Boston, MA, August 2015

Poster Presentations

- 1) “Solid-State Photochemistry and Kinetics of Δ^2 -1,2,3-Triazolines to form Aziridines” Chung T.S.; Garcia-Garibay, M. A. *Inter-American Photochemical Society*, Sarasota, FL, January 2017.
- 2) “Cultivating a Culture of Safety in an Organic Chemistry Lab at UCLA” Vadehra, G. S.; Staehle, I. O.; Chung, T. S.; Commins, P. J.; Garcia-Garibay, M. A. *UC Center for Laboratory Safety: Workshop on Laboratory Safety*, Irvine, CA, April 2014.

Chapter 1

Background and Introduction:

Solid-state Photochemistry and Nanocrystalline Suspensions

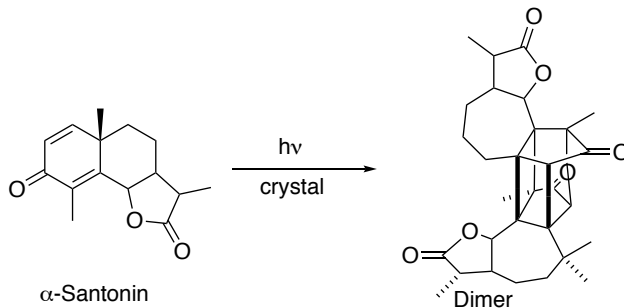
1.1 Overview and Purpose:

This introductory chapter will shed light on the background, progress, limitations and the current available tools to study mechanistic solid-state photochemistry. The ultimate purpose of this dissertation is dedicated to expanding the frontiers of solid-state photochemistry of denitrogenation reactions of various Δ^2 -1,2,3-triazolines as well as selected aryl azides. The first part of this introductory chapter will discuss the first discovery of solid-state photochemistry by Trommsdorff and will lead to the discussion of the topochemical postulate by Cohen and Schmidt. The latter half of this chapter will highlight the seminal works of McBride, Techert and Scaiano in pursuit of observing reactive intermediates in solid-state photochemistry. Finally, the use of nanocrystals suspended in water to overcome complications with performing conventional transmission spectroscopy will be discussed.

1.2 Origin of Solid-state Photochemistry: Topochemical Postulate

Solid-state photochemistry is the study of the interaction of light with molecules in the solid state. Trommsdorff reported the first solid-state photochemical reaction in 1834 when he found that α -santonin crystals turned yellow and would “burst” when exposed to ambient sunlight.¹ The “bursting” effect of α -santonin crystals is found to be the result of a large change in crystal volume from a rearrangement and subsequent cyclization to form the dimer product shown in Scheme 1.1.² However, since its discovery, the progress in solid-state photochemistry has been relatively sluggish compared to solution-state photochemistry. The slow development of this field may be attributed to the general lack of analytical tools necessary to study solid-state photochemistry. This fact is evident from finding only 127 hits for “crystalline organic photochemistry” from 1900 to current.³

Scheme 1.1

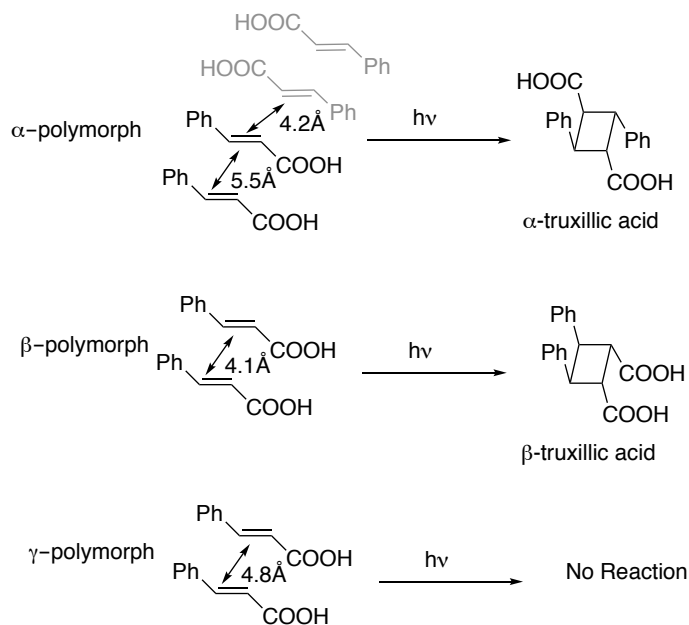


Historically, most of solid-state photochemical studies were performed through product analysis. The crystalline product would be dissolved in solvent to carry out further analysis of the photoproduct, with mechanistic analysis rationalized by the structure of the product.⁴ However, atoms in the crystalline solid are locked in specific arrangements in the crystalline lattice and by dissolving the crystal, one loses vital chemical information. One of the remarkable breakthroughs of solid-state photochemistry came in the 1960's when X-ray crystallography became available to chemists. X-ray crystallography allowed chemists to elucidate chemical structure with precision and gave insight into the atomic arrangements and geometries in the solid state. Using x-ray crystallography, Schmidt and Cohen studied the reaction of *trans*-cinnamic acid (Scheme 1.2) and developed the foundation of solid-state photochemistry: the Topochemical Postulate.⁵

Trans-cinnamic acid was known to crystallize in three different polymorphs in the solid-state (α , β , and γ).⁶ The α , β , and γ polymorphs were shown to have different distances as well as different positions between its nearest neighbors in the crystal. In the α polymorph, one molecule of *trans*-cinnamic acid has a closest neighbor which is 4.2Å away in a different stack and another neighbor in the same stack which is 5.5Å away. When this crystal is irradiated with UV light, a [2+2] cycloadduct is formed with the closest neighbor to form the centrosymmetric dimer (α -truxillic acid). In the β polymorph, *trans*-cinnamic acid packs with short

intermolecular distance of 4.1Å away from its neighbor. When the β polymorph is irradiated, a [2+2] cycloaddition occurs with the closest neighboring molecule to form the mirror symmetric dimer β -truxillic acid. In the case of the γ polymorph, the intermolecular distance is too far as the nearest molecule is 4.8Å away and no product is formed in this polymorph. These experimental data led Cohen and Schmidt to confirm what Kohlschutter first suggested in 1918,⁷ and establish the Topochemical Postulate: (1) solid-state reactions occur with a minimum amount of molecular motion and (2) crystal packing and molecular geometry plays a more crucial role than the inherent photo-reactivity. This postulate was a cornerstone and foundation for solid-state photochemistry and gave rise to seminal discoveries in the field following the Topochemical Postulate.⁸⁻¹⁰

Scheme 1.2



1.3 Direct Observation of Reactive Intermediates in Crystals

Pump-probe spectroscopy is a two-pulse experiment in which the first laser (pump) excites the sample in the UV region and a second pulse (usually a broadband lamp) flashes the sample at a later time to analyze the various transient species.¹¹ Most solution-state photochemical mechanisms are deduced from transient absorption spectroscopy in the form of a laser flash photolysis to detect which transients are formed, their lifetimes, which can be computationally confirmed. However, performing common transmission spectroscopic techniques of bulk powders or crystals to directly observe intermediates are complicated by high optical density, dichroism, birefringence, and light scattering. One can perform laser flash photolysis in solution and analyze geometries from x-ray crystal structures to infer a mechanism of the solid-state photoreaction. However, this practice is often invalid as excitons and energy transfer within the crystal plays a large role in crystalline photochemistry.¹²

The McBride group reported one of the first examples of direct detection of intermediates in crystals. McBride and co-workers studied various azo and peroxide species at cryogenic temperatures in crystals to directly observe radicals within crystals.¹³ These radicals were observed by a combination of EPR and IR techniques and led to the development of the “Local Stress” postulate. Additionally, one of the most elegant techniques developed by the Techert group used a pulsed laser excitation with a single-crystal X-ray diffraction to detect the excited states, reactive intermediates and reversible reaction of α -Styrylpyrylium Trifluoromethanesulfonate.^{14,15} Scaiano and co-workers have also provided significant progress in the use of diffuse reflectance transient absorption spectroscopy to directly observe reactive intermediates as a function of reaction progress in solids.¹⁶ Rather than using a transmitted light source as frequently done in pump-probe spectroscopy, Scaiano monitored changes of the

reflected light from the solid. Although this technique was a significant discovery, there were many complications and issues using diffuse reflectance. For example, the increased laser power needed for detection of reflected light often would lead to delocalization of excited states within the crystalline solid which would yield multiphotonic processes. The current bottleneck in mechanistic solid-state photochemistry is the technical difficulty as well as the available analytical tools necessary to directly observe reactive intermediates in solids.

1.4 Nanocrystalline Suspensions in Water

As discussed in Section 1.3, performing pump-probe spectroscopy to directly observe transients in the solid state are complicated due to high optical density, dichroism, birefringence, and light scattering of the solid sample. In order to further advance the field of solid-state photochemistry, a simpler and efficient technique to perform pump-probe spectroscopy is vital. Since 2006, the Garcia-Garibay group has used nanocrystalline suspensions in water to overcome the challenges of performing transmission spectroscopy in the solid state.¹⁷⁻²¹ Using the reprecipitation method, or a solvent shift, first reported by Kasai and co-workers is an efficient method to make polydispersed nanocrystals in the 50-200 nm range.²² One may view nanocrystals as a state in transition between supramolecular systems and bulk solids, such that conventional transmission spectroscopic methods can be used to study mechanistic solid-state photochemistry. Often times, submicellular cetrimonium bromide (CTAB) or sodium dodecyl sulfate (SDS) can be used to as surface passivators to prevent aggregation. The crystallinity and particle size of nanocrystalline suspensions can be identified by using powder X-ray diffraction (PXRD) and dynamic light scattering (DLS), respectively. Figure 1.1 depicts the PXRD pattern for 2-azidobiphenyl in the bulk powder (bottom blue line) and for nanocrystals (top black line) collected by centrifugation and air-drying. The two diffractograms illustrate very similar peak positions but display some

differences in peak intensities, indicating that the two solid forms adopt in specific crystallite alignments. However, the similar peak positions indicate that the two solids are in fact in the same polymorph.

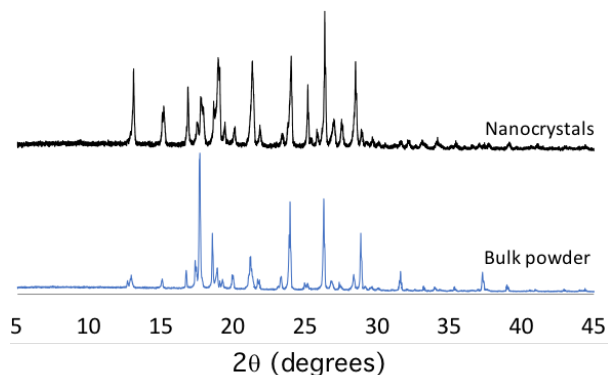


Figure 1.1. Powder X-Ray Diffraction (PXRD) patterns of bulk powder and nanocrystals of 2-azidobiphenyl.

Additionally, the sizes of these nanocrystals can be identified by using dynamic light scattering (DLS) to verify that the crystals are in the suitable range (50-200 nm) to perform pump-probe spectroscopy. Using nanocrystals suspended in water in a flow system to make sure a fresh sample is being pulsed, one can perform laser flash photolysis to detect various transient profiles and their decays, thereby giving insight into the photochemical mechanism in the solid-state. It has been shown that the use of nanocrystalline suspensions in water provide an efficient and promising avenue to study mechanistic solid-state photochemistry. Further mechanistic details on the photochemical denitrogenation of Δ^2 -1,2,3-triazolines and 2-azido biphenyls are disclosed in Chapters 3 and 4 of this dissertation using nanocrystals in water.

1.5 Conclusions

Progress in mechanistic solid-state photochemistry has been relatively slower than that in solution due to the lack of necessary analytical tools available. This chapter has highlighted the current state as well as limitations on mechanistic solid-state photochemistry. Nanocrystalline suspensions in water is a simple and promising technique to perform pump-probe spectroscopy in the solid-state using conventional pump-probe techniques. This thesis is dedicated to understanding the scope, specificity of the photochemistry of Δ^2 -1,2,3-triazolines in solution and in the solid-state. Additionally, the mechanism of the solid-state photochemical reactions of Δ^2 -1,2,3-triazolines and 2-azido biphenyls are reported by using laser flash photolysis of nanocrystalline suspensions in water.

1.6 References

- 1) (a) Trommsdorf, H. *Ann. Chem. Pharm.* **1834**, 11. (b) Roth, H. D. *Angew. Chem. Int. Ed.* **1989**, 28, 1193. (c) Garcia-Garibay, M. A. *Acc. Chem. Res.* **2003**, 36, 491.
- 2) Natarajan, A.; Tsai, C.K.; Khan, S.I.; McCarren, P.; Houk, K.N.; Garcia-Garibay, M.A. *J. Am. Chem. Soc.* **2007**, 129, 9846-9847.
- 3) Web of Knowledge only found 127 hits for “crystalline organic photochemistry” from 1900 to current in peer-reviewed journals.
- 4) Examples of topotactic reactions which retain their crystallinity throughout the reaction:
(a) Natarajan, A.; Mague, J. T.; Ramamurthy, V. *J. Am. Chem. Soc.* **2005**, 127, 3568. (b) Papaefstathiou, G. S.; Zhong, Z.; Geng, L.; MacGillivray, L. R. *J. Am. Chem. Soc.* **2004**, 126, 9158. (c) Irie, M.; Kobatake, S.; Horichi, M. *Science* **2001**, 291, 1769. (d) Fomitchev, D. V.; Bagley, K. A.; Coppens, P. *J. Am. Chem. Soc.* **2000**, 122, 532.
- 5) Ginsburg, D.; Schmidt, G. M. J. in *Reactivity of the Photoexcited Organic Molecule*. Ginsburg, D., Ed.; Wiley Interscience: New York, 1967.
- 6) (a.) Cohen, M. D.; Schmidt, G. M. J. *J. Am. Chem. Soc.* **1964**, 53, 1996. (b.) Cohen, M. D.; Schmidt, G. M. J.; Sonntag, F. I. *J. Am. Chem. Soc.* **1964**, 53, 2000. (c.) Schmidt, G. M. J. *J. Am. Chem. Soc.* **1964**, 53, 2014
- 7) Kohlshutter, H. W. *Z. Anorg. Allg. Chem.* **1918**, 105, 111.
- 8) Scheffer, J. R.; Scott, C. *Science*, **2001**, 291, 1712.
- 9) (a) Gnanaguru, K.; Ramasubbu, N.; Venkatesan, K.; Ramamurthy, V. *J. Photochem.* **1984**, 27, 355. (b) Ramasubbu, N. T.; Guru Row, N. K.; Venkatesan, V.; Ramamurthy, V.; Rao, C. N. R. *J. Chem. Soc. Chem. Commun.* **1982**, 178. (c) Ramasubbu, N. K.; Gnanaguru, K. K.; Ramamurthy, V. *Can. J. Chem.* **1982**, 60, 2169.

- 10) Gudmundsdottir, A. D.; Lew, T. J.; Randall, L. H., Scheffer, J. R.; Rettig, S. J.; Trotter, J. Wu, C.-H. *J. Am. Chem. Soc.* **1996**, *118*, 6167.
- 11) Weiner, A., Ed.; *Ultrafast Optics*. Wiley Publications: New York, 2009.
- 12) Powel, R. C; Soos, Z. G. *J. Lumin.* **1975**, *11*, 1.
- 13) McBride, J. M. *Acc. Chem. Res.* **1983**, *16*, 304 and references therein.
- 14) Hallmann, J. R.; Morgenroth, W.; Paulmann, C.; Davaasambuu, J.; Kong, Q.; Wulff, M.; Techert, S. *J. Am. Chem. Soc.* **2009**, *131*, 15018–15025.
- 15) Techert, S. *Crystallogr. Rev.* **2006**, *12*, 25-45.
- 16) Wilkinson, F.; Kelly, G. In *Handbook of Organic Photochemistry*, Vol. 1 Scaiano, J. C, Ed. CRC Press: Boca Raton, 1989.
- 17) Chin, K. K.; Natarajan, A.; Gard, M. N.; Campos, L. M.; Johansson, E.; Shepherd, H.; Garcia-Garibay, M. A. *Chem. Commun.* **2007**, *41*, 4266-4268.
- 18) Kuzmanich, G.; Simoncelli, S.; Gard, M.N.; Spänig, F.; Hoekstra, R.; Guldi, D. M.; Garcia-Garibay, M. A. *J. Am. Chem. Soc.*, **2011**, *133*, 17296-17306.
- 19) Doan, S. C.; Kuzmanich, G.; Gard, M. N.; Garcia-Garibay, M. A.; Schwarts, B. J. *J. Phys. Chem. Lett.*, **2012**, *3*, 81-86.
- 20) Kuzmanich, G.; Vogelsberg C. S.; Maverick, E. F.; Netto-Ferreira, J. C.: Scaiano, J. C.; Garcia-Garibay, M. A. *J. Am. Chem. Soc.*, **2012**, *134*, 1115-1123.
- 21) Ayitou, A. J.-L.; Flynn, K.; Jockusch, S.; Khan, S. I.; Garcia-Garibay, M. A. *J. Am. Chem. Soc.*, **2016**, *138*, 2644-2648.
- 22) Kasai, H.; Nalwa, H. S.; Oikawa, H.; Okada, S.; Matsuda, H.; Minami, N.; Kuakuta, A.; Ono, K.; Mukoh, A.; Nakanishi, H. *Jpn. J. Appl. Phys.*, **1992**, *31*, 1132-1134.

Chapter 2

Stereospecific Synthesis of Substituted Aziridines by a Crystal-to-Crystal

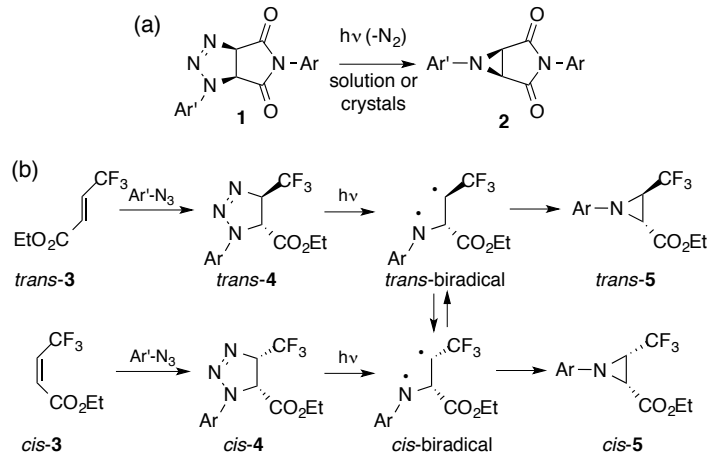
Photodenitrogenation of Δ^2 -1,2,3-Triazolines

2.1 Introduction

Aziridines are highly strained, nitrogen-containing, saturated, three-membered heterocycles with excellent synthetic potential and valuable biological properties.¹ For this reason, there have been numerous recent efforts to synthesize aziridines in a highly stereoselective manner.^{1,2} Having recently shown that crystalline bicyclic Δ^2 -1,2,3-triazolines derived from N-aryl maleimides (**1**, Scheme 1a) can undergo an efficient solid-state photodenitrogenation to form bicyclic aziridines (**2**) in quantitative chemical yields,⁶ we set out to explore the potential of a two-step strategy to prepare ring-substituted aziridines in a stereospecific manner.³⁻⁵ As indicated in Scheme 1b, this approach intends to take advantage of a stereospecific 1,3-dipolar cycloaddition between suitable azides and *cis*- or *trans*-activated alkenes to form the corresponding *cis*- or *trans*- Δ^2 -1,2,3-triazoline precursors. Subsequent crystallization and exposure of the resulting solid to UV light is expected to result in cleavage of C-N and N-N bonds to release N₂, with the formation of a 1,3-alkyl-aminyl biradical intermediate confined in the rigid environment of its crystalline precursor.⁷ Photochemistry performed in this rigid environment should provide minimal rotational freedom to conserve stereospecificity in forming aziridines.^{8,9}

In order to test the synthetic hypothesis illustrated in Scheme 1b, we prepared and crystallized samples of diastereomerically pure 1-aryl- Δ^2 -1,2,3-triazolines *cis*-**4** and *trans*-**4**, shown in Scheme 1b, and we determined the stereospecificity of their photodenitrogenation reaction in solution and in the solid state. As illustrated in the scheme, one may expect that the 1,3-biradical in solution may be able to explore conformations leading to the loss of stereochemical information in a measure that will depend on its lifetime. Singlet biradicals should display greater stereochemical memory than those generated by sensitization in the triplet state.

Scheme 2.1

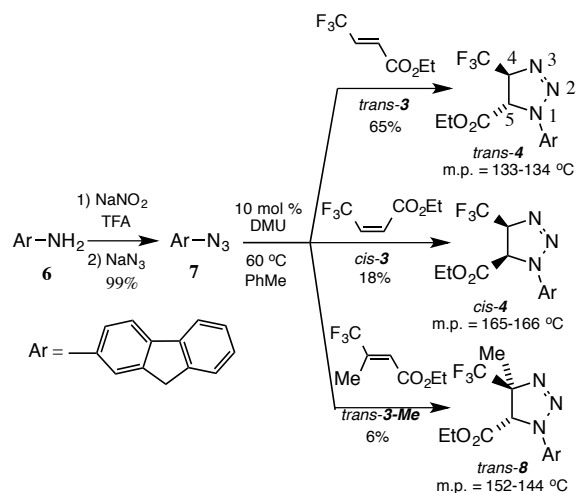


2.2 Results and Discussion

2.2.1 Synthesis and Characterization

As shown in Scheme 2, samples of Δ^2 -1,2,3-triazolines *trans-4*, *cis-4* and *trans-8* were obtained by a 1,3-dipolar cycloaddition of aryl azide **7** with dipolarophiles *trans-3* and *cis-3* and the methyl substituted derivative *trans-3-Me*, catalyzed by N,N-dimethylurea (DMU). While *trans-3* and *trans-3-Me* are commercially available, *cis-4* was obtained by photoisomerization of *trans-3* using wavelengths $\lambda \geq 220$ nm, which yielded a photostationary state with a ratio *trans-3*:*cis-3*=76:24. A sample of fluorenyl amine **6** was converted to the corresponding azide **7** in quantitative yield, using standard protocols.¹⁰ We selected the fluorenyl group as a model system with expectations that it would lead to the formation of high melting solids.

Scheme 2.2



The desired role of the fluorenyl substituent was confirmed as the three triazolines were shown to be crystalline solids with melting points ranging from 133 °C to 165 °C, which should be suitable for the exploration of solid-to-solid reactions. The stereochemical identity of isomeric triazolines *cis-4* and *trans-4* could be determined by ^1H NMR experiments and was subsequently confirmed by single crystal X-ray diffraction in the case of *trans-4* and *trans-8*. Briefly, the identity of the heterocycle H4 signal (for numbering see *trans-4* in Scheme 2) was established by its vicinal coupling to the CF_3 group ($J_{4,\text{CF}_3} \approx 8$ Hz) and the *cis*- or *trans*- relation with H5 was established by their vicinal coupling constants ($J_{\text{cis}} \approx 13$ Hz and $J_{\text{trans}} \approx 8$ Hz) and presence (*cis*) or absence (*trans*) of a 2D NOESY correlations. The regiochemistry of the triazolines was also determined by a 2D NOESY between H5 and the fluorenyl *ortho*-hydrogens. These assignments were all consistent with the X-ray structure shown in Figure 1, which displays the trifluoromethyl and ethoxycarbonyl groups of *trans-4* (Figure 1, top) to be on opposite faces of the heterocycle, with the ester being adjacent to the N-Aryl fragment. Similar features were observed in the case of *trans-8* (Figure 1, bottom), which included a conformation with the planes of fluorenyl and

triazoline rings nearly coplanar and the corresponding carbonyl oxygens pointing in the direction of the N-Aryl nitrogen.

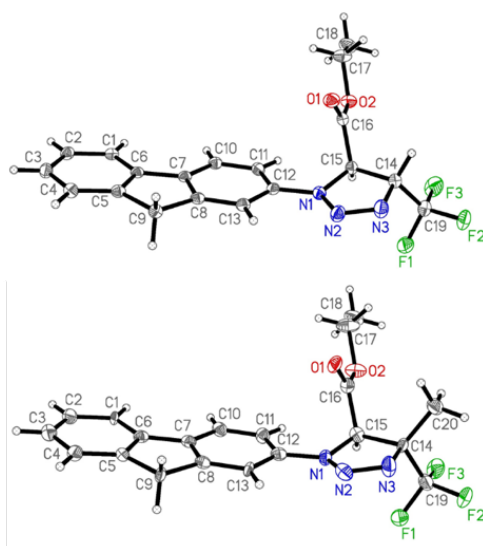


Figure 2.2.1. X-Ray determined molecular structures of triazolines *trans-4* (top) and *trans-8* (bottom) in with 30% probability ellipsoids, illustrating the *trans* relationship between the ester and trifluoromethyl groups.

2.2.2 Computational Analysis

The regioselectivity of the 1,3-dipolar cycloaddition could be explained from theoretical calculations using the M06-2X¹¹ density functional theory. The methyl ester analog of *trans-3* is activated by DMU and phenyl azide is a model 1,3-dipole. The lowest energy transition structures **TS1** and **TS2** lead to the two possible regioisomeric cycloadducts (Figure 2). **TS2** is 3.8 kcal mol⁻¹ lower in free energy than **TS1**, corresponding to the observed regioisomer.¹²

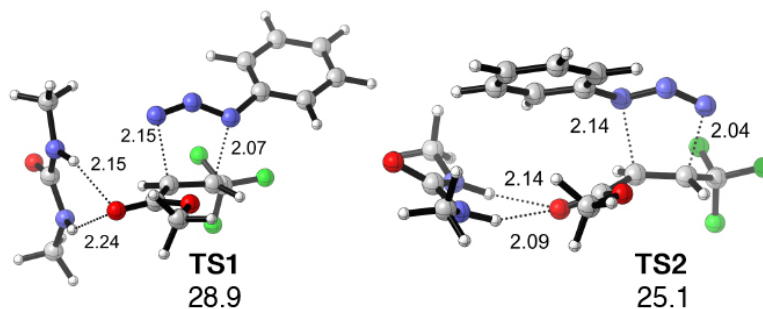


Figure 2.2.2. Transition structures for the DMU-catalyzed (3+2) cycloaddition of PhN_3 and *trans*-**3**. Bond lengths are reported in Å and energies in kcal mol^{-1} .

Analysis of the reactant and reaction energetics showed that DMU-complexed *trans*-**3** has a LUMO energy (-2.21 eV) that is 0.44 eV lower than the non-complexed dipolarophile (-1.87 eV), which accounts for the increased reactivity in the presence of the catalyst.¹³ We found that the frontier orbital coefficients of the two carbon atoms in the dipolarophile are essentially identical, with or without the catalyst, suggesting that the reaction regioselectivity is determined by factors affecting the energies of the two transition states, as expected by the distortion/interaction model,¹⁴ rather than by the intrinsic properties of the reactants. Thus, the computed activation free energies (ΔE^\ddagger) of **TS1** and **TS2** are 14.1 and 9.6 kcal mol^{-1} , respectively, and agree with the observed regioselectivity. The distortion energies for the competing transition states (ΔE_d^\ddagger) are 30.0 and 33.3 kcal mol^{-1} , for **TS1** and **TS2** respectively, indicating that the reactants must distort further to reach the geometry of **TS2**. However, the corresponding interaction energies (ΔE_i^\ddagger), -15.9 and -23.7 kcal mol^{-1} , respectively, reveal a stronger stabilizing effect for **TS2** as compared to **TS1**. In fact, the interaction energy difference favoring **TS2**, $\Delta\Delta E_i^\ddagger$, is much greater than the distortion energy difference favoring **TS1**, $\Delta\Delta E_d^\ddagger$ (7.8 vs. 3.3 kcal mol^{-1} , respectively). The large $\Delta\Delta E_i^\ddagger$ value in favor of **TS2** is likely due to a combination of favorable π - π dispersive interactions between the phenyl group and the ester-DMU complex (Figure 2) and the binding mode of DMU

to the alkene in the transition structure. **TS2** shows DMU coordinated to both in-plane carbonyl lone pair orbitals, which further improves the FMO interaction in **TS1**, where DMU is coordinated to the carbonyl π^* orbital. In fact, azide **7** with a more extensive fluorenyl π -system may contribute to the larger preference for **TS2** beyond that predicted by DFT computations for a phenyl group.

2.2.3 Photochemistry of Triazolines

The solution photochemistry of triazolines *trans*-**4** and *cis*-**4** was analyzed with samples of ca. 5-8 mg dissolved in MeCN-d₃ in an NMR tube, and degassed with Argon for approximately 15 minutes. After exposure to the output of a medium pressure 400 W Hanovia Hg arc lamp equipped with a Pyrex filter (cutoff of $\lambda \leq 290$ nm), the reactions were analyzed by ¹H-NMR to determine conversion to product and the relative amounts of the *cis*- and *trans*-aziridines. The two aziridines were purified and characterized by spectroscopic methods with their identity easily established from the coupling constants of the aziridine hydrogens, with values $J_{trans} \approx 2.3$ Hz and $J_{cis} \approx 6.5$ Hz.¹⁵

As shown in Table 1, photochemical reactions in solution yielded aziridines **5** and **9** as the only product with significant stereochemical retention. While reaction of *trans*-**4** resulted in preferential formation of *trans*-**5** in 76% yield in MeCN-d₃, *cis*-**4** preferentially yielded *cis*-**5** in 68%. Similarly, methyl triazoline *trans*-**8** yielded aziridine *trans*-**9** in 86% yield in MeCN-d₃. Recognizing that high stereochemical retention values are indicative of a short lived 1,3-biradical singlet biradical where bond formation must be competitive with conformational relaxation, we also carried out experiments using acetone-d₆ as solvent and triplet sensitizer. In all three cases the triplet sensitized reaction resulted in the exclusive formation of the less sterically encumbered *trans*-aziridine, suggesting that a longer-lived triplet 1,3-biradical has an opportunity to relax and give thermodynamically more stable product.

In order to establish the conditions required for a solid state photochemical reaction we determined the thermal stability of the three triazoline crystals using differential scanning calorimetric (DSC) and thermogravimetric analysis (TGA). The DSC results showed a relatively sharp endothermic transition which correlated with the melting temperature determined visually at 133-134 °C for *trans*-4, and 165-166 °C for *cis*-4 (DSC for *trans*-8 does not show sharp endothermic transition but only shows denitrogenation). In all three cases, a melting endotherm was followed by a broad exothermic transition corresponding to the thermal denitrogenation of the corresponding triazoline (See SI section). The loss of mass corresponding to N₂ was also documented by TGA. After noting that the purified aziridines were crystalline, and with melting points in the range of 84-125°C, we recognized that the triazoline reactant-to-aziridine product mixture could be a good candidate for a solid-to-solid reaction at room temperature. This was confirmed with solid-state photochemical experiments carried out with ca. 5-10 mg of triazoline crystals ground between two microscope slides and subsequently exposed to Pyrex-filtered UV light. We also note that the bulk powder triazolines used for solid-state photochemistry were shown to be different polymorphs than those used for single crystal x-ray diffractions. We were not able to replicate the same polymorphic triazolines after numerous crystallization attempts and we were not able to get good quality single crystals of the new forms.

Table 2.2.1 Ratio of *cis*- and *trans*-aziridines from photoreactions in solution and in the solid-state.^a

triazoline	MeCN-d ₃ <i>trans</i> -5/ <i>cis</i> -5	Me ₂ CO-d ₆ <i>trans</i> -5/ <i>cis</i> -5	crystals <i>trans</i> -5/ <i>cis</i> -5
<i>trans</i> -4	76:24	99:1	83:17
<i>cis</i> -4	32:68	99:1	10:90
<i>trans</i> -8	86:14 ^b	99:1 ^b	99:1 ^b

^aRatios were determined by ¹H NMR. ^bThese entries pertain to product ratios from aziridine **9**.

The solid-state photochemistry shown in the last column of Table 1 was fully reacted to the aziridine product with quantitative conversions. As expected, reactions in the solid-state were more stereoselective than reactions in solution (Table 1), suggesting a decrease in conformational relaxation for the postulated 1,3-biradical. Samples of *trans*-**4** and *cis*-**4** yielded *trans*-**5** and *cis*-**5** in 83% and 90% yield, respectively. The highest level of retention was observed upon reaction of the trisubstituted triazoline, *trans*-**8**, where the added methyl group further hinders rotation of the 1,3-biradical intermediate. The *trans*-aziridine was obtained in quantitative yield. A small loss of stereochemical retention in the case of *trans*-**4** and *cis*-**4** indicates that a fraction of the 1,3-biradical is able to change the configuration of the carbon bearing the CF₃ group within the rigid crystalline lattice.

2.3 Conclusions

In conclusion, the synthesis of substituted aziridines by a stereospecific dipolar cycloaddition of activated alkenes and azides followed by the photodenitrogenation of the resulting triazolines in the crystalline phase presents some promise and also some challenges. Although we confirmed a remarkably high regioselectivity and stereospecificity for the hydrogen-bond DMU-catalyzed dipolar cycloaddition of CF₃-activated acrylates, reaction yields are moderate to low. DFT calculations suggest that dispersive π - π stacking interactions are responsible for the regioselectivity of the (3+2) dipolar cycloaddition and suggest that more active catalysts would be needed. By contrast, we showed that solution photochemistry of Δ^2 -1,2,3-triazolines gives good to excellent results. Direct photochemical excitation generates the singlet 1,3-biradicals, which afford the kinetically controlled *trans*- or *cis*- aziridine products with good to excellent stereospecificities, as previously reported by Schreiner with different Δ^2 -1,2,3-triazolines.¹⁶ We also found that reactions carried out using acetone as a triplet sensitizer

proceed through the longer-lived triplet 1,3-birdical and give the thermodynamically favored *trans*-product regardless of the nature of the precursor. Finally, photochemical solid-to-solid reactions occur with the highest stereochemical retention values and in quantitative yields, suggesting that the reaction has synthetic potential.

Author's note. Chapter 2 is adapted from the following publication: Chung, T.S.; Lopez, S.A.; Houk, K.N.; Garcia-Garibay, M.A. "Stereospecific Synthesis of Substituted Aziridines by a Crystal-to-Crystal Photodenitrogenation of Δ^2 -1,2,3-Triazolines." *Org. Lett.*, **2015**, *17*, 4568–4571. I performed the synthesis, characterization, and photochemical studies and Dr. Steven Lopez assisted with computational data.

2.4 Experimental

Synthesis of 2-azido-9*H*-fluorene (**7**):

Compound **2** was synthesized according to literature from 2-Aminofluorene. Crude product from the reaction was purified by silica gel chromatography (eluent: EtOAc/Hexanes 20/80). Yield 99%, orange solid, R_f 0.89. IR (ATR): 3045, 2386, 2104, 1603, 1580, 1450, 1290, 1280, 836 cm^{-1} . ^1H NMR (500 MHz, CDCl_3) δ 7.74 (d, $J = 8.1$ Hz, 2H), 7.53 (d, $J = 7.5$ Hz, 1H), 7.37 (d, $J = 7.5$ Hz, 1H), 7.30 (td, $J = 7.4, 1.0$ Hz, 1H), 7.22 (s, 1H), 7.04 (dd, $J = 8.1, 2.1$ Hz, 1H), 3.90 (s, 2H). ^{13}C NMR (125 MHz, CDCl_3) δ 145.13, 142.93, 140.97, 138.97, 138.48, 126.95, 126.68, 125.05, 120.88, 119.67, 117.85, 115.75, 36.87. The spectra of this compound is reported in previous literature.

Synthesis of ethyl (*Z*)-4,4,4-trifluorobut-2-enoate (*cis*-**3**):

Ethyl 4,4,4-trifluorocrotonate *trans*-**3** (638mg, 3.8mmol) was dissolved in 5mL of dry DCM. The mixture was irradiated using a medium-pressure Hg Hanovia lamp with a quartz emersion well filter with cutoff of $\lambda \leq 220$ nm. After 3 days, the mixture reached a photostationary state of 76% *trans*-**3** and 24% *cis*-**3**. The DCM was concentrated under vacuum and the mixture was purified by silica gel column chromatography using pentane/diethyl ether (90/10) as eluent. Clear liquid, R_f 0.45, stained with Potassium permanganate. IR(ATR): 2952, 2924, 1742, 1668, 1460, 1371, 1312, 1262, 1183 cm^{-1} . ^1H NMR (500 MHz, CDCl_3) δ 6.28 (d, $J = 12.5$ Hz, 1H), 6.03 (dq, $J = 12.5, 8.0$ Hz, 1H), 4.27 (q, $J = 7.1$ Hz, 2H), 1.20 (t, $J = 7.1$ Hz, 3H). ^{13}C NMR (125 MHz, CDCl_3) δ 163.46, 130.12, 130.07, 130.03, 129.99, 127.38, 127.08, 126.79, 126.50, 124.46, 122.30, 120.14, 117.97, 61.67, 34.12, 13.86.

Synthesis of Ethyl (4*R*,5*R*)-1-(8*a*,9-dihydro-4*bH*-fluoren-2-yl)-4-(trifluoromethyl) Δ^2 -1,2,3-triazoline-5-carboxylate (*trans*-**4**):

Ethyl 4,4,4-trifluorocrotonate (0.3 mmol), **7** (0.3 mmol), and $\text{N,N}'$ -dimethylurea (0.03 mmol) was dissolved in 1.5mL of dry toluene the reaction was stirred for 32 hours at 60 $^{\circ}\text{C}$ under argon atmosphere. After the initial 32 hours, an additional 0.3 mmol of ethyl 4,4,4-trifluorocrotonate was added to the solution. After 33 more hours of heating, the reaction was cooled when the disappearance of azide by TLC was observed. The product mixture was purified by silica gel column chromatography (eluent 10/70 EtOAc/Hexanes). Obtained 73 mg, yield 65%, white solid, R_f 0.39. IR (ATR): 2996, 1738, 1615, 1584, 1487-1337, 1274, 1241, 1199-1107, 1017, 986 cm^{-1} . ^1H NMR (500 MHz, CDCl_3) δ 7.75 (t, $J = 8.7$ Hz, 2H), 7.57 (d, $J = 1.6$ Hz, 1H), 7.53 (d, $J = 7.4$ Hz, 1H), 7.38 (td, $J = 7.4, 1.1$ Hz, 1H), 7.30 (td, $J = 7.4, 1.1$ Hz, 1H), 7.27 – 7.23 (m, 2H), 5.28 (p, $J = 7.8$ Hz, 1H), 4.69 (d, $J = 7.8$ Hz, 1H), 4.31 – 4.23 (m, 2H), 3.92 (s, 2H), 1.24 (t, $J = 7.1$

Hz, 3H). ^{13}C NMR (125 MHz, CDCl_3) δ 167.85, 144.98, 142.94, 140.92, 138.48, 137.74, 126.97, 126.66, 125.04, 123.76, 121.54, 120.68, 119.66, 114.37, 112.77, 82.60, 82.37, 82.13, 81.89, 63.13, 57.30, 37.09, 13.98. IonSense ID-CUBE DART ion source $\text{C}_{19}\text{H}_{16}\text{F}_3\text{N}_3\text{O}_2+\text{H}^+$ calcd, 376.12282, $\text{C}_{19}\text{H}_{16}\text{F}_3\text{N}_3\text{O}_2+\text{H}^+$ found, 376.12532. Melting Point: 132.7-133.6°C

Synthesis of Ethyl (4*S*,5*R*)-1-(8*a*,9-dihydro-4*bH*-fluoren-2-yl)-4-(trifluoromethyl) Δ^2 -1,2,3-triazoline-5-carboxylate (*cis*-4):

Ethyl (*Z*)-4,4,4-trifluorobut-2-enoate (*cis*-3) (0.48 mmol), **7** (0.24 mmol), and $\text{N,N}'$ -dimethylurea (0.024 mmol) was dissolved in 1 mL of dry toluene the reaction was stirred for 62 hours at 60°C under argon atmosphere. The reaction was cooled when the disappearance of azide by TLC was observed. The product mixture was purified by silica gel column chromatography (eluent 10/70 EtOAc/Hexanes). Obtained 10 mg, yield 18%, white solid, R_f 0.33. IR (ATR): 2919, 2850, 1743, 1615, 1585, 1483-1329, 1277, 1223, 1203, 1173-1021, 968, 821 cm^{-1} . ^1H NMR (500 MHz, CDCl_3) δ 7.74 (t, $J = 7.7$ Hz, 2H), 7.57 – 7.49 (m, 2H), 7.37 (td, $J = 7.4, 1.1$ Hz, 1H), 7.29 (td, $J = 7.4, 1.1$ Hz, 1H), 7.15 (dd, $J = 8.3, 2.2$ Hz, 1H), 5.21 (dq, $J = 12.9, 7.8$ Hz, 1H), 4.91 (d, $J = 12.9$ Hz, 1H), 4.22 – 4.10 (m, 2H), 3.92 (s, 2H), 1.14 (t, $J = 7.1$ Hz, 3H). ^{13}C NMR (125 MHz, CDCl_3) δ 165.32, 145.04, 142.92, 140.96, 138.30, 138.02, 126.95, 126.61, 125.80, 125.03, 123.58, 121.36, 120.72, 119.61, 119.14, 114.09, 112.59, 81.02, 80.78, 80.53, 80.29, 62.79, 57.56, 37.10, 13.69. ESI-TOF $\text{C}_{19}\text{H}_{16}\text{F}_3\text{N}_3\text{O}_2+\text{H}^+$ calcd, 376.12282, $\text{C}_{19}\text{H}_{16}\text{F}_3\text{N}_3\text{O}_2+\text{H}^+$ found, 376.12581. Melting Point: 165.1-166.4°C.

Synthesis of Ethyl (4*R*,5*R*)-1-(8*a*,9-dihydro-4*bH*-fluoren-2-yl)-4-methyl-4-(trifluoromethyl) Δ^2 -1,2,3-triazoline-5-carboxylate (*trans*-8):

Ethyl 3-(trifluoromethyl) crotonate (0.483 mmol), **7** (0.483 mmol), and $\text{N,N}'$ -dimethylurea (0.048 mmol) was dissolved in 1.5mL of dry toluene the reaction was stirred for 48 hours at

60°C under argon atmosphere. After the initial 48 hours, an additional 0.483 mmol of ethyl 3-(trifluoromethyl)crotonate was added to the solution. After 40 more hours of heating, the reaction was cooled when the disappearance of azide by TLC was observed. The product mixture was purified by silica gel column chromatography (eluent 10/70 EtOAc/Hexanes). Obtained 10 mg, yield 6%, white solid, R_f 0.35. IR (ATR): 3079, 3051, 2961, 1745, 1615, 1585, 1480-1351, 1256, 1201, 1165, 1101, 1041, 1021, 980 cm^{-1} . ^1H NMR (500 MHz, CD_3CN) δ 7.84 (d, $J = 8.3$ Hz, 1H), 7.80 (d, $J = 7.6$ Hz, 1H), 7.60 – 7.55 (m, 1H), 7.54 (d, $J = 1.6$ Hz, 1H), 7.38 (td, $J = 7.5, 0.9$ Hz, 1H), 7.30 (td, $J = 7.4, 1.1$ Hz, 1H), 7.25 (dd, $J = 8.3, 2.2$ Hz, 1H), 5.03 (s, 1H), 4.31 – 4.20 (m, 2H), 3.95 (s, 2H), 1.62 (s, 3H), 1.23 (t, $J = 7.1$ Hz, 3H). ^{13}C NMR (126 MHz, CDCl_3) δ 166.32, 145.00, 142.90, 140.99, 138.15, 137.95, 127.64, 126.93, 126.55, 125.39, 125.01, 124.90, 123.14, 120.89, 120.68, 119.59, 113.95, 112.39, 86.43, 86.21, 86.00, 85.78, 62.66, 60.85, 37.09, 15.06, 14.10. IonSense ID-CUBE DART ion source $\text{C}_{20}\text{H}_{18}\text{F}_3\text{N}_3\text{O}_2+\text{H}^+$ calcd, 390.13847, $\text{C}_{20}\text{H}_{18}\text{F}_3\text{N}_3\text{O}_2+\text{H}^+$ found, 390.14137. Melting Point: 152.4-154.2°C.

Synthesis of Aziridines from Triazolines:

For solid-state photolysis:

Triazoline *trans*-**4**, *cis*-**4**, and *trans*-**8** (5-8 mg) was crushed between two microscope slides and photolyzed using a medium-pressure Hg Hanovia lamp with a pyrex emersion well filter with cutoff of $\lambda \leq 290$ nm. The reaction was monitored by ^1H NMR and was completed in less than one hour.

For solution-state photolysis:

Triazoline (5-8mg) was dissolved in deuterated acetonitrile or acetone in an NMR tube and the solution was degassed with argon using a long needle for approximately 10 minutes. The NMR

tube was photolyzed using a medium-pressure Hg Hanovia lamp with a pyrex emersion well filter with cutoff of $\lambda \leq 290$ nm. The reactions were monitored by ^1H NMR and showed completion in less than one hour.

Ethyl (2*R*,3*R*)-1-(8*a*,9-dihydro-4*bH*-fluoren-2-yl)-3-(trifluoromethyl)-2-aziridinecarboxylate (*trans*-**5**):

IR(ATR): 2997, 1735, 1613, 1579, 1486-1402, 1373, 1338, 1278, 1214, 1096, 1078, 1029 cm^{-1} .

^1H NMR (500 MHz, CD_3CN) δ 7.76 (d, $J = 7.6$ Hz, 1H), 7.72 (d, $J = 8.1$ Hz, 1H), 7.54 (dd, $J = 7.5, 0.8$ Hz, 1H), 7.36 (td, $J = 7.5, 0.8$ Hz, 1H), 7.28 (td, $J = 7.4, 1.1$ Hz, 1H), 7.16 (d, $J = 1.3$ Hz, 1H), 6.96 (dd, $J = 8.1, 2.1$ Hz, 1H), 4.12 – 3.99 (m, 2H), 3.87 (s, 2H), 3.66 (qd, $J = 5.1, 2.3$ Hz, 1H), 3.53 (d, $J = 2.2$ Hz, 1H), 1.08 (t, $J = 7.1$ Hz, 3H). ^{13}C NMR (125 MHz, CD_3CN) δ 165.51, 146.38, 145.38, 143.70, 141.57, 138.07, 127.37, 127.16, 126.91, 125.63, 124.99, 122.82, 120.93, 119.13, 117.13, 62.48, 42.56, 42.24, 41.92, 41.60, 40.22, 40.20, 36.99, 13.87. IonSense ID-CUBE DART ion source $\text{C}_{19}\text{H}_{16}\text{F}_3\text{NO}_2 + \text{H}^+$ calcd, 348.11667, $\text{C}_{19}\text{H}_{16}\text{F}_3\text{NO}_2 + \text{H}^+$ found, 348.11927. Melting Point: 124.7-125.6 $^\circ\text{C}$.

Ethyl (2*R*,3*S*)-1-(8*a*,9-dihydro-4*bH*-fluoren-2-yl)-3-(trifluoromethyl)-2-aziridinecarboxylate (*cis*-**5**):

IR(ATR): 2924, 1756, 1615, 1456, 1379, 1288, 1260, 1228, 1207, 1151, 1060 cm^{-1} . ^1H NMR (500 MHz, CD_3CN) δ 7.77 (t, $J = 8.0$ Hz, 2H), 7.55 (d, $J = 7.5$ Hz, 1H), 7.43 – 7.34 (m, 1H), 7.29 (td, $J = 7.5, 1.1$ Hz, 2H), 7.09 (dd, $J = 8.1, 2.1$ Hz, 1H), 4.27 (dddd, $J = 17.9, 10.8, 7.1, 3.7$ Hz, 2H), 3.89 (s, 1H), 3.38 (d, $J = 6.5$ Hz, 1H), 3.35 – 3.25 (m, 1H), 1.38 – 1.24 (m, 3H). ^{13}C NMR (125 MHz, CD_3CN) δ 165.81, 149.12, 144.99, 143.23, 140.90, 137.96, 126.84, 126.47, 125.10, 124.06, 122.63, 120.53, 119.57, 118.54, 116.60, 61.65, 42.39, 42.07, 41.46, 29.35, 13.34.

IonSense ID-CUBE DART ion source $C_{19}H_{16}F_3NO_2+H^+$ calcd, 348.11667, $C_{19}H_{16}F_3NO_2+H^+$ found, 348.11936. Melting Point: 84.8-86.9°C

Ethyl(2*R*,3*R*)-1-(8*a*,9-dihydro-4*bH*-fluoren-2-yl)-3-methyl-3-(trifluoromethyl)-2-aziridinecarboxylate (*trans*-**9**):

IR (ATR): 2984, 2857, 1751, 1651, 1580, 1486. 1455, 1430, 1310, 1251, 1194, 1181, 1170, 1138, 1121, 1049, 1018, 941, 833 cm^{-1} . 1H NMR (500 MHz, CD_3CN) δ 7.76 (d, $J = 7.6$ Hz, 1H), 7.72 (d, $J = 8.2$ Hz, 1H), 7.56 – 7.51 (m, 1H), 7.36 (dd, $J = 10.7, 4.2$ Hz, 1H), 7.27 (td, $J = 7.4, 1.1$ Hz, 1H), 7.15 (d, $J = 1.3$ Hz, 1H), 6.95 (dd, $J = 8.2, 2.1$ Hz, 1H), 4.25 (m, 2H), 3.87 (s, 1H), 3.52 (s, 1H), 1.65 (s, 3H), 1.30 (t, $J = 7.1$ Hz, 3H). ^{13}C NMR (126 MHz, $CDCl_3$) δ 166.62, 144.36, 144.11, 142.82, 141.43, 137.31, 127.57, 126.77, 126.09, 124.90, 124.48, 121.45, 120.19, 119.37, 118.45, 118.21, 115.97, 77.27, 77.02, 76.76, 61.99, 41.36, 36.86, 30.95, 30.34, 29.71, 29.05, 14.25, 12.04. IonSense ID-CUBE DART ion source $C_{20}H_{18}F_3NO_2+H^+$ calcd, 362.13232, $C_{20}H_{18}F_3NO_2+H^+$ found, 362.13508. Melting Point: 113.6-115.2°C

The ratios of all other aziridine products were analyzed by analogy using coupling constants and chemical shifts of aziridines trans-5 and cis-5.

2.5 Appendix

Characterization for Chapter 2

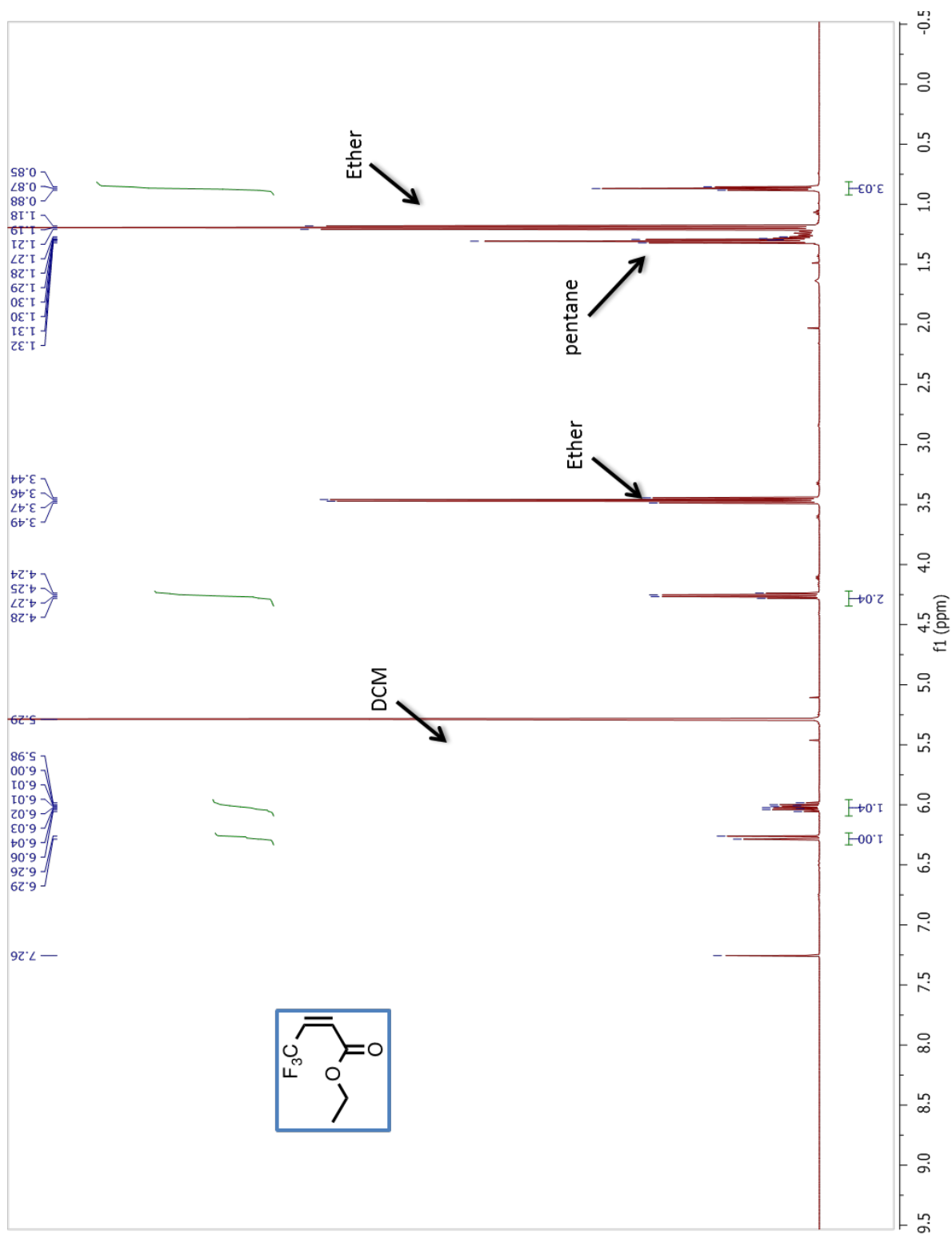
2.5.1	General Information.....	27
2.5.2	Compound Spectra (¹ H NMR, ¹³ C NMR, 2D NMR, UV-Vis).....	28
2.5.3	Crystal Pictures.....	58
2.5.4	Thermal Analysis.....	59
2.5.5	PXRD Analysis.....	62
2.5.6	Computational Supplemental Information.....	64

2.5.1 General Information

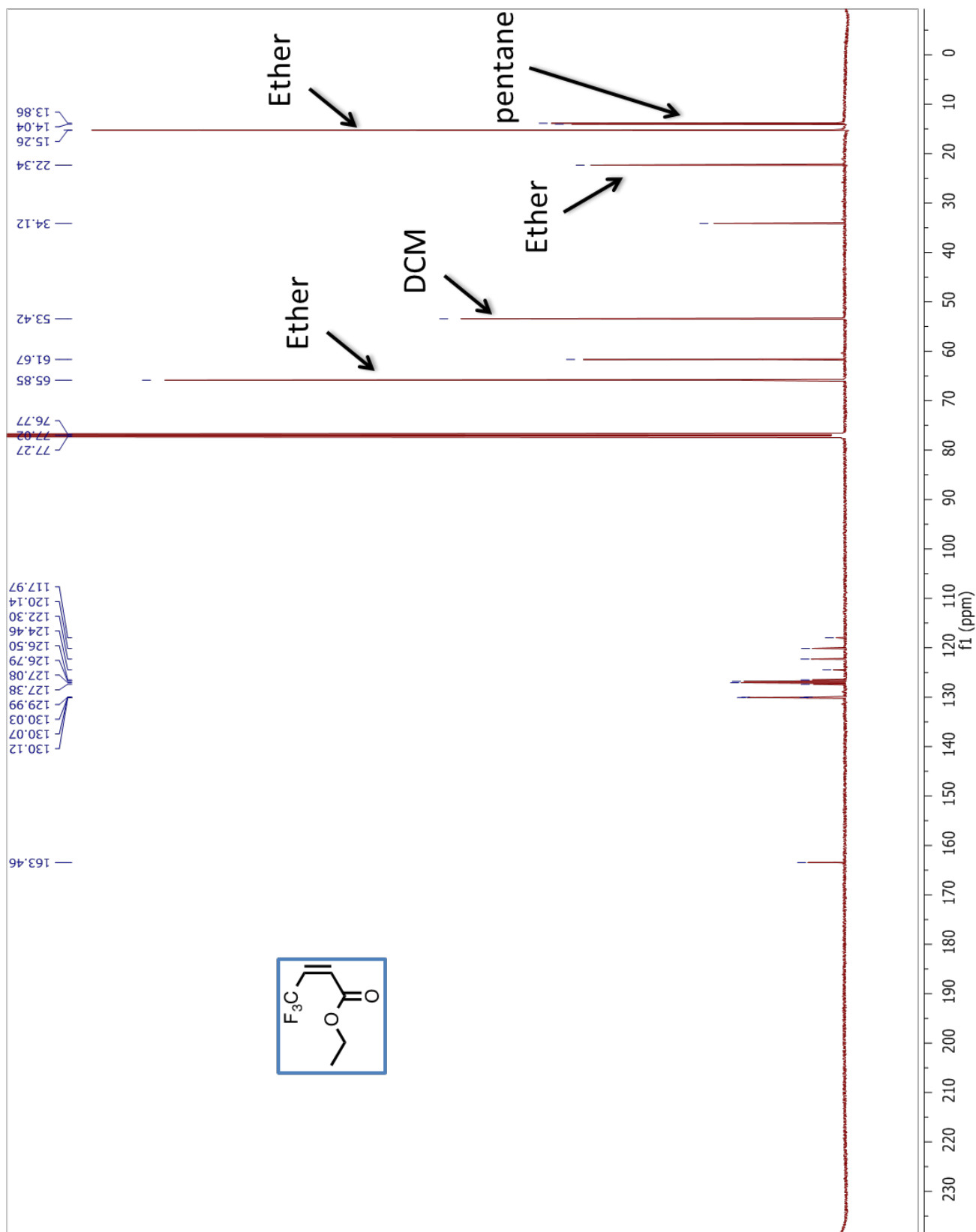
All reactions were carried out under an inert atmosphere of argon in oven or flame-dried glassware, unless the reaction procedure states otherwise. All chemicals were purchased from commercial suppliers and used as received. The 2-Aminofluorene is commercially available and the corresponding aryl azide was synthesized according to literature. Room temperature reactions were carried out between 20-25 °C, reactions at 0 °C were performed using a water-ice bath and reactions at -78 °C were carried out in an acetone-dry ice bath. Analytical thin-layer chromatography (TLC) was performed using pre-coated TLC plates with Silica Gel 60 F254 and visualized using combinations of UV, and potassium permanganate (KMnO₄) staining. Flash column chromatography was performed using silica gel (230-400 mesh) as the stationary phase. Proton magnetic resonance spectra were recorded at 500 MHz, and carbon-13 magnetic resonance spectra were recorded at 125 MHz, respectively. All chemical shifts are reported in ppm on the δ -scale relative to TMS (δ 0.0) using residual solvent as reference (CDCl₃ δ 7.26 and δ 77.16 for proton and carbon, respectively, CD₃CN δ 1.94 and 1.32, 118.26 for proton and carbon respectively, (CD₃)₂CO δ 2.05 and 29.84, 206.26 for proton and carbon, respectively). Coupling constants *J* are reported in Hz. Multiplicities are reported as broad (br), singlet (s), doublet (d), triplet (t), quartet (q), pentet (p), sextet (sxt), septuplet (spt) and multiplet (m). Uncorrected melting points were recorded on a melting point apparatus using open glass capillaries. IR spectral data were obtained using an Attenuated Total Reflectance (ATR) spectrometer as the neat compound and the units are stated in cm⁻¹. PXRD analyses were carried out using Cu-K α 1 = 1.5406 Å radiation. Data were collected at room temperature in the range of $2\theta = 4$ -50° (steps of 0.017, step time 120 s).

2.5.2 Compound Spectra (^1H NMR, ^{13}C NMR, 2D NMR, UV-Vis)

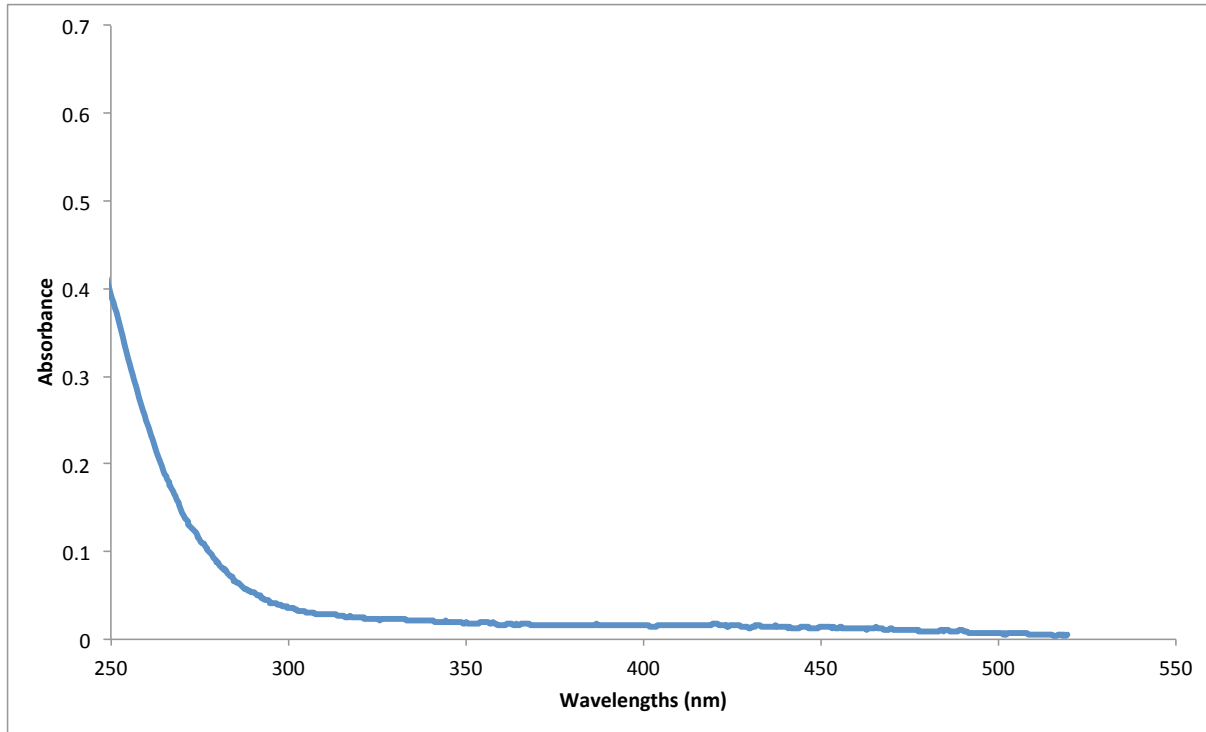
^1H NMR (CDCl_3 , 500 MHz) spectrum of *cis*-3



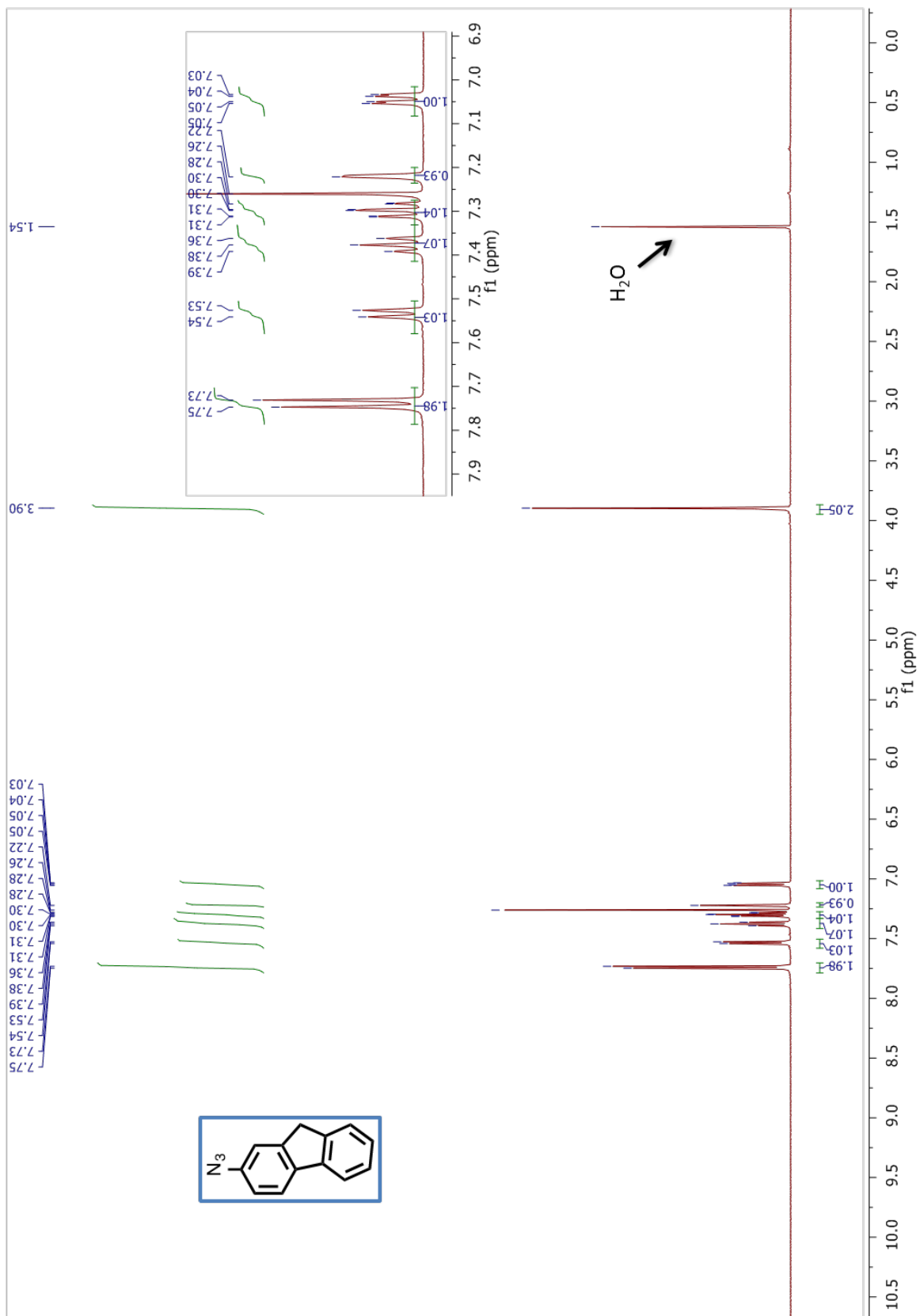
^{13}C NMR (CDCl_3 , 125 MHz) spectrum of *trans*-3



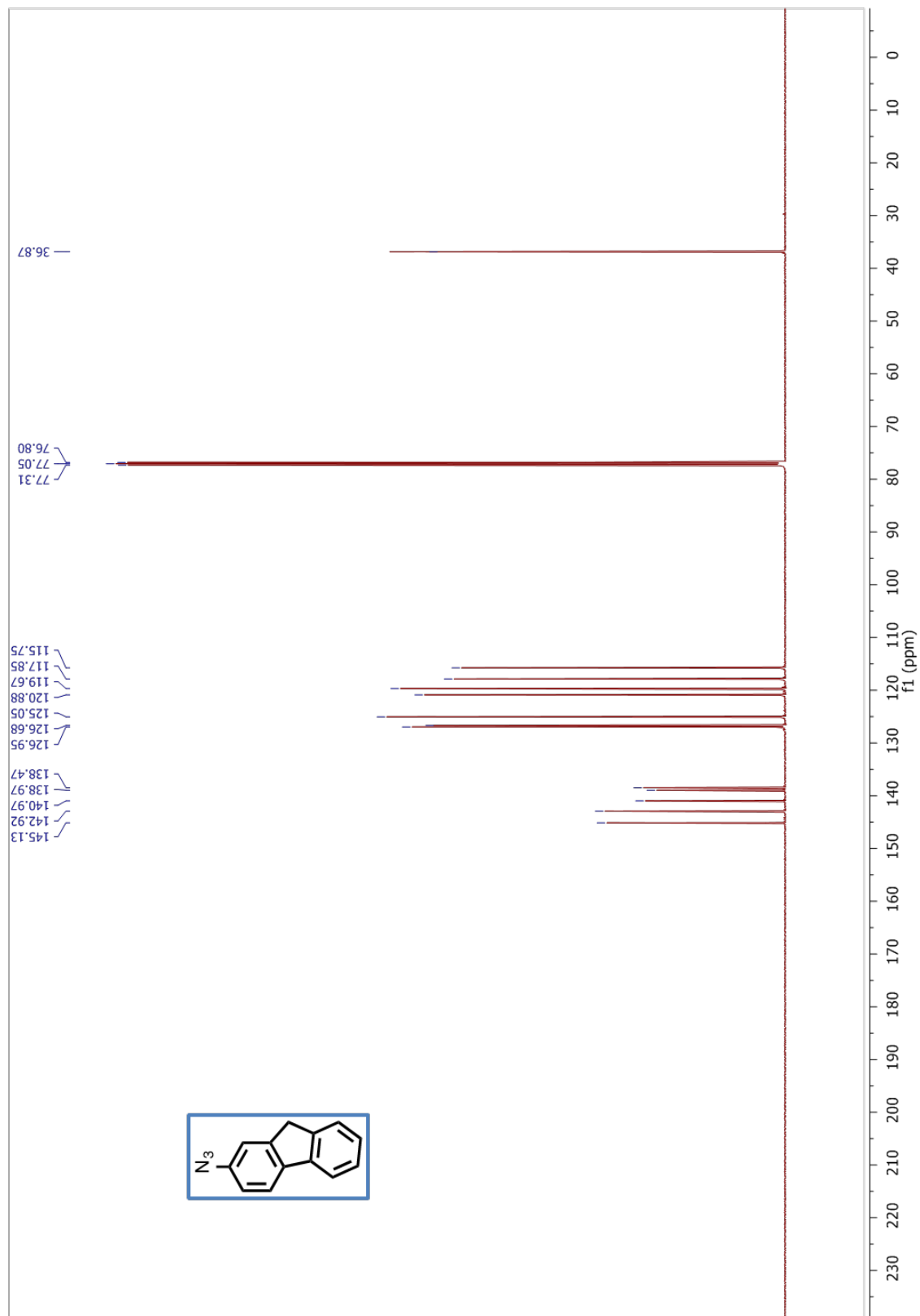
UV-Vis Spectrum of *trans*-**3** in dichloromethane.



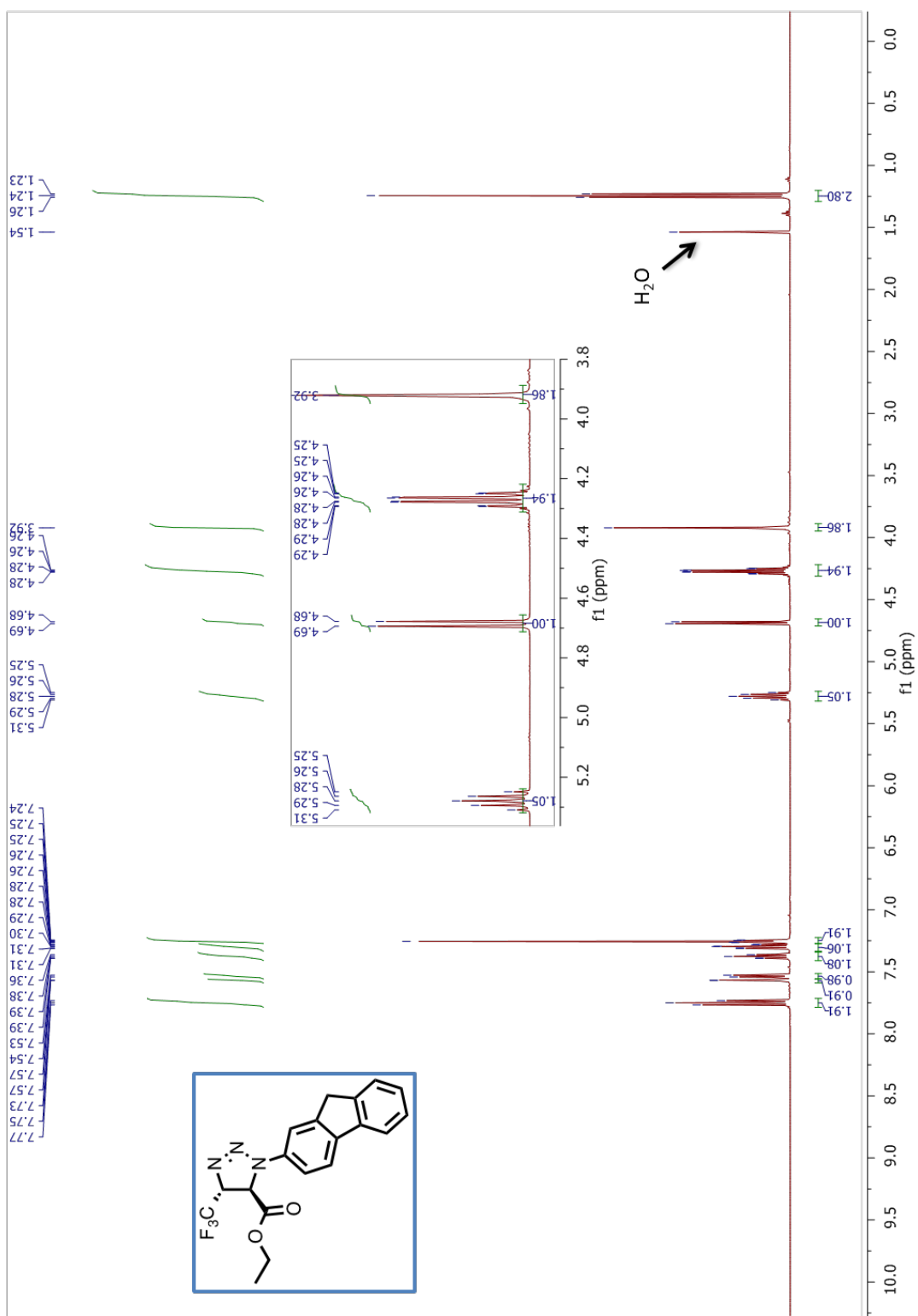
^1H NMR (CDCl_3 , 500 MHz) spectrum of **7**



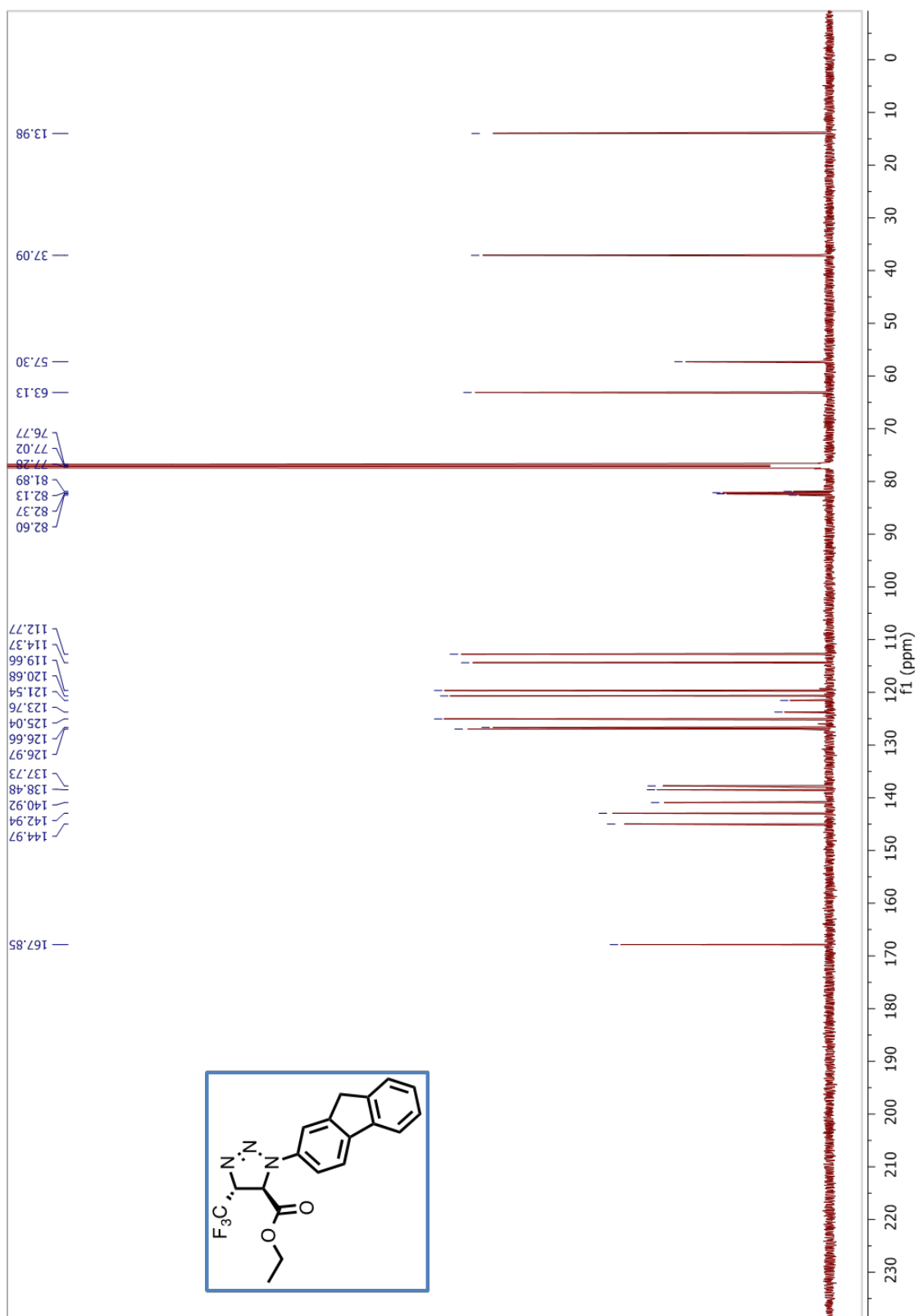
^{13}C NMR (CDCl_3 , 125 MHz) spectrum of 7



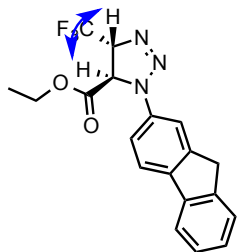
^1H NMR (CDCl_3 , 500 MHz) spectrum of *trans*-4



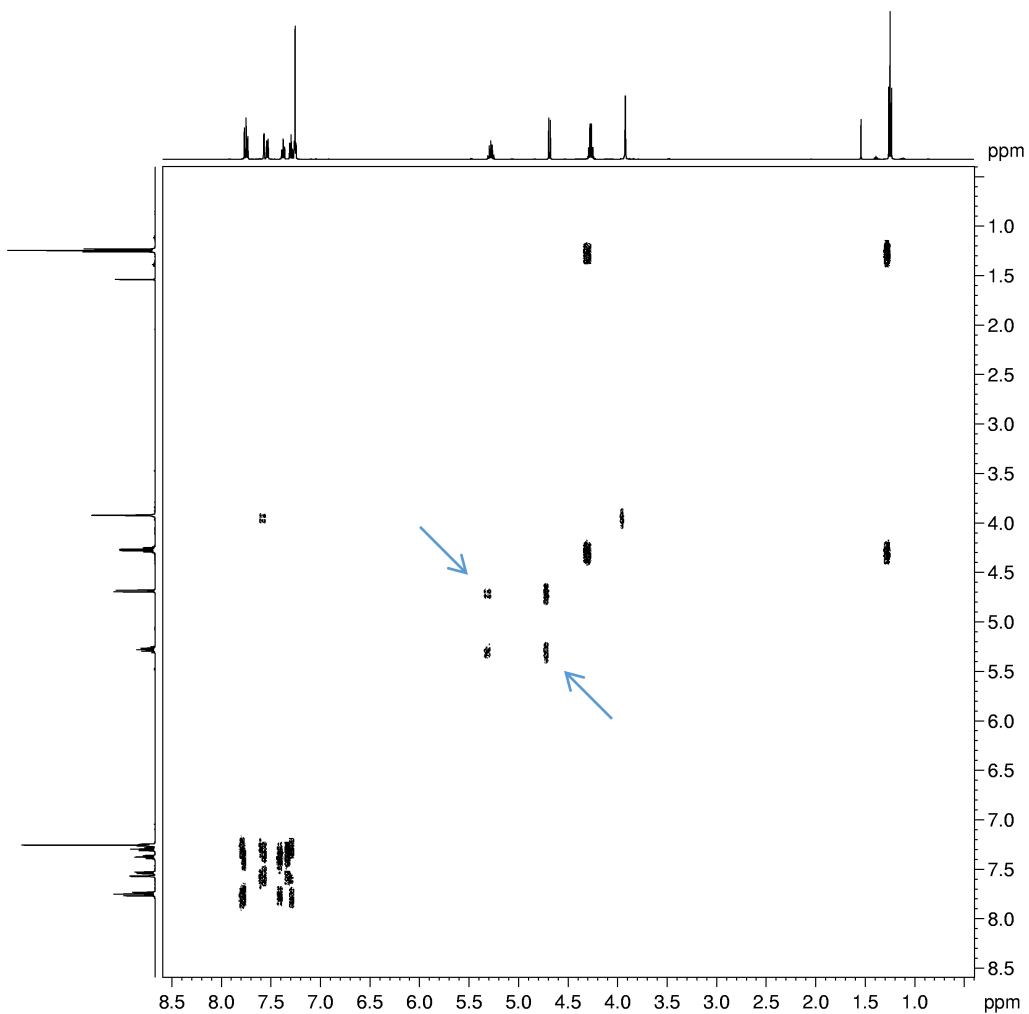
^{13}C NMR (CDCl_3 , 125 MHz) spectrum of *trans*-4



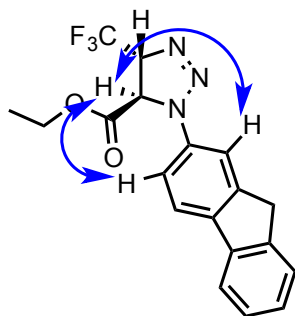
COSY NMR (CDCl₃, 500 MHz) spectrum of *trans*-4



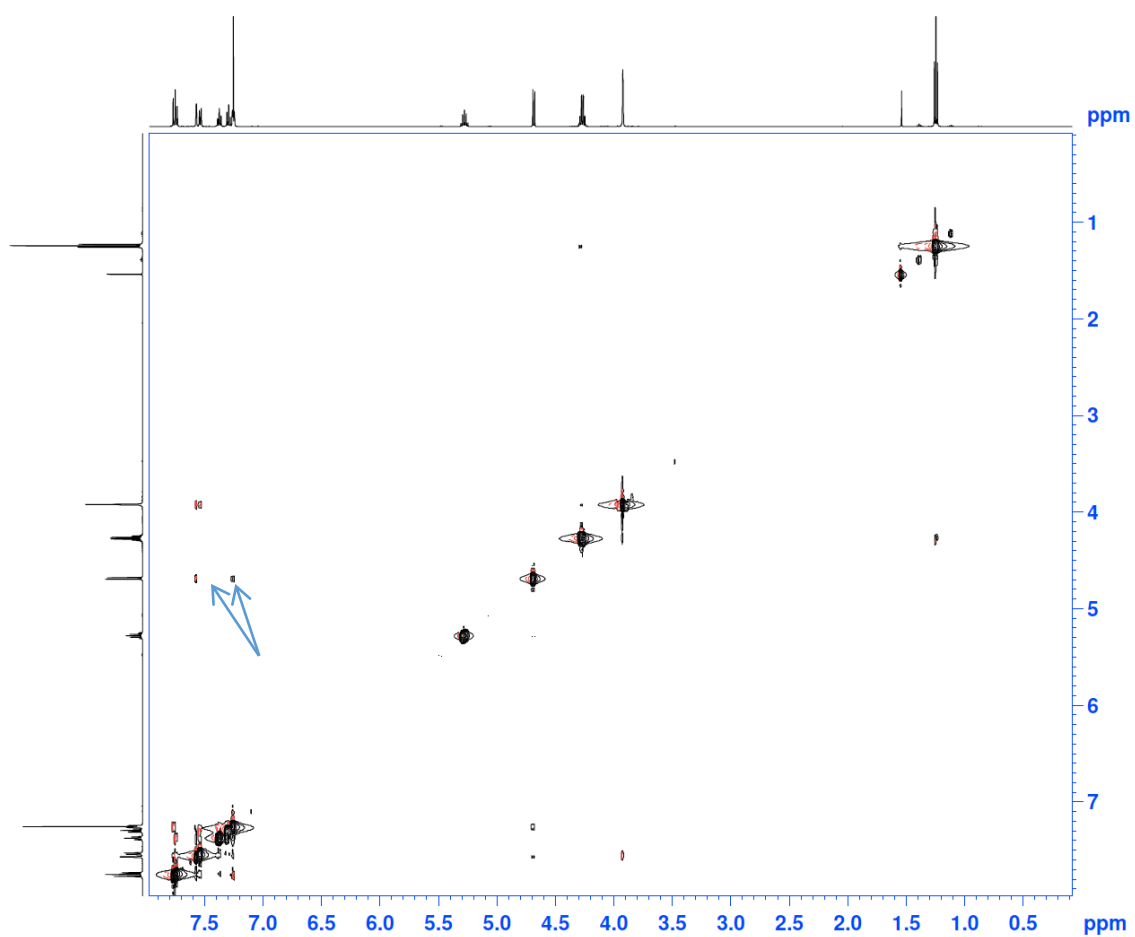
The two blue arrows below shows positive COSY correlation of the two ring protons shown in the structure.



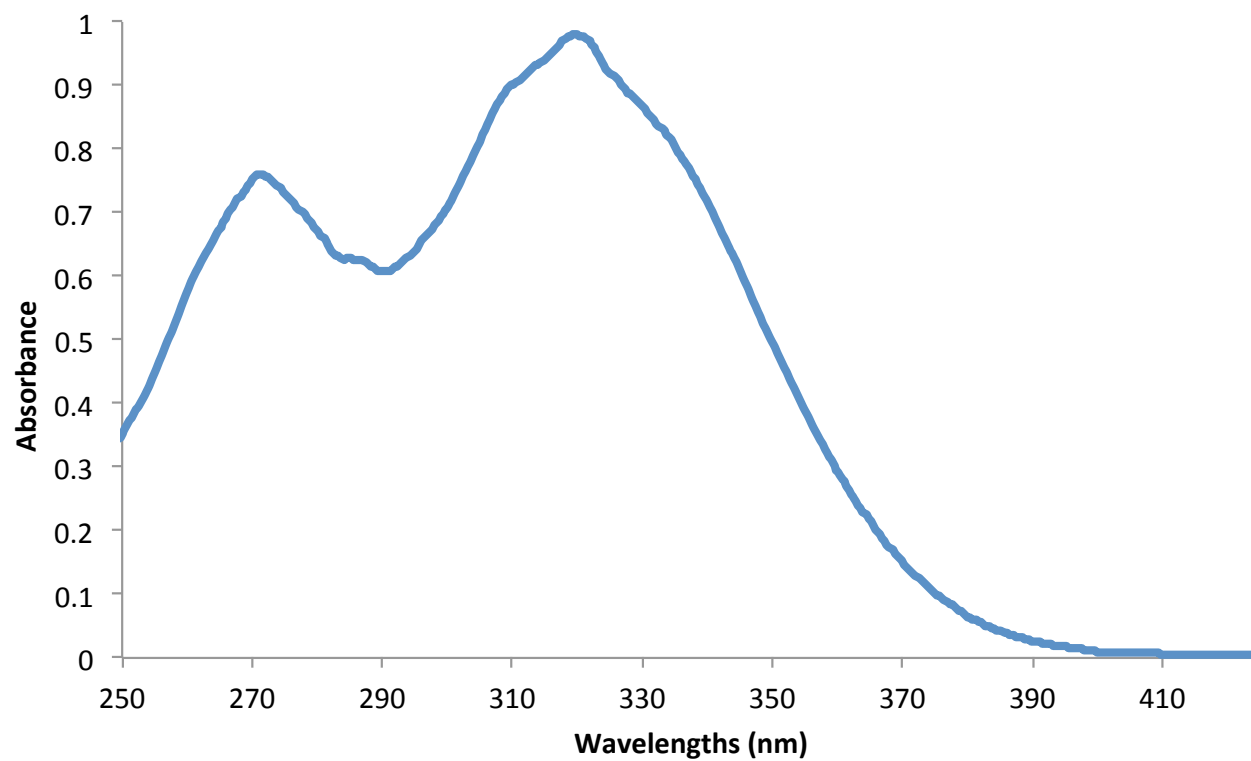
NOESY NMR (CDCl_3 , 500 MHz) spectrum of *trans*-4



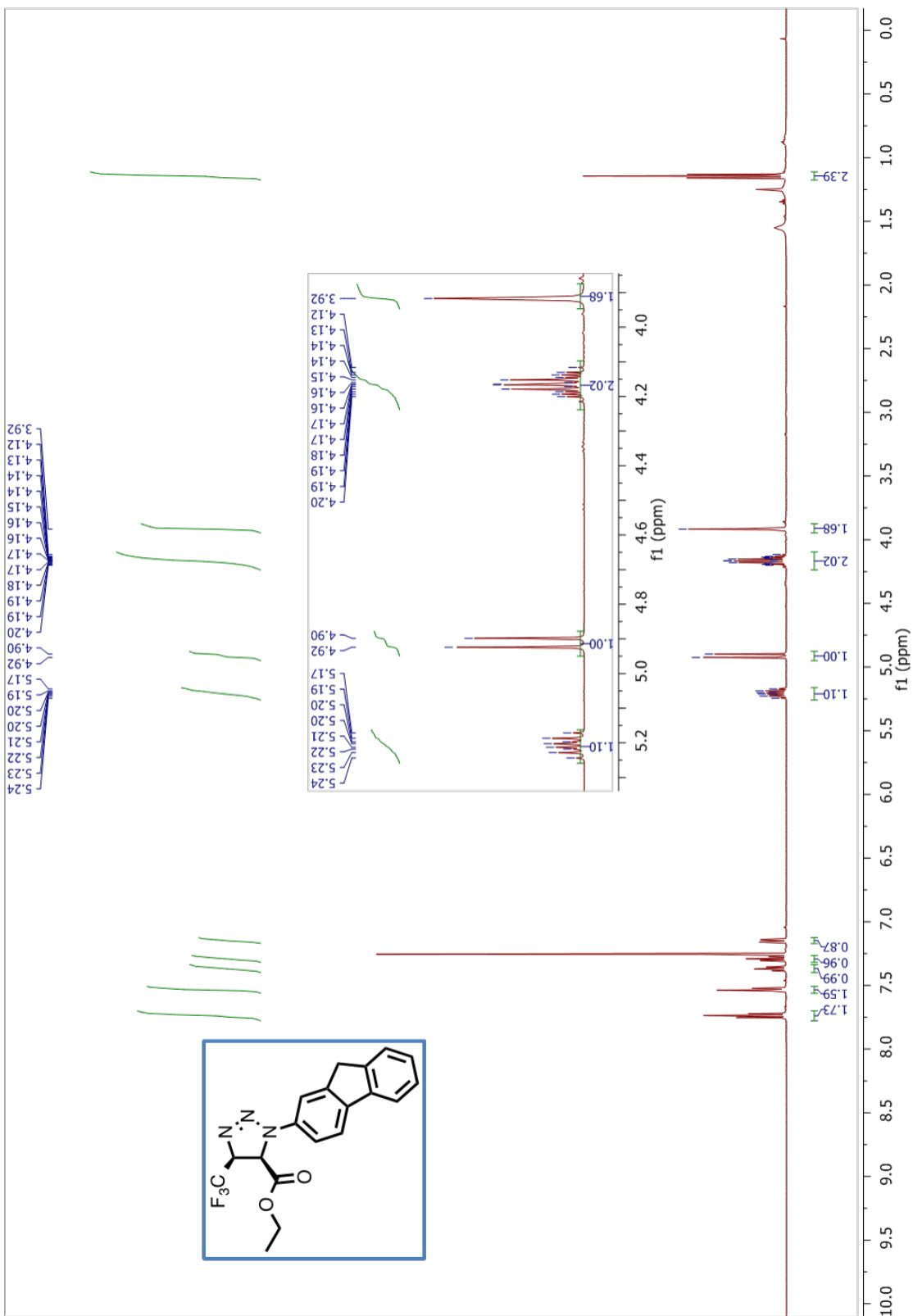
The two blue arrows below shows positive NOESY correlation of the methine proton to the aromatic protons, indicating regiochemistry of the cycloaddition product.



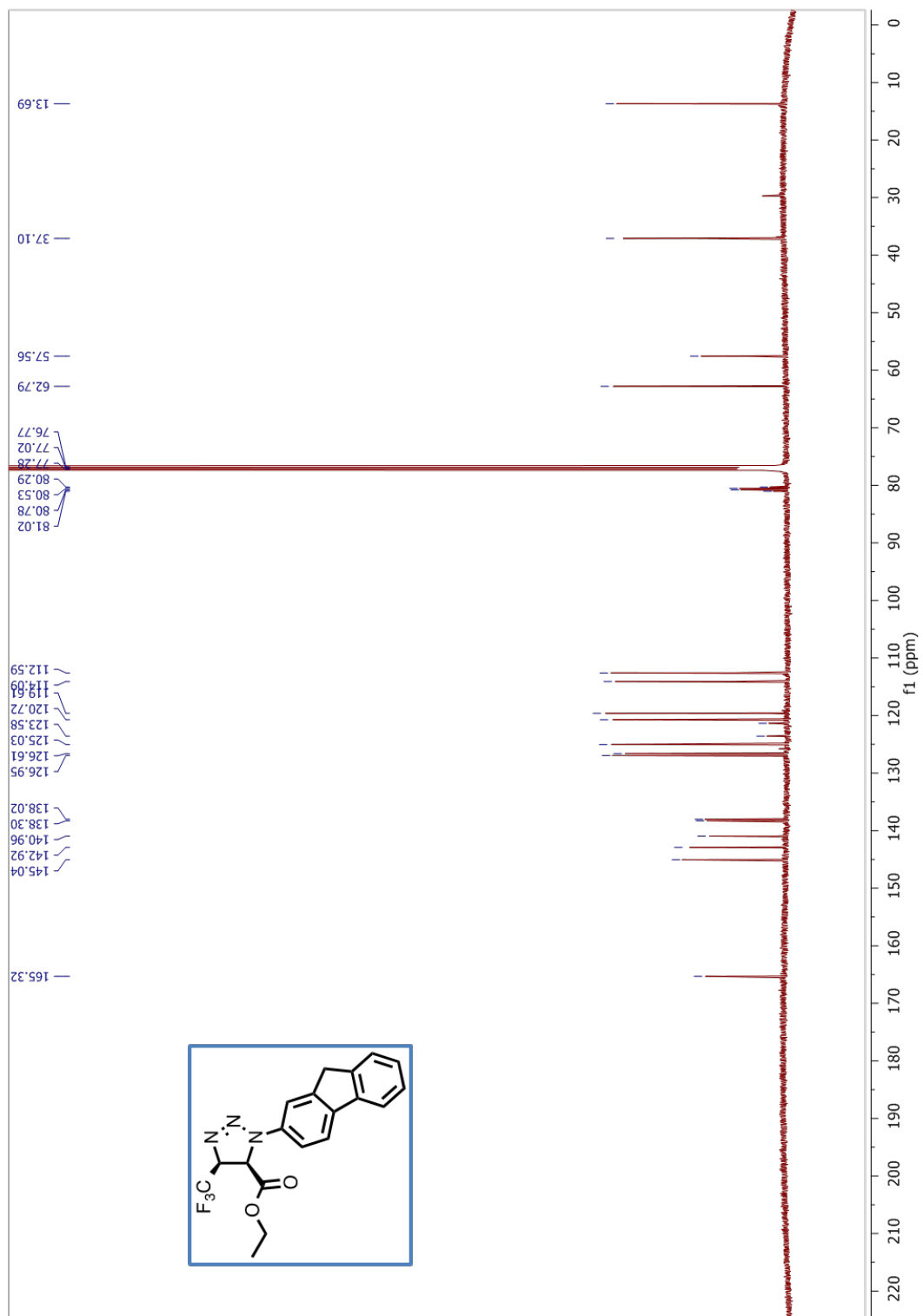
UV-Vis Spectrum of *trans*-4 in dichloromethane.



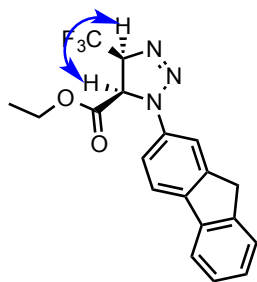
^1H NMR (CDCl_3 , 500 MHz) spectrum of *cis*-4



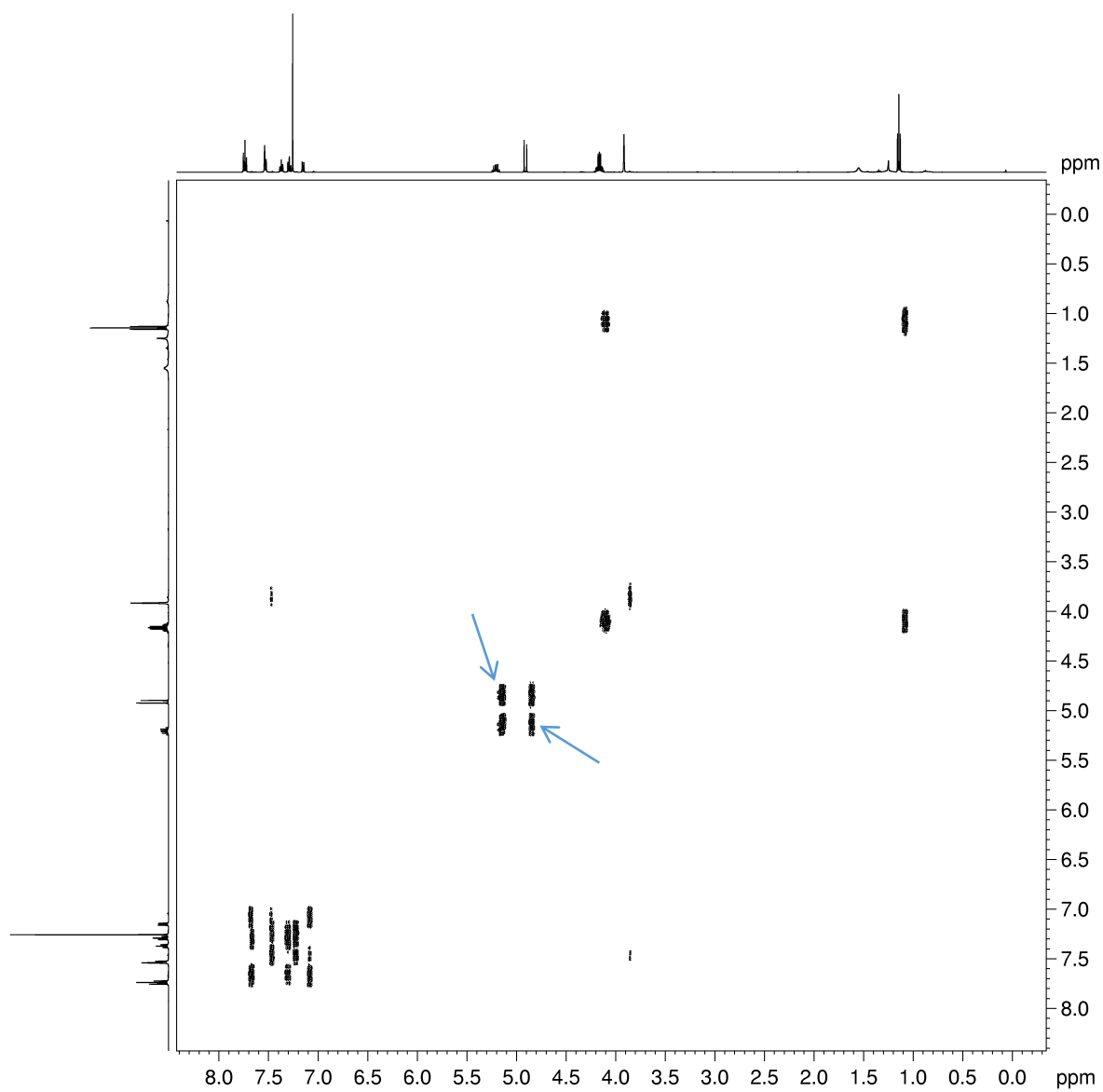
^{13}C NMR (CDCl_3 , 125 MHz) spectrum of *cis*-4



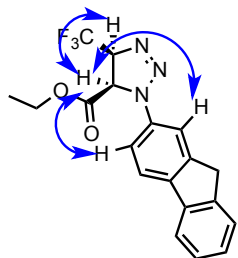
COSY NMR (CDCl₃, 500 MHz) spectrum of *cis*-4



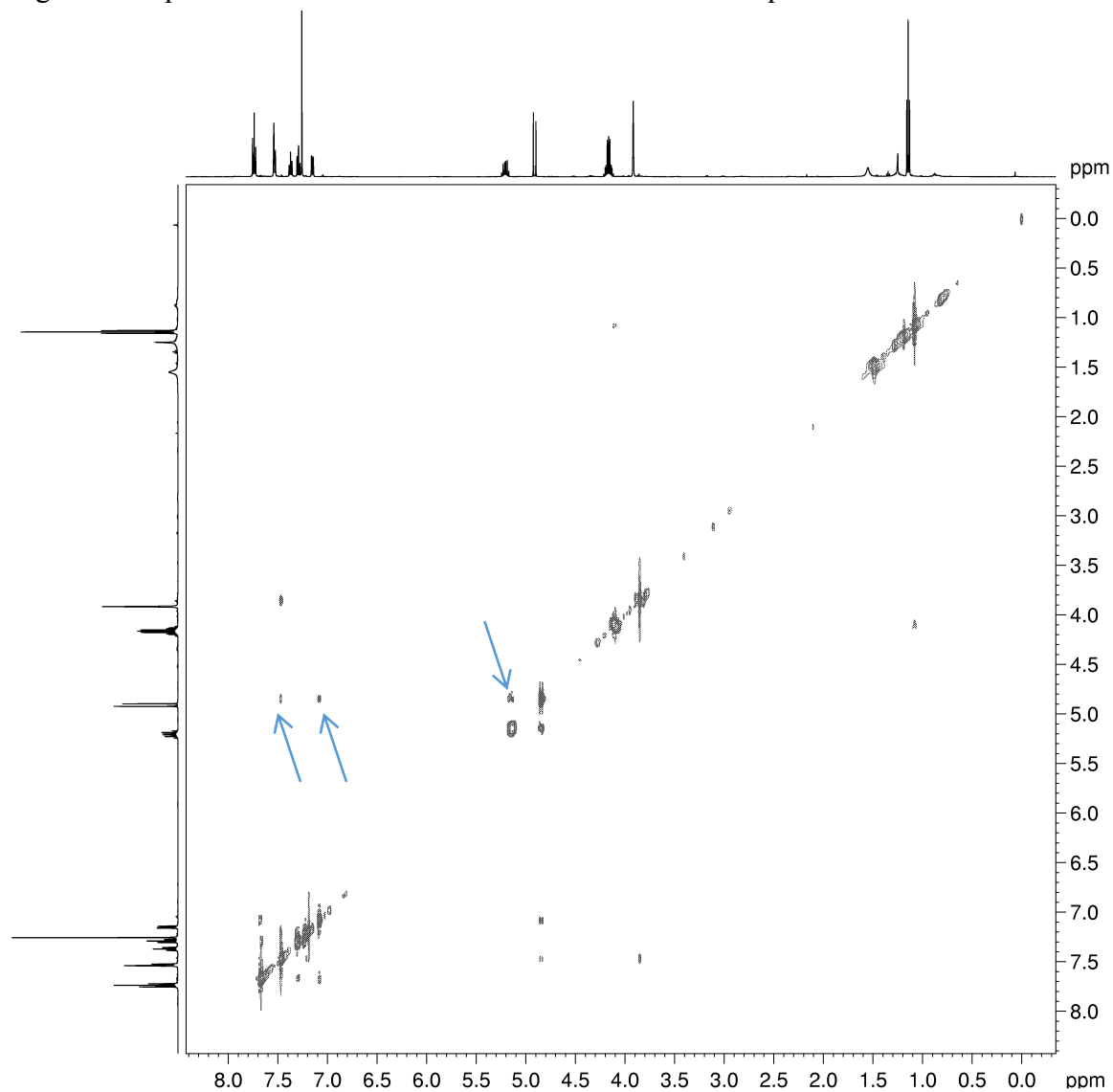
The two blue arrows below shows positive COSY correlation of the two ring protons shown in the structure.



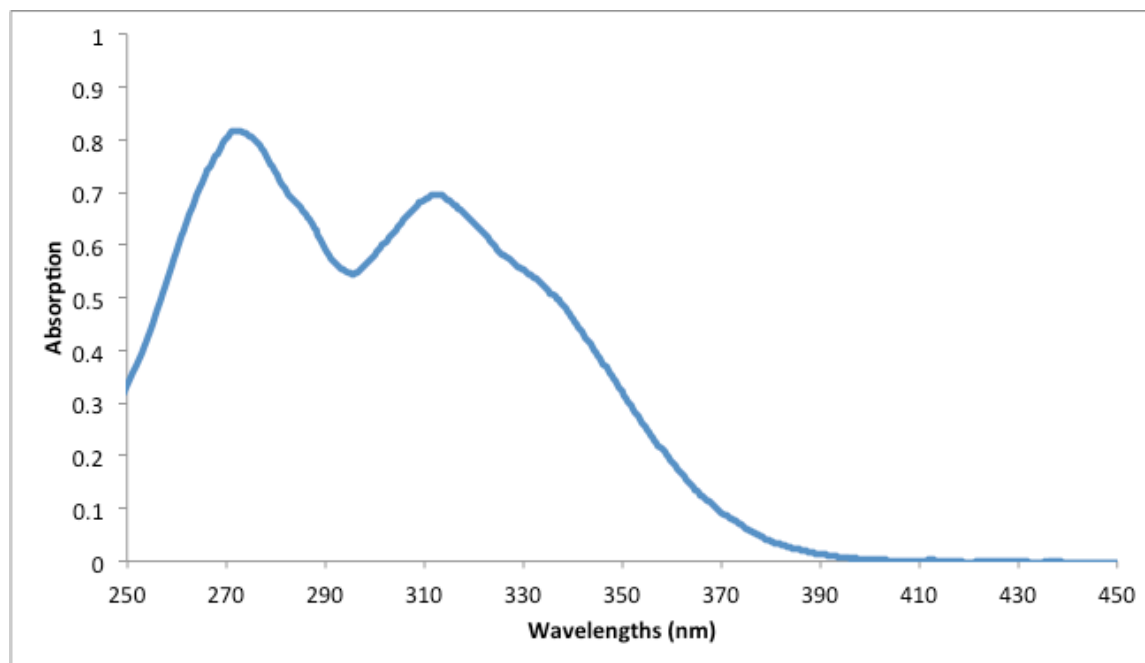
NOESY NMR (CDCl₃, 500 MHz) spectrum of *cis-4*



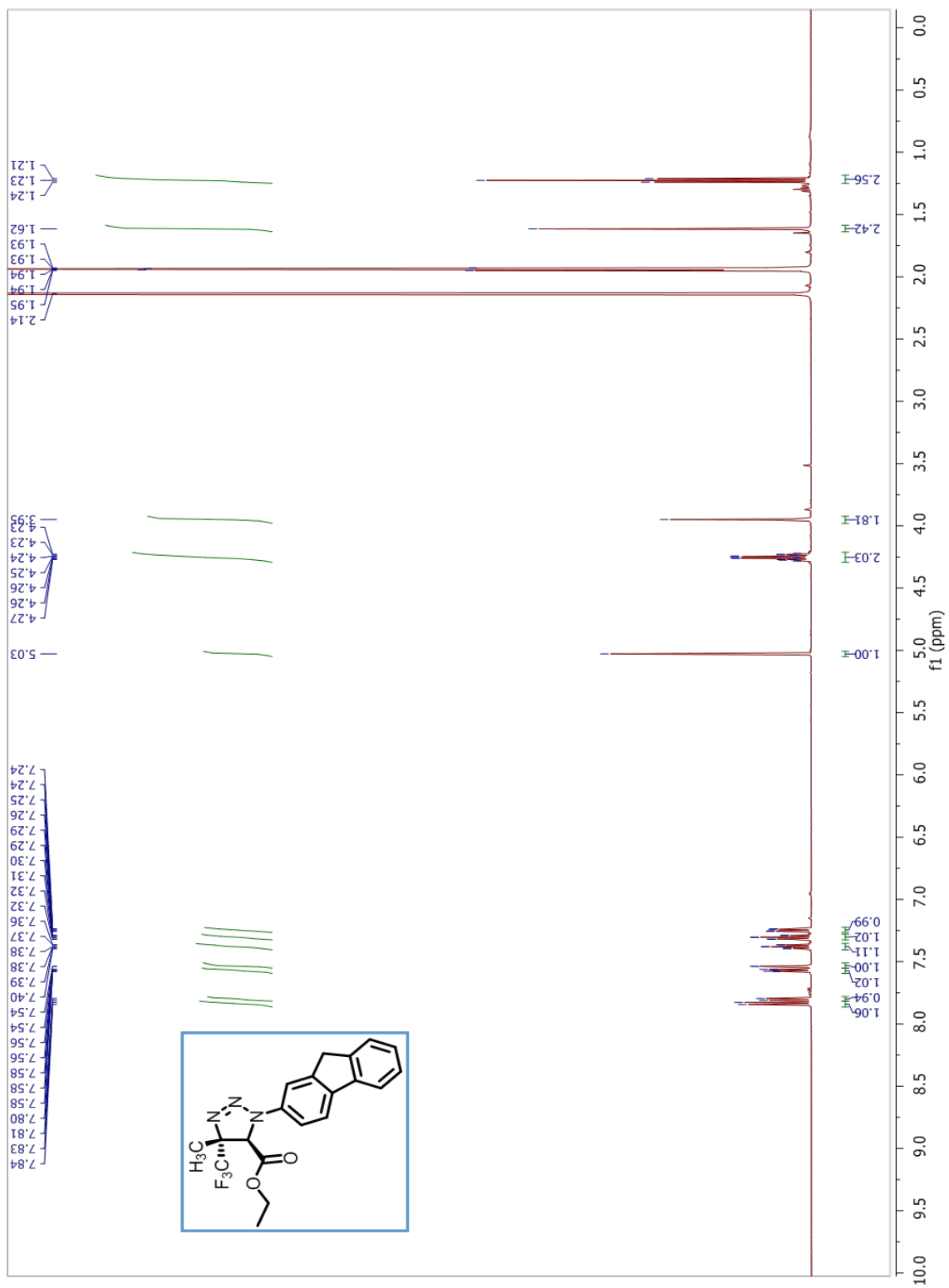
The three blue arrows below shows positive NOESY correlation of the two ring methine protons as well as the correlation to the aromatic protons shown in structure.



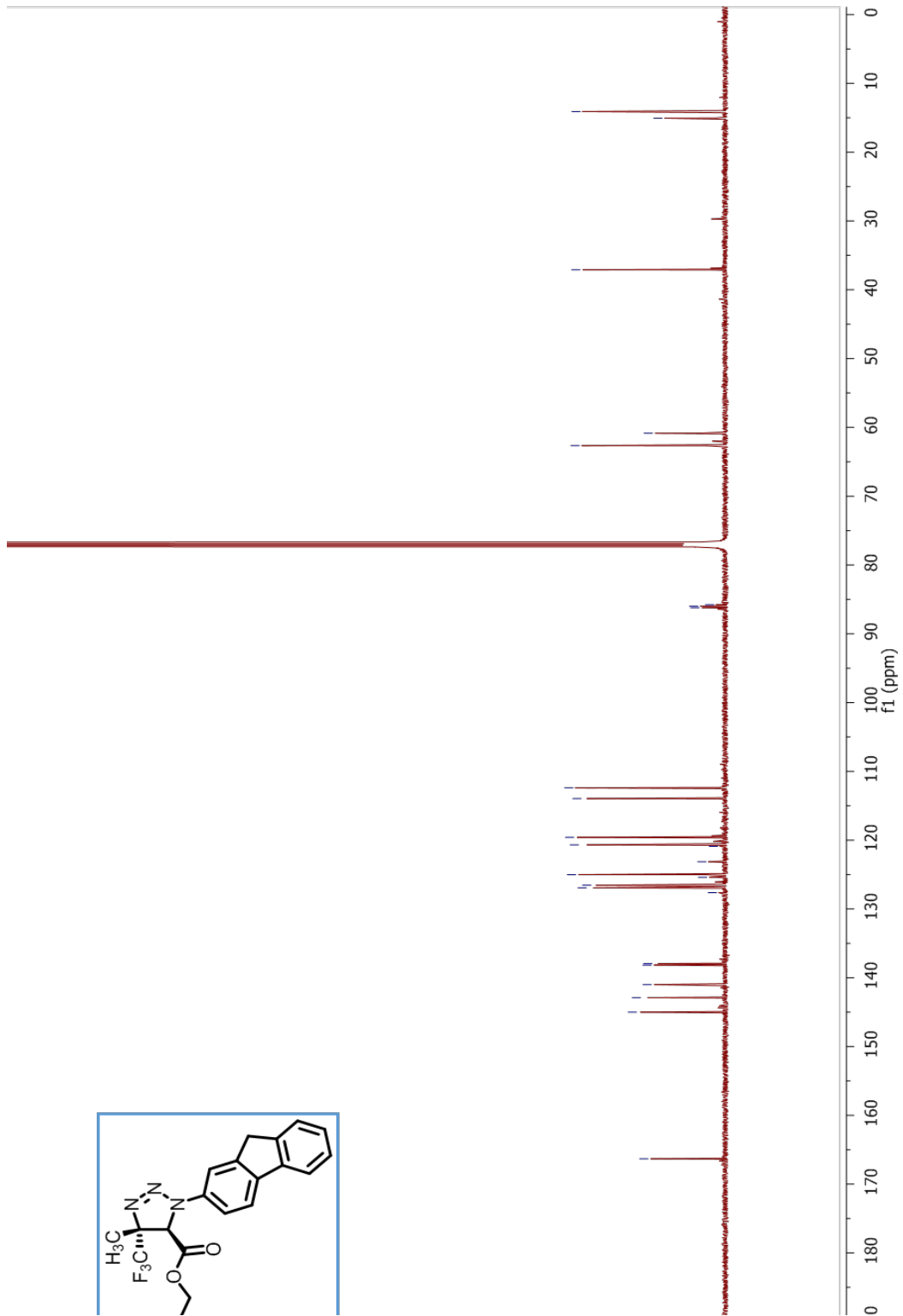
UV-Vis Spectrum of *cis*-4 in dichloromethane.



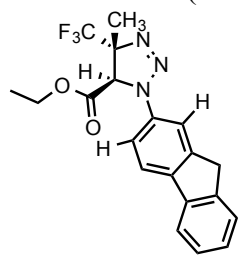
^1H NMR (CD_3CN , 500 MHz) spectrum of *trans*-8



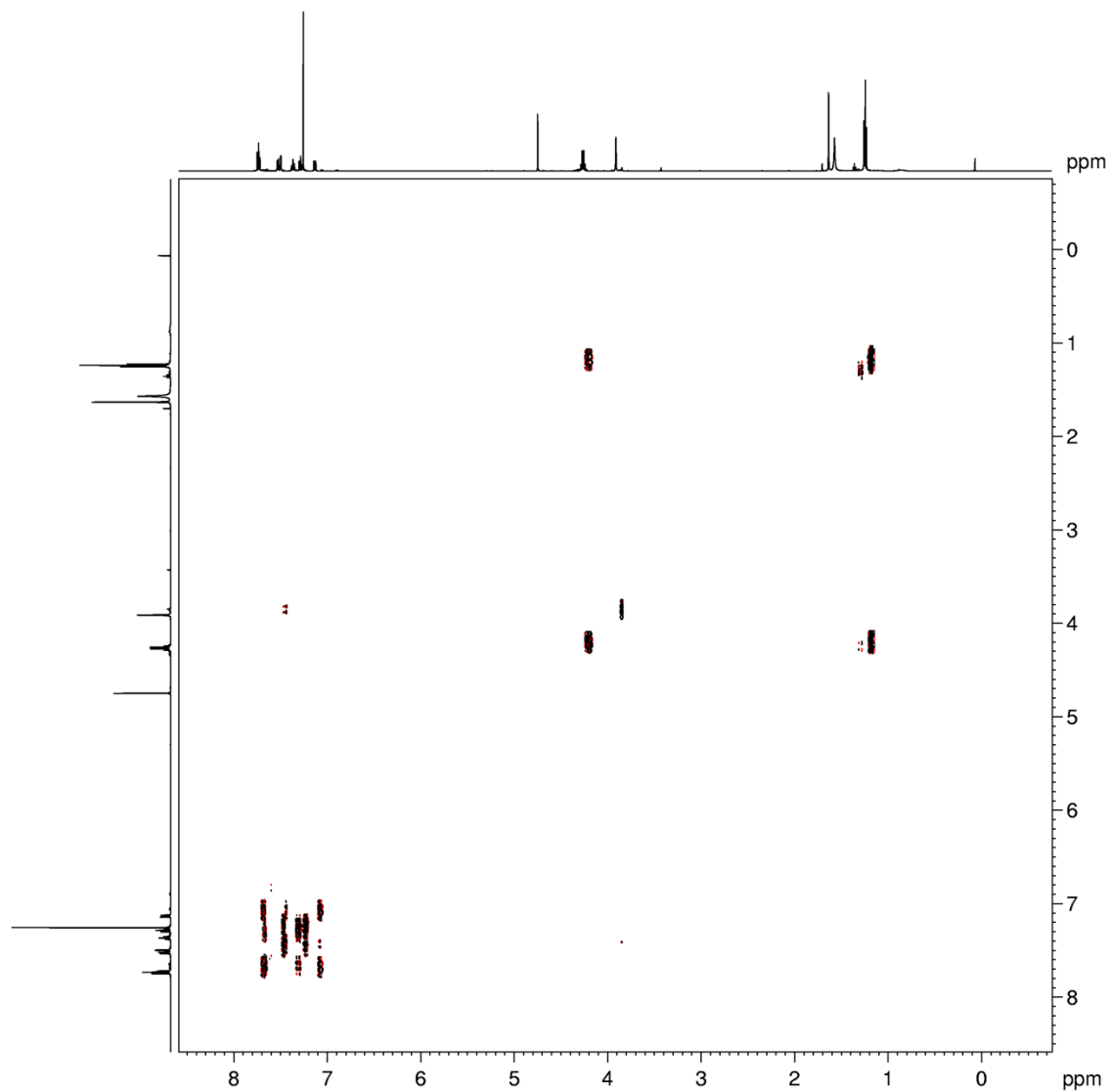
^{13}C NMR (CD_3CN , 125 MHz) spectrum of *trans*-8



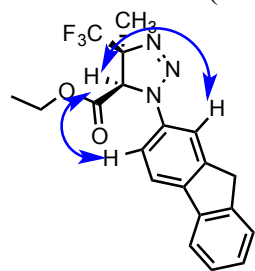
COSY NMR (CDCl₃, 500 MHz) spectrum of *trans*-**8**



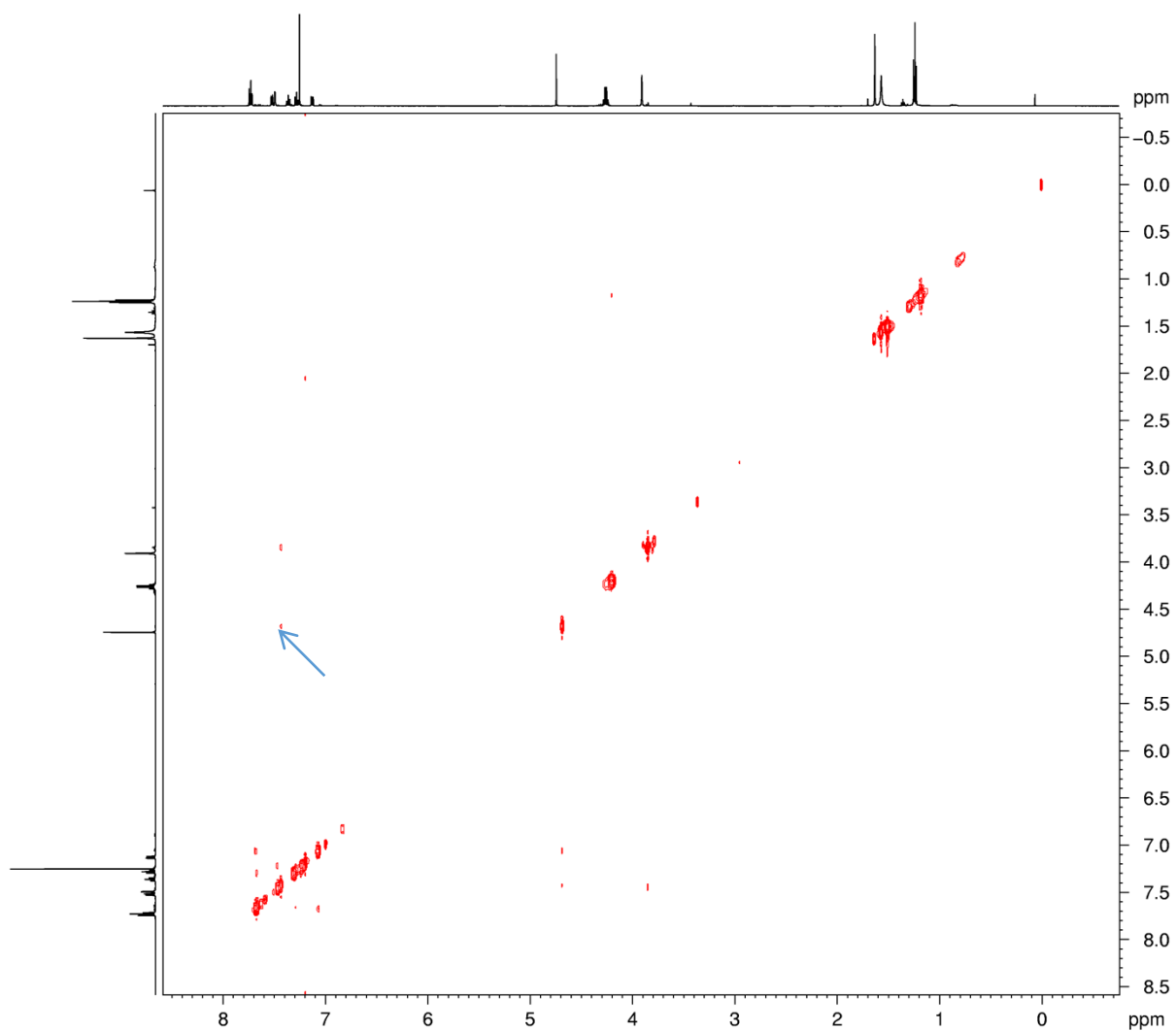
No significant COSY correlation present in this molecule.



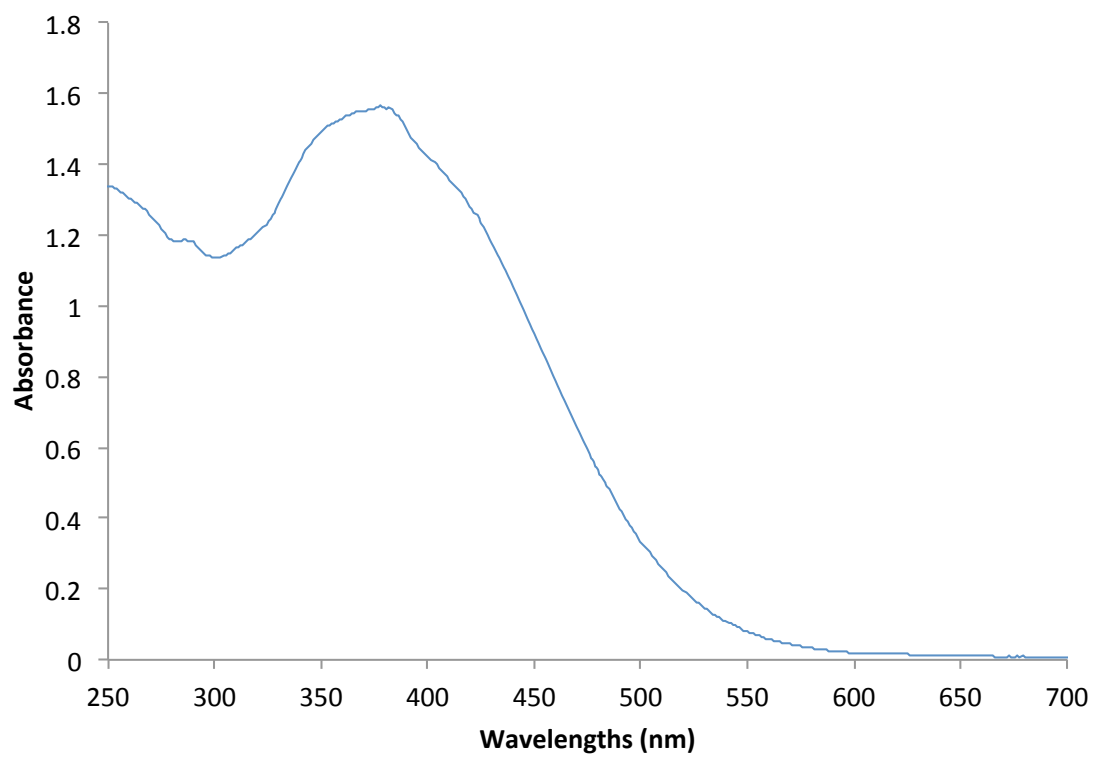
NOESY NMR (CDCl₃, 500 MHz) spectrum of *trans*-**8**



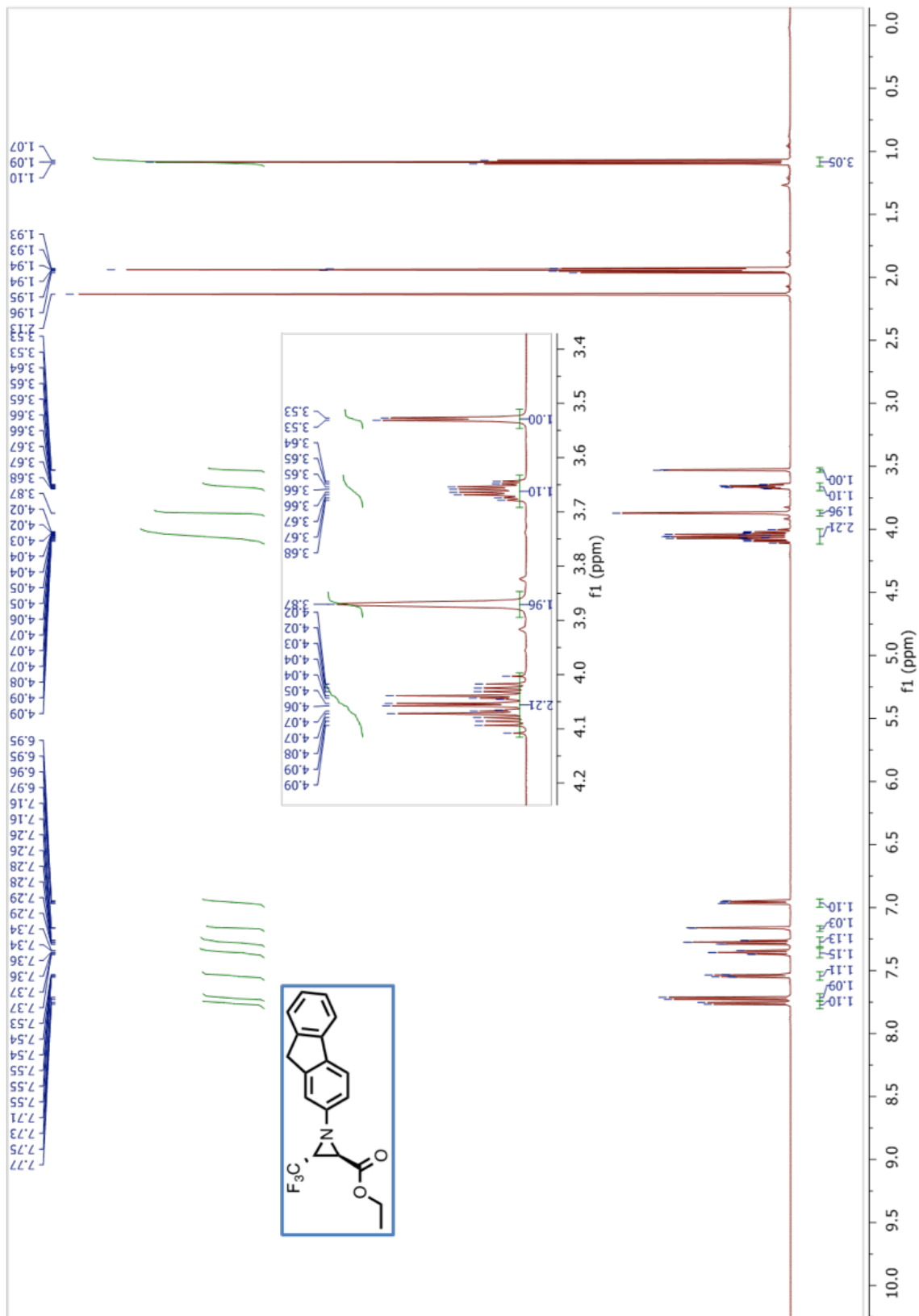
Positive NOESY correlation between methine proton to aromatic protons, indicating regiochemistry of the cycloaddition product as shown in structure.



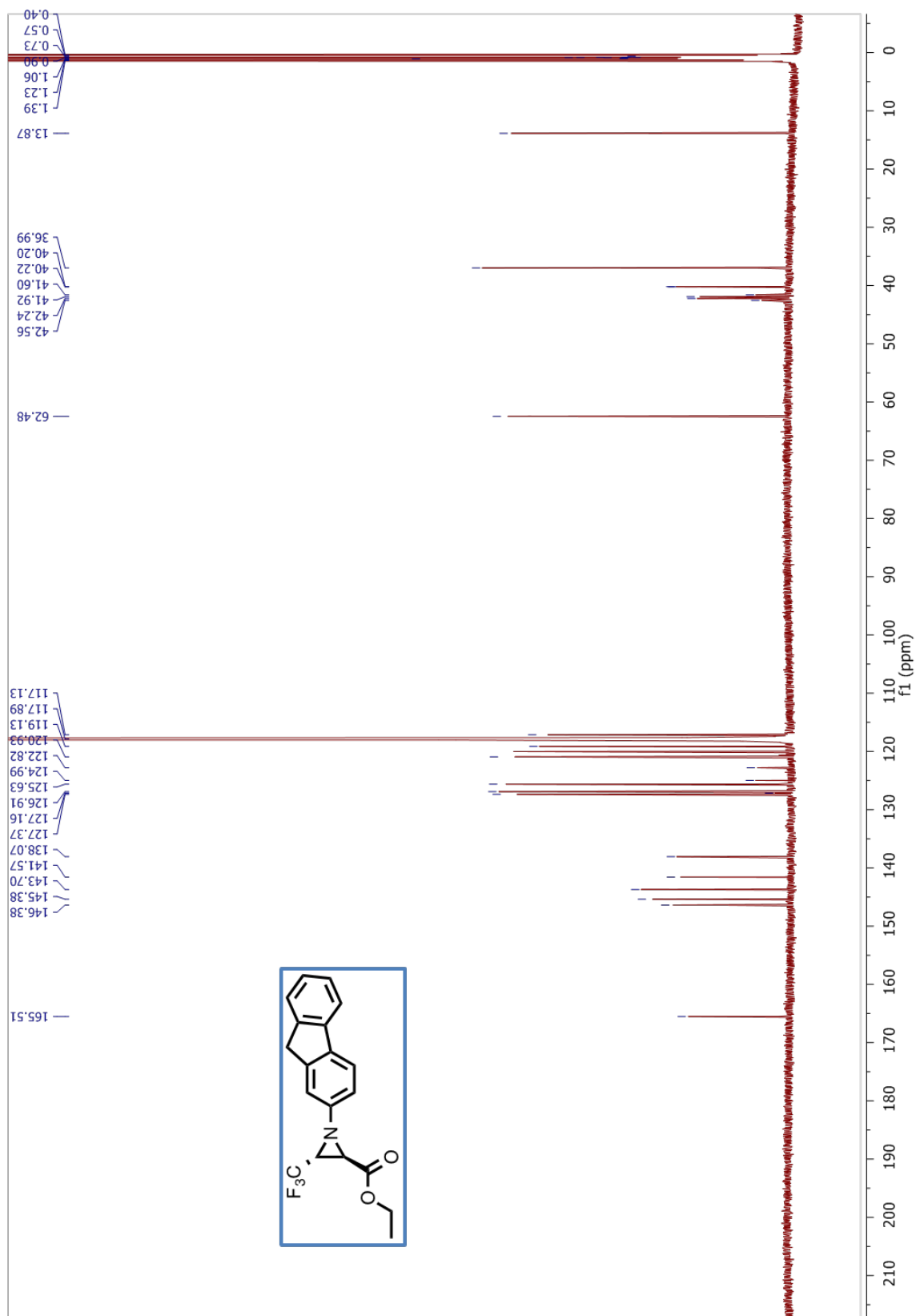
UV-Vis Spectrum of *trans*-**8** in dichloromethane.



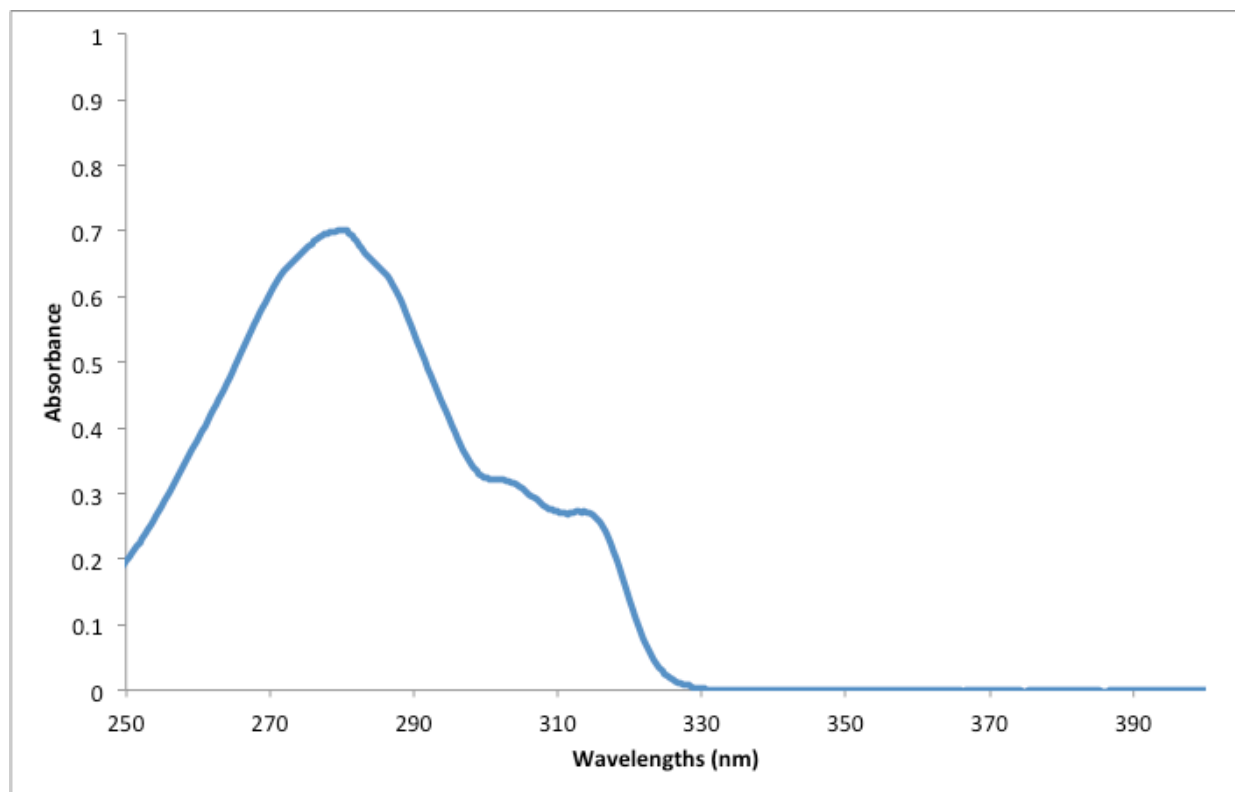
^1H NMR (CD_3CN , 500 MHz) spectrum of *trans*-**5**



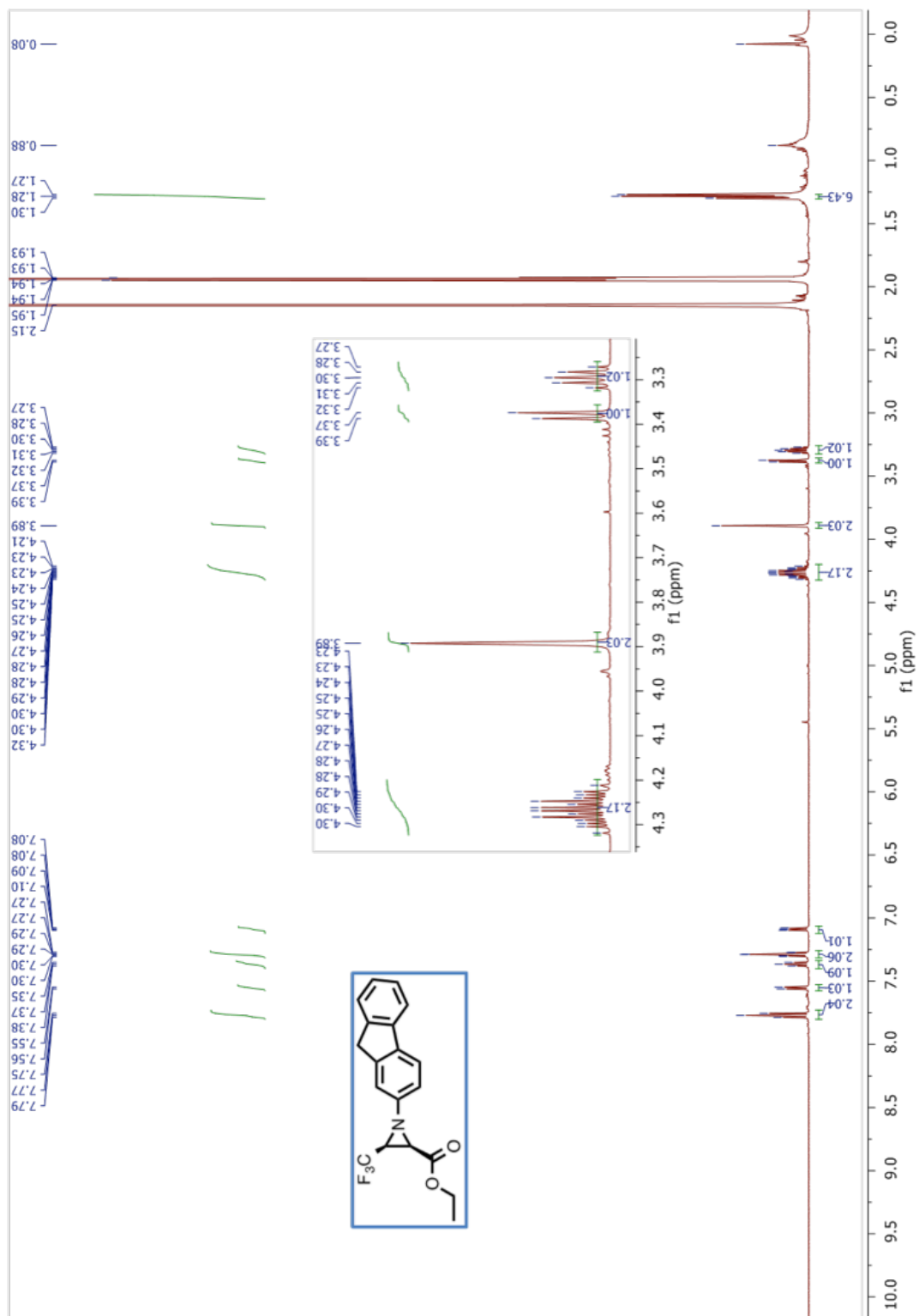
^{13}C NMR (CD_3CN , 125 MHz) spectrum of *trans*-5



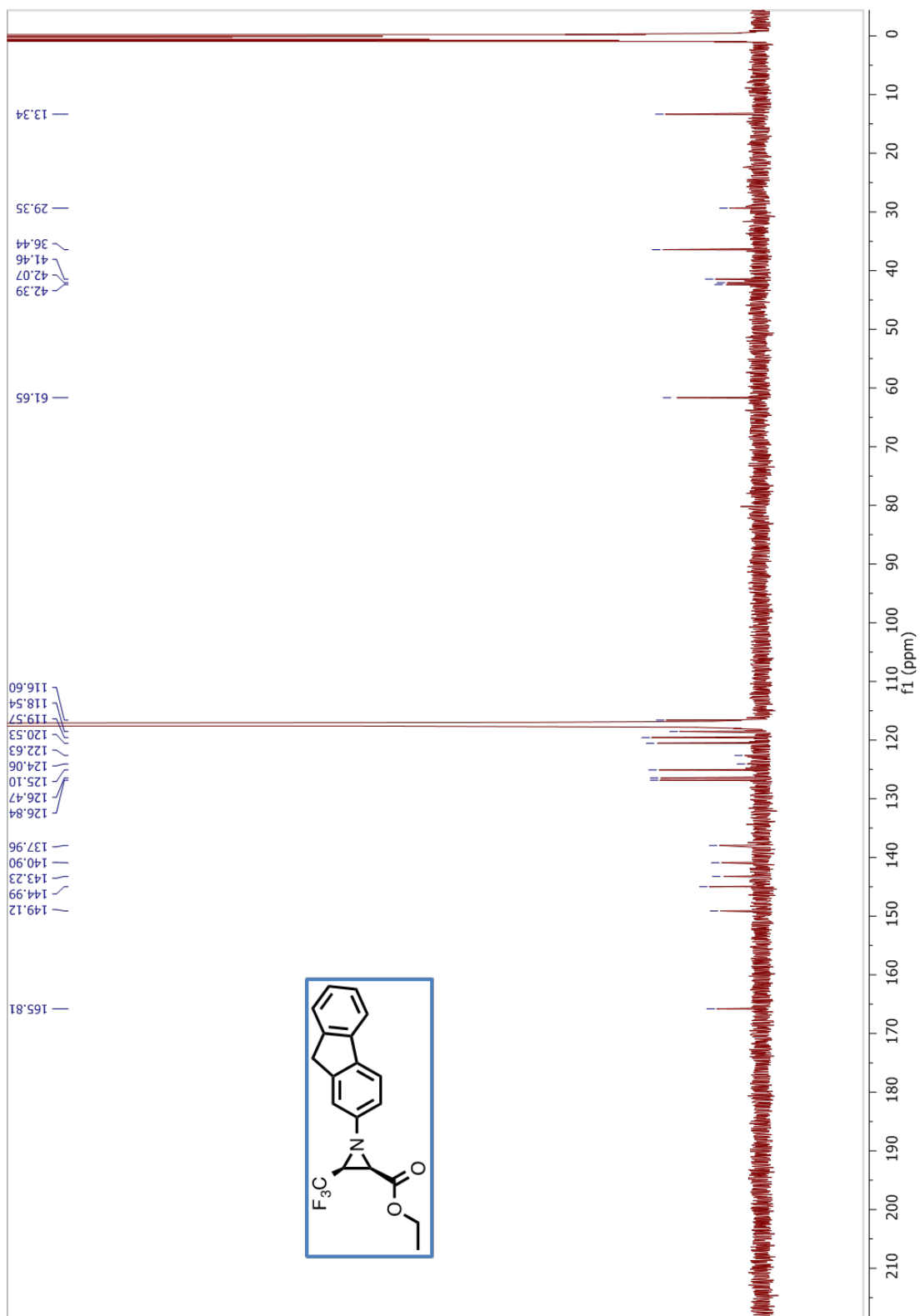
UV-Vis Spectrum of *trans*-5 in dichloromethane.



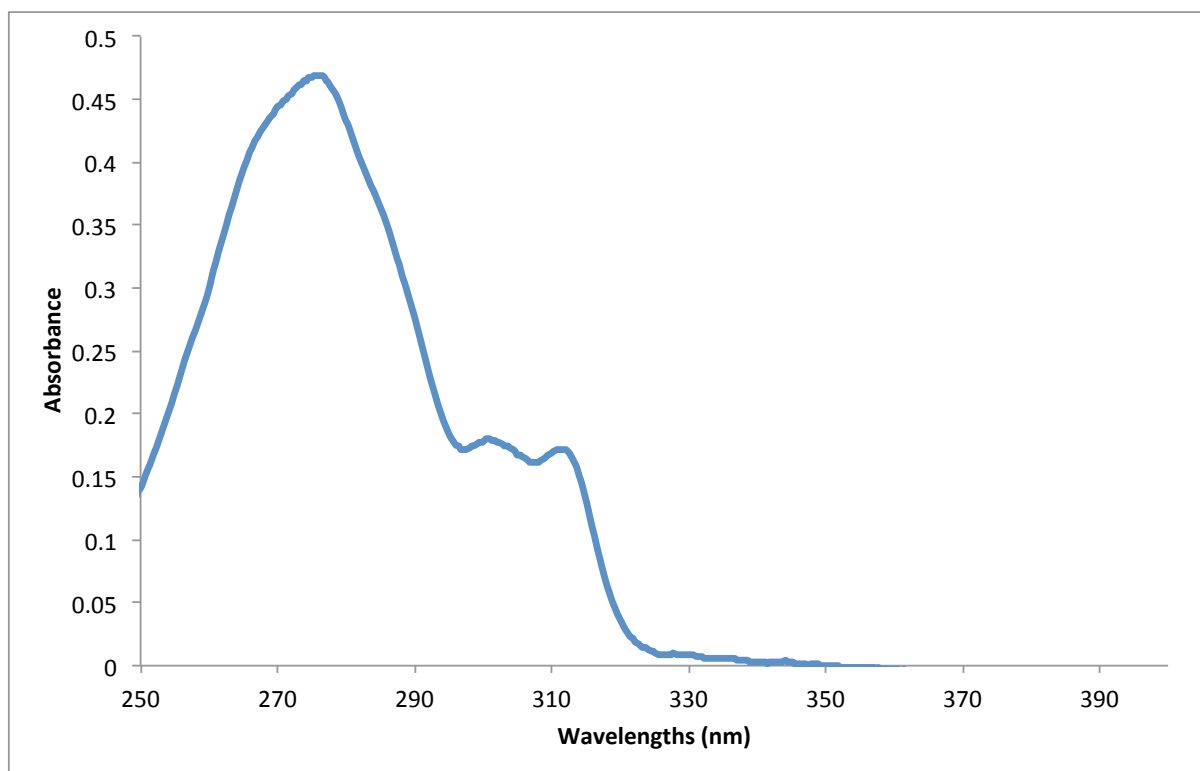
^1H NMR (CD_3CN , 500 MHz) spectrum of *cis*-5



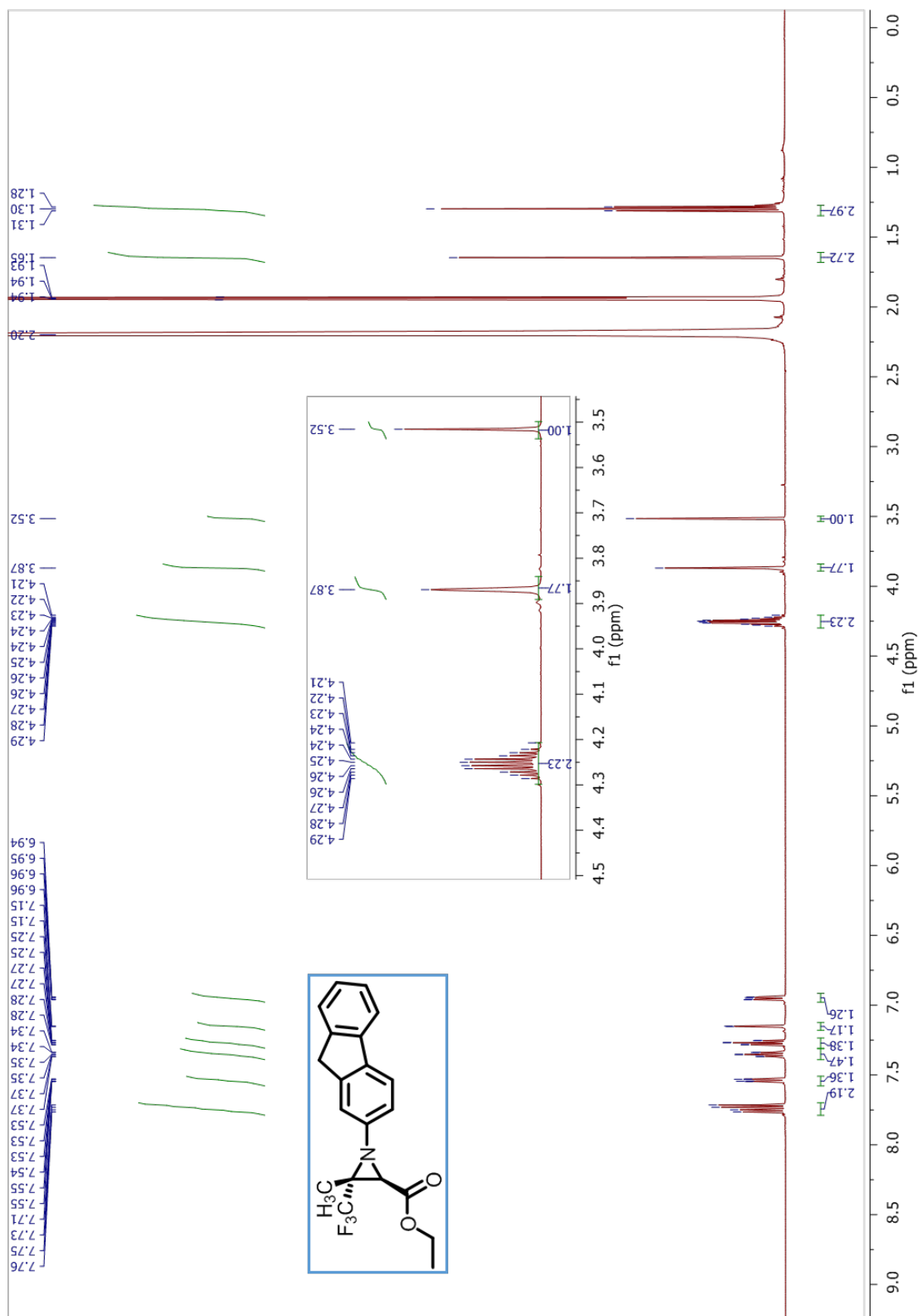
^{13}C NMR (CD_3CN , 125 MHz) spectrum of *cis*-5



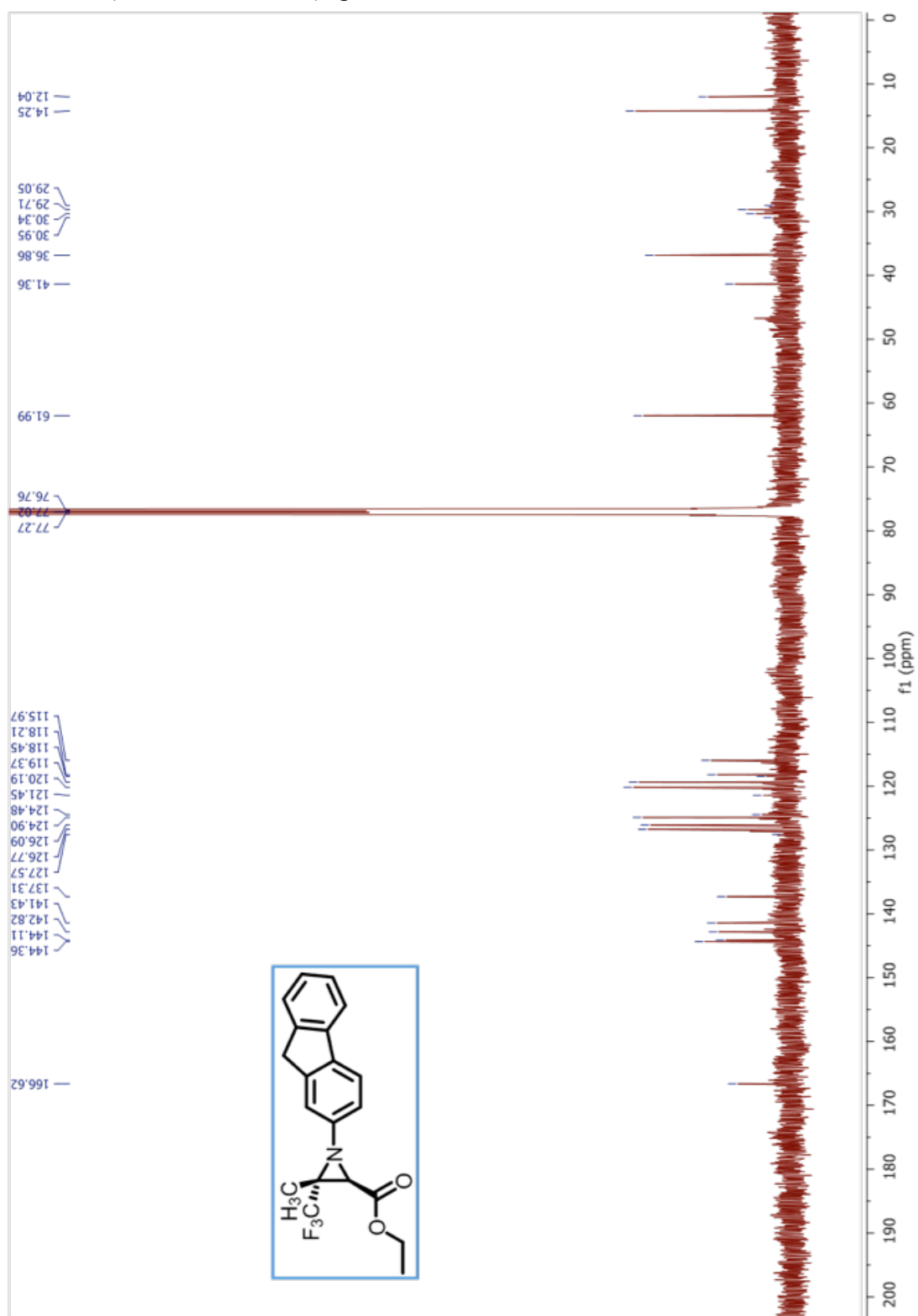
UV-Vis Spectrum of *trans*-**5** in dichloromethane.



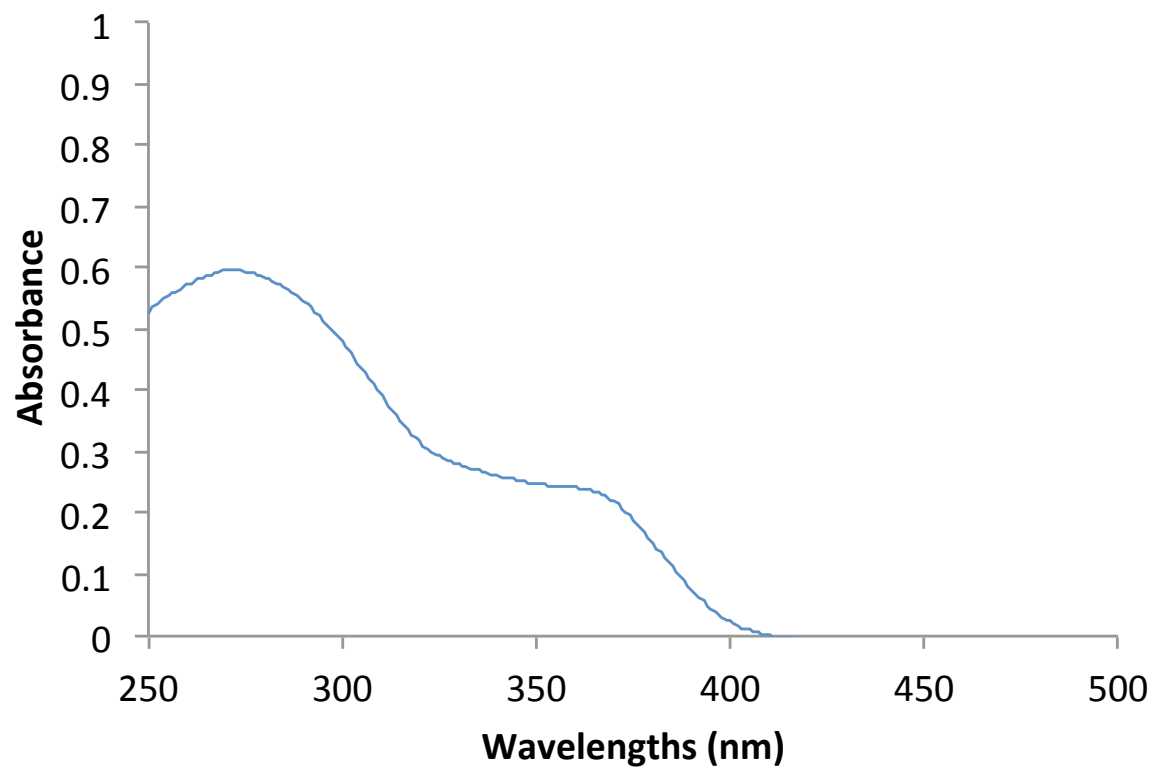
¹H NMR (CD₃CN, 500 MHz) spectrum of *trans*-9



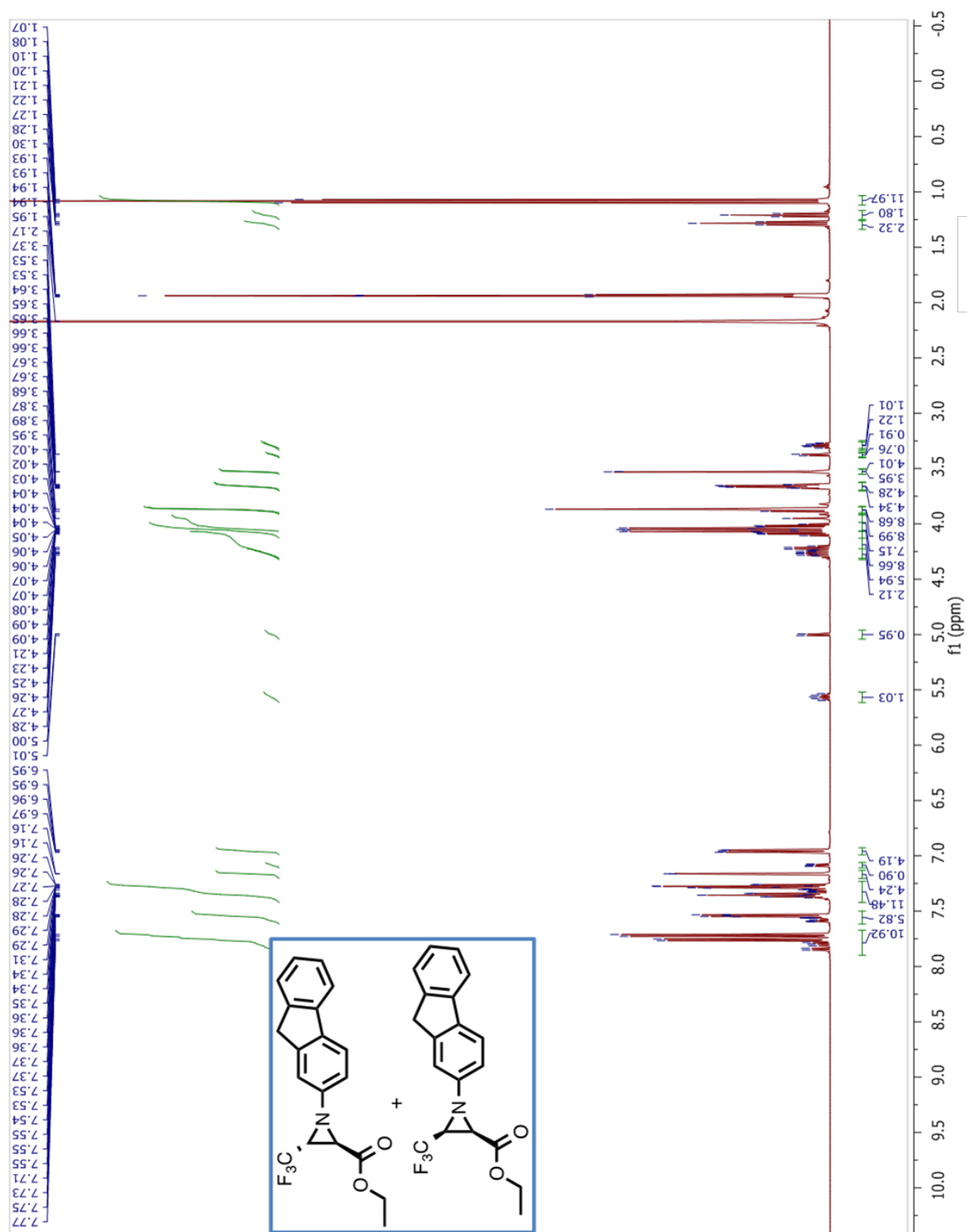
^{13}C NMR (CD_3CN , 125 MHz) spectrum of *trans*-9



UV-Vis Spectrum of *trans*-**9** in dichloromethane.

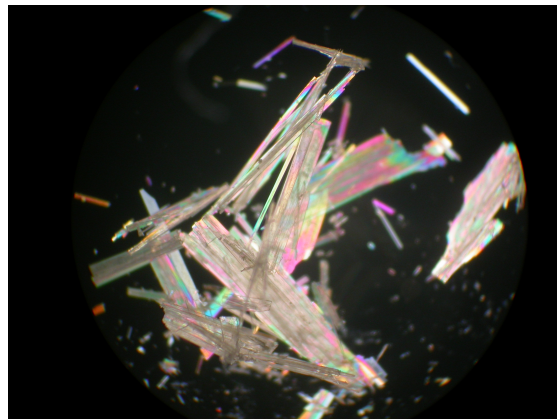
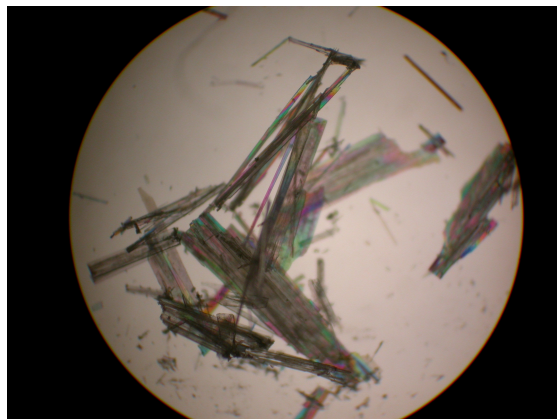


Crude ^1H NMR (CD_3CN , 500 MHz) spectrum of *trans*-4 photolysis.

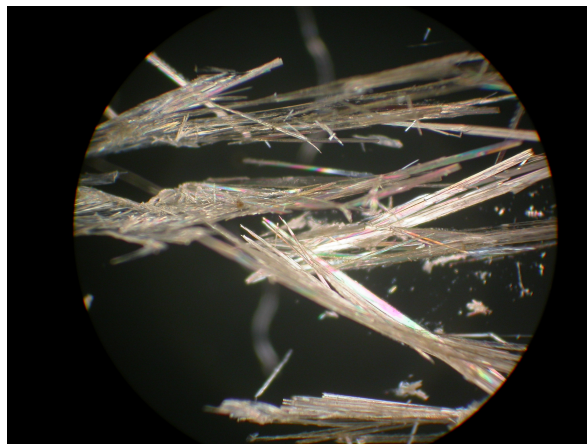


2.5.3 Crystal Pictures

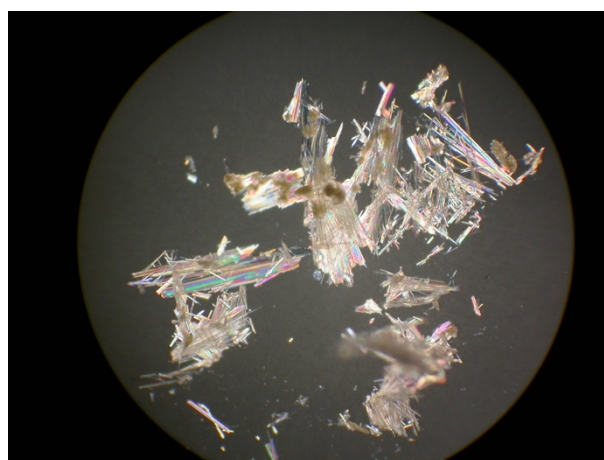
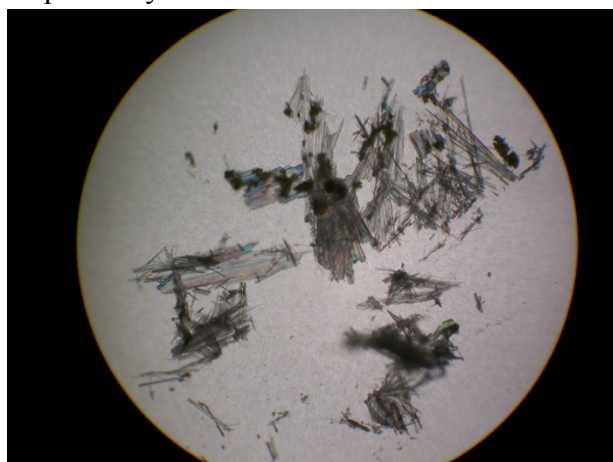
Pictures of Ethyl (4*R*,5*R*)-1-(8*a*,9-dihydro-4*bH*-fluoren-2-yl)-4-(trifluoromethyl) Δ^2 -1,2,3-triazoline-5-carboxylate (compound *trans*-4) under microscope with parallel and cross polarizer, respectively:



Pictures of Ethyl (4*S*,5*R*)-1-(8*a*,9-dihydro-4*bH*-fluoren-2-yl)-4-(trifluoromethyl) Δ^2 -1,2,3-triazoline-5-carboxylate (compound *cis*-4) under microscope with parallel and cross polarizer, respectively:



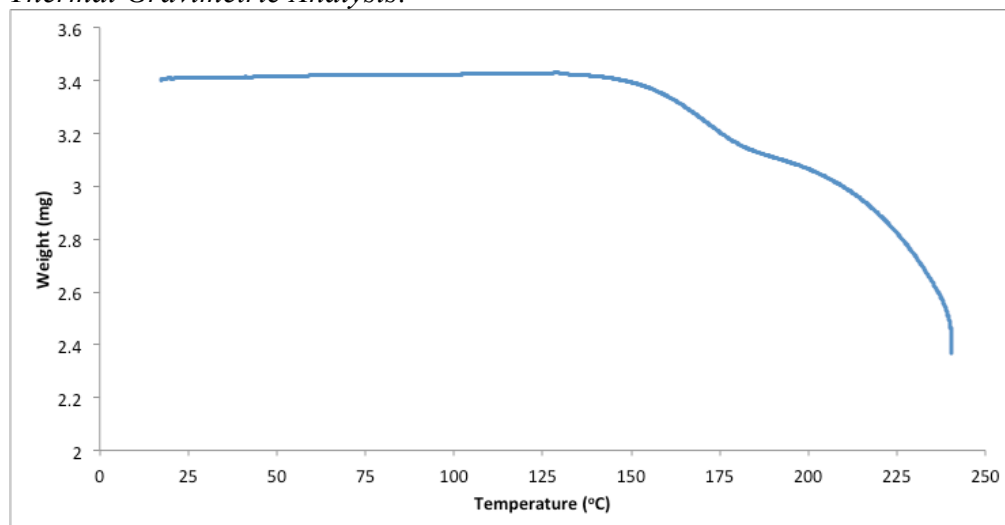
Pictures of Ethyl (4*R*,5*R*)-1-(8*a*,9-dihydro-4*bH*-fluoren-2-yl)-4-methyl-4-(trifluoromethyl) Δ^2 -1,2,3-triazoline-5-carboxylate (*trans*-8) under microscope with parallel and cross polarizer, respectively:



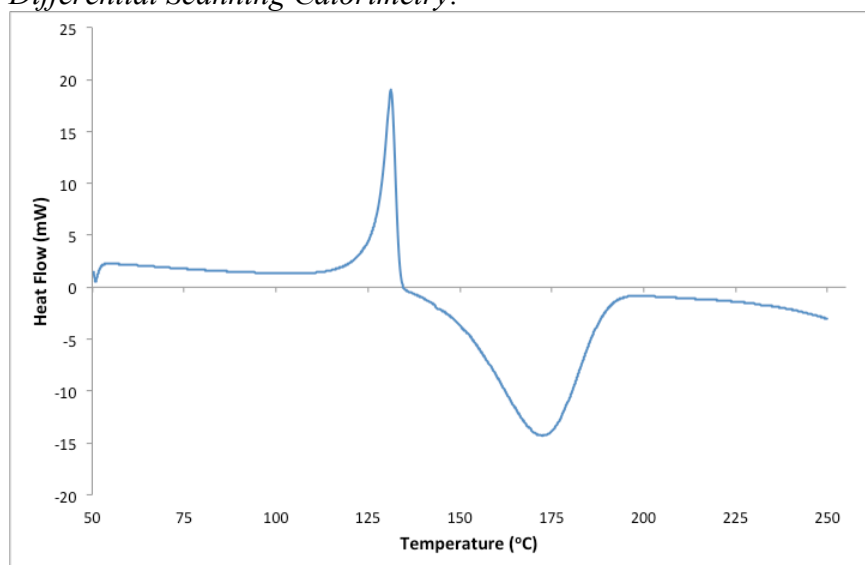
2.5.4 Thermal Analysis

Ethyl (4*R*,5*R*)-1-(8*a*,9-dihydro-4*bH*-fluoren-2-yl)-4-(trifluoromethyl) Δ^2 -1,2,3-triazoline-5-carboxylate (*trans*-4):

Thermal Gravimetric Analysis:

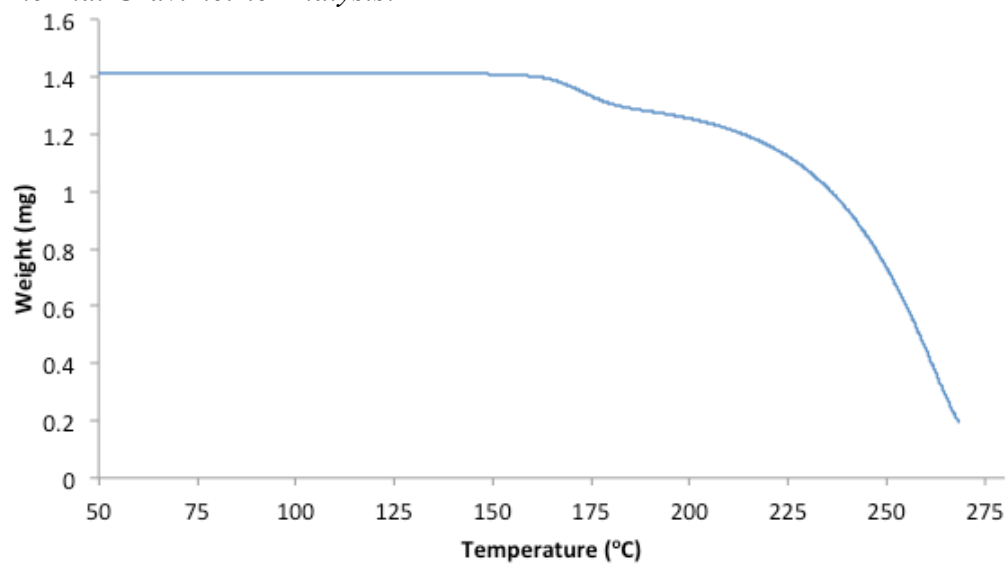


Differential Scanning Calorimetry:

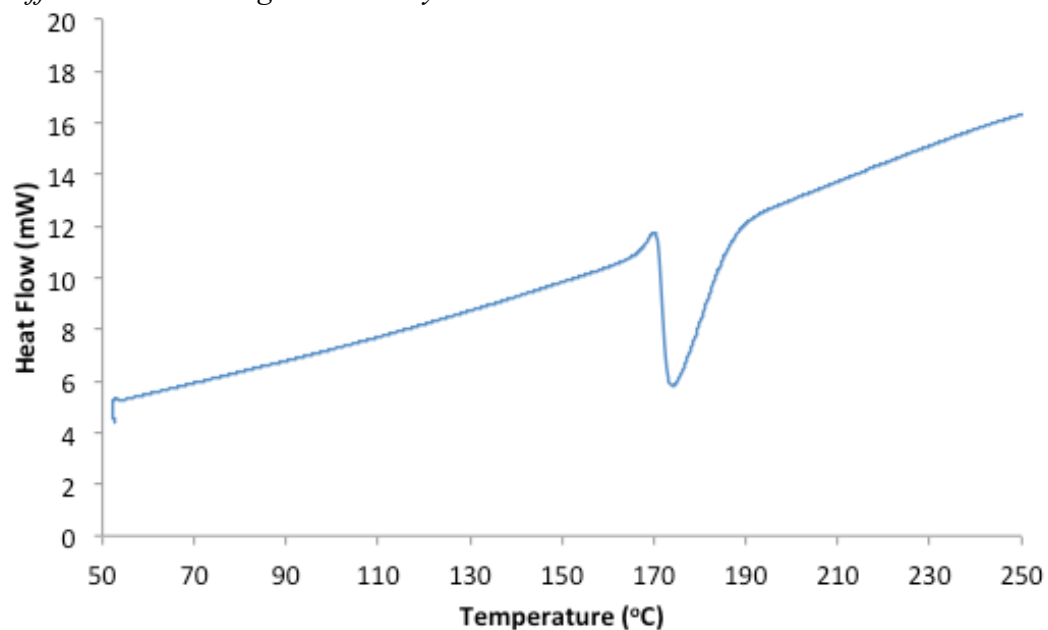


Ethyl (4*S*,5*R*)-1-(8*a*,9-dihydro-4*bH*-fluoren-2-yl)-4-(trifluoromethyl) Δ^2 -1,2,3-triazoline-5-carboxylate (*cis*-4):

Thermal Gravimetric Analysis:

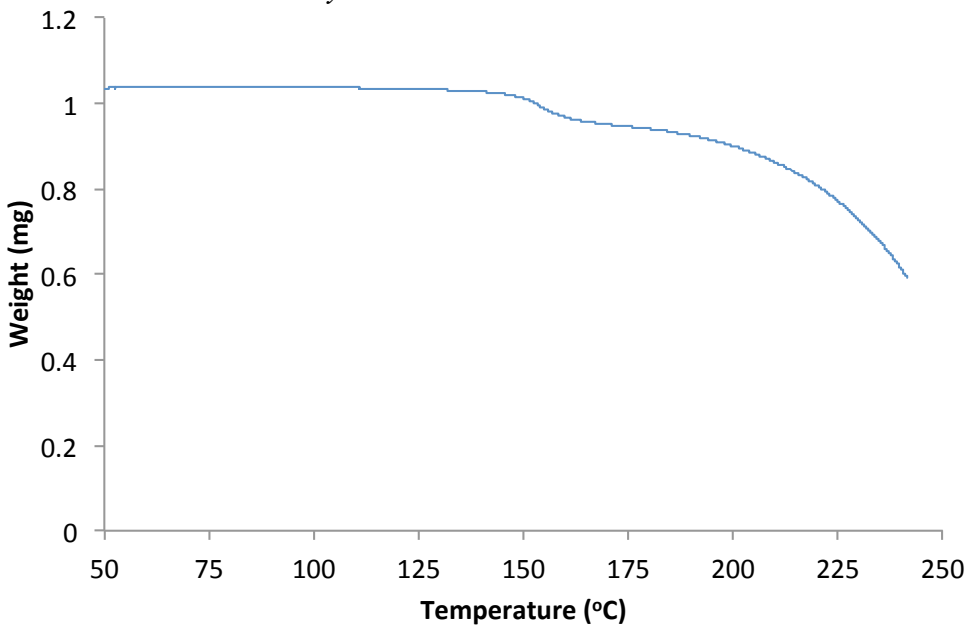


Differential Scanning Calorimetry:

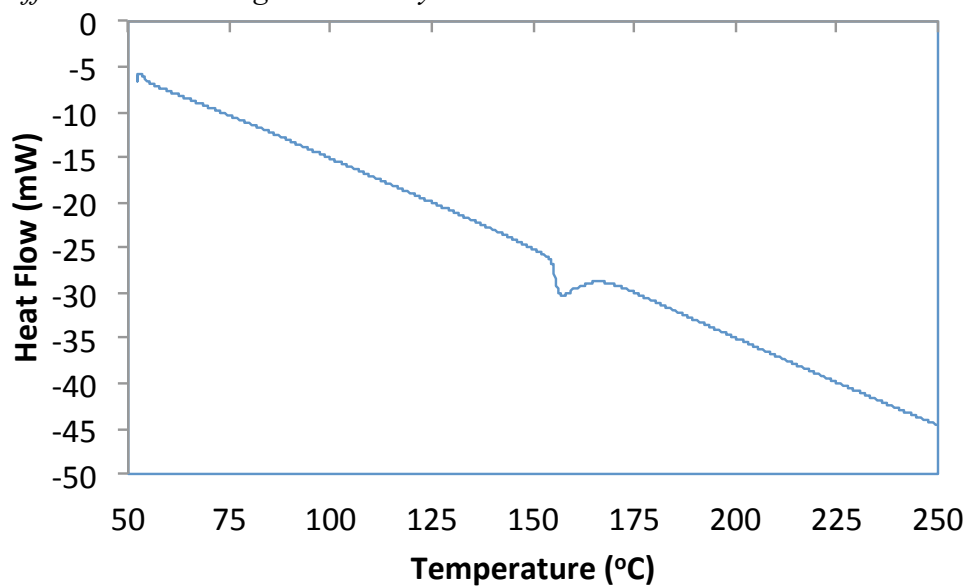


Ethyl (4*R*,5*R*)-1-(8*a*,9-dihydro-4*bH*-fluoren-2-yl)-4-methyl-4-(trifluoromethyl) Δ^2 -1,2,3-triazoline-5-carboxylate (*trans*-**8**):

Thermal Gravimetric Analysis:

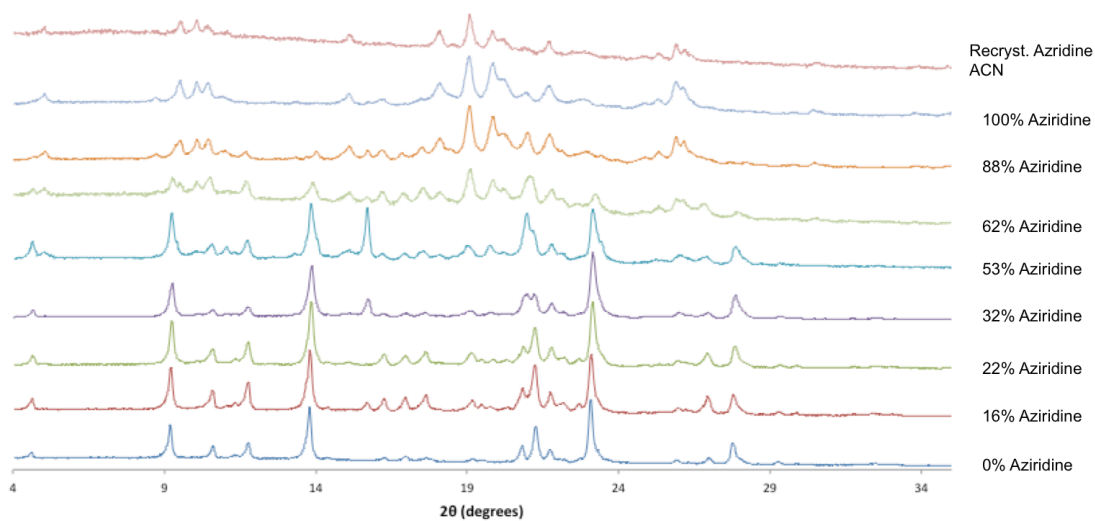
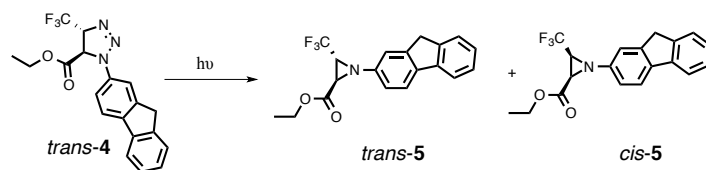


Differential Scanning Calorimetry:

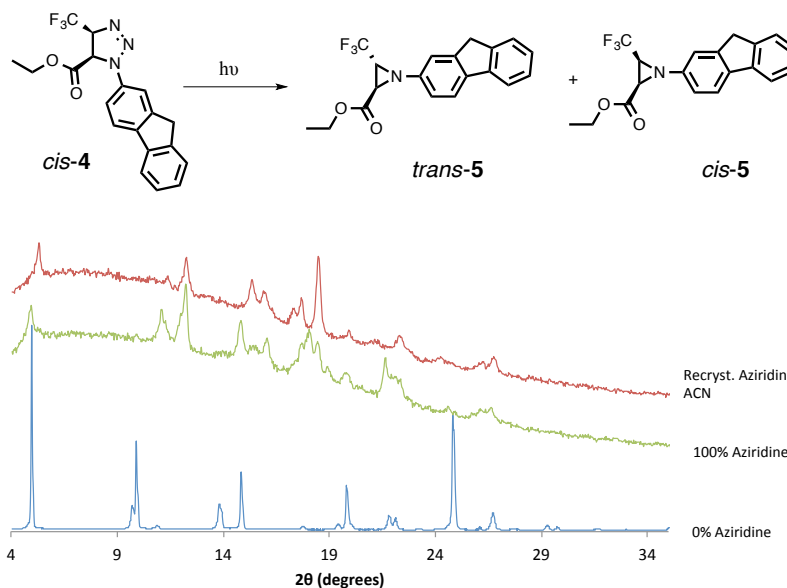


2.5.5 PXRD Analysis

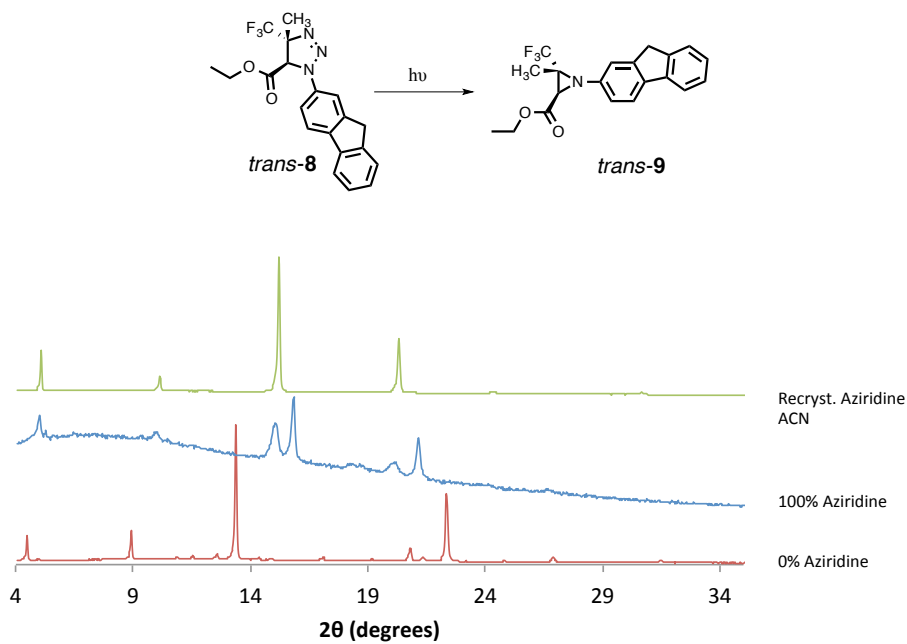
Powder X-Ray Diffraction of triazoline *trans-4* as progression of photo reaction and recrystallized in acetonitrile:



Powder X-Ray Diffraction of triazoline **cis-4** as progression of photo reaction and recrystallized in acetonitrile:



Powder X-Ray Diffraction of triazoline **trans-8** as progression of photo reaction and recrystallized in acetonitrile:



2.5.6 Computational Supplemental Information

We also performed computational analysis using the M06-2X density functional for the uncatalyzed cycloaddition reaction (shown in **Figure S42**). **TS3** and **TS4** are both concerted, but slightly asynchronous. The internal nitrogen–carbon ($N_{\text{int}}\text{-C}$) bonds are shorter than the terminal nitrogen–carbon ($N_{\text{term}}\text{-C}$) bonds. The activation free energies of **TS3** and **TS4** are nearly identical (27.3 and 27.1 kcal mol⁻¹, respectively) but **TS4** is slightly favored. These results suggest a slight inherent preference exists for the experimentally observed product (55:45). We confirmed this computational indifference by experimental evidence (**Figure S43**).

Figure S43: Transition states for the two regioisomers without DMU activation.

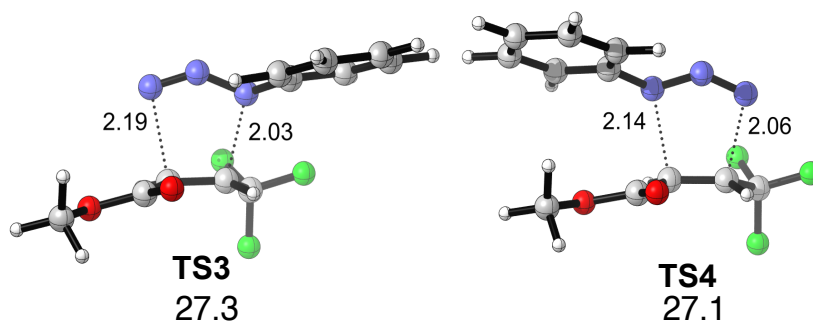
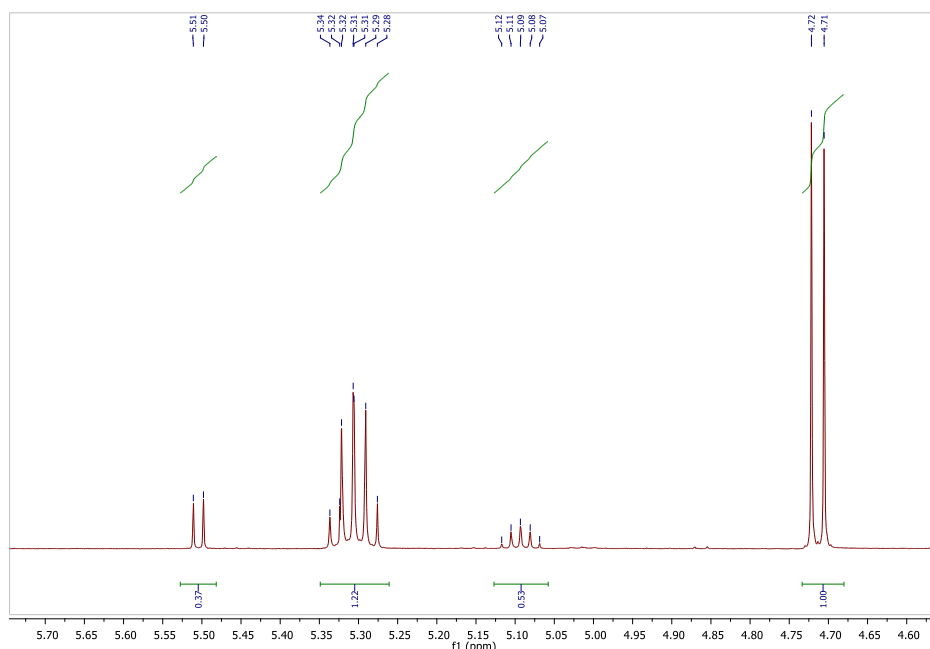


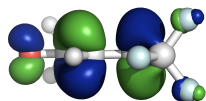
Figure S44: Zoomed NMR spectrum from 4.6 to 5.7 ppm of the cycloaddition reaction without the DMU catalyst. It shows two pentets and two doublets between 4.7 and 5.5 ppm. This data suggests that one may form the two regioisomers of triazoline *trans*-4 without urea coordination. Integration of the peaks indicates that ca. 29% of the unobserved regioisomer can be formed without DMU coordination.



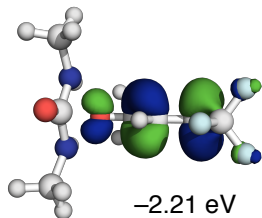
We computed the π^* orbital coefficients of *trans*-3 and *trans*-3 with urea coordination. Surprisingly, they are nearly unchanged (0.71, -0.71 and 0.70, -0.71, respectively).

Figure S45: Computed HOMO of PhN3 and the LUMOs of 1 and DMU-1. Orbital energies are reported in eV and calculated using B3LYP/6-31G(d)/M06-2X/6-31G+(d,p)/IEF-PCMtoluene.

Alkene LUMO

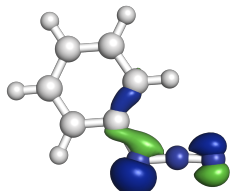


-1.87 eV



-2.21 eV

Azide HOMO



-8.66 eV

PhN₃

Zero-point correction=	0.104593 (Hartree/Particle)		
Thermal correction to Energy=	0.111520		
Thermal correction to Enthalpy=	0.112464		
Thermal correction to Gibbs Free Energy=	0.072733		
Sum of electronic and zero-point Energies=	-395.584855		
Sum of electronic and thermal Energies=	-395.577928		
Sum of electronic and thermal Enthalpies=	-395.576984		
Sum of electronic and thermal Free Energies=	-395.616715		

N	2.39557200	-0.09888800	-0.00000200
N	3.30939700	0.56391400	-0.00000500
N	1.47007800	-0.91695000	0.00000000
C	0.15323800	-0.37772500	0.00000100
C	-0.12533500	0.99177400	-0.00000200
C	-0.88629800	-1.31058900	0.00000300
C	-1.45156800	1.41926800	-0.00000100
C	-2.20511900	-0.87007500	0.00000400
C	-2.49503300	0.49541300	0.00000200
H	-0.64329200	-2.36786100	0.00000500
H	-3.01033400	-1.59769600	0.00000700
H	-3.52493800	0.83586700	0.00000200
H	-1.66565700	2.48327300	-0.00000300
H	0.67958300	1.72149800	-0.00000400

1

Zero-point correction=	0.102034 (Hartree/Particle)		
Thermal correction to Energy=	0.111970		
Thermal correction to Enthalpy=	0.112914		
Thermal correction to Gibbs Free Energy=	0.065078		
Sum of electronic and zero-point Energies=	-643.203364		
Sum of electronic and thermal Energies=	-643.193428		

Sum of electronic and thermal Enthalpies= -643.192484
 Sum of electronic and thermal Free Energies= -643.240319

C	0.53987200	-0.31452200	-0.00000100
H	0.21062800	-1.34885700	-0.00001700
C	-0.31021700	0.70695300	0.00001300
H	0.02494000	1.73869800	0.00002700
C	-1.78883200	0.52767400	0.00000400
O	-2.56296900	1.45771400	-0.00001100
O	-2.16167800	-0.75490500	0.00001200
C	-3.57648000	-0.98670500	-0.00000400
H	-3.69521700	-2.06772200	0.00001400
H	-4.02704700	-0.54664300	0.89115300
H	-4.02702000	-0.54667600	-0.89119100
C	2.02356400	-0.11483800	-0.00000100
F	2.58682400	-0.68644400	-1.08032800
F	2.58683600	-0.68650200	1.08028900
F	2.38005600	1.17709700	0.00003200

1

Zero-point correction= 0.223968 (Hartree/Particle)
 Thermal correction to Energy= 0.243615
 Thermal correction to Enthalpy= 0.244559
 Thermal correction to Gibbs Free Energy= 0.170666
 Sum of electronic and zero-point Energies= -946.861684
 Sum of electronic and thermal Energies= -946.842037
 Sum of electronic and thermal Enthalpies= -946.841093
 Sum of electronic and thermal Free Energies= -946.914986

C	-0.93055700	0.35063400	0.05363700
C	-2.18612200	-0.08107000	-0.01338400
H	-3.03630100	0.59157000	-0.07022000
C	-2.52491100	-1.54043600	-0.01788100
H	-0.08074300	-0.32403100	0.10926200
F	-1.44949800	-2.32957800	0.08226600
F	-3.17101500	-1.87819000	-1.14917700
F	-3.34603300	-1.84282500	1.00468200
C	-0.58782700	1.79822900	0.05499900
O	0.55949900	2.20510400	0.09338800
O	-1.64551300	2.59973100	0.01008700
C	-1.36834400	4.00855900	0.00684100
H	-2.34019700	4.49458900	-0.02932600
H	-0.82898000	4.28328000	0.91444000

H	-0.77062100	4.26771700	-0.86821700
C	2.76595100	-0.61687500	-0.02122300
N	2.32127000	0.02020400	-1.15285000
H	1.94861600	0.95499600	-1.05002600
C	2.84611900	-0.38035900	-2.44524900
H	3.91120400	-0.14571100	-2.55201800
H	2.71892300	-1.45605500	-2.57330000
H	2.28496500	0.13795700	-3.22376400
N	2.33249400	-0.06968600	1.16183900
H	1.96414700	0.87243100	1.13438700
C	2.88139000	-0.56256400	2.41192900
H	2.77626900	-1.64733700	2.45186600
H	3.94322300	-0.31641400	2.52585500
H	2.32038200	-0.12100000	3.23651700
O	3.45319900	-1.63570900	-0.06426700

TS1

Zero-point correction=	0.207802 (Hartree/Particle)
Thermal correction to Energy=	0.225021
Thermal correction to Enthalpy=	0.225965
Thermal correction to Gibbs Free Energy=	0.160326
Sum of electronic and zero-point Energies=	-1038.761437
Sum of electronic and thermal Energies=	-1038.744218
Sum of electronic and thermal Enthalpies=	-1038.743273
Sum of electronic and thermal Free Energies=	-1038.808912

C	-1.93152200	0.57108800	-0.49816700
C	-0.89829000	0.68265500	0.41732800
H	-1.00341200	0.29884200	1.42543700
N	-0.19793500	-1.17147300	-1.23304000
N	-1.18163600	-0.94437700	-1.80212900
N	0.36978300	-0.86160000	-0.14874700
C	1.78959700	-0.85704100	-0.05983400
C	2.60715300	-0.63547900	-1.17053800
C	2.33940200	-1.03227500	1.20963000
C	3.98821200	-0.60674800	-1.00184300
C	3.72067900	-0.98076900	1.36938800
C	4.54777600	-0.77310500	0.26547100
C	0.04537100	1.84187800	0.26415000
H	-2.03024600	1.28369600	-1.30910800
H	2.16357700	-0.49023700	-2.15115300
H	4.62790200	-0.44428400	-1.86313000
H	5.62488900	-0.74176400	0.39141100
H	4.15143700	-1.11241200	2.35644200
H	1.67976500	-1.20137400	2.05479900
F	0.50911800	1.94497400	-0.99500900

F	1.10396800	1.74762300	1.08192900
F	-0.56194200	3.01031800	0.55106500
C	-3.17158900	-0.16806300	-0.16689500
O	-4.22439900	-0.02437500	-0.74688800
O	-2.98970500	-1.03979900	0.83806900
C	-4.14347900	-1.80466500	1.20534300
H	-3.81947800	-2.45266600	2.01688100
H	-4.94467500	-1.14147700	1.53631100
H	-4.48856000	-2.39386900	0.35402300

TS2

Zero-point correction=	0.208069 (Hartree/Particle)
Thermal correction to Energy=	0.225034
Thermal correction to Enthalpy=	0.225978
Thermal correction to Gibbs Free Energy=	0.161812
Sum of electronic and zero-point Energies=	-1038.764969
Sum of electronic and thermal Energies=	-1038.748004
Sum of electronic and thermal Enthalpies=	-1038.747060
Sum of electronic and thermal Free Energies=	-1038.811226

C	-1.94425500	0.29614900	-0.39129800
C	-0.97507900	0.63281500	0.54123600
H	-1.18062900	0.55199700	1.60285600
N	-0.38201800	-1.70127400	-0.42743700
N	-1.36955100	-1.58074900	-1.02599700
N	0.25509000	-1.11233800	0.49341500
C	1.65999600	-0.96250700	0.35160000
C	2.34072400	-1.25935200	-0.83477500
C	2.33847800	-0.42678900	1.44756600
C	3.71013100	-1.02816500	-0.90912900
C	3.70516700	-0.17874800	1.35129200
C	4.39509300	-0.48166800	0.17811800
H	-1.92308000	0.72833800	-1.38571600
H	1.80245100	-1.67411400	-1.68178100
H	4.24277400	-1.27053000	-1.82305200
H	5.46203500	-0.29710100	0.11094100
H	4.23054700	0.24732700	2.19936900
H	1.78719900	-0.19561200	2.35311100
C	0.14195700	1.54872500	0.20190300
O	0.72287800	2.23091900	1.01569000
O	0.47146600	1.48607400	-1.09431500
C	1.65046900	2.21474600	-1.46141100
H	1.78759900	2.03212200	-2.52512900
H	1.51391600	3.27911700	-1.26381700
H	2.50494700	1.83948700	-0.89125000
C	-3.30529900	-0.09219600	0.09884200

F	-4.02087200	0.98104700	0.49747300
F	-4.02975700	-0.70120400	-0.85205000
F	-3.23953300	-0.92367900	1.15568100

TS3

Zero-point correction=			0.329999 (Hartree/Particle)
Thermal correction to Energy=			0.356700
Thermal correction to Enthalpy=			0.357644
Thermal correction to Gibbs Free Energy=			0.268513
Sum of electronic and zero-point Energies=			-1342.422630
Sum of electronic and thermal Energies=			-1342.395929
Sum of electronic and thermal Enthalpies=			-1342.394985
Sum of electronic and thermal Free Energies=			-1342.484116
C	-1.17778360	-0.84134614	-0.01541803
C	-2.44369360	-0.69667714	0.52789697
H	-2.86033060	0.28635386	0.71596997
N	-2.79700060	-1.41873614	-1.92212303
N	-1.64405060	-1.46578314	-2.02127403
N	-3.67327060	-1.03637214	-1.09895003
C	-4.95201960	-1.66207014	-1.06584903
C	-5.13671760	-2.99681914	-1.43263703
C	-6.01488160	-0.89389114	-0.59287103
C	-6.40755560	-3.55556114	-1.33776703
C	-7.27687760	-1.46954714	-0.48294203
C	-7.47701160	-2.79779014	-0.85895303
C	-2.93637360	-1.78692714	1.43920097
H	-0.58872760	-1.73348514	0.17627797
H	-4.29502560	-3.58511714	-1.78612303
H	-6.55921860	-4.58955014	-1.62942203
H	-8.46352560	-3.24214314	-0.77949403
H	-8.10619360	-0.87704614	-0.11112303
H	-5.83974760	0.13999586	-0.31299303
F	-2.79747160	-3.00285214	0.88501797
F	-4.22843260	-1.62884114	1.76278997
F	-2.24603360	-1.80140814	2.59573197
C	-0.39918060	0.32759986	-0.46961303
O	0.78890140	0.28499786	-0.74146803
O	-1.13192260	1.43662586	-0.58847003
C	-0.43450460	2.60046186	-1.05414003
H	-1.18090560	3.39051786	-1.09256103
H	0.36764740	2.85794386	-0.36086403
H	-0.01579360	2.41342586	-2.04415003
C	1.72634840	-3.17110514	-0.67019903
N	1.40194940	-2.52591214	-1.83157403
H	1.16097140	-1.54444214	-1.78103203
C	0.96878640	-3.29296914	-2.98260703
H	0.82839840	-2.60893714	-3.82024003

H	1.72941340	-4.03026014	-3.24659303
H	0.02744040	-3.82156814	-2.79317403
N	1.88393640	-2.35394414	0.42411697
H	1.94939640	-1.35736014	0.25605497
C	2.47722240	-2.88992814	1.63496197
H	3.53848840	-3.13299914	1.50762697
H	2.37219640	-2.15161614	2.43105897
H	1.95049340	-3.80023414	1.92369397
O	1.85179740	-4.39435214	-0.60397203

TS4

Zero-point correction=	0.330706 (Hartree/Particle)
Thermal correction to Energy=	0.356748
Thermal correction to Enthalpy=	0.357692
Thermal correction to Gibbs Free Energy=	0.272473
Sum of electronic and zero-point Energies=	-1342.429363
Sum of electronic and thermal Energies=	-1342.403321
Sum of electronic and thermal Enthalpies=	-1342.402377
Sum of electronic and thermal Free Energies=	-1342.487596

C	-3.033661	-0.220246	0.563804
C	-1.795765	-0.687487	0.143797
H	-1.727164	-1.463672	-0.610022
N	-2.232804	1.600313	-0.989841
N	-3.261178	1.530158	-0.453032
N	-1.208514	0.884583	-1.18744
C	0.070336	1.483264	-1.023036
C	0.248364	2.735538	-0.422929
C	1.168888	0.721038	-1.423348
C	1.537766	3.223095	-0.239337
C	2.456545	1.210456	-1.214592
C	2.642899	2.460991	-0.625889
H	-3.145428	0.227115	1.545644
H	-0.61398	3.319758	-0.115271
H	1.679725	4.199846	0.211805
H	3.647516	2.843156	-0.476807
H	3.317056	0.618451	-1.513604
H	1.003677	-0.248014	-1.885212
C	-0.589481	-0.544215	0.985635
O	0.378311	-1.277436	0.900451
O	-0.647855	0.506533	1.80216
C	0.561804	0.818117	2.507861
H	0.336503	1.704077	3.097184
H	0.845215	-0.013468	3.156946
H	1.359748	1.030932	1.788219

C	-4.264774	-0.89775	0.040221
F	-4.476486	-2.083236	0.648506
F	-5.368026	-0.162746	0.238637
F	-4.173137	-1.150357	-1.278332
C	3.741936	-1.409287	-0.013133
N	3.367665	-1.030242	1.249613
H	2.38159	-1.097513	1.470125
N	2.819693	-2.15839	-0.693156
H	1.873445	-2.185528	-0.335963
C	4.166522	-0.054243	1.963239
H	5.217899	-0.33721	1.906156
H	4.05995	0.956964	1.547173
H	3.860455	-0.044899	3.011073
C	3.050713	-2.482535	-2.086414
H	2.28851	-3.19192	-2.411059
H	3.013946	-1.596344	-2.734473
H	4.034128	-2.940599	-2.201205
O	4.839476	-1.121528	-0.496146

2.6 References

- 1) (a) Botuha, C.; Chemla, F.; Ferreira, F.; Perez-Luna, A. In *Heterocycles in Natural Product Synthesis*, K.C. Majumdar, S. K. Chattopadhyay, Eds. (Wiley-VCH, Weinheim, Germany, 2011) pp. 3-39. (b) Padwa, A. In *Comprehensive Heterocyclic Chemistry III*; Katrizky, A. R., Ramsden, C. A., Scriven, E. F. V., Taylor, R. J. K., Eds.; Elsevier: New York, 2008; Vol. 1, pp 1–104. (c) Sweeney, J. B. In *Science of Synthesis*; Schaumann, E., Enders, D., Eds.; Georg Thieme Verlag: Stuttgart, Germany, 2008; Vol. 40a, p 643. (d) Zwanenburg, B.; ten Holte, P. *Top. Curr. Chem.* **2001**, *216*, 93. (e) Lindstrom, U. M.; Somfai, P. *Synthesis* **1998**, 109.
- 2) (a) Harada, K.; Tomita, K.; Fujii, K.; Masuda, K.; Mikami, Y.; Yazawa, K.; Komaki, H. *J. Antibiot.* **2004**, *57*, 125. (b) Tsuchida, T.; Inuma, H.; Kinoshita, N.; Ikeda, T.; Sawa, T.; Hamada, M.; Takeuchi, T. *J. Antibiot.* **1995**, *48*, 217. (c) Metzger, J. O.; Furmeier, S. *Eur. J. Org. Chem.* **2003**, 649.
- 3) Jat, J. L.; Paudyal, M. P.; Gao, H.; Xu, Q-L.; Yousufuddin, M.; Devarajan, D.; Ess, D. H.; Kürti, L.; Falck, J. R. *Science* **2014**, *343*, 61.
- 4) Llaveria, J.; Beltrán, Á.; Díaz-Requejo, M. M.; Matheu, M. I.; Castellón, S.; Pérez, P. J. *Angew. Chem.* **2010**, *122*, 7246–7249.
- 5) (a) Li, Z.; Conser, K. R.; Jacobsen, E. N.; *J. Am. Soc. Chem.* **1993**, *115*, 5326. (b) Antilla, J. C.; Wulff, W. D. *Angew. Chem.* **2000**, *122*, 4692-4695. (c) For a review of stereospecific synthesis of aziridines see: Degennaro, L.; Trinchera, P.; Luisi, R. *Chem. Rev.* **2014**, *114*, 7881-7929.
- 6) de Loera, D.; Garcia-Garibay, M. A. *Org. Lett.* **2012**, *14*, 3874–3877.
- 7) Cohen, M. D. *Angew. Chem. Int. Ed.* **1975**, *14*, 38.

8) (a) *Photochemistry in Organized and Constrained Media*, Ramamurthy, V., Ed.; VCH Publishers: New York, 1991. (b) Shiraki, S.; Garcia-Garibay, M.A. in *Handbook of Synthetic Photochemistry*, Albini, A., Fagnoni, M. Eds., Wiley-VCH, Weinheim, 2010, pp. 25-66.

9) (a) Scheffer, J. R. In *Solid State Organic Chemistry*; Desiraju, G. R., Ed.; VCH: Amsterdam, 1987; pp 1–45. (b) Zimmerman, H. E.; Sebek, P.; Zhu, Z. *J. Am. Chem. Soc.* **1998**, *120*, 8549. (c) MacGillivray, L. R. *CrystEngComm* **2002**, *4*, 37.

10) Leyva, E.; de Loera, D.; Jimenez-Catano, R. *Tetrahedron Lett.* **2010**, *51*, 3978.

11) Zhao, Y.; Truhlar, D. G. *Theor. Chem. Acc.* **2008**, *120*, 215.

12) Calculations were also carried out for the non-catalyzed reaction and are included in the Supporting Information section.

13) (a) Fleming, I. *Frontier Orbitals and Organic Chemical Reactions*. London: Wiley, 1978. (b) Houk, K. N.; Sims, J.; Duke, R. E.; Strozier, R. W.; George, J. K. *J. Am. Chem. Soc.* **1973**, *95*, 7287.

1⁴) Ess, D. H.; Houk, K. N. *J. Am. Chem. Soc.* **2007**, *129*, 10646.

1⁵) Crews, P., Rodriguez, J., and Jaspars, M. *Organic structure analysis*. 2nd ed. New York: Oxford University Press, 2010.

16) Schreiner, P. *J. Am. Chem. Soc.*, **1968**, *90*, 988.

17) Legault, C. Y. *CYLview 1.0b*; Université de Sherbrooke; 2014 (www.cylview.org)

Chapter 3

**Stereospecific Photochemistry of Δ^2 -1,2,3-Triazolines in Solution and in the Solid-State:
Scope and Mechanistic Studies.**

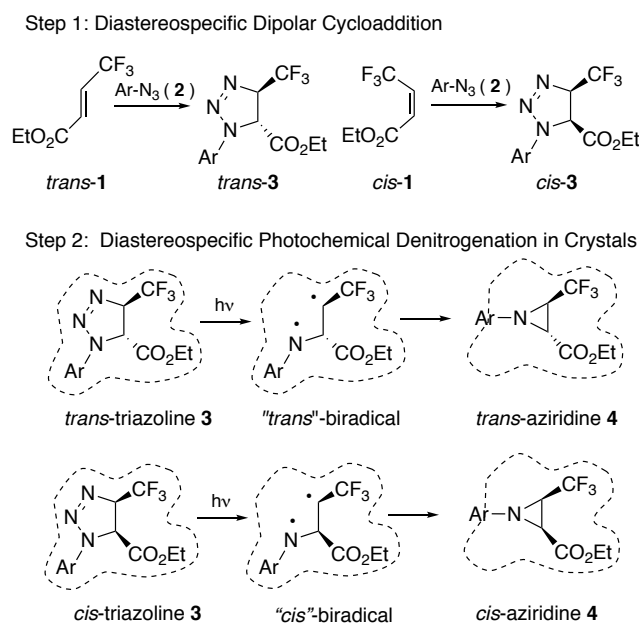
3.1 Introduction

Aziridines are nitrogen-containing three-membered heterocycles widely explored for their interesting reactivity and biological potential.¹⁻⁶ Some of the most common strategies for the stereospecific synthesis of aziridines⁷ involves the addition of nitrenes to alkenes, or the addition of carbenes into imine double bonds. Unfortunately, improved selectivity requires the use of expensive metal catalysts and toxic volatile solvents, such that alternatives strategies are desirable. Knowing that solid-state photochemistry is a viable green-chemistry alternative for the preparation of valuable synthetic targets,⁸⁻¹² we recognized an opportunity to explore a two-step strategy for the stereospecific synthesis of substituted aziridines. As illustrated in Scheme 1, we proposed the use of (*cis*)- or (*trans*)-alkenes **1** to carry out 1,3-dipolar cycloadditions with azides **2** to form (*cis*)- or (*trans*)-substituted 1,2,3-triazolines **3**.⁴ The second step would involve the photoinduced diastereospecific generation of the desired aziridines **4** by formation of an intermediate 1,3-alkylaminy radical in crystals of the pure 1,2,3-triazoline **3**.

The viability of the strategy shown in Scheme 1 was recently reported in a brief letter.⁸ It was shown that the hydrogen-bond-catalyzed dipolar cycloadditions of trifluoromethyl acrylates *trans*-**1** and *cis*-**1** with 2-fluorenyl azide **2D** (Scheme 2) are not only stereospecific, but remarkably regioselective, giving the compound where the N-Aryl group is located vicinal to the ester group. The crystallization of the two triazoline isomers proceeded well, and the solid state photochemistry occurred with high diastereomeric yields. In this article, we increased the number of aryl azides studied to include phenyl azide (**2A**), 2-naphthyl azide (**2B**), 4-biphenyl azide (**2C**), and 4-(triphenylmethyl)phenyl azide (**2E**). All the dipolar cycloaddition reactions were highly regioselective and stereospecific, each giving a single triazoline diastereomer (Scheme 2). Eight out of the ten triazolines prepared turned out to be crystalline solids and

photochemical experiments showed that the previously observed results are robust, with solid state diastereomeric ratios that are consistently greater (99:1 to 87:13) than those observed in acetonitrile solution (85:15 to 66:34).

Scheme 3.1.1



3.2 Results and Discussion

3.2.1 Synthesis and Characterization

To establish the stereospecificities of product formation in terms of the ratios of *trans*- and *cis*-aziridine products, various 1,2,3-triazolines were synthesized using a 1,3-dipolar cycloaddition of five different aryl azides (**2A-2E**) and the two geometric isomers of dipolarophile **1** (Table 1). The aryl groups used in this study contain phenyl (**2A**), 2-naphthyl (**2B**), 4-biphenyl (**2C**), 2-fluorenyl (**2D**), 4-trityl phenyl (**2E**) as illustrated in Table 1.

shown to display the characteristic IR stretch at ca. 2200 cm⁻¹ (See SI). With the aryl azides in hand for the 1,3-dipolar cycloaddition, we used commercially available ethyl (*E*)-4,4,4-trifluorobut-2-enoate (*trans*-**1**) as the dipolarophile for the cycloaddition. Alkene *trans*-**1** was selected due to its inherently electron poor nature resulting from the effects of the ethoxy ester and trifluoromethyl groups. Ethyl (*Z*)-4,4,4-trifluorobut-2-enoate (*cis*-**1**) was obtained by isomerizing *trans*-**1** under UV irradiation to afford a photostationary state of 3:1 (*trans*-**1**: *cis*-**1**). Samples of *cis*-**1** were subsequently purified by column chromatography. Triazolines were synthesized by performing a 1,3-dipolar cycloadditions by heating azides **1A-E** with either *trans*-**1** or *cis*-**1** in toluene with 10 mol% of dimethyl urea, which served as a hydrogen bond-donor catalyst, to obtain triazolines *trans*-**3A-E** and *cis*-**3A-E** in low to modest yields. The regiochemistry and stereochemistry of the triazolines were assigned based ¹H, and ¹³C, which matched with previous reports on Δ²-1,2,3-triazolines *cis*-**3D** and *trans*-**3D**, which included their single crystal X-Ray structures.⁸ Furthermore, differential scanning calorimetric analysis of triazoline *trans*-**3D** shows a relatively sharp endothermic transition which correlated to the melting temperature determined visually, and was immediately followed by a broad exothermic transition that corresponds to the thermal denitrogenation. This is illustrated in Figure 1 with the DSC data from *trans*-**3D**, which melts at 131°C and has a minimum for the decomposition peak at 171 °C.

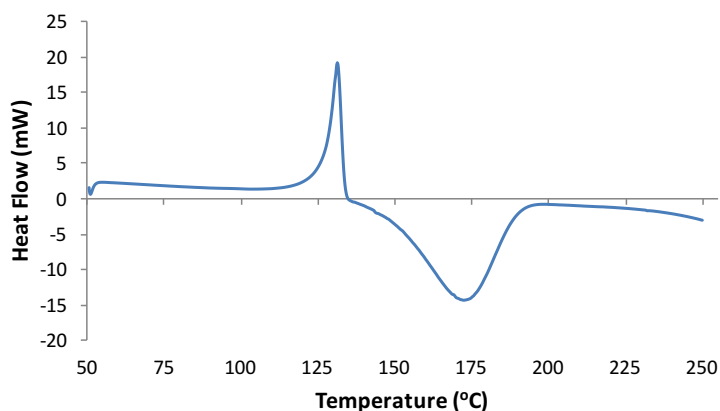


Figure 3.2.1. Differential Scanning Calorimetry (DSC) of triazoline *trans*-**3D**. Sharp peak at 131°C indicates melting and broad peak at 171°C shows denitrogenation of triazoline to form aziridine.

3.2.2 Photochemical Studies

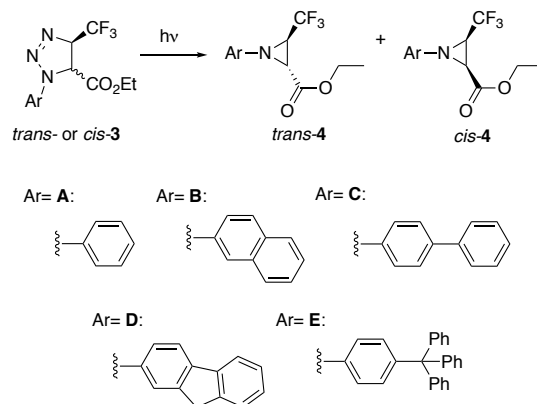
Triazolines *trans*-**3A-E** and *cis*-**3A-E** were irradiated in solution using either acetonitrile- d_3 or acetone- d_6 , or in the neat solid-state, using a medium-pressure Hg lamp (450 watts) equipped with a Pyrex filter to provide $\lambda \geq$ ca. 290 nm. To our delight, only the corresponding aziridine photoproducts were observed both in solution and in the solid-state (Table 2). Solution experiments were carried with ca. 5 mg/ml triazoline solutions that had been subject to three freeze-pump-thaw cycles to ensure that photoreactions occurred free from oxygen. Solid state experiments were carried out with ca. 3 mg of finely powdered crystals sandwiched between two microscope slides. Reaction progress was monitored by ^1H NMR spectroscopy, which was also used to determine the ratio of *trans*- to *cis*-aziridines identified by the different ^1H coupling constants, $J_{trans} \approx 2.3$ Hz and $J_{cis} \approx 6.5$ Hz.¹³

The photochemical results summarized in Table 2 include product ratios obtained in triplicate with all five *trans*-triazolines in the top five entries, and the ones determined with

the *cis*-triazolines in the bottom five. It is estimated that errors in the table are in the range of $\pm 3\%$. The results obtained under direct excitation in acetonitrile solutions, upon triplet sensitization in acetone, and by direct irradiation in the crystalline solid state, are included in the left, middle, and right columns, respectively. The results of experiments carried out in acetonitrile revealed a high level of stereospecificity, with each triazoline isomer resulting in the preferential formation of the corresponding same isomeric aziridine product. As in previous examples, this result implies that the biradical intermediates resulting by denitrogenation from the five-membered heterocycle are formed in the singlet state and have no time to equilibrate before bond formation to form the three-membered ring. Thus, irradiation of *trans*-triazolines resulted in *trans:cis* ratios ranging from 85:15 to 73:27 (Table 2, third column, entries 1-5) and direct photoexcitation of *cis*-triazolines resulted in analogous but opposite selectivities, from 21:79 to 34:66 (Table 2, third column, entries 6-10).

Experiments carried out in acetone, which is used both as solvent and as triplet sensitizer, are expected to reveal the reactivity of the longer-lived triplet state biradicals. In this case, unable to form the singlet state photoproduct before intersystem crossing to the singlet state, triplet biradicals are expected to have a greater opportunity for conformational equilibration. Thus, at a first approximation, one may expect the stability of the triplet state biradical to parallel the stability of the product, such that the *trans*-aziridine isomers should be preferred in the triplet-sensitized reaction. To verify this we performed calculations on the ground state energies of the equilibrium conformers of *trans*-**4A-D** and *cis*-**4A-D** at the B3LYP/6-31G* level of theory. We confirmed that the *trans* aziridines are indeed more stable than the *cis* aziridines. Energy differences of 2.6 and 2.3 kcal/mol were observed,

respectively, for the N-phenyl (**4A**) and N-(4-phenyl) (**4C**), compounds, with corresponding values of 6.3 and 6.4 kcal/mol for the analogous 2-naphthyl (**4B**) and 2-fluorenyl (**4D**) structures. We omitted aziridines **4E** due to their large size and long computing time, assuming that similar results should be observed. While our expectations on the relative energies of the *cis* and *trans* N-aryl aziridines were confirmed, we discovered that the experimental results of reactions carried out in acetone are not straightforward, as shown in the fourth column in Table 2. On one hand, one can see that five entries, including *trans-3C*, *trans-3D*, *trans-3E*, *cis-3C* and *cis-3D* yield the *trans*-aziridine isomer in yields greater than 96% and conform to our original expectations. However, the stereoselectivities observed with compounds *trans-3A*, *trans-3B*, are diminished to ca. 75 and 79% *trans*, respectively, and the ones observed from *cis-3A*, *cis-3B* and *cis-3E* are closer to 50:50. Additional measurements revealed that the product ratios are not dependent on the extent of conversion or irradiation time, and experiments carried out with other triplet sensitizers, including benzophenone, xanthone and biacetyl, showed that the products in the table do reflect the reactivity of the triplet excited state. The fact that different product ratios are observed from triplet sensitized experiments that start from the *cis*- and *trans*-isomers of the same triazoline indicate that biradical equilibration does not take place. For example, *trans-3A* and *cis-3A* give aziridine **4A** in *trans*:*cis* ratios that are 79:21 and 52:48, respectively. This observation indicates that intersystem crossing and ring closure compete with the rate of conformational equilibration, a fact that has been shown for a number of short chain 1,3-biradicals and 1,4-biradicals.¹⁴⁻¹⁷

Table 3.2.2. Ratios of *cis*- and *trans*-aziridines from triazolines in solution and solid-state.^a

Entry	Compound	CD ₃ CN <i>trans</i> : <i>cis</i>	(CD ₃) ₂ CO <i>trans</i> : <i>cis</i>	Crystals <i>trans</i> : <i>cis</i>
1	<i>trans</i> - 3A	85:15	79:21	n.a. ^o
2	<i>trans</i> - 3B	83:17	75:25	n.a. ^o
3	<i>trans</i> - 3C	82:18	99:1	90:10
4	<i>trans</i> - 3D	76:24	99:1	83:17
5	<i>trans</i> - 3E	73:27	97:3	83:17
6	<i>cis</i> - 3A	29:71	52:48	1:99
7	<i>cis</i> - 3B	21:79	43:57	6:94
8	<i>cis</i> - 3C	34:66	96:4	17:83
9	<i>cis</i> - 3D	32:68	99:1	10:90
10	<i>cis</i> - 3E	28:72	43:57	12:88

^a Product ratios determined in triplicate with estimated errors of $\pm 3\%$; ^b Triazolines were liquids at 300 K.

Photochemical experiments in the crystalline solid state included samples of *trans*-triazolines **3C-E** and *cis*-triazolines **3A-E**. Samples of *trans*-(N-phenyl)- and *trans*-N-(2-Naphthyl)-triazolines *trans*-**3A** and *trans*-**3B** were liquids under ambient conditions. We were able to confirm that, as expected, stereospecificities obtained in the solid state are greater than those obtained under direct irradiation in solution. For example, reaction of N-(4-biphenyl)-*trans*-triazoline **3C** improved the formation of *trans*-aziridine **4C** from 82%

in solution to 90% in the solid state (entry 3, columns 3 and 5). Similar observations were made with *trans*-triazolines **3D** and **3E**, and with all *cis*-triazolines, which systematically give the *cis*-aziridine as the preferred photoproduct with yields that range from 83% (*cis*-**3C**) to 99% (*cis*-**3A**). While a higher stereospecificity was expected in the solid state as compared to solution, it appears that hindered bond rotation in the 1,3-biradical intermediate is not large enough to guarantee very high specificity in all cases. The lack of correlation with respect to the size of the N-aromatic substituent suggests that isomerization occurs by bond rotation about the biradical ArNC(CO₂Et)—CHCF₃ bond. This hypothesis is suggested by a previously reported example where the stereospecificity of a 4-methyl-4-trifluoromethyl triazoline analog was shown to be quantitative.⁸

3.2.3 Mechanistic Analysis

To explore the type and range of experimental parameters that affect the photoreaction, and perhaps the subtle differences between product ratios of *trans*:*cis* aziridine in solution and in the solid-state, we first analysed the role of solvent polarity. While we postulated a biradical intermediate resulting from a homolytic cleavage reaction (Figure 2), we reasoned that a zwitterionic intermediate would have different stabilizing interactions in different solvents, which may result in different *trans*:*cis* aziridine ratios.¹⁸ The results of photochemical experiments using triazoline *trans*-**3C** in methanol, acetonitrile and carbon tetrachloride, which range in E_T(30) values from 32-55 kcal/mol,¹⁹ showed no changes in stereospecificity (Table 3).

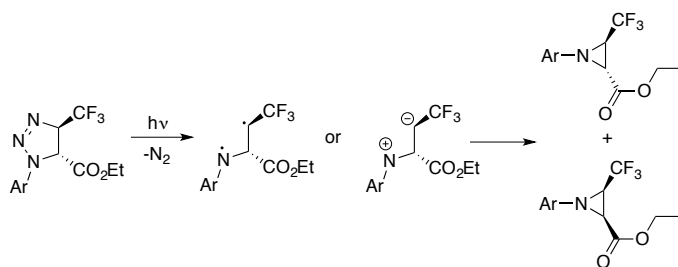
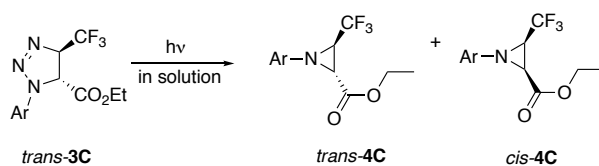


Figure 3.2.2. Plausible biradical intermediate versus zwitterionic intermediate to form aziridines.

Table 3.2.3. Solution-state photochemistry of triazoline *trans*-**3C** in solvents with different polarity.^a



Solvent	$E_T(30)$ (kcal/mol)	<i>trans</i> - 4C (%)	<i>cis</i> - 4C (%)
Methanol ^{a,b}	55	80	20
Acetonitrile ^a	46	82	18
Carbon Tetrachloride ^a	32	81	19

^aProduct ratios determined in triplicate with estimated errors of $\pm 3\%$. ^bProducts showed both methyl ester and ethyl ester.

A plausible mechanism to account for different *trans*:*cis* aziridine ratios under direct excitation in solution and in solids would be that the *trans*-triazolines form stereospecifically to the *trans*-aziridine product, but continuous irradiation may provide a pathway for isomerization. However, experiments carried out with pure aziridine *trans*-**4C** in solution and in the solid state for several hours under the previously utilized reaction conditions led to no observable change, ruling out the possibility of *trans*-aziridine

isomerization. In order to determine whether one can steer the ratios of *cis*- to *trans*-aziridines in the solid-state, we analysed the effects of temperature from 25 °C to -196 °C. We observed a decrease in the stereospecificity of the reaction through this temperature range with the *trans:cis* ratio changing from 84:16 at 25 °C to 66:33 at -40 °C and below, showing that that the optimum temperature to provide the highest *trans/cis* aziridine ratios is around room temperature.

3.3 Conclusions

In conclusion, we have synthesized ten different diastereomerically pure triazolines and investigated their stereospecificities to form aziridines in solution and in the solid state. We have shown that photochemistry of Δ^2 -1,2,3-triazolines are moderately stereospecific in solution and more so in the solid-state. Solid-state photochemistry of triazolines provides an efficient and solvent-free method to synthesize their corresponding aziridines. Specifically, we found that photochemistry of Δ^2 -1,2,3-triazolines under singlet excited states would afford the kinetically controlled *trans*- to *cis*-aziridine ratios, whereas efficient triplet sensitization would form the thermodynamically controlled product ratios. Using various solvent studies, variable temperature studies, and product analysis, we propose the photochemistry of Δ^2 -1,2,3-triazolines to form aziridines follows a homolytic cleavage to expel nitrogen and form the 1,3-biradical species.

Author's note: This chapter is in the final stages of manuscript editing for submission. This article will be submitted shortly.

3.4 Experimental

A. Experimental for compound *cis*-1

The synthesis of ethyl (*Z*)-4,4,4-trifluorobut-2-enoate (compound *cis*-1) was reported in the literature and was synthesized accordingly.¹ The synthesized compound matched spectroscopic data of the published compound. Ethyl 4,4,4-trifluorocrotonate *trans*-1 (638mg, 3.8mmol) was dissolved in 5mL of dry DCM. The mixture was irradiated using a medium-pressure Hg Hanovia lamp with a quartz emission well filter with cutoff of $\lambda \leq 220$ nm. After 3 days, the mixture reached a photostationary state of 76% *trans*-1 and 24% *cis*-1. The DCM was concentrated under vacuum and the mixture was purified by silica gel column chromatography using pentane/diethyl ether (90/10) as eluent. Clear liquid, R_f 0.45, stained with Potassium permanganate. IR(ATR): 2952, 2924, 1742, 1668, 1460, 1371, 1312, 1262, 1183 cm^{-1} . ¹H NMR (500 MHz, CDCl_3) δ 6.28 (d, $J = 12.5$ Hz, 1H), 6.03 (dq, $J = 12.5, 8.0$ Hz, 1H), 4.27 (q, $J = 7.1$ Hz, 2H), 1.20 (t, $J = 7.1$ Hz, 3H). ¹³C NMR (125 MHz, CDCl_3) δ 163.46, 130.12, 130.07, 130.03, 129.99, 127.38, 127.08, 126.79, 126.50, 124.46, 122.30, 120.14, 117.97, 61.67, 34.12, 13.86.

B. Experimental for compounds 2A-2E

All of the aryl azides were synthesized following a reported protocol.¹ All of the corresponding amines were commercially available and used without further purification.

Synthesis of phenyl azide (compound 2A): Crude product was purified by silica gel chromatography (eluent: EtOAc/Hexanes 20/80). Yield 74%, yellow liquid, R_f 0.92. IR (ATR): 2122, 2090, 1593, 1491, 1293, 1279, 744, 685, 668 cm^{-1} . ¹H NMR (500 MHz, CDCl_3) δ 7.40 – 7.32 (m, 2H), 7.18 – 7.12 (m, 1H), 7.07 – 6.97 (m, 2H). ¹³C NMR (126 MHz, CDCl_3) δ 140.01, 129.78, 124.89, 119.04.

Synthesis of 2-azidonaphthalene (compound **2B**): Crude product was purified by silica gel chromatography (eluent: EtOAc/Hexanes 20/80). Yield 98%, yellow liquid, R_f 0.88. IR (ATR): 2101, 1625, 1596, 1508, 1281, 845, 805, 741 cm^{-1} . ^1H NMR (500 MHz, CDCl_3) δ 7.83 (d, $J = 8.7$ Hz, 2H), 7.77 (d, $J = 8.2$ Hz, 1H), 7.52 (ddd, $J = 8.2, 6.9, 1.3$ Hz, 1H), 7.49 – 7.43 (m, 2H), 7.17 (dd, $J = 8.8, 2.3$ Hz, 1H). ^{13}C NMR (126 MHz, CDCl_3) δ 137.53, 134.03, 131.08, 129.95, 127.91, 127.04, 125.46, 118.79, 115.85.

Synthesis of 4-azidobiphenyl (compound **2C**): Crude product was purified by silica gel chromatography (eluent: EtOAc/Hexanes 10/90). Yield 83%, yellow solid, R_f 0.91. IR (ATR): 2129, 2092, 1584, 1517, 1482, 1289, 833, 759. 689 cm^{-1} . ^1H NMR (500 MHz, CDCl_3) δ 7.63 – 7.53 (m, 4H), 7.50 – 7.41 (m, 2H), 7.39 – 7.31 (m, 1H), 7.18 – 7.07 (m, 2H). ^{13}C NMR (126 MHz, CDCl_3) δ 140.15, 139.15, 138.01, 128.89, 128.46, 127.39, 126.88, 119.42.

Synthesis of 2-azido-9H-fluorene (compound **2D**): Crude product was purified by silica gel chromatography (eluent: EtOAc/Hexanes 10/90). Yield 99%, yellow solid, R_f 0.91. IR (ATR): 3045, 2386, 2104, 1603, 1580, 1450, 1290, 1280, 836 cm^{-1} . ^1H NMR (500 MHz, CDCl_3) δ 7.74 (d, $J = 8.1$ Hz, 2H), 7.53 (d, $J = 7.5$ Hz, 1H), 7.37 (d, $J = 7.5$ Hz, 1H), 7.30 (td, $J = 7.4, 1.0$ Hz, 1H), 7.22 (s, 1H), 7.04 (dd, $J = 8.1, 2.1$ Hz, 1H), 3.90 (s, 2H). ^{13}C NMR (125 MHz, CDCl_3) δ 145.13, 142.93, 140.97, 138.97, 138.48, 126.95, 126.68, 125.05, 120.88, 119.67, 117.85, 115.75, 36.87.

Synthesis of ((4-azidophenyl)methanetriyl)tribenzene (compound **2E**): Crude product was purified by silica gel chromatography (eluent: EtOAc/Hexanes 20/80). Yield 86%, yellow solid,

R_f 0.84. IR (ATR): 2122, 2084, 1500, 1490, 1442, 1291, 752, 701 cm^{-1} . ^1H NMR (500 MHz, CDCl_3) δ 7.31 – 7.13 (m, 17H), 6.99 – 6.87 (m, 2H). ^{13}C NMR (126 MHz, CDCl_3) δ 146.54, 143.78, 137.62, 132.52, 131.04, 127.60, 126.08, 118.10, 64.56.

C. Experimental for compounds *trans*-3A-3E and *cis*-3A-3E

All triazolines were synthesized using the following general procedure published in the literature:¹ Ethyl 4,4,4-trifluorocrotonate (0.3 mmol), **2A** (0.3 mmol), and $\text{N,N}'$ -dimethylurea (0.03 mmol) was dissolved in 1.5 mL of dry toluene the reaction was stirred for 32 hours at 60°C under argon atmosphere. After the initial 32 hours, an additional 0.3 mmol of ethyl 4,4,4-trifluorocrotonate was added to the solution. After 33 more hours of heating, the reaction was cooled when the disappearance of azide by TLC was observed. The crude mixture was rotary evaporated under vacuum and the reaction mixture was purified by column chromatography.

Synthesis of ethyl (4*R*,5*R*)-1-phenyl-4-(trifluoromethyl)-4,5-dihydro-1*H*-1,2,3-triazole-5-carboxylate (*trans*-**3A**): Crude product was purified by silica gel chromatography (eluent: EtOAc/Hexanes 10/60). Yield 22%, white liquid, R_f 0.45. IR (ATR): 2989, 1732, 1598, 1499, 1477, 1330 1268, 1133, 752, 692 cm^{-1} . ^1H NMR (500 MHz, CDCl_3) δ 7.44 – 7.34 (m, 2H), 7.34 – 7.28 (m, 2H), 7.15 (t, $J = 7.4$ Hz, 1H), 5.29 – 5.22 (m, 1H), 4.61 (d, $J = 8.1$ Hz, 1H), 4.26 (q, $J = 7.1$ Hz, 2H), 1.24 (t, $J = 7.1$ Hz, 3H). ^{13}C NMR (126 MHz, CDCl_3) δ 167.79, 138.87, 129.62, 124.43, 123.70, 121.48, 115.38, 82.67, 82.43, 82.19, 81.95, 63.15, 56.90, 13.95.

Synthesis of ethyl (4*R*,5*S*)-1-phenyl-4-(trifluoromethyl)-4,5-dihydro-1*H*-1,2,3-triazole-5-carboxylate (*cis*-**3A**): Crude product was purified by silica gel chromatography (eluent: EtOAc/Hexanes 10/60). Yield 12%, white solid, R_f 0.35. IR (ATR): 2898, 1732, 1598, 1329, 1267, 1172, 1133, 1064, 752, 692, 668 cm^{-1} . ^1H NMR (500 MHz, CD_3CN) δ 7.50 – 7.35 (m,

2H), 7.29 – 7.23 (m, 2H), 7.19 – 7.06 (m, 1H), 5.60 – 5.32 (m, 1H), 5.09 (d, $J = 12.9$ Hz, 1H), 4.27 – 4.04 (m, 2H), 1.15 (t, $J = 7.1$ Hz, 3H). ^{13}C NMR (126 MHz, CD_3CN) δ 166.38, 139.84, 130.25, 126.90, 124.69, 124.53, 122.47, 120.26, 115.69, 81.20, 80.96, 80.72, 80.49, 63.13, 57.16, 13.61. Melting Point: 90-91 °C

Synthesis of ethyl (4*R*,5*R*)-1-(naphthalen-2-yl)-4-(trifluoromethyl)-4,5-dihydro-1*H*-1,2,3-triazole-5-carboxylate (*trans*-**3B**): Crude product was purified by silica gel chromatography (eluent: EtOAc/Hexanes 10/60). Yield 80%, yellow liquid, R_f 0.47. IR (ATR): 3063, 2984, 1745, 1633, 1602, 1471, 1234, 1262, 1178, 1126, 966 cm^{-1} . ^1H NMR (500 MHz, CDCl_3) δ 7.88 (d, $J = 9.0$ Hz, 1H), 7.85 – 7.78 (m, 2H), 7.76 (dd, $J = 8.2, 0.5$ Hz, 1H), 7.50 (ddd, $J = 8.2, 6.9, 1.3$ Hz, 1H), 7.43 (ddd, $J = 8.1, 6.9, 1.2$ Hz, 1H), 7.37 (d, $J = 2.2$ Hz, 1H), 5.46 – 5.26 (m, 1H), 4.75 (d, $J = 8.1$ Hz, 1H), 4.27 (qq, $J = 10.8, 7.1$ Hz, 2H), 1.25 (t, $J = 7.1$ Hz, 3H). ^{13}C NMR (126 MHz, CDCl_3) δ 167.83, 136.61, 133.61, 130.61, 129.96, 127.86, 127.37, 127.19, 125.30, 123.74, 121.52, 116.51, 110.57, 82.84, 82.60, 82.36, 82.12, 63.19, 57.03, 57.02, 13.98.

Synthesis of ethyl (4*R*,5*S*)-1-(naphthalen-2-yl)-4-(trifluoromethyl)-4,5-dihydro-1*H*-1,2,3-triazole-5-carboxylate (*cis*-**3B**): Crude product was purified by silica gel chromatography (eluent: EtOAc/Hexanes 10/70). Yield 14%, white solid, R_f 0.43. IR (ATR): 2924, 1745, 1629, 1600, 1483, 1370, 1326, 1277, 1172, 1135, 1063, 809 cm^{-1} . ^1H NMR (500 MHz, CD_3CN) δ 7.95 (d, $J = 9.0$ Hz, 1H), 7.86 (ddd, $J = 16.9, 8.2, 0.6$ Hz, 2H), 7.77 (dd, $J = 9.0, 2.3$ Hz, 1H), 7.52 (ddd, $J = 8.2, 6.9, 1.3$ Hz, 1H), 7.45 (ddd, $J = 8.1, 6.9, 1.2$ Hz, 1H), 7.38 (d, $J = 2.3$ Hz, 1H), 5.51 (dd, $J = 12.9, 8.3$ Hz, 1H), 5.22 (d, $J = 12.9$ Hz, 1H), 4.15 (q, $J = 7.1$ Hz, 2H), 1.14 (t, $J = 7.1$ Hz, 3H). ^{13}C NMR (126 MHz, CD_3CN) δ 166.33, 137.60, 134.32, 130.91, 130.42, 128.30, 127.82,

127.77, 126.91, 125.72, 124.70, 122.49, 120.28, 116.73, 111.01, 81.36, 81.12, 80.88, 80.65, 63.18, 60.54, 57.33, 57.32, 13.63. Melting Point: 114-116 °C

Synthesis of ethyl (4*R*,5*R*)-1-([1,1'-biphenyl]-4-yl)-4-(trifluoromethyl)-4,5-dihydro-1*H*-1,2,3-triazole-5-carboxylate (*trans*-**3C**): Crude product was purified by silica gel chromatography (eluent: EtOAc/Hexanes 10/60). Yield 51%, white solid, R_f 0.39. IR (ATR): 2964, 1736, 1606, 1526, 1449, 1474, 1323, 1201, 1241, 1170, 1142, 1124, 1101, 762 cm^{-1} . ^1H NMR (500 MHz, CDCl_3) δ 7.69 – 7.59 (m, 2H), 7.59 – 7.54 (m, 2H), 7.52 – 7.41 (m, 2H), 7.41 – 7.29 (m, 3H), 5.35 – 5.23 (m, 1H), 4.65 (d, J = 8.1 Hz, 1H), 4.29 (q, J = 7.1 Hz, 2H), 1.27 (t, J = 7.1 Hz, 3H). ^{13}C NMR (126 MHz, CDCl_3) δ 167.74, 167.71, 140.06, 138.09, 137.41, 128.89, 128.24, 127.37, 126.82, 125.93, 123.70, 121.48, 119.26, 115.73, 82.76, 82.53, 82.29, 82.05, 63.21, 56.93, 13.98. Melting Point: 146-147°C

Synthesis of ethyl (4*R*,5*S*)-1-([1,1'-biphenyl]-4-yl)-4-(trifluoromethyl)-4,5-dihydro-1*H*-1,2,3-triazole-5-carboxylate (*cis*-**3C**): Crude product was purified by silica gel chromatography (eluent: EtOAc/Hexanes 10/60). Yield 21%, white solid, R_f 0.33. IR (ATR): 2966, 2929, 1748, 1486, 1369, 1327, 1275, 1139, 1062, 1022, 968, 924, 769 cm^{-1} . ^1H NMR (500 MHz, CDCl_3) δ 7.67 – 7.53 (m, 4H), 7.53 – 7.38 (m, 2H), 7.38 – 7.27 (m, 3H), 5.21 (dq, J = 12.9, 7.8 Hz, 1H), 4.88 (d, J = 12.9 Hz, 1H), 4.19 (qdd, J = 14.3, 9.0, 5.4 Hz, 2H), 1.18 (dd, J = 8.7, 5.6 Hz, 3H). ^{13}C NMR (126 MHz, CDCl_3) δ 165.21, 140.05, 138.30, 137.18, 128.88, 128.25, 127.33, 126.78, 123.54, 121.32, 115.57, 81.15, 80.91, 80.67, 80.42, 62.87, 57.18, 13.68. Melting Point: 163-164°C

Synthesis of ethyl (4*R*,5*R*)-1-(9*H*-fluoren-2-yl)-4-(trifluoromethyl)-4,5-dihydro-1*H*-1,2,3-triazole-5-carboxylate (*trans*-**3D**): The product mixture was purified by silica gel column chromatography (eluent 10/70 EtOAc/Hexanes). Yield 65%, white solid, R_f 0.39. IR (ATR): 2996, 1738, 1615, 1584, 1487, 1337, 1274, 1241, 1199, 1107, 1017, 986 cm^{-1} . ^1H NMR (500 MHz, CDCl_3) δ 7.75 (t, $J = 8.7$ Hz, 2H), 7.57 (d, $J = 1.6$ Hz, 1H), 7.53 (d, $J = 7.4$ Hz, 1H), 7.38 (td, $J = 7.4, 1.1$ Hz, 1H), 7.30 (td, $J = 7.4, 1.1$ Hz, 1H), 7.27 – 7.23 (m, 2H), 5.28 (p, $J = 7.8$ Hz, 1H), 4.69 (d, $J = 7.8$ Hz, 1H), 4.31 – 4.23 (m, 2H), 3.92 (s, 2H), 1.24 (t, $J = 7.1$ Hz, 3H). ^{13}C NMR (125 MHz, CDCl_3) δ 167.85, 144.98, 142.94, 140.92, 138.48, 137.74, 126.97, 126.66, 125.04, 123.76, 121.54, 120.68, 119.66, 114.37, 112.77, 82.60, 82.37, 82.13, 81.89, 63.13, 57.30, 37.09, 13.98. Melting Point: 133-134°C

Synthesis of ethyl (4*R*,5*S*)-1-(9*H*-fluoren-2-yl)-4-(trifluoromethyl)-4,5-dihydro-1*H*-1,2,3-triazole-5-carboxylate (*cis*-**3D**): The product mixture was purified by silica gel column chromatography (eluent 10/70 EtOAc/Hexanes). Yield 18%, white solid, R_f 0.33. IR (ATR): 2919, 2850, 1743, 1615, 1585, 1483, 1329, 1277, 1223, 1203, 1173, 1021, 968, 821 cm^{-1} . ^1H NMR (500 MHz, CDCl_3) δ 7.74 (t, $J = 7.7$ Hz, 2H), 7.57 – 7.49 (m, 2H), 7.37 (td, $J = 7.4, 1.1$ Hz, 1H), 7.29 (td, $J = 7.4, 1.1$ Hz, 1H), 7.15 (dd, $J = 8.3, 2.2$ Hz, 1H), 5.21 (dq, $J = 12.9, 7.8$ Hz, 1H), 4.91 (d, $J = 12.9$ Hz, 1H), 4.22 – 4.10 (m, 2H), 3.92 (s, 2H), 1.14 (t, $J = 7.1$ Hz, 3H). ^{13}C NMR (125 MHz, CDCl_3) δ 165.32, 145.04, 142.92, 140.96, 138.30, 138.02, 126.95, 126.61, 125.80, 125.03, 123.58, 121.36, 120.72, 119.61, 119.14, 114.09, 112.59, 81.02, 80.78, 80.53, 80.29, 62.79, 57.56, 37.10, 13.69. Melting Point: 165-166°C.

Synthesis of ethyl (4*R*,5*R*)-4-(trifluoromethyl)-1-(4-tritylphenyl)-4,5-dihydro-1*H*-1,2,3-triazole-5-carboxylate (*trans*-**3E**): Crude product was purified by silica gel chromatography (eluent: EtOAc/Hexanes 10/60). Yield 74%, white solid, R_f 0.41. IR (ATR): 2993, 1768, 1508, 1489, 1441, 1134, 1032, 701 cm^{-1} . ^1H NMR (500 MHz, CDCl_3) δ 7.50 – 6.91 (m, 17H), 5.32 – 5.11 (m, 1H), 4.56 (d, $J = 8.2$ Hz, 1H), 4.34 – 4.16 (m, 2H), 1.22 (t, $J = 7.1$ Hz, 3H). ^{13}C NMR (126 MHz, CDCl_3) δ 167.84, 146.52, 143.13, 136.72, 132.25, 131.91, 131.05, 127.59, 127.47, 126.07, 125.96, 123.69, 121.47, 118.56, 114.40, 82.74, 82.50, 82.26, 82.02, 64.51, 63.13, 56.99, 13.94. Melting Point: 167-168°C.

Synthesis of ethyl (4*R*,5*S*)-4-(trifluoromethyl)-1-(4-tritylphenyl)-4,5-dihydro-1*H*-1,2,3-triazole-5-carboxylate (*cis*-**3E**): Crude product was purified by silica gel chromatography (eluent: EtOAc/Hexanes 10/60). Yield 22%, white solid, R_f 0.35. IR (ATR): 2997, 1767, 1594, 1509, 1441, 1231, 1206, 1133, 701 cm^{-1} . ^1H NMR (500 MHz, CD_3CN) δ 7.63 – 6.91 (m, 14H), 5.56 – 5.34 (m, 1H), 5.04 (d, $J = 13.0$ Hz, 1H), 4.28 – 3.92 (m, 2H), 1.12 (t, $J = 7.1$ Hz, 3H). ^{13}C NMR (126 MHz, CD_3CN) δ 165.76, 146.86, 142.65, 137.03, 131.95, 130.67, 127.75, 126.05, 124.09, 121.88, 80.46, 80.22, 64.48, 62.57, 59.97, 56.55, 13.07. Melting Point: 173-174°C.

D. Experimental for compounds *trans*-4A-4E and *cis*-4A-4E

For solid-state photolysis:

Triazoline *trans*-**3A-E** and *cis*-**3A-E** (5-8 mg) was crushed between two microscope slides and photolyzed using a medium-pressure Hg Hanovia lamp with a pyrex emersion well filter with cutoff of $\lambda \leq 290$ nm. The reaction was monitored by ^1H NMR and was completed in less than one hour.

For solution-state photolysis:

Triazoline (5-8mg) was dissolved in deuterated acetonitrile or acetone in an NMR tube and the solution was freeze-pump-thawed for 3 cycles to ensure no gas was present in the reaction. The NMR tube was photolyzed using a medium-pressure Hg Hanovia lamp with a pyrex emersion well filter with cutoff of $\lambda \leq 290$ nm. The reactions were monitored by ^1H NMR and showed completion in less than one hour.

Ethyl (2*R*,3*R*)-1-phenyl-3-(trifluoromethyl)aziridine-2-carboxylate (*trans*-4A): IR (ATR): 2985, 1738, 1600, 1494, 1336, 1279, 1145, 1082, 757, 692 cm^{-1} . ^1H NMR (500 MHz, CD_3CN) δ 7.32 – 7.22 (m, 2H), 7.12 – 7.01 (m, 1H), 7.01 – 6.87 (m, 2H), 4.19 – 3.95 (m, 2H), 3.60 (qd, $J = 5.1$, 2.3 Hz, 1H), 3.48 (d, $J = 2.2$ Hz, 1H), 1.10 (t, $J = 7.1$ Hz, 3H). ^{13}C NMR (126 MHz, CD_3CN) δ 165.49, 147.17, 129.94, 129.72, 129.56, 127.86, 127.12, 124.95, 124.29, 122.78, 120.61, 120.21, 62.44, 42.34, 42.02, 41.70, 41.37, 39.88, 39.86, 13.82. Compound was a white liquid at room temperature.

Ethyl (2*S*,3*R*)-1-phenyl-3-(trifluoromethyl)aziridine-2-carboxylate (*cis*-4A): IR (ATR): 2990, 2931, 1753, 1599, 1492, 1380, 1268, 1206, 1146, 1060, 763, 694 cm^{-1} . ^1H NMR (500 MHz, CD_3CN) δ 7.43 – 7.27 (m, 2H), 7.18 – 7.09 (m, 1H), 7.09 – 7.01 (m, 2H), 4.25 (qq, $J = 10.8$, 7.1 Hz, 2H), 3.33 (d, $J = 6.5$ Hz, 1H), 3.24 (dq, $J = 11.4$, 5.7 Hz, 1H), 1.27 (t, $J = 7.1$ Hz, 3H). ^{13}C NMR (126 MHz, CD_3CN) δ 166.33, 150.49, 129.96, 127.52, 125.34, 124.85, 123.17, 120.99, 120.20, 62.19, 43.01, 42.69, 42.37, 42.05, 13.90. Compound was a slightly yellow liquid at room temperature.

Ethyl (2*R*,3*R*)-1-(naphthalen-2-yl)-3-(trifluoromethyl)aziridine-2-carboxylate (*trans*-**4B**): IR (ATR): 2984, 1737, 1632, 1600, 1334, 1279, 1146, 695 cm⁻¹. ¹H NMR (500 MHz, CD₃CN) δ 7.80 (ddd, *J* = 15.7, 8.6, 0.5 Hz, 3H), 7.49 (ddd, *J* = 8.2, 6.9, 1.2 Hz, 1H), 7.45 – 7.35 (m, 2H), 7.15 (dd, *J* = 8.7, 2.3 Hz, 1H), 4.13 – 3.94 (m, 2H), 3.74 (qd, *J* = 5.1, 2.3 Hz, 1H), 3.59 (d, *J* = 2.3 Hz, 1H), 1.05 (t, *J* = 7.1 Hz, 3H). ¹³C NMR (126 MHz, CD₃CN) δ 165.53, 144.88, 134.40, 131.12, 129.69, 128.24, 127.38, 127.33, 127.16, 125.44, 124.99, 122.82, 120.87, 120.65, 116.30, 62.51, 42.59, 42.26, 41.94, 41.62, 40.03, 40.02, 40.00, 13.83. Compound was a clear liquid at room temperature.

Ethyl (2*S*,3*R*)-1-(naphthalen-2-yl)-3-(trifluoromethyl)aziridine-2-carboxylate (*cis*-**4B**): IR (ATR): 2985, 1739, 1631, 1601, 1509, 1471, 1275, 1232, 1146, 1060, 854, 813, 749 vcm⁻¹. ¹H NMR (500 MHz, CD₃CN) δ 7.93 – 7.77 (m, 3H), 7.56 – 7.37 (m, 3H), 7.30 (dd, *J* = 8.8, 2.3 Hz, 1H), 4.38 – 4.20 (m, 2H), 3.45 (d, *J* = 6.5 Hz, 1H), 3.42 – 3.32 (m, 1H), 1.29 (t, *J* = 7.1 Hz, 3H). ¹³C NMR (126 MHz, CD₃CN) δ 166.34, 148.09, 134.36, 131.35, 130.01, 128.27, 127.54, 127.46, 125.70, 125.36, 123.19, 120.95, 116.15, 62.27, 43.12, 42.80, 42.48, 42.16, 41.92, 41.91, 13.92. Compound was a slightly orange liquid at room temperature.

Ethyl (2*R*,3*R*)-1-([1,1'-biphenyl]-4-yl)-3-(trifluoromethyl)aziridine-2-carboxylate (*trans*-**4C**): IR (ATR): 2924, 1733, 1605, 1523, 1487, 1373, 1336, 1221, 1144, 1082, 762, 722 cm⁻¹. ¹H NMR (500 MHz, CD₃CN) δ 7.66 – 7.52 (m, 3H), 7.52 – 7.39 (m, 2H), 7.39 – 7.28 (m, 1H), 7.09 – 6.91 (m, 2H), 4.16 – 4.01 (m, 2H), 3.65 (qd, *J* = 5.0, 2.3 Hz, 1H), 3.52 (d, *J* = 2.3 Hz, 1H), 1.12 (t, *J* = 7.1 Hz, 3H). ¹³C NMR (126 MHz, CD₃CN) δ 165.50, 146.64, 140.72, 136.99, 129.47, 128.20,

127.76, 127.16, 124.92, 122.75, 120.76, 62.53, 42.42, 42.10, 41.78, 41.46, 39.99, 39.97, 13.84.

Melting Point: 99-101 °C

Ethyl (2*S*,3*R*)-1-([1,1'-biphenyl]-4-yl)-3-(trifluoromethyl)aziridine-2-carboxylate (*cis*-**4C**): IR (ATR): 2986, 1754, 1599, 1493, 1454, 1380, 1296, 1206, 1266, 1143, 1059, 758, 694 cm⁻¹. ¹H NMR (500 MHz, CD₃CN) δ 7.64 – 7.55 (m, 3H), 7.49 – 7.41 (m, 2H), 7.38 – 7.31 (m, 1H), 7.21 – 7.10 (m, 2H), 4.35 – 4.18 (m, 2H), 3.38 (d, *J* = 6.5 Hz, 1H), 3.34 – 3.26 (m, 1H), 1.28 (t, *J* = 7.1 Hz, 3H). ¹³C NMR (126 MHz, CD₃CN) δ 166.28, 149.89, 140.61, 137.52, 129.52, 129.49, 128.42, 127.86, 127.78, 127.22, 125.31, 123.14, 120.75, 62.23, 43.07, 42.75, 42.43, 42.12, 41.85, 13.89. Melting Point: 94-95°C

Ethyl (2*R*,3*R*)-1-(9*H*-fluoren-2-yl)-3-(trifluoromethyl)aziridine-2-carboxylate (*trans*-**4D**): IR(ATR): 2997, 1735, 1613, 1579, 1486-1402, 1373, 1338, 1278, 1214, 1096, 1078, 1029cm⁻¹. ¹H NMR (500 MHz, CD₃CN) δ 7.76 (d, *J* = 7.6 Hz, 1H), 7.72 (d, *J* = 8.1 Hz, 1H), 7.54 (dd, *J* = 7.5, 0.8 Hz, 1H), 7.36 (td, *J* = 7.5, 0.8 Hz, 1H), 7.28 (td, *J* = 7.4, 1.1 Hz, 1H), 7.16 (d, *J* = 1.3 Hz, 1H), 6.96 (dd, *J* = 8.1, 2.1 Hz, 1H), 4.12 – 3.99 (m, 2H), 3.87 (s, 2H), 3.66 (qd, *J* = 5.1, 2.3 Hz, 1H), 3.53 (d, *J* = 2.2 Hz, 1H), 1.08 (t, *J* = 7.1 Hz, 3H). ¹³C NMR (125 MHz, CD₃CN) δ 165.51, 146.38, 145.38, 143.70, 141.57, 138.07, 127.37, 127.16, 126.91, 125.63, 124.99, 122.82, 120.93, 119.13, 117.13, 62.48, 42.56, 42.24, 41.92, 41.60, 40.22, 40.20, 36.99, 13.87. Melting Point: 125-126°C.

Ethyl (2*S*,3*R*)-1-(9*H*-fluoren-2-yl)-3-(trifluoromethyl)aziridine-2-carboxylate (*cis*-**4D**): IR(ATR): 2924, 1756, 1615, 1456, 1379, 1288, 1260, 1228, 1207, 1151, 1060cm⁻¹. ¹H NMR (500 MHz,

CD₃CN) δ 7.77 (t, J = 8.0 Hz, 2H), 7.55 (d, J = 7.5 Hz, 1H), 7.43 – 7.34 (m, 1H), 7.29 (td, J = 7.5, 1.1 Hz, 2H), 7.09 (dd, J = 8.1, 2.1 Hz, 1H), 4.27 (dddd, J = 17.9, 10.8, 7.1, 3.7 Hz, 2H), 3.89 (s, 1H), 3.38 (d, J = 6.5 Hz, 1H), 3.35 – 3.25 (m, 1H), 1.38 – 1.24 (m, 3H). ¹³C NMR (125 MHz, CD₃CN) δ 165.81, 149.12, 144.99, 143.23, 140.90, 137.96, 126.84, 126.47, 125.10, 124.06, 122.63, 120.53, 119.57, 118.54, 116.60, 61.65, 42.39, 42.07, 41.46, 29.35, 13.34. Melting Point: 85-87°C

Ethyl (2*R*,3*R*)-3-(trifluoromethyl)-1-(4-tritylphenyl)aziridine-2-carboxylate (*trans*-**4E**): IR (ATR): 3035, 3002, 1965, 1740, 1596, 1492, 1444, 1336, 1279, 1208, 1149, 701 cm⁻¹. ¹H NMR (500 MHz, CD₃CN) δ 7.32 – 7.10 (m, 17H), 6.88 – 6.81 (m, 2H), 4.08 – 3.89 (m, 2H), 3.61 (qd, J = 5.0, 2.3 Hz, 1H), 3.45 (d, J = 2.3 Hz, 1H), 1.00 (t, J = 7.1 Hz, 3H). ¹³C NMR (126 MHz, CD₃CN) δ 165.38, 147.52, 144.95, 142.99, 132.09, 131.27, 128.22, 127.06, 126.56, 124.89, 122.72, 120.55, 119.40, 64.99, 62.39, 42.14, 41.82, 41.50, 41.18, 40.04, 40.03, 13.89. Melting Point: 135-137°C

Ethyl (2*S*,3*R*)-3-(trifluoromethyl)-1-(4-tritylphenyl)aziridine-2-carboxylate (*cis*-**4E**): IR (ATR): 3032, 1983, 1739, 1603, 1491, 1273, 1148, 1027, 832, 700 cm⁻¹. ¹H NMR (500 MHz, CD₃CN) δ 7.47 – 7.10 (m, 18H), 7.03 – 6.91 (m, 1H), 4.34 – 4.11 (m, 2H), 3.30 (d, J = 6.5 Hz, 1H), 3.27 – 3.17 (m, 1H), 1.25 (t, J = 7.1 Hz, 3H). ¹³C NMR (126 MHz, CD₃CN) δ 166.26, 148.17, 147.51, 143.58, , 133.07, 132.29, 130.34, 128.96, 128.51, 128.35, 126.88, 126.58, 126.56, 119.33, 65.03, 62.18, 42.65, 42.33, 41.82, 41.73, 41.18, 40.05, 13.89. Melting Point: 132-133°C

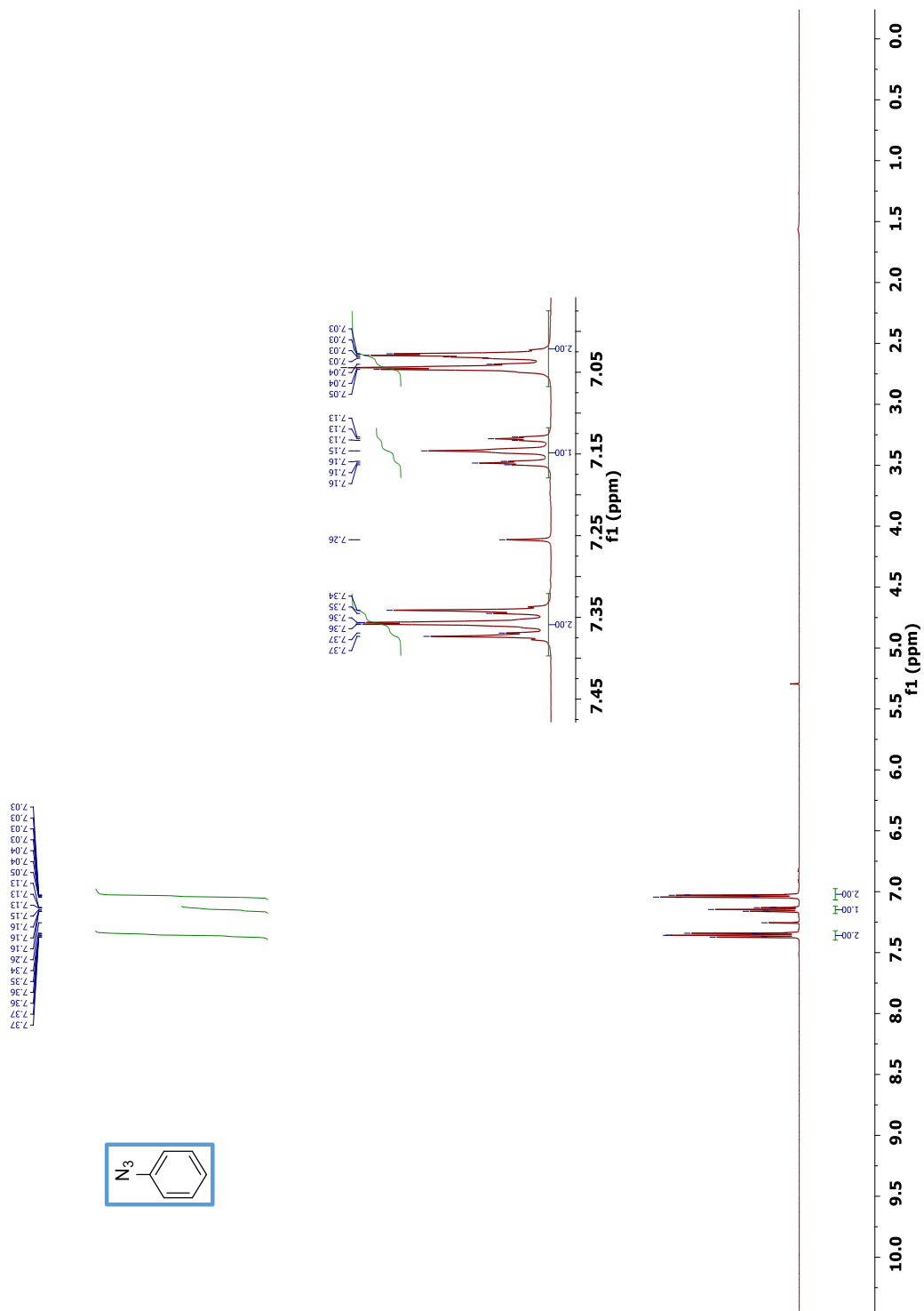
3.5 Appendix

Characterization for Chapter 3

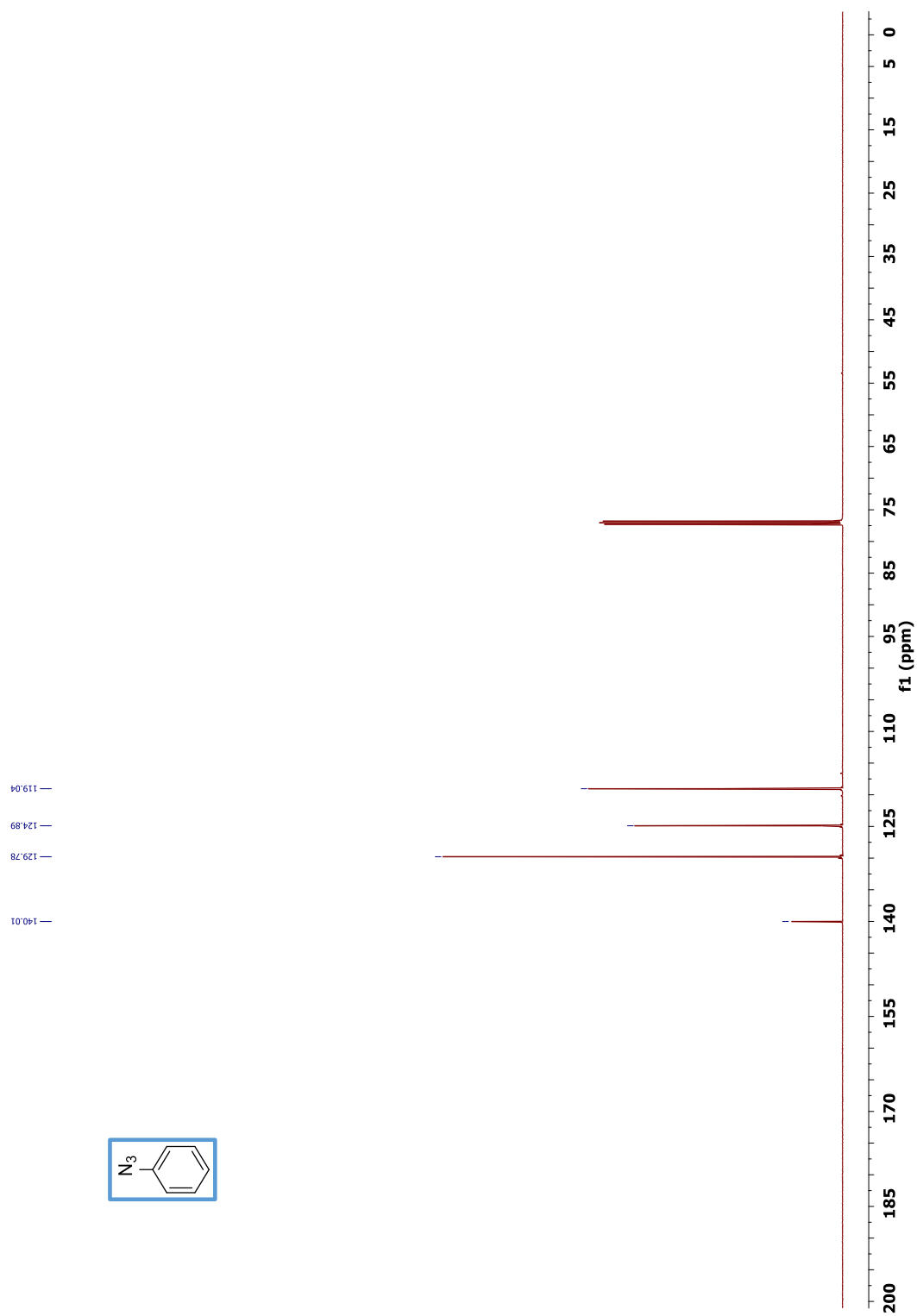
3.5.1	Compound Spectra (^1H NMR, ^{13}C NMR, UV-Vis).....	98
3.5.2	Computational Data.....	156

3.5.1 Compound Spectra (^1H NMR, ^{13}C NMR, UV-Vis)

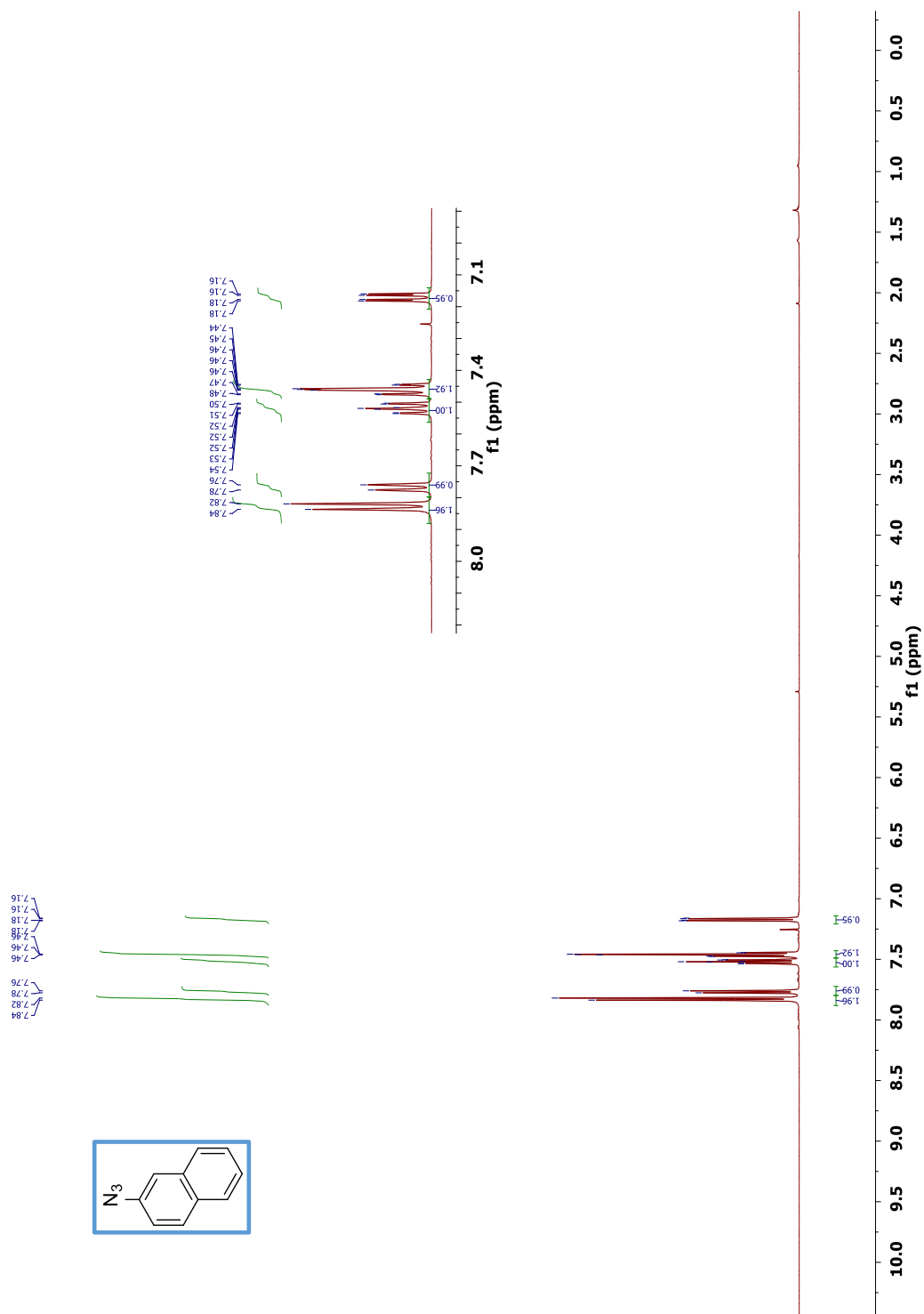
^1H NMR (500 MHz, CDCl_3) of compound **2A**.



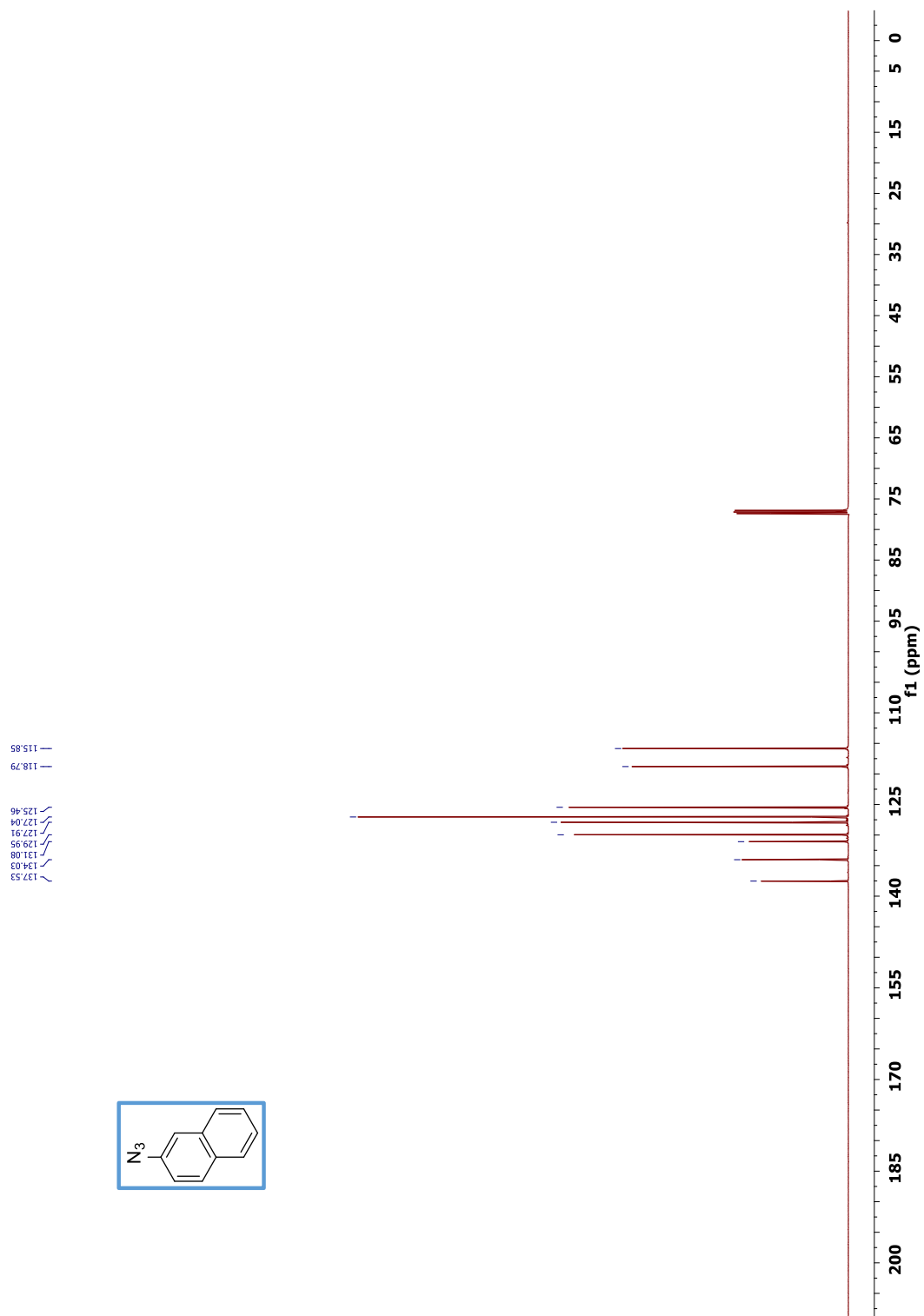
^{13}C NMR (126 MHz, CDCl_3) of compound **2A**.



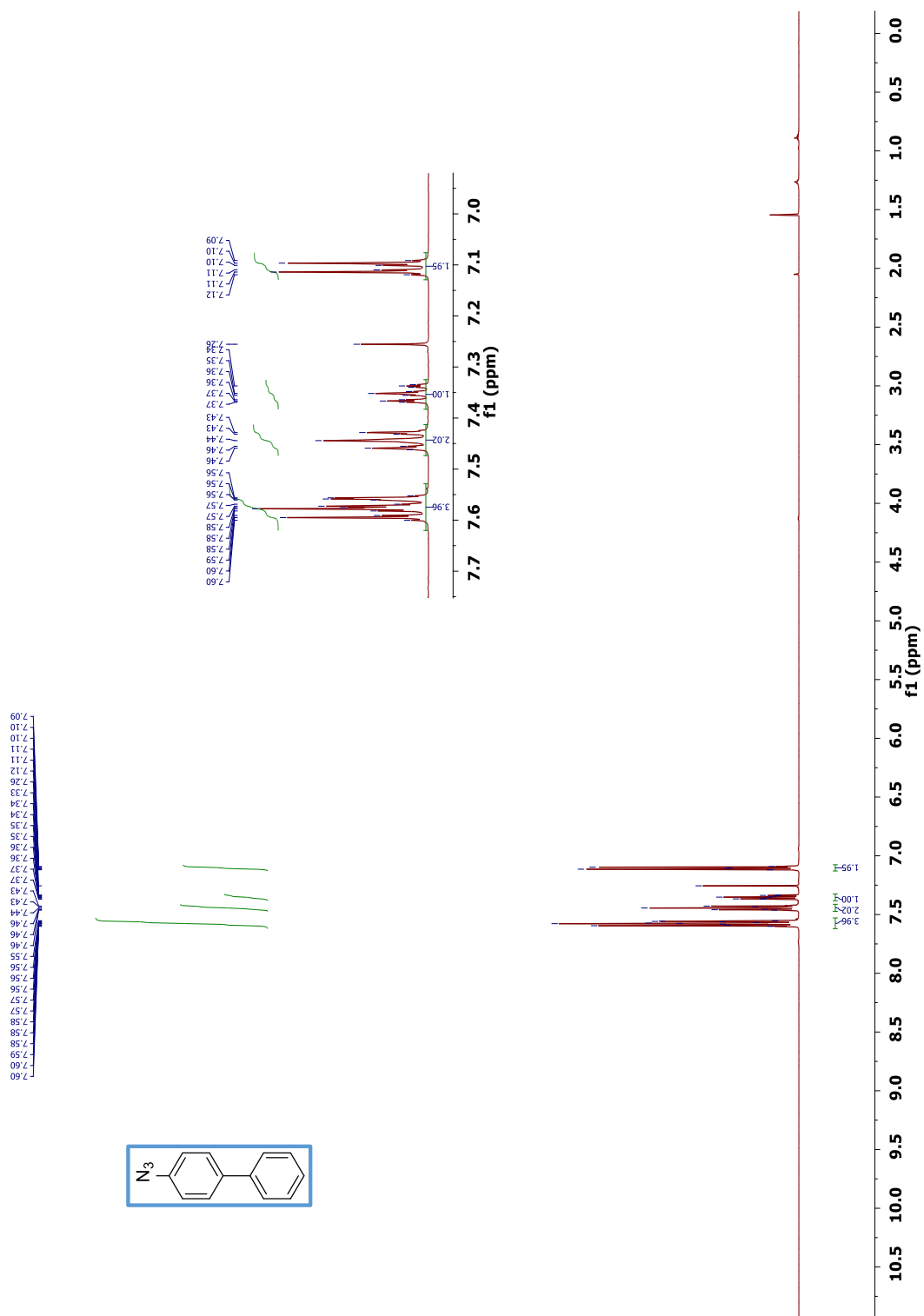
^1H NMR (500 MHz, CDCl_3) of compound **2B**.



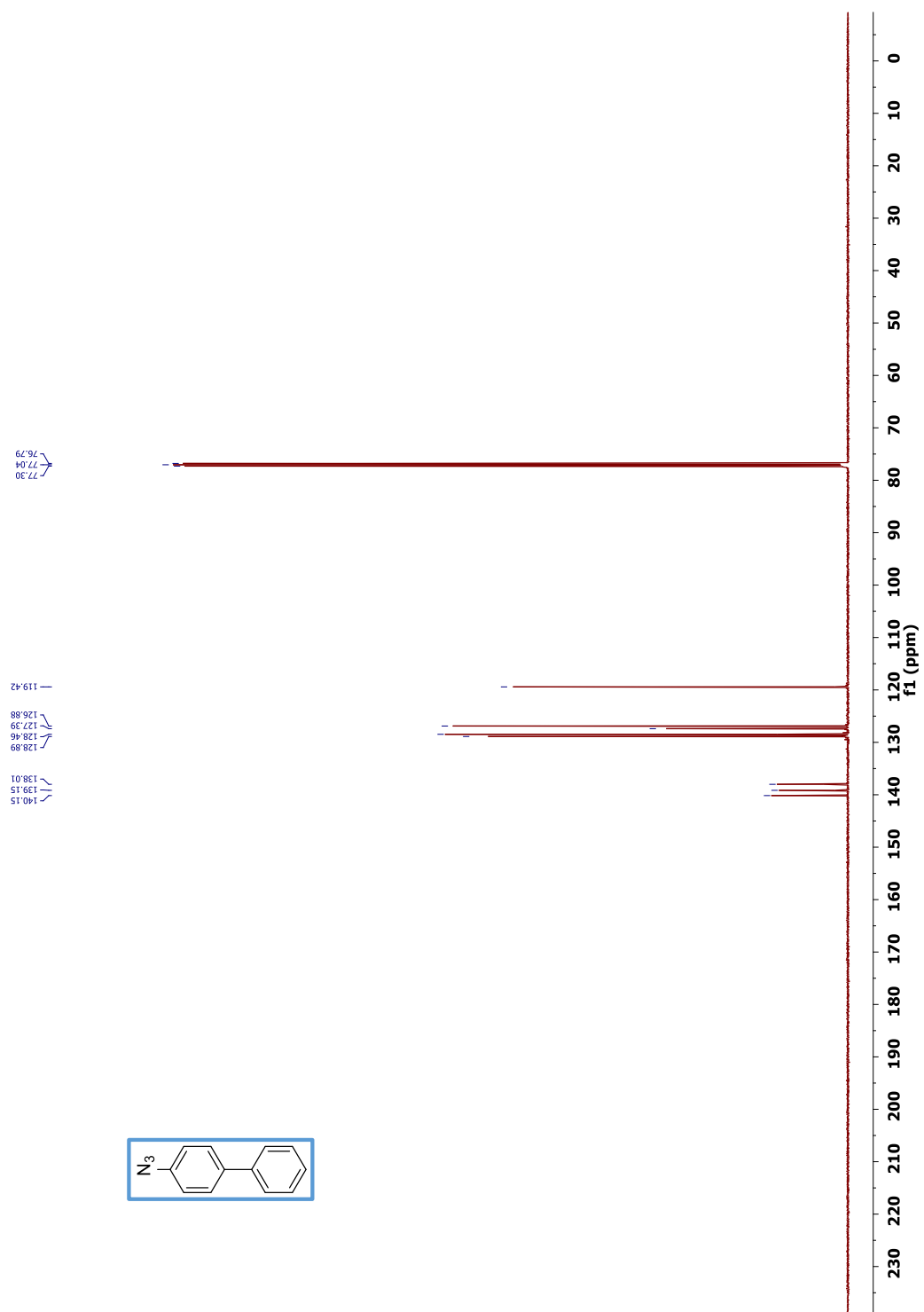
^{13}C NMR (126 MHz, CDCl_3) of compound **2B**.



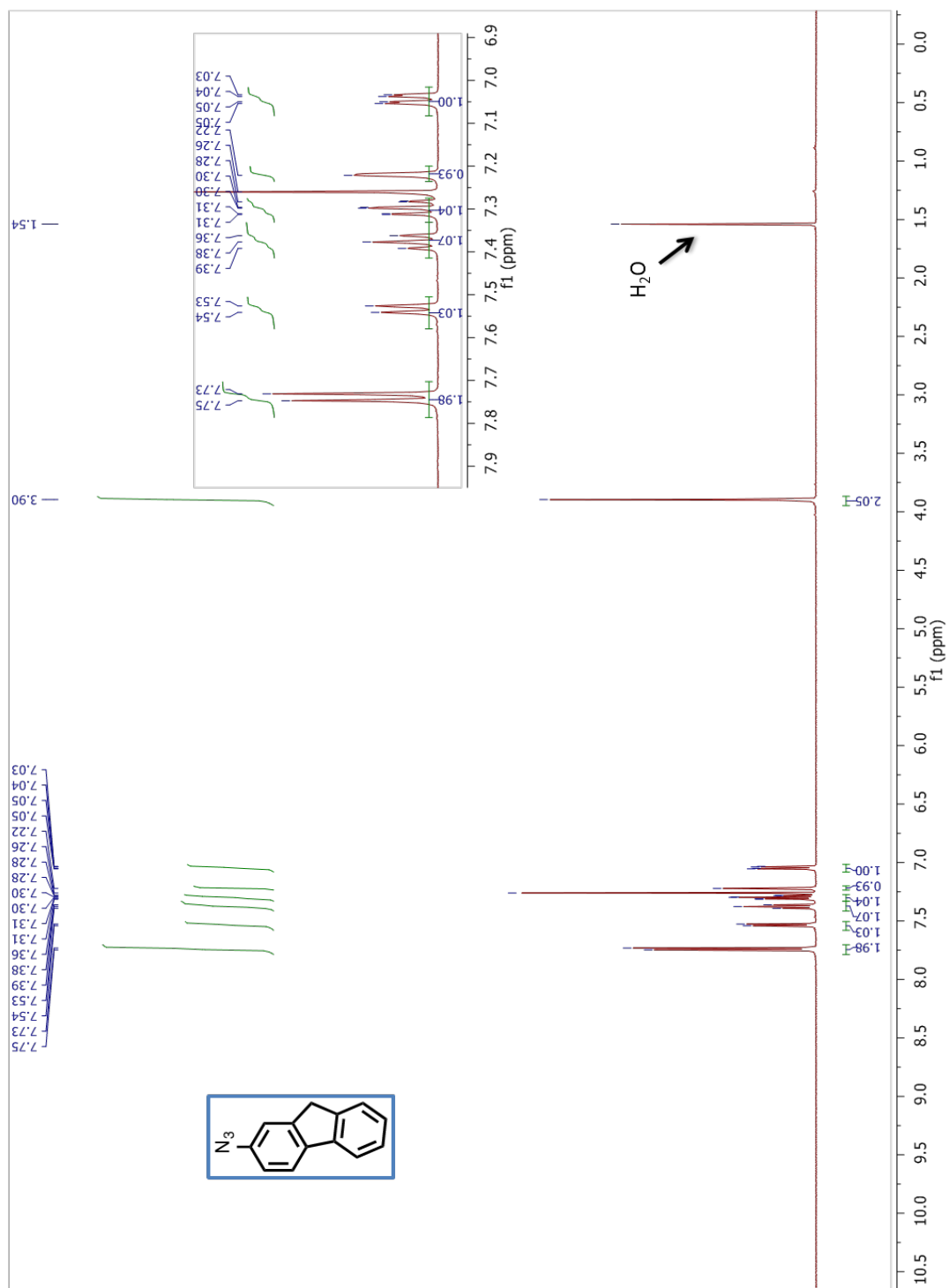
^1H NMR (500 MHz, CDCl_3) of compound **2C**.



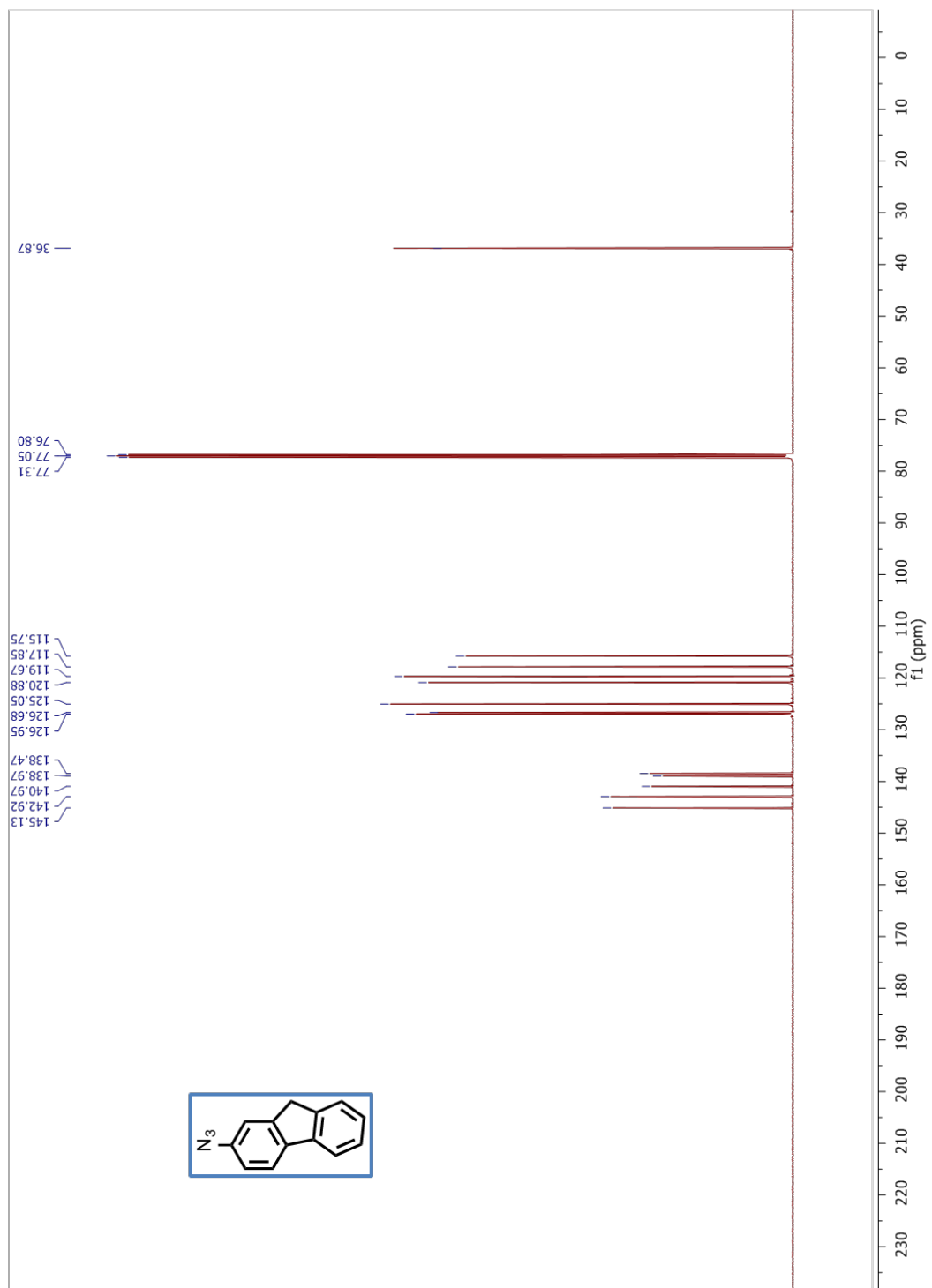
^{13}C NMR (126 MHz, CDCl_3) of compound **2C**.



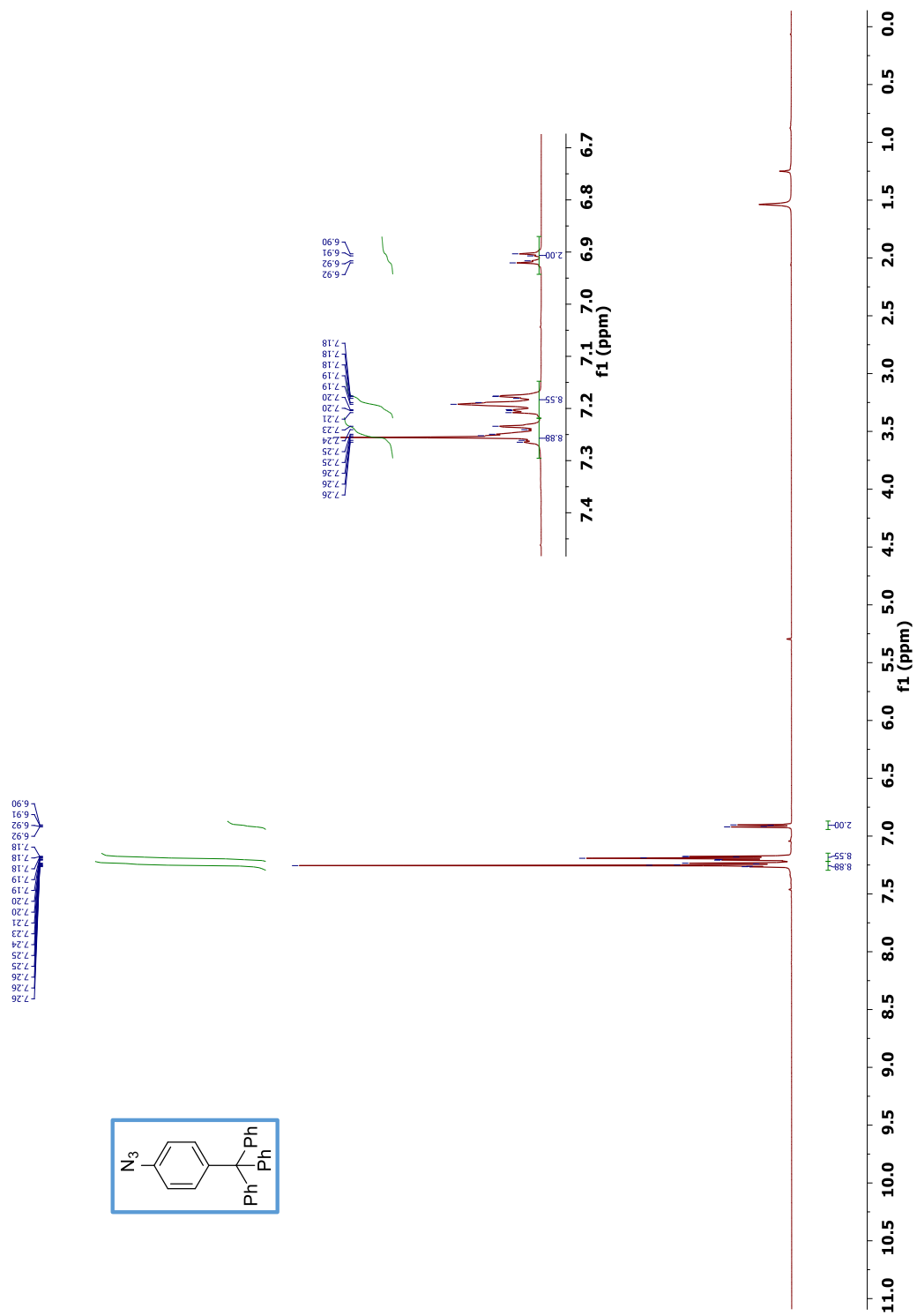
^1H NMR (500 MHz, CDCl_3) of compound **2D**.



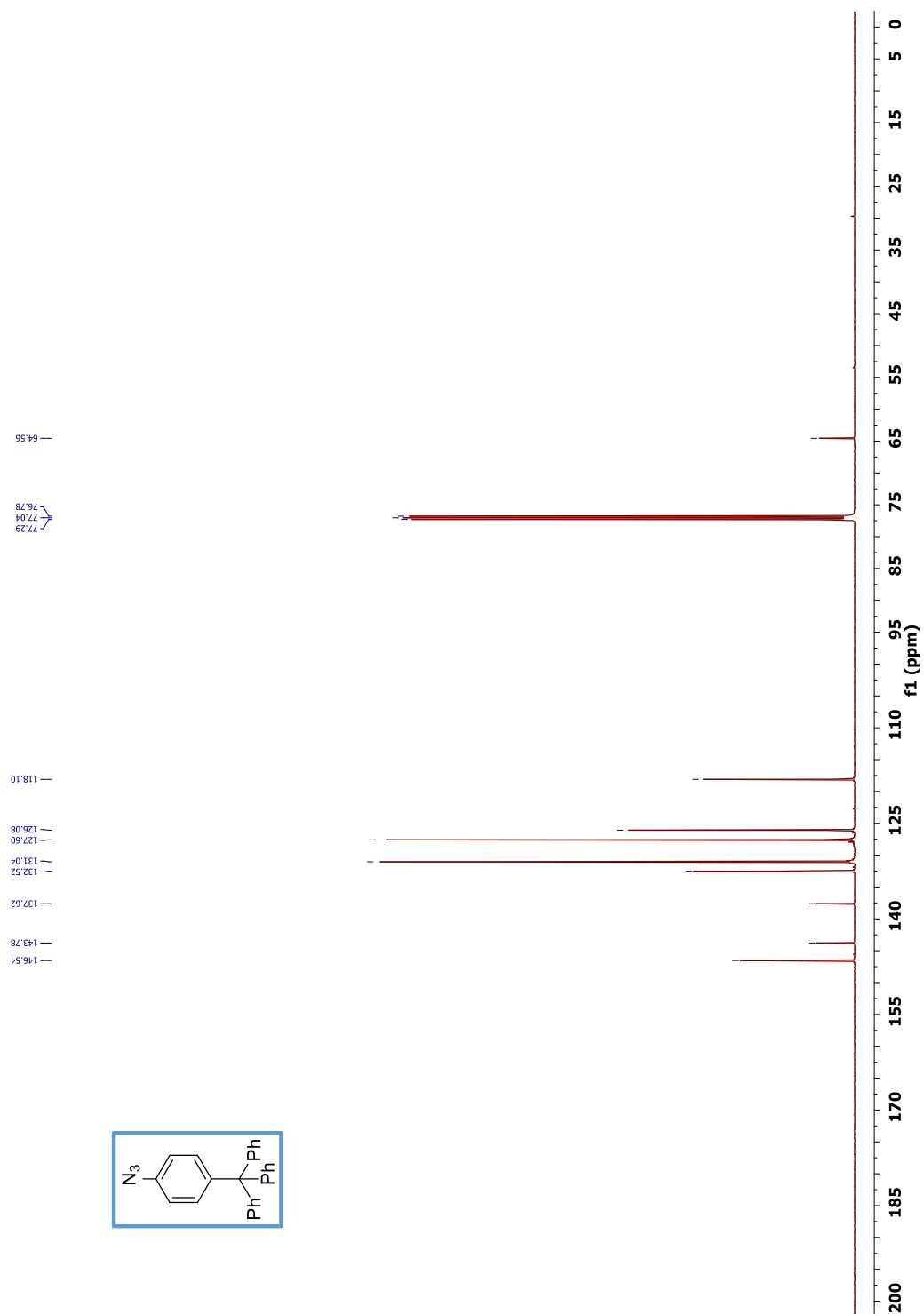
^{13}C NMR (126 MHz, CDCl_3) of compound **2D**.



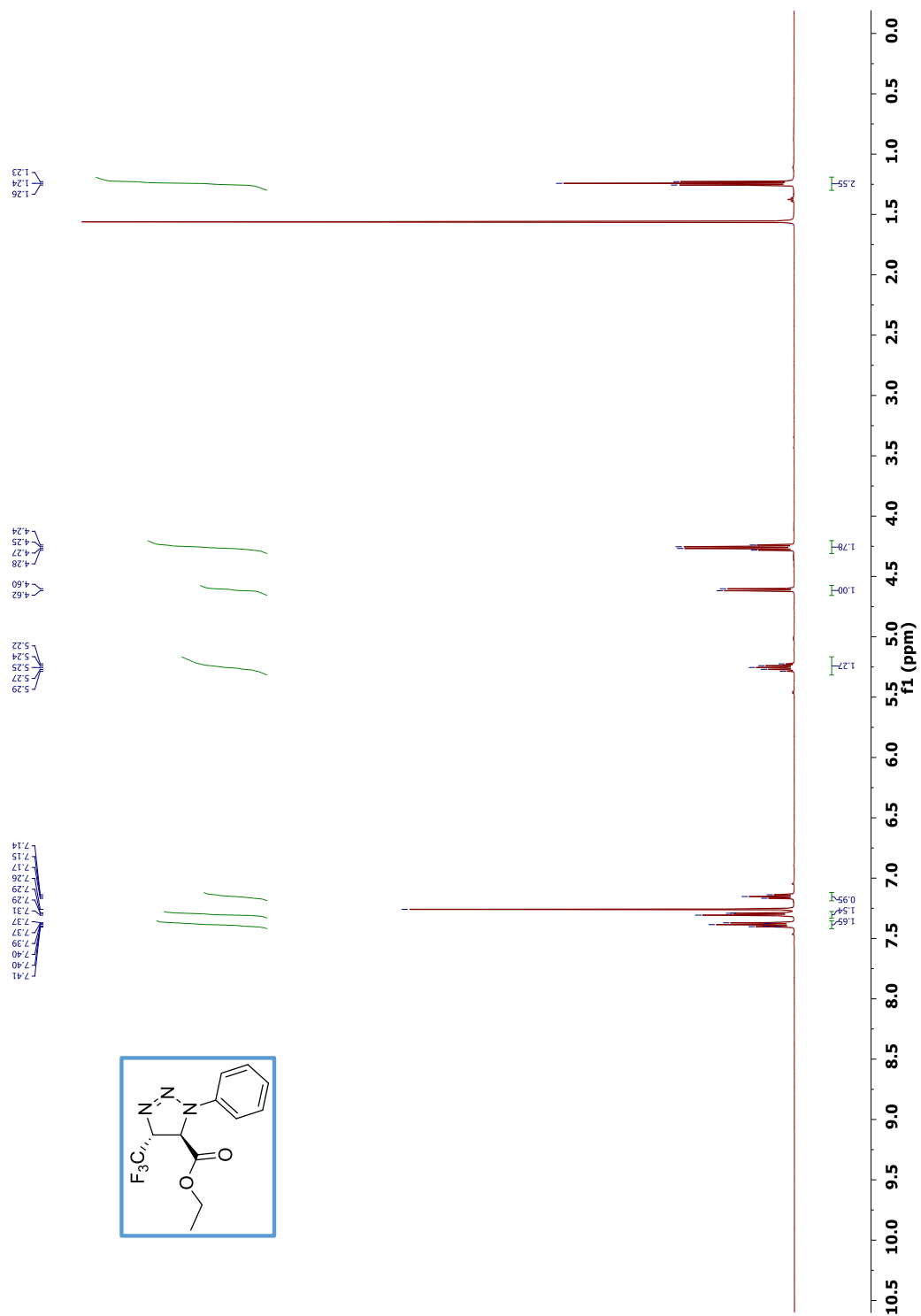
^1H NMR (500 MHz, CDCl_3) of compound **2E**.



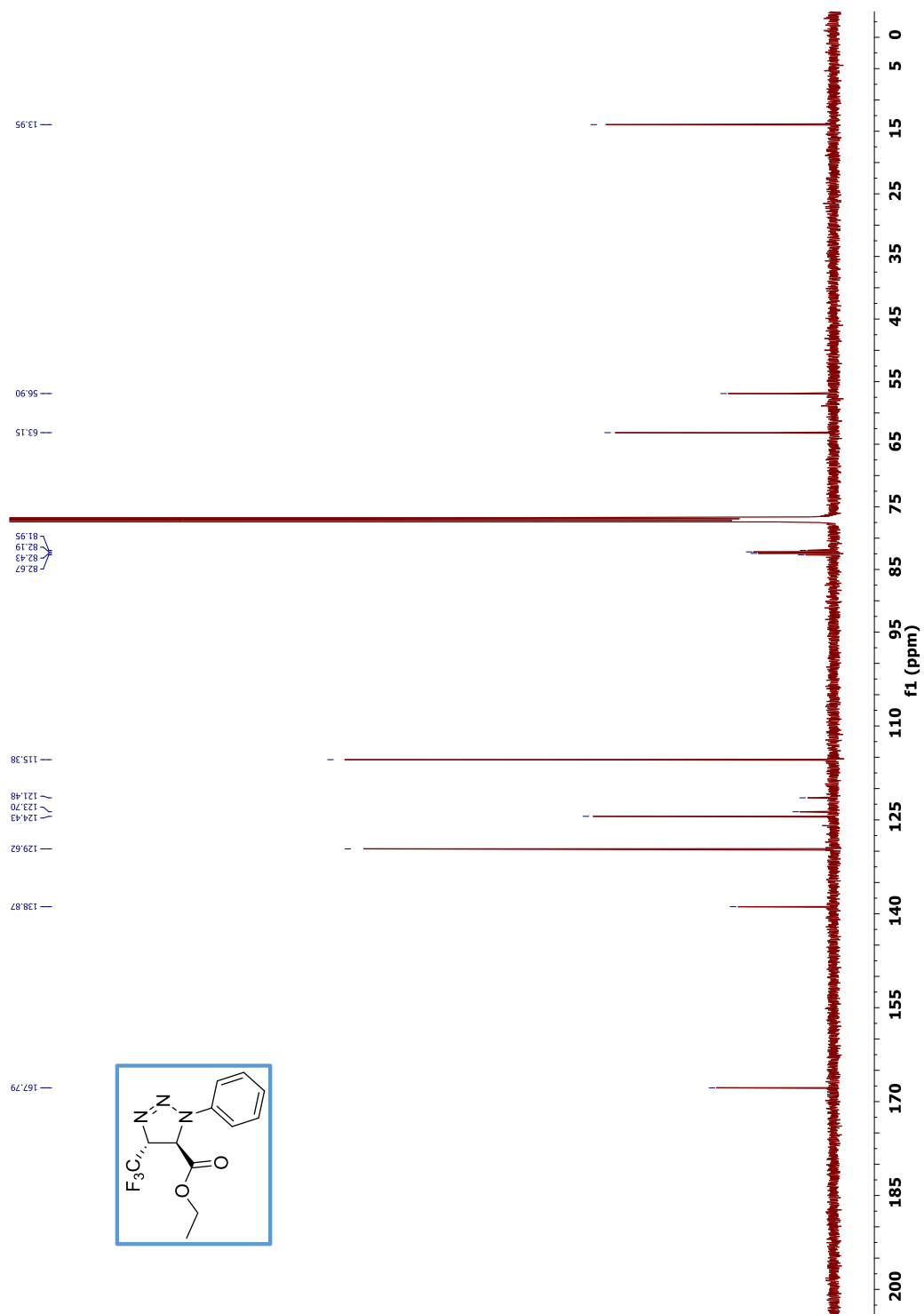
^{13}C NMR (126 MHz, CDCl_3) of compound **2E**.



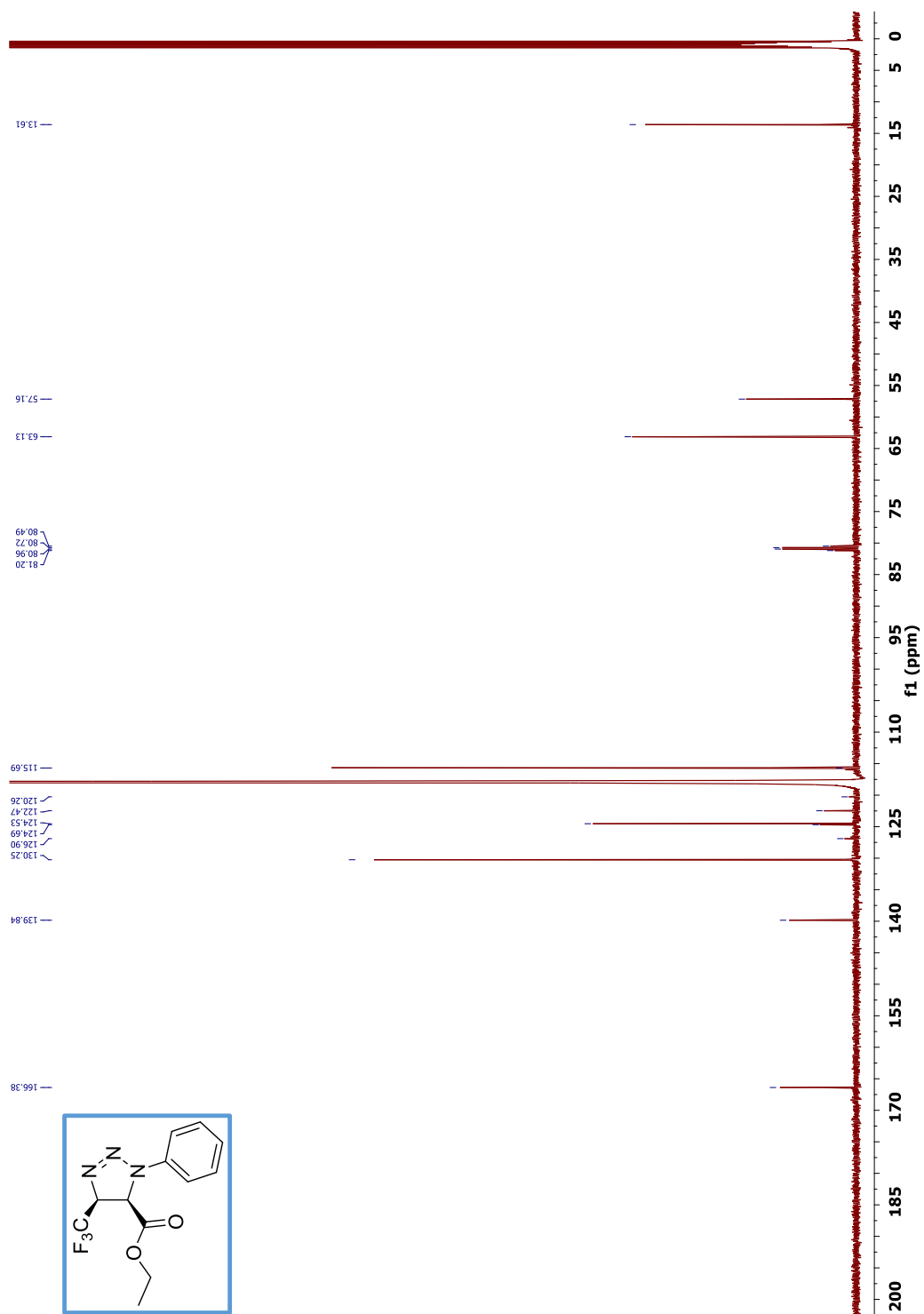
^1H NMR (500 MHz, CDCl_3) of compound *trans*-3A.



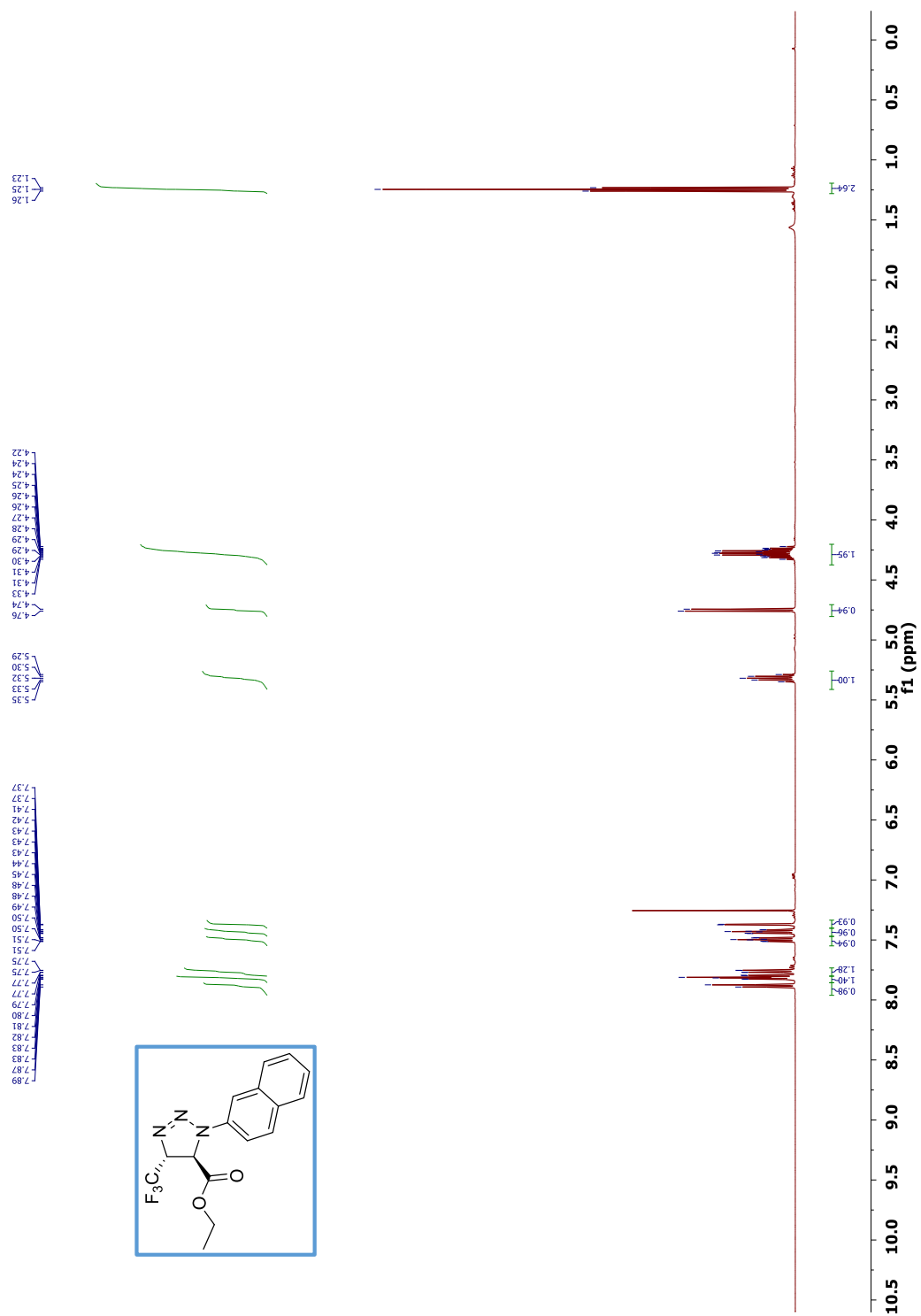
^{13}C NMR (126 MHz, CDCl_3) of compound *trans*-3A.



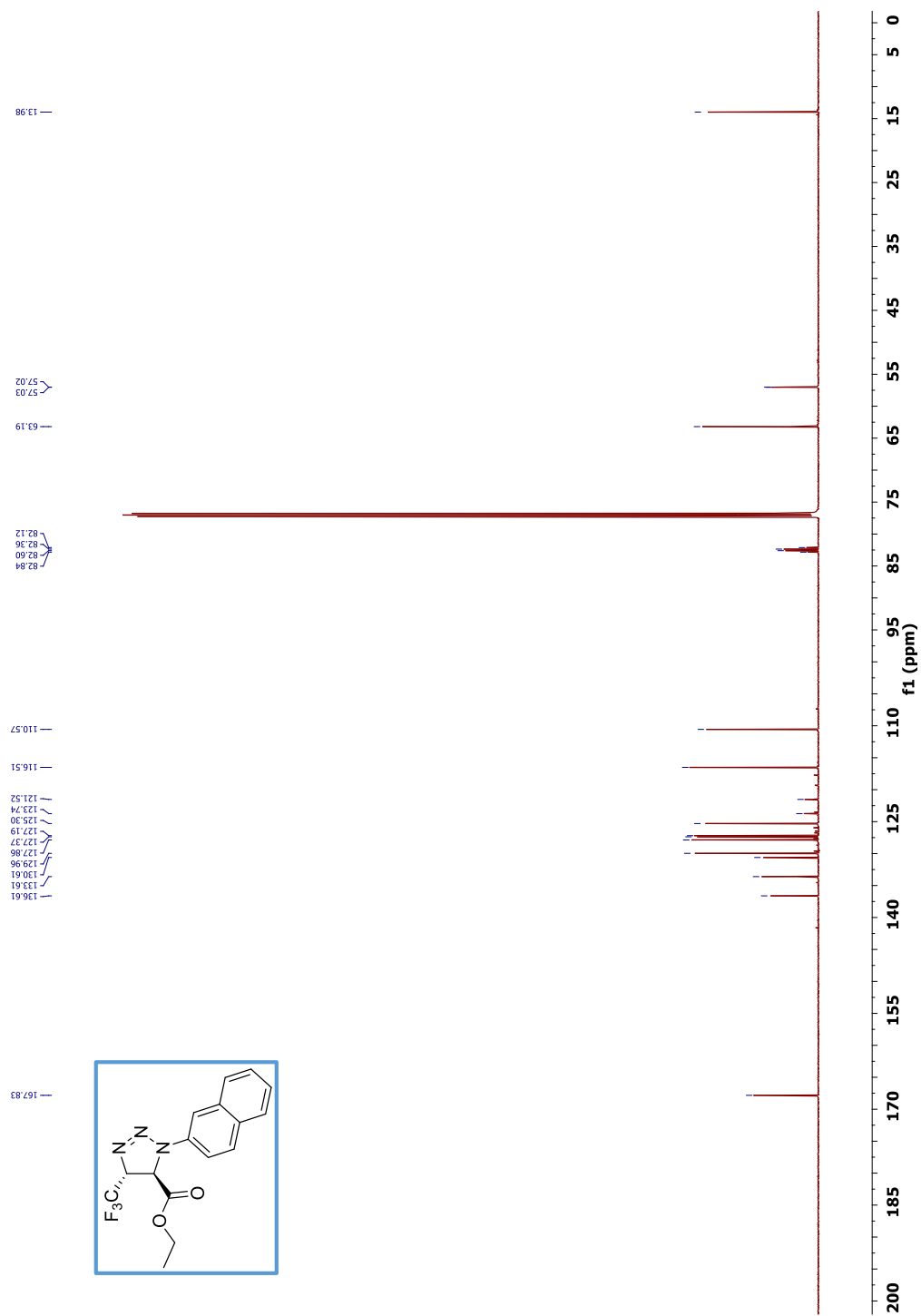
^{13}C NMR (126 MHz, CD_3CN) of compound *cis*-3A.



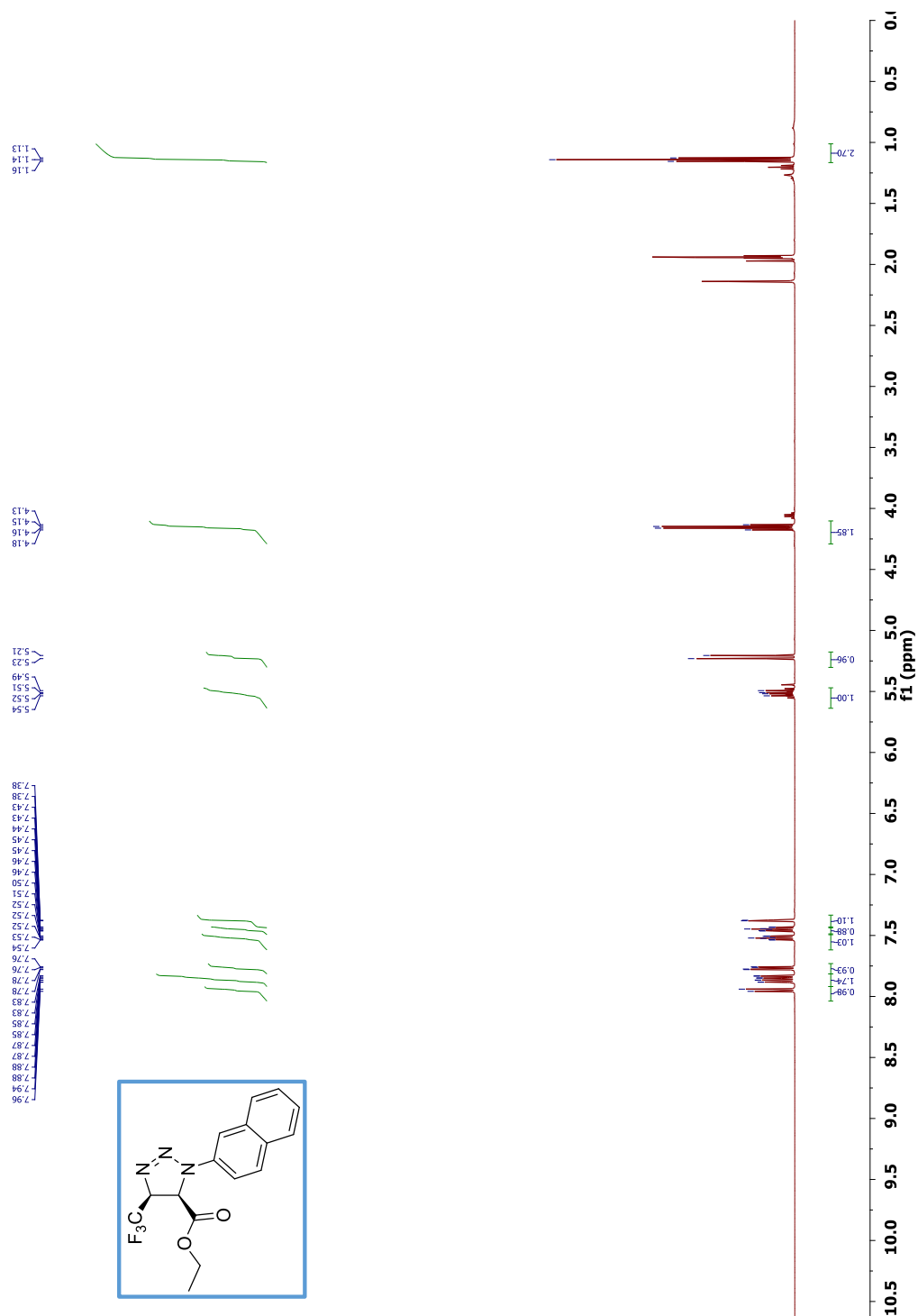
^1H NMR (500 MHz, CDCl_3) of compound *trans*-**3B**.



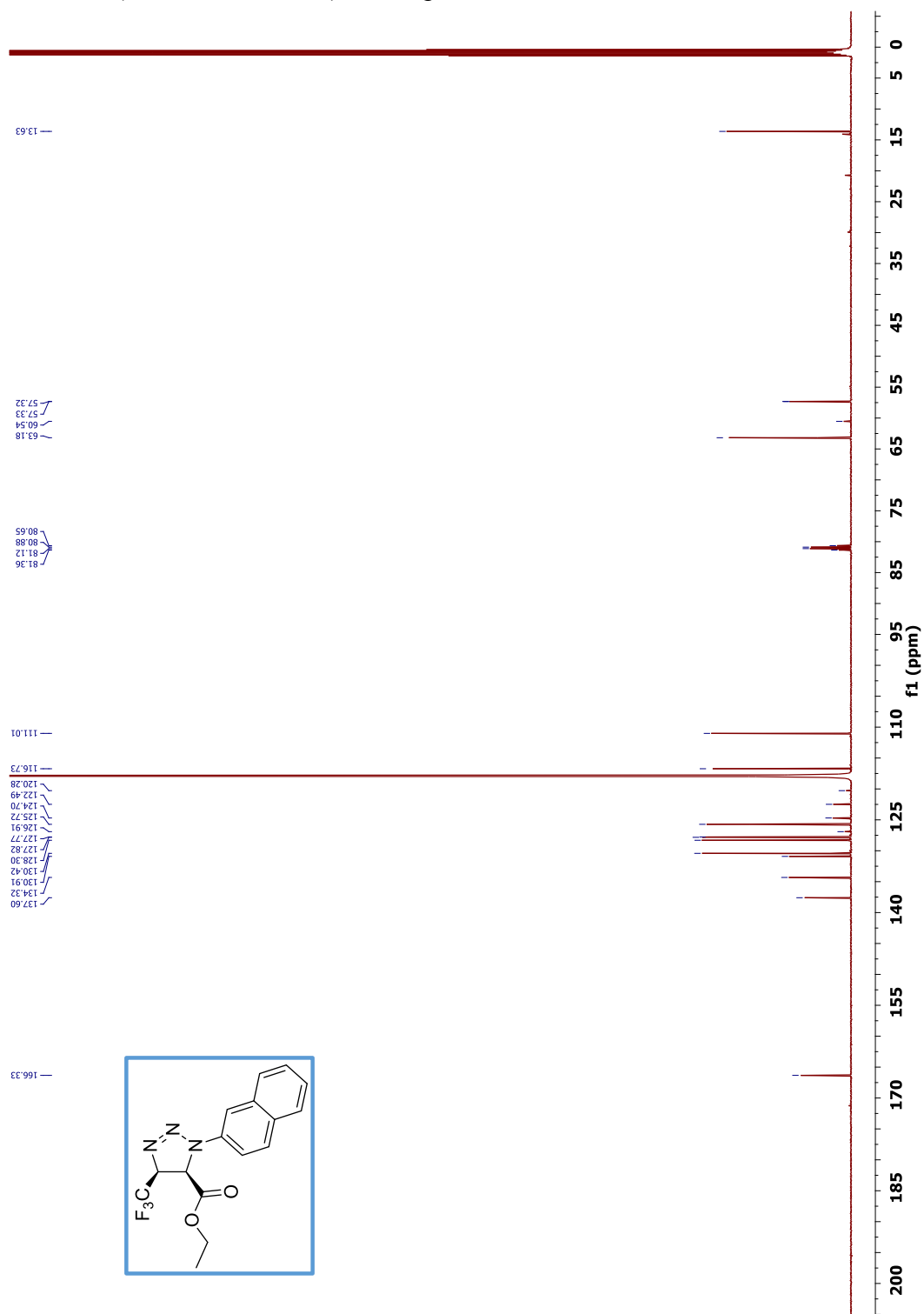
^{13}C NMR (126 MHz, CDCl_3) of compound *trans*-**3B**.



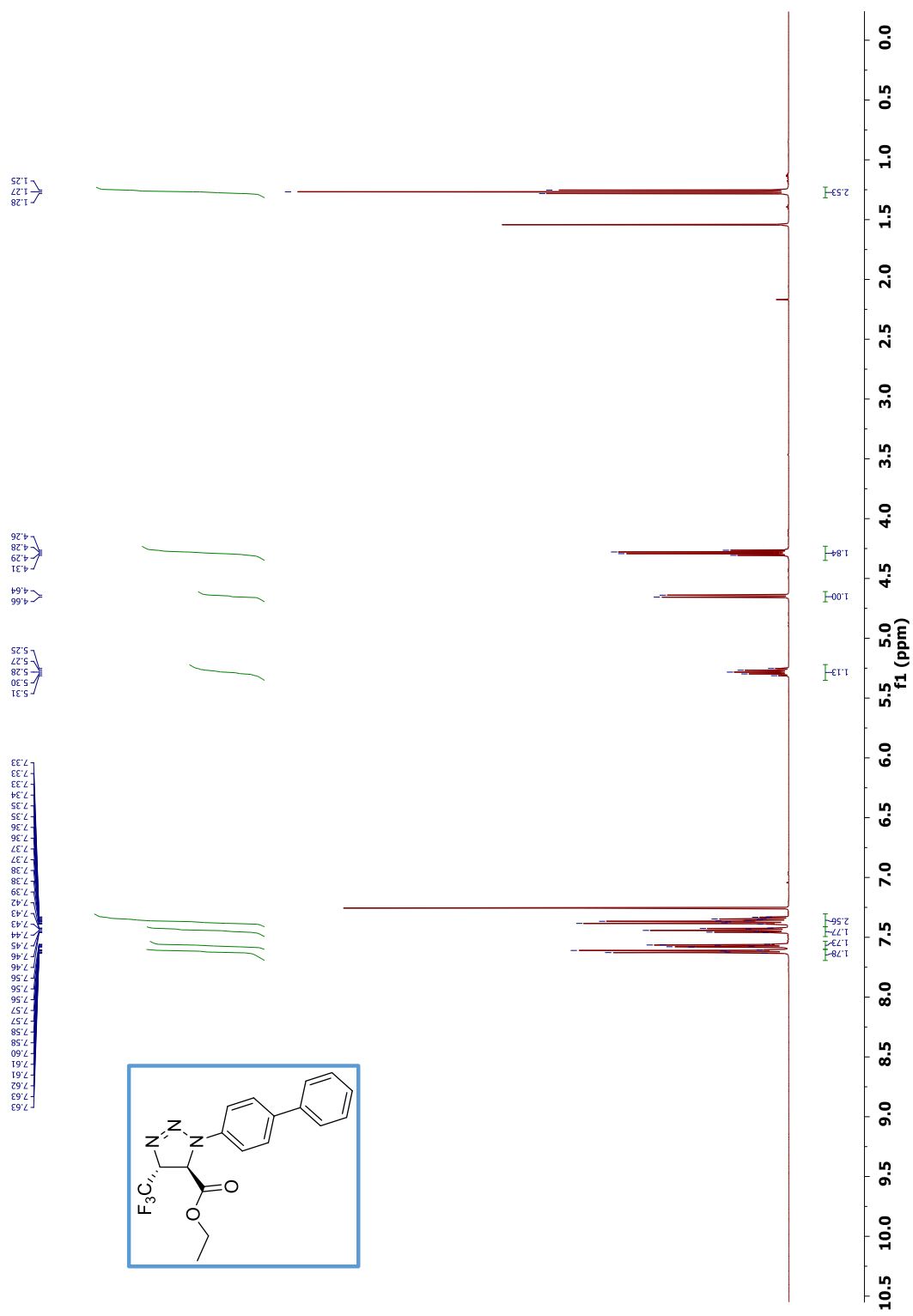
^1H NMR (500 MHz, CD_3CN) of compound *cis*-**3B**.



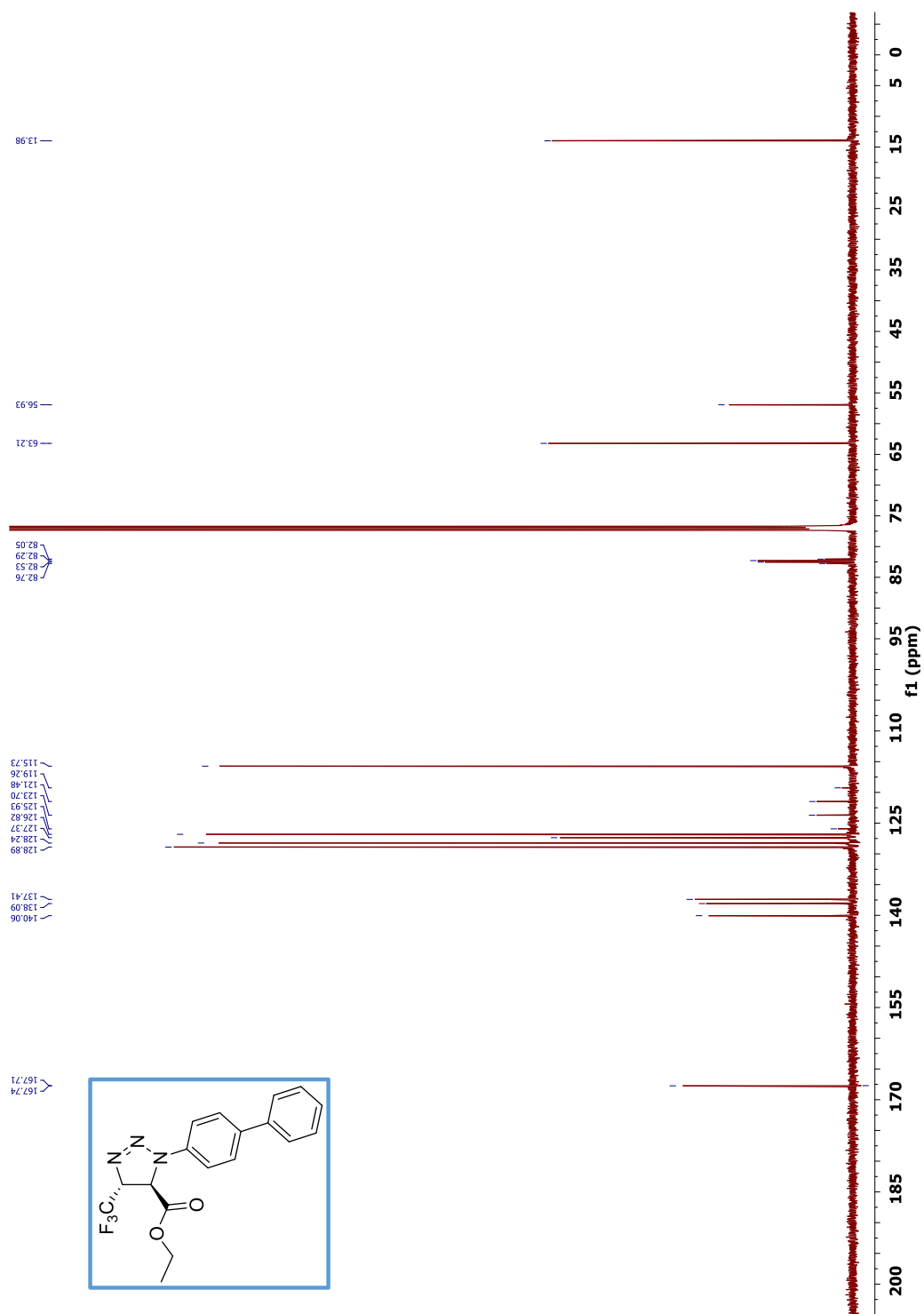
^{13}C NMR (126 MHz, CD_3CN) of compound *cis*-**3B**.



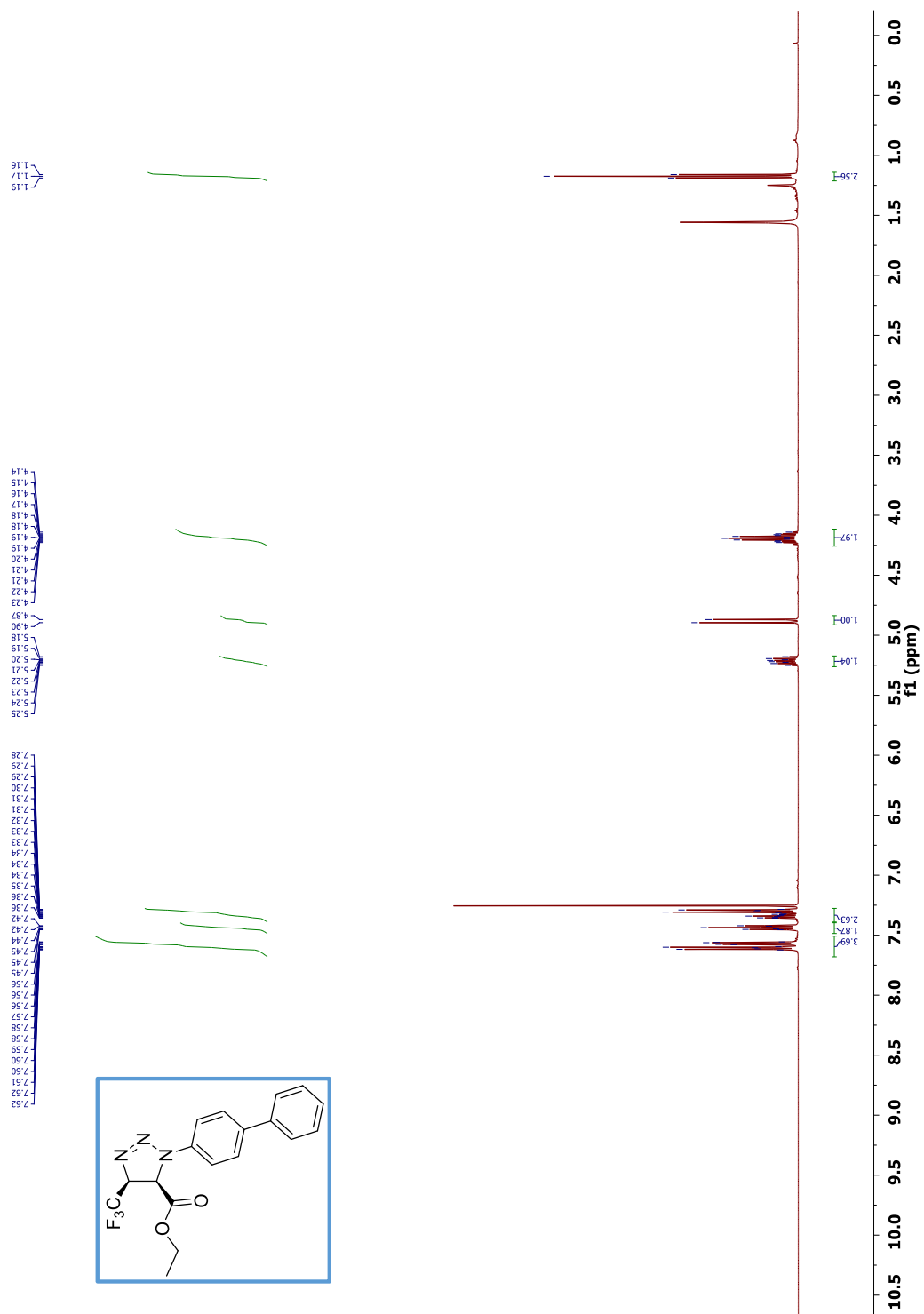
^1H NMR (500 MHz, CDCl_3) of compound *trans*-3C.



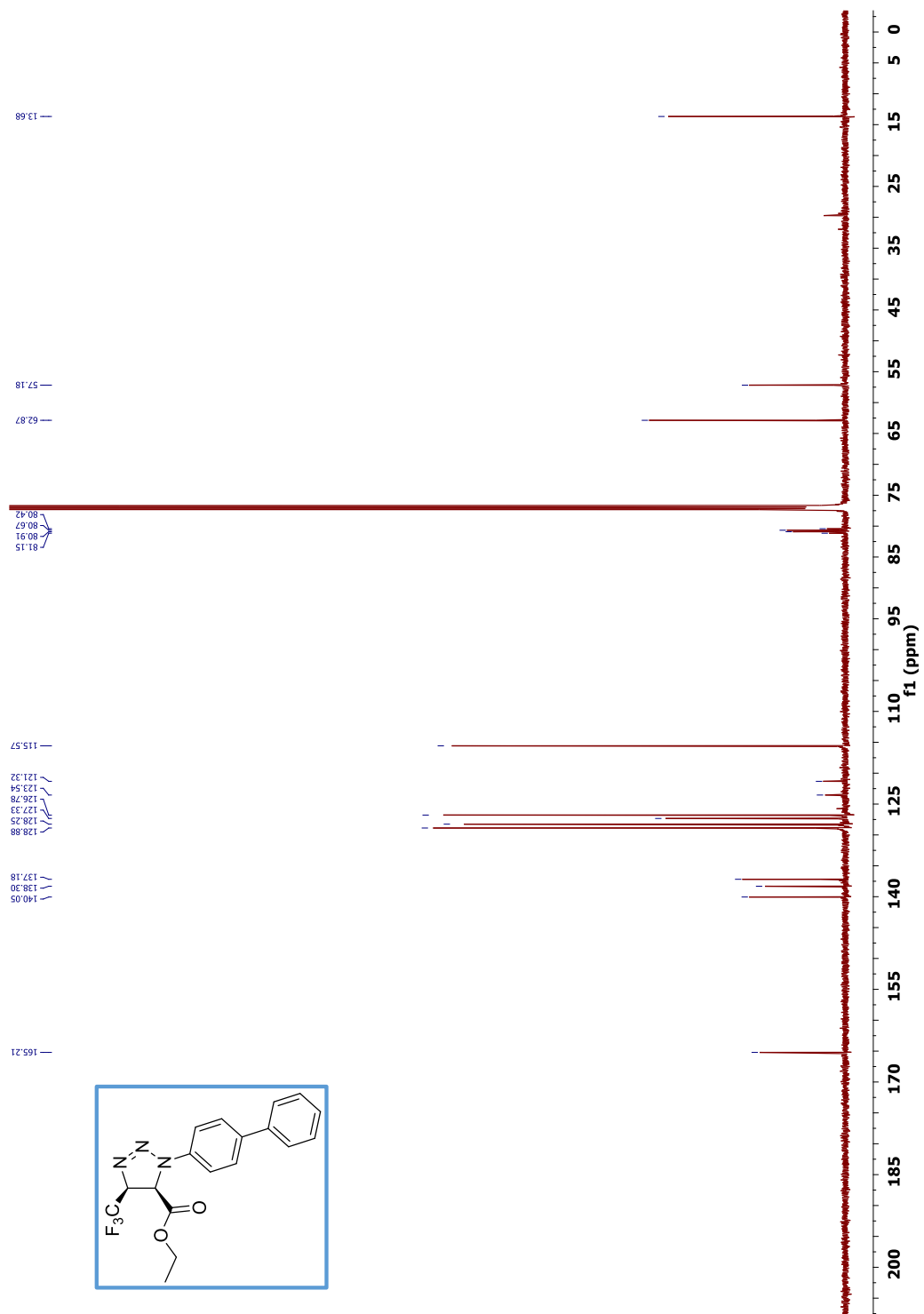
^{13}C NMR (126 MHz, CDCl_3) of compound *trans*-3C.



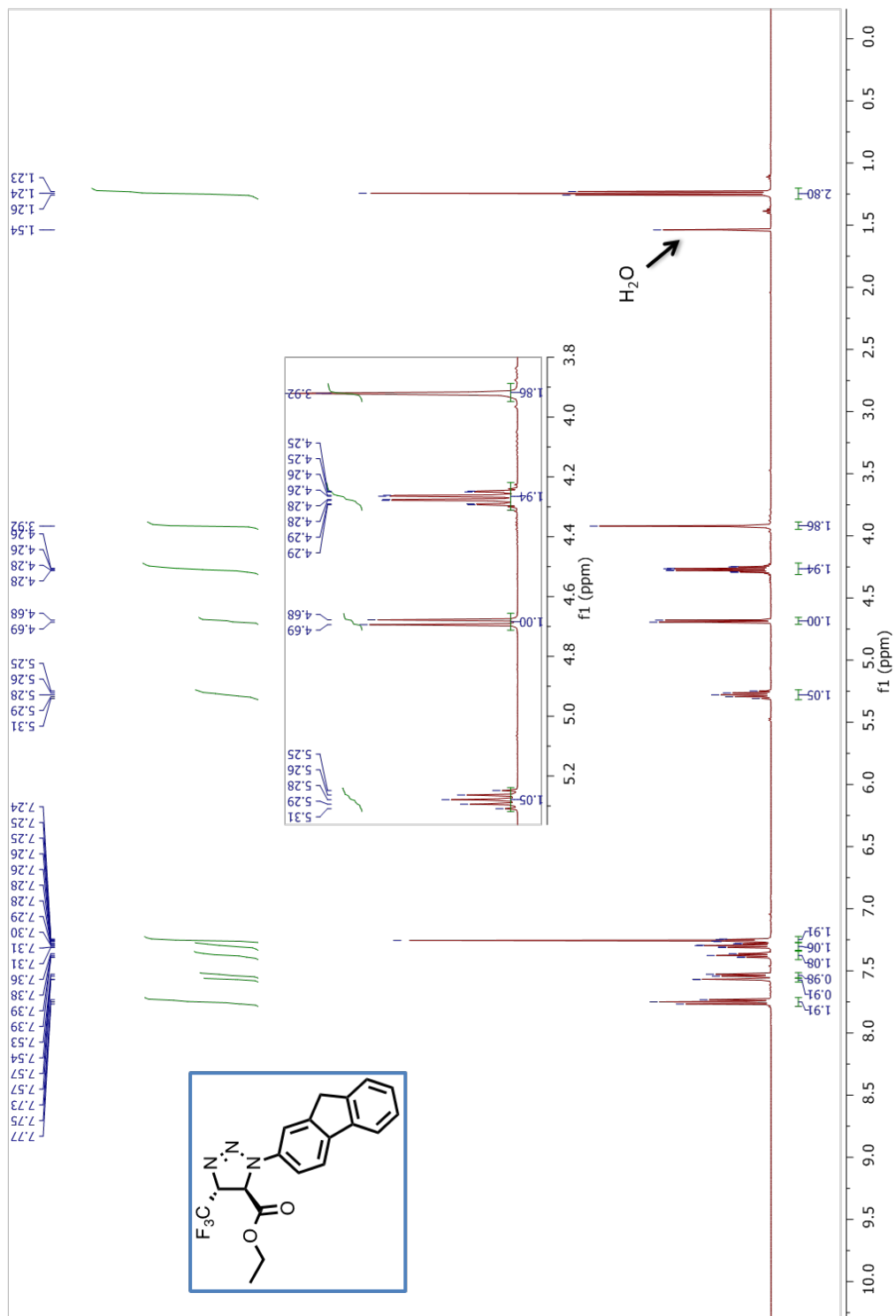
^1H NMR (500 MHz, CDCl_3) of compound *cis*-3C.



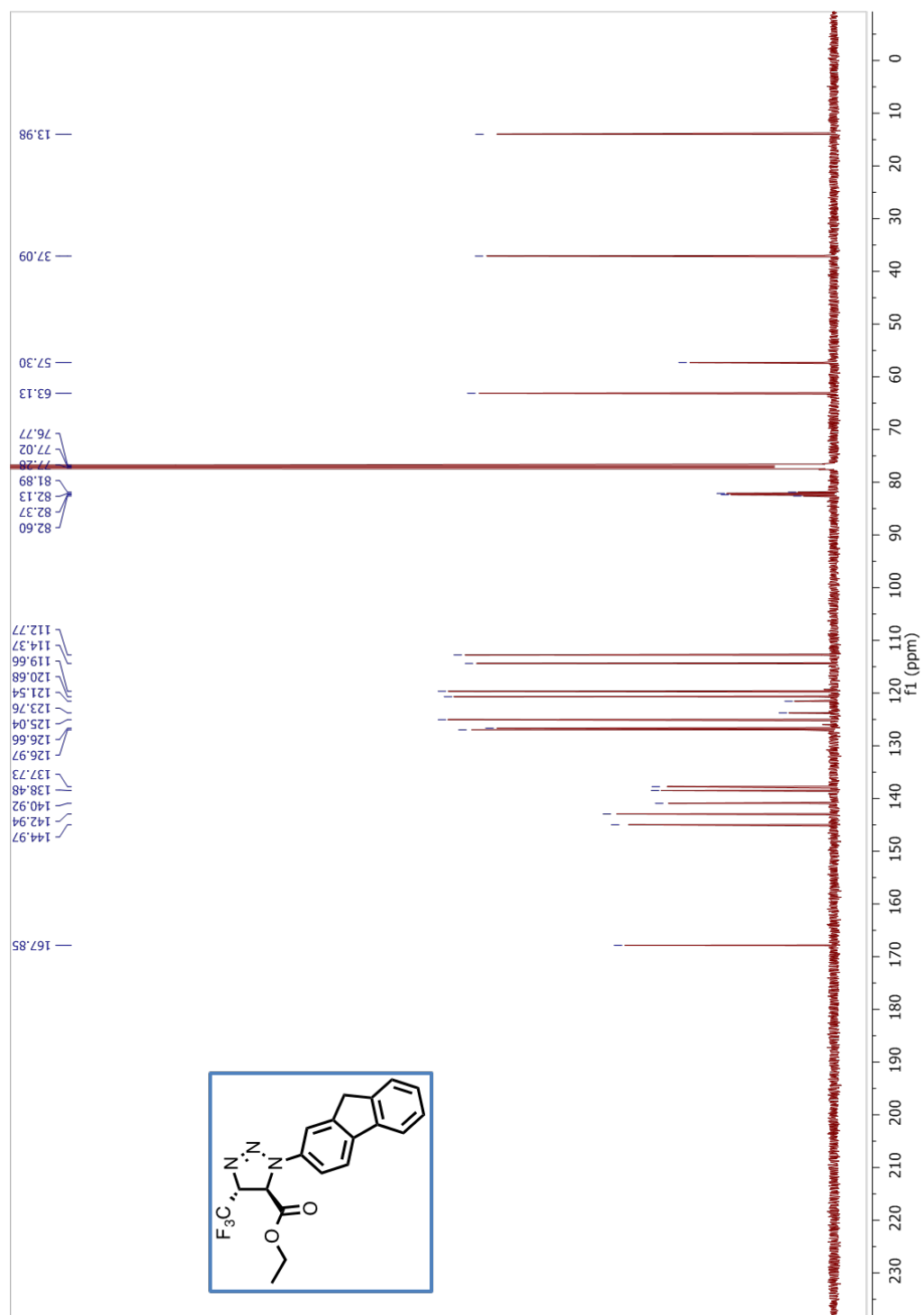
^{13}C NMR (126 MHz, CDCl_3) of compound *cis*-3C.



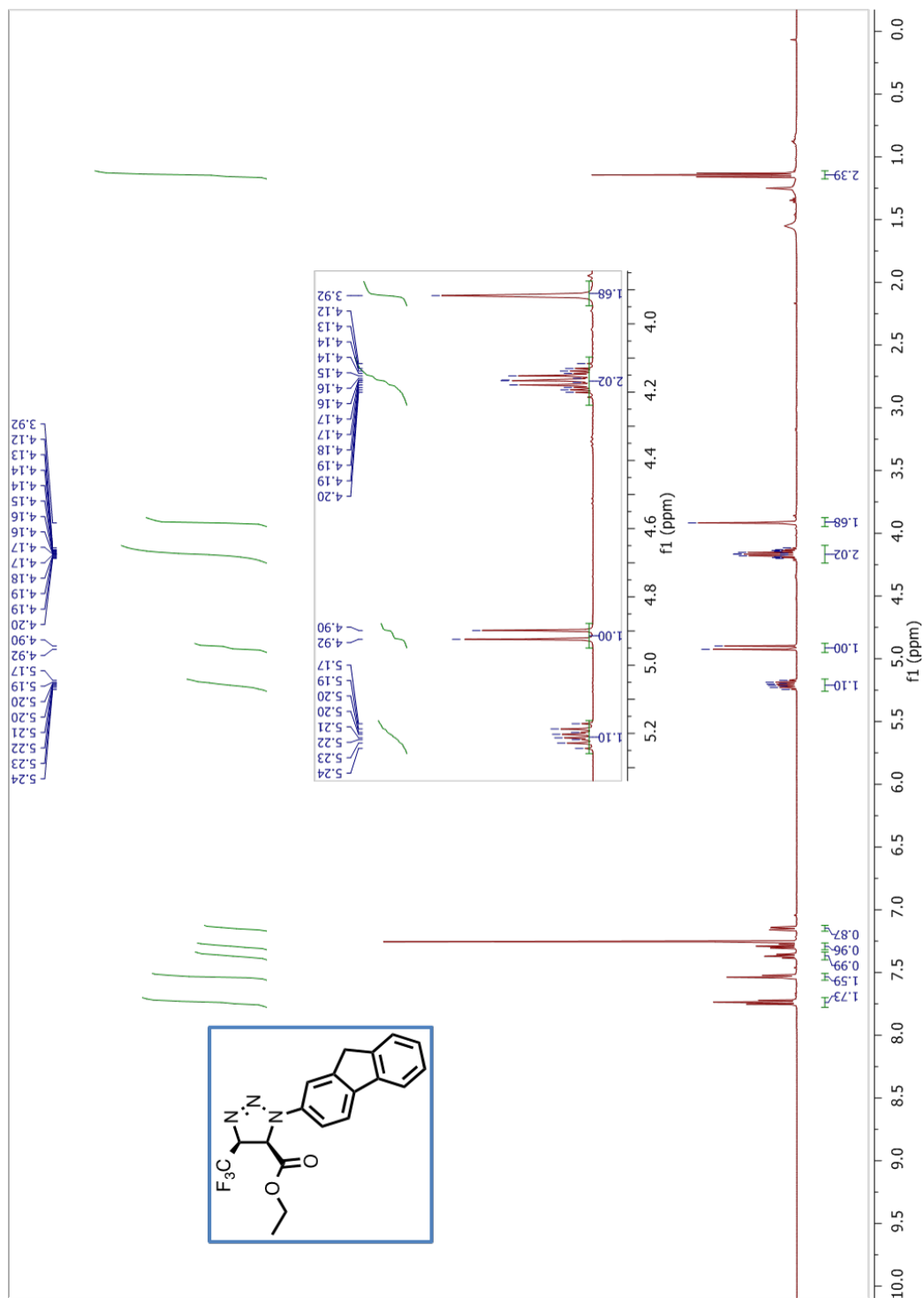
^1H NMR (500 MHz, CDCl_3) of compound *trans*-3D.



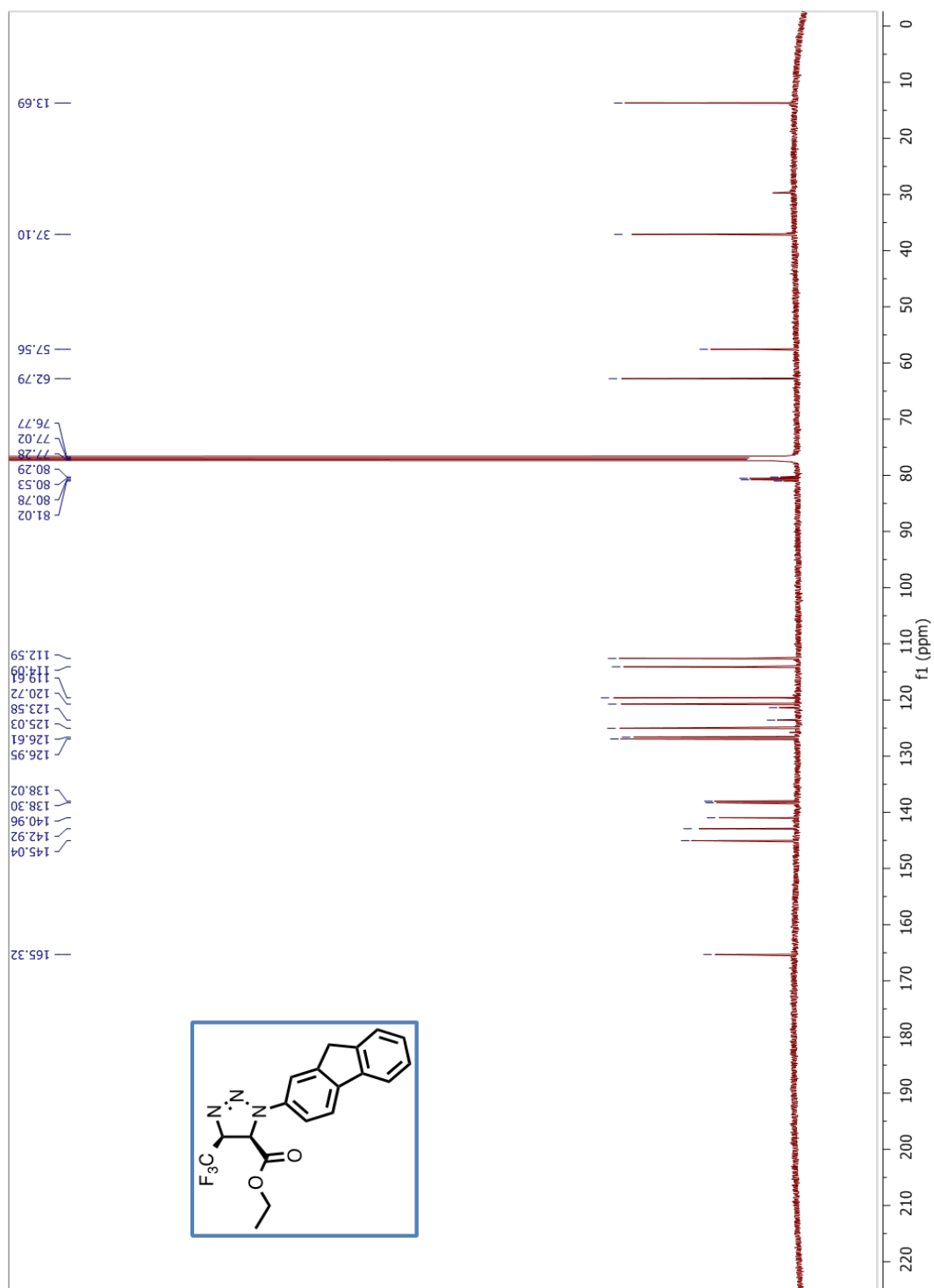
^{13}C NMR (126 MHz, CDCl_3) of compound *trans*-**3D**.



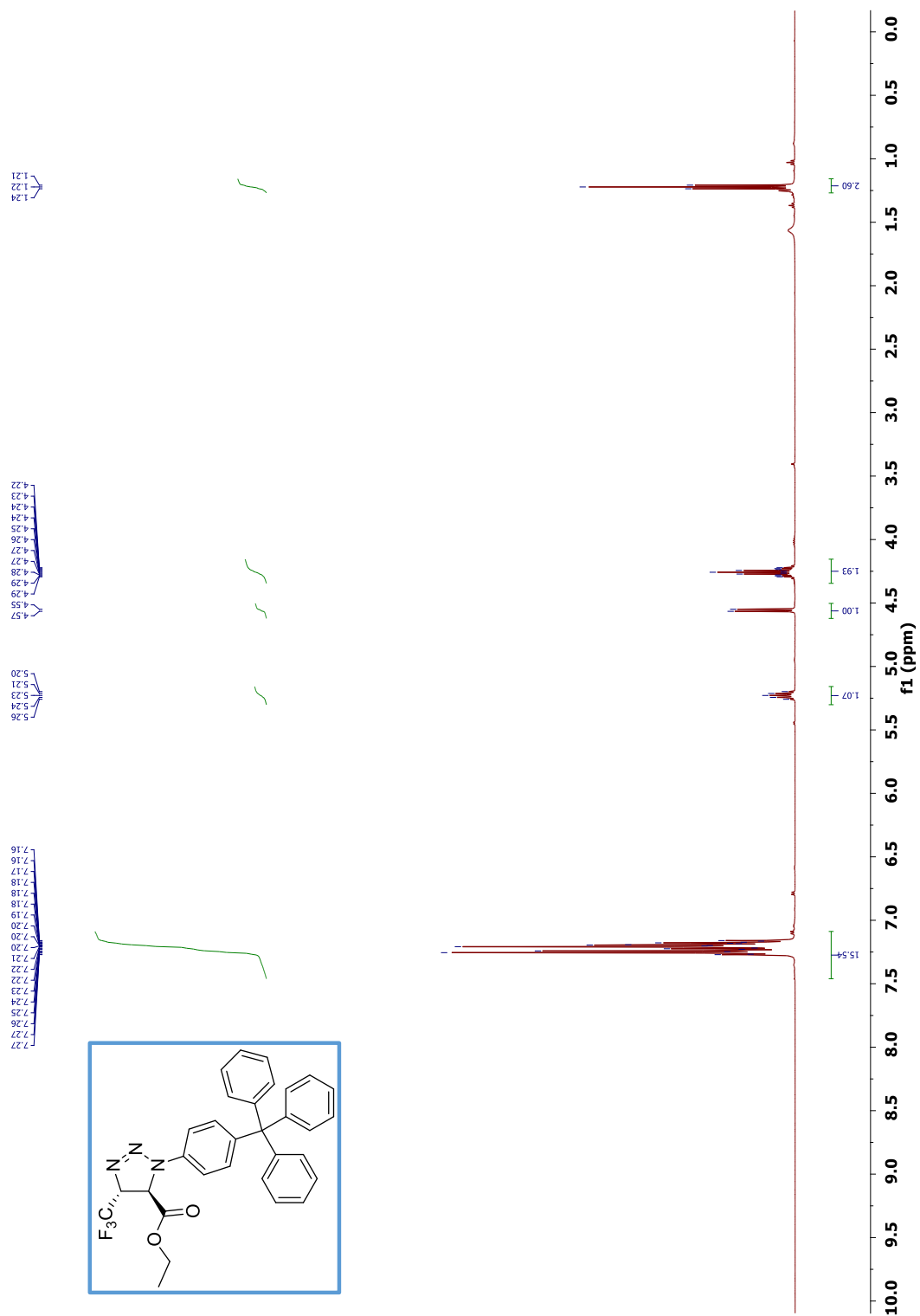
^1H NMR (500 MHz, CDCl_3) of compound *cis*-3D.



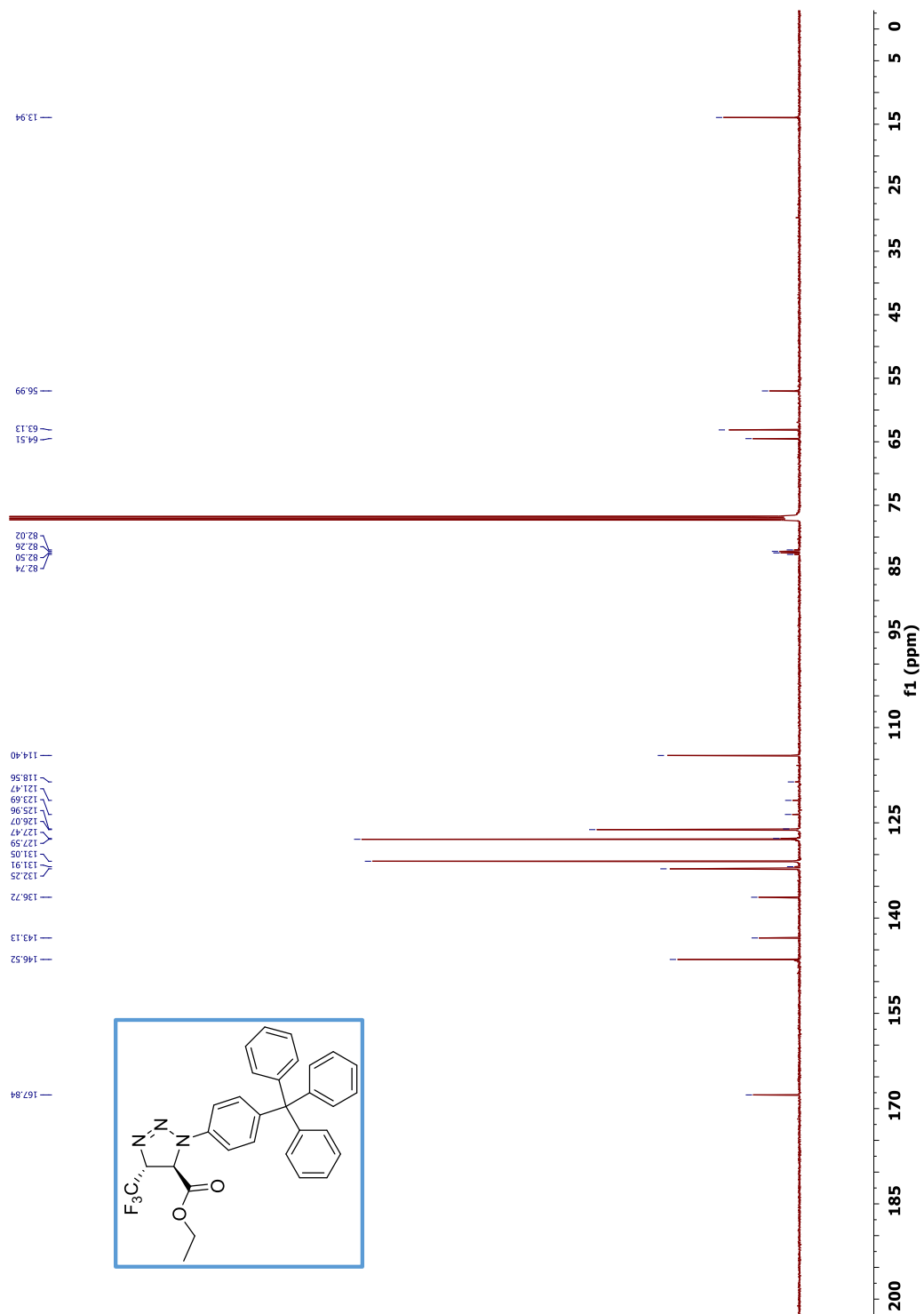
^{13}C NMR (126 MHz, CDCl_3) of compound *cis*-**3D**.



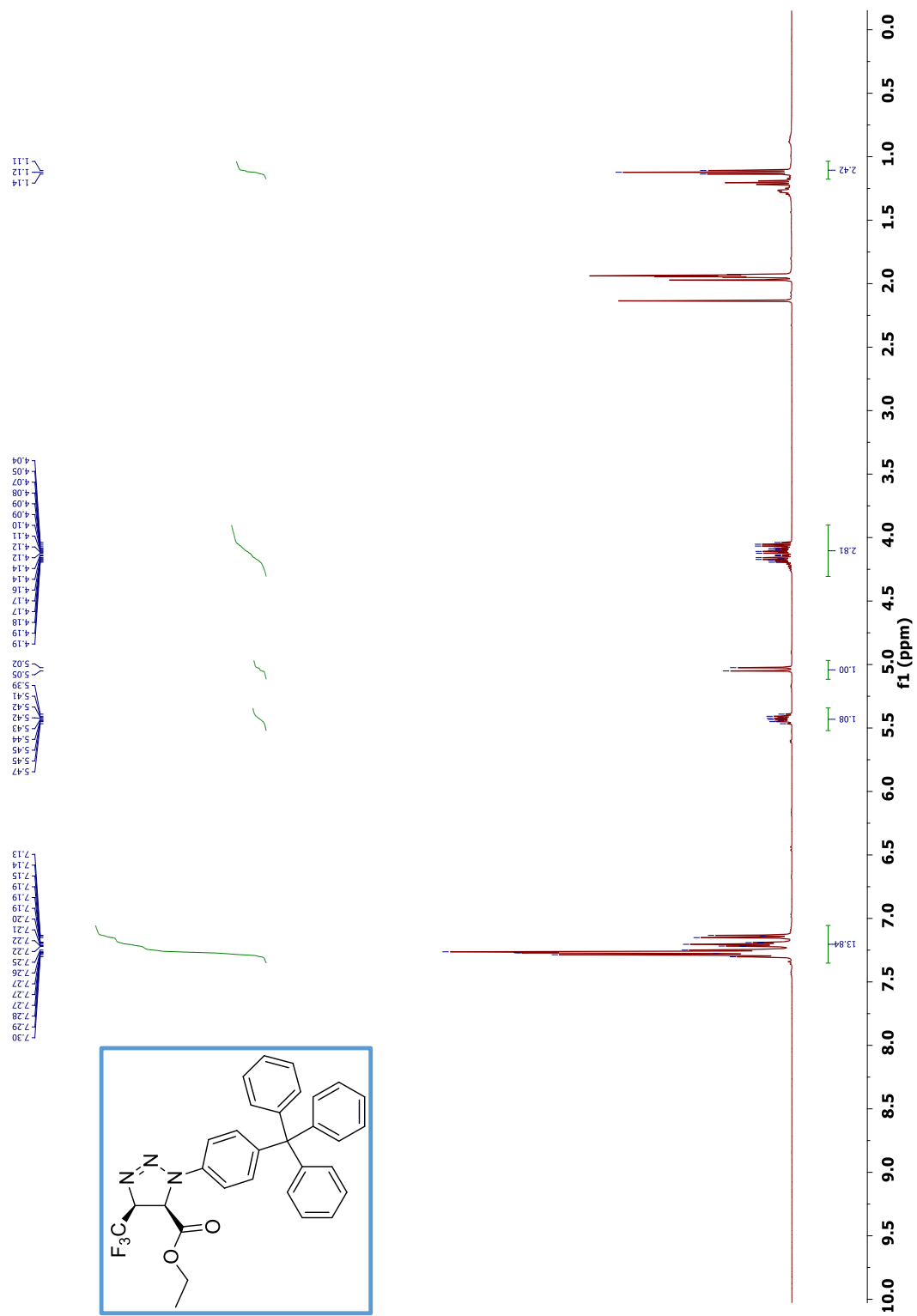
^1H NMR (500 MHz, CDCl_3) of compound *trans*-3E.



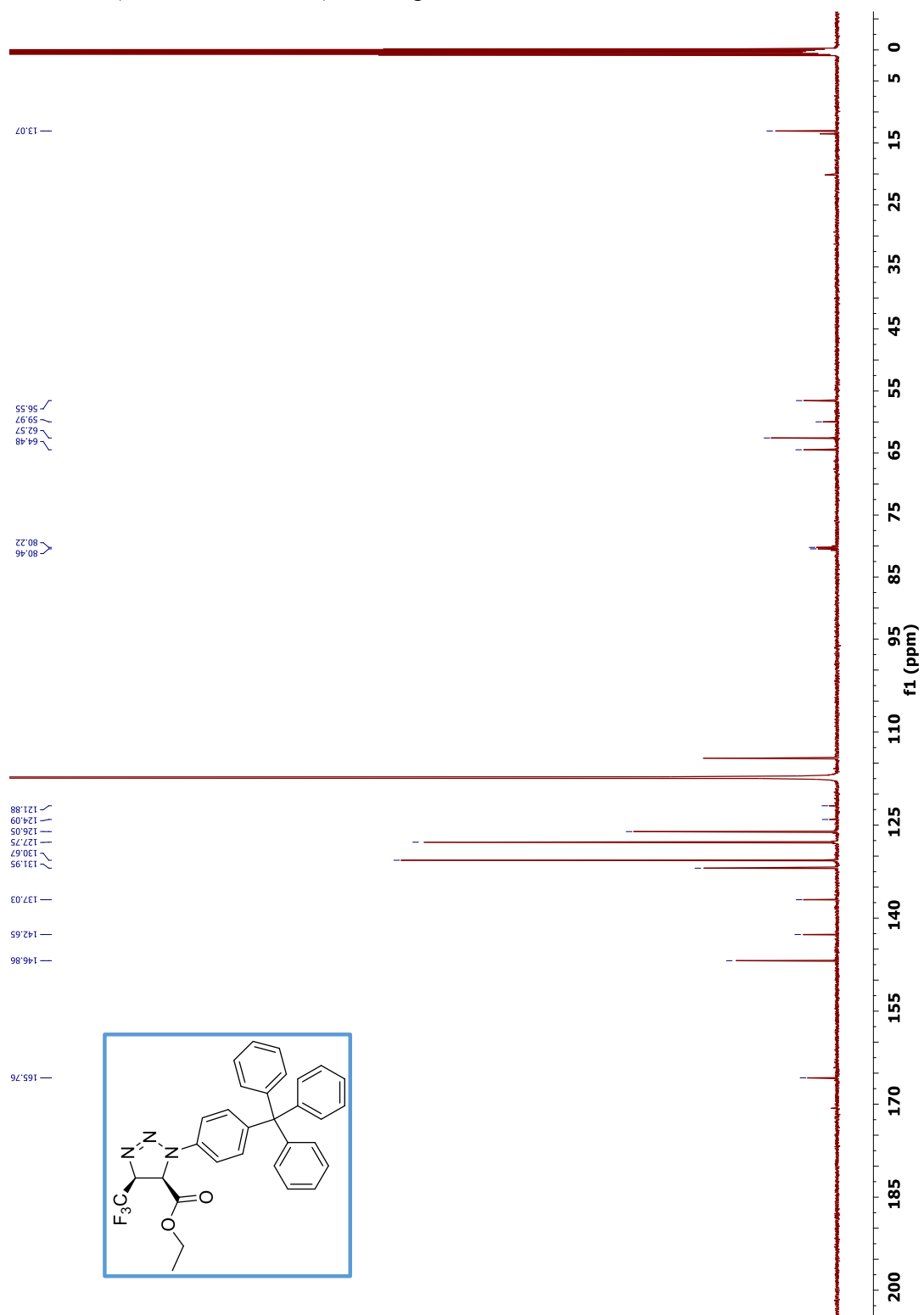
^{13}C NMR (126 MHz, CDCl_3) of compound *trans*-**3E**.



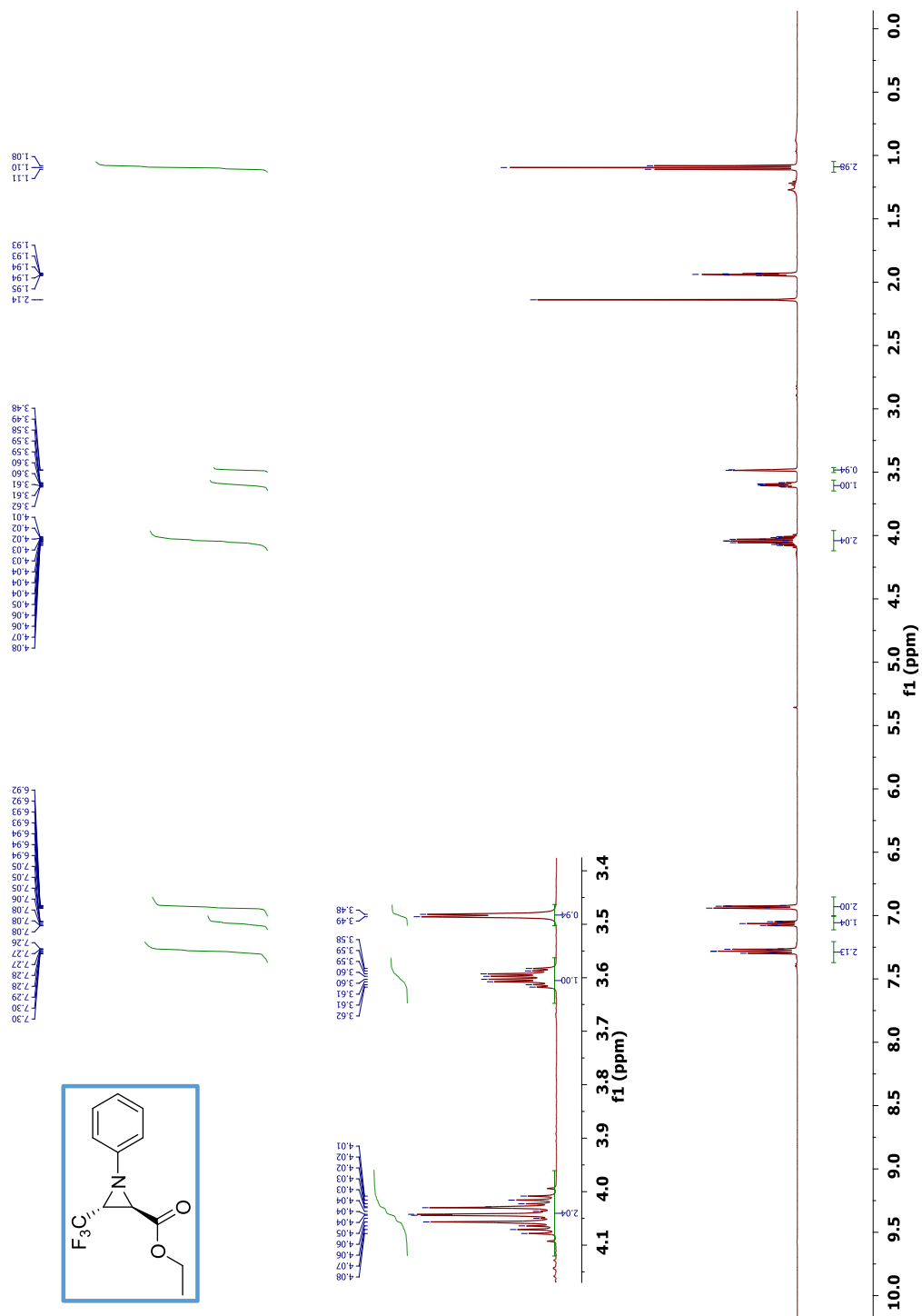
^1H NMR (500 MHz, CD_3CN) of compound *cis*-**3E**.



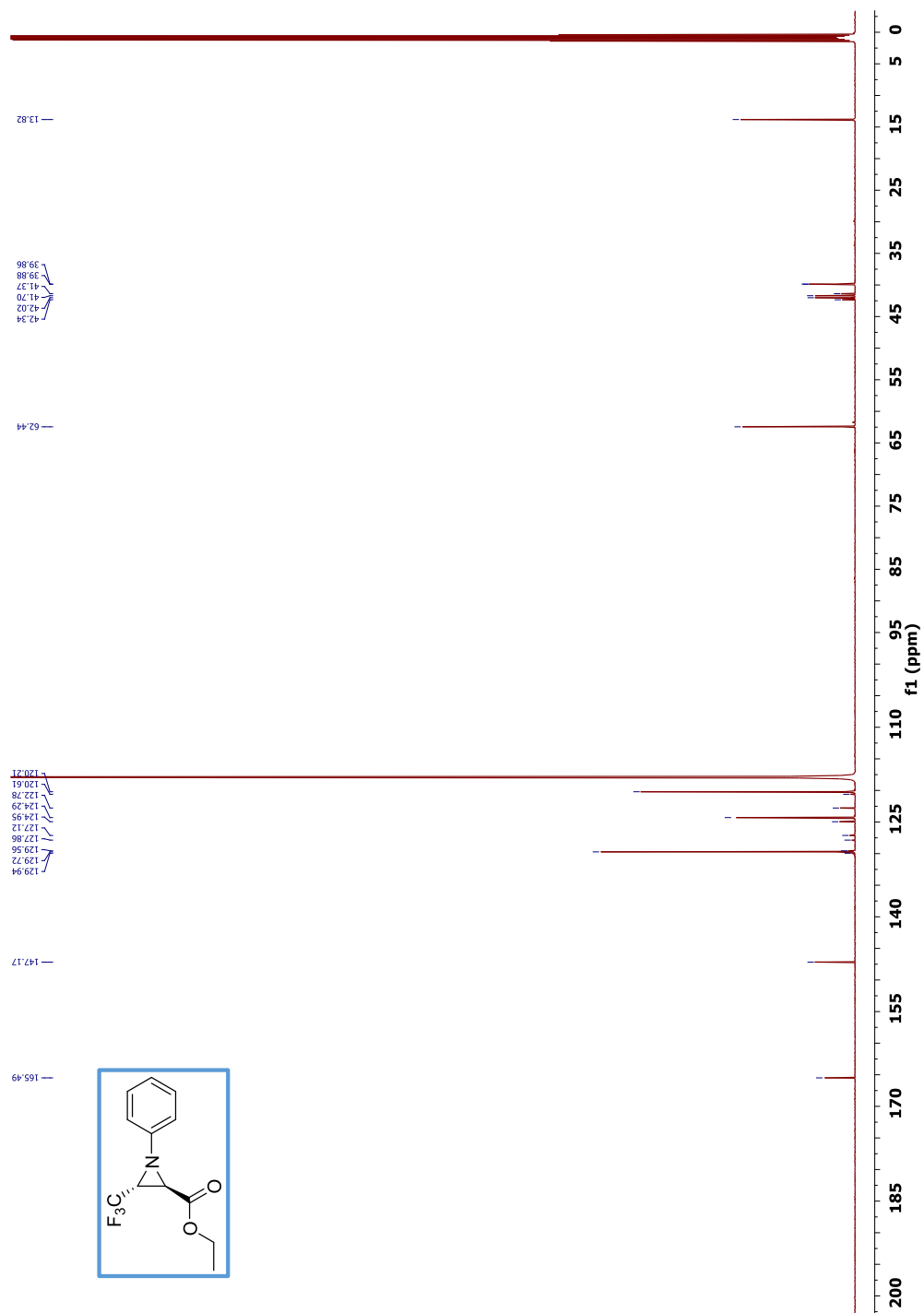
^{13}C NMR (126 MHz, CD_3CN) of compound *cis*-**3E**.



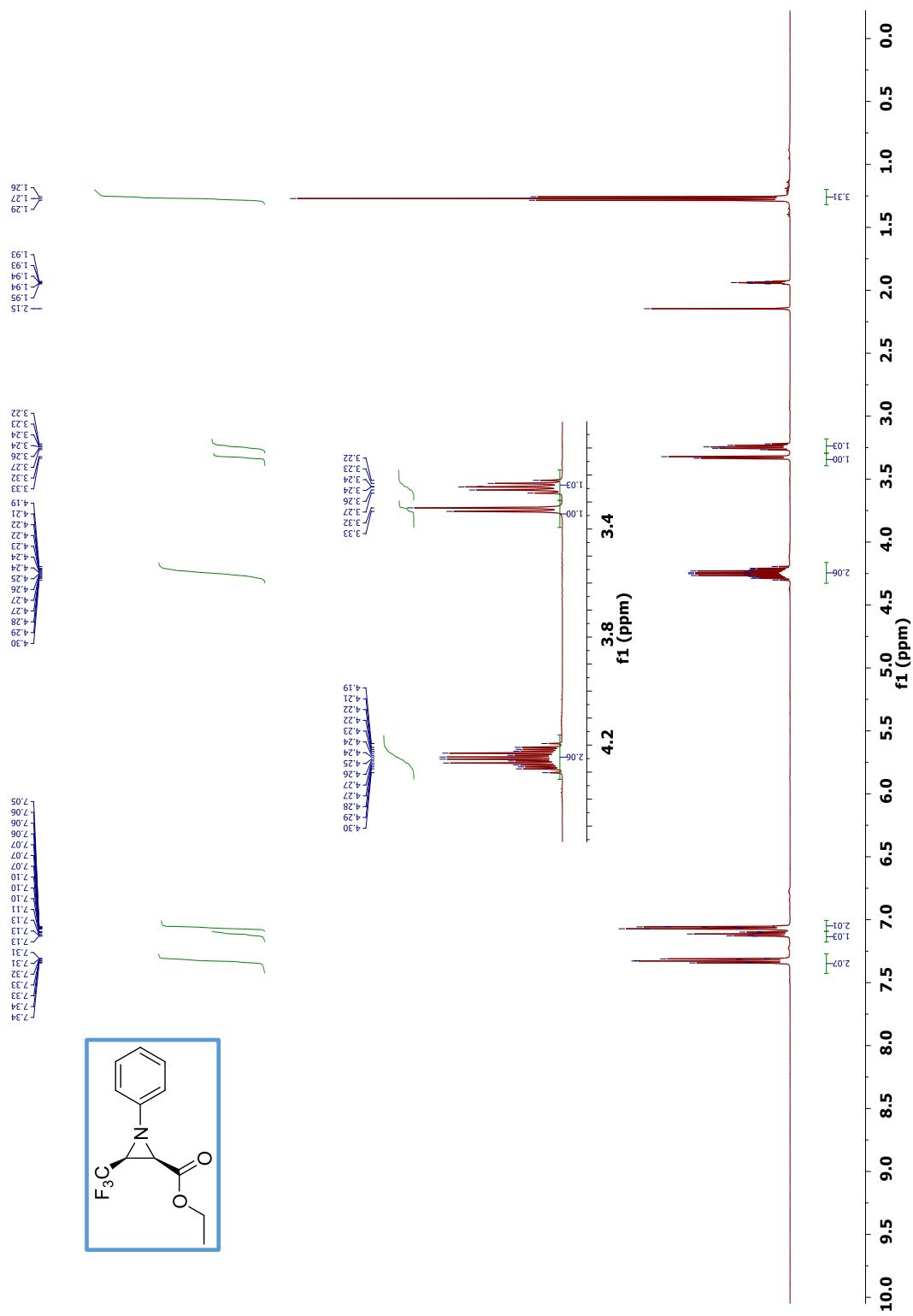
^1H NMR (500 MHz, CD_3CN) of compound *trans*-4A.



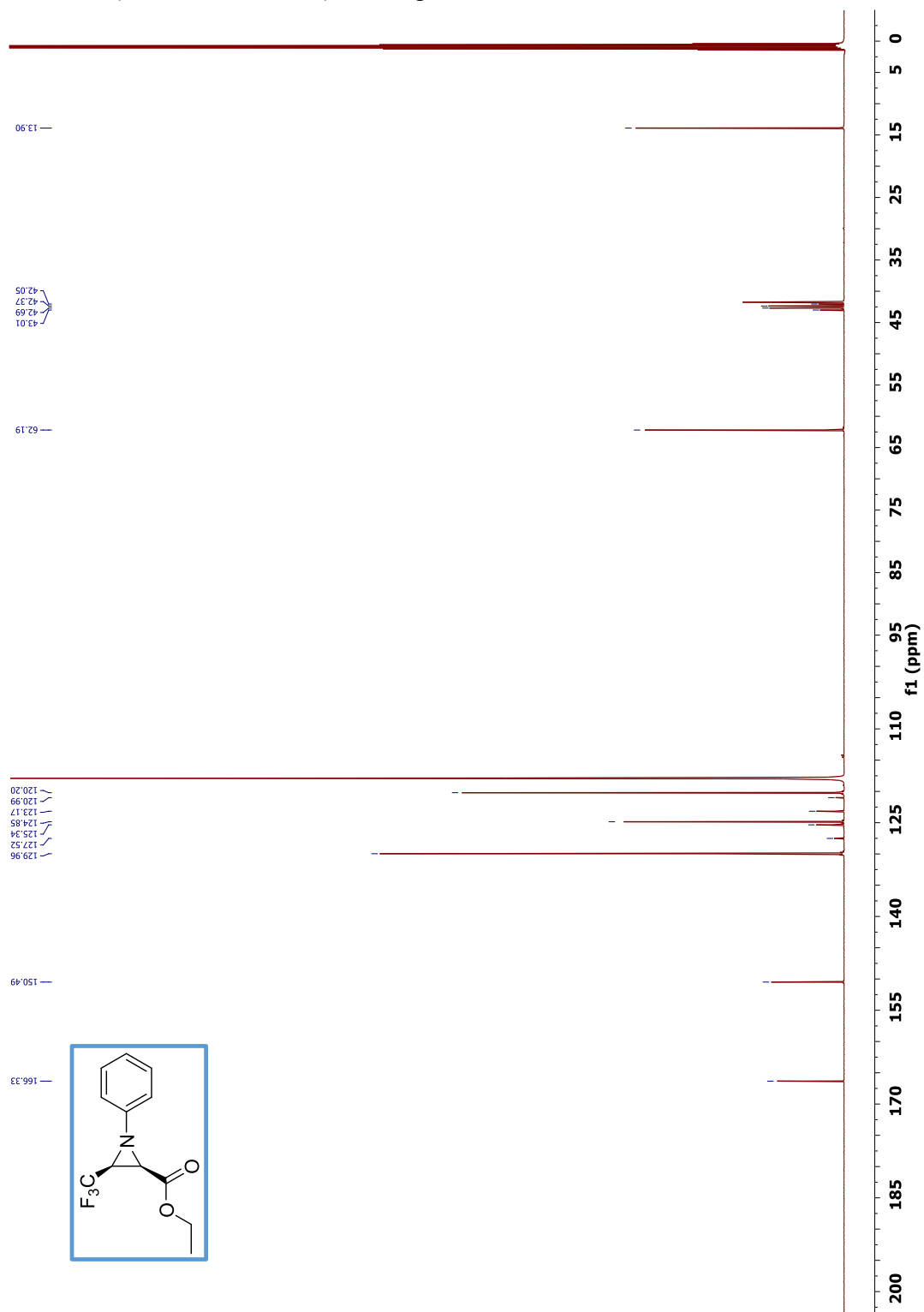
^{13}C NMR (126 MHz, CD_3CN) of compound *trans*-4A.



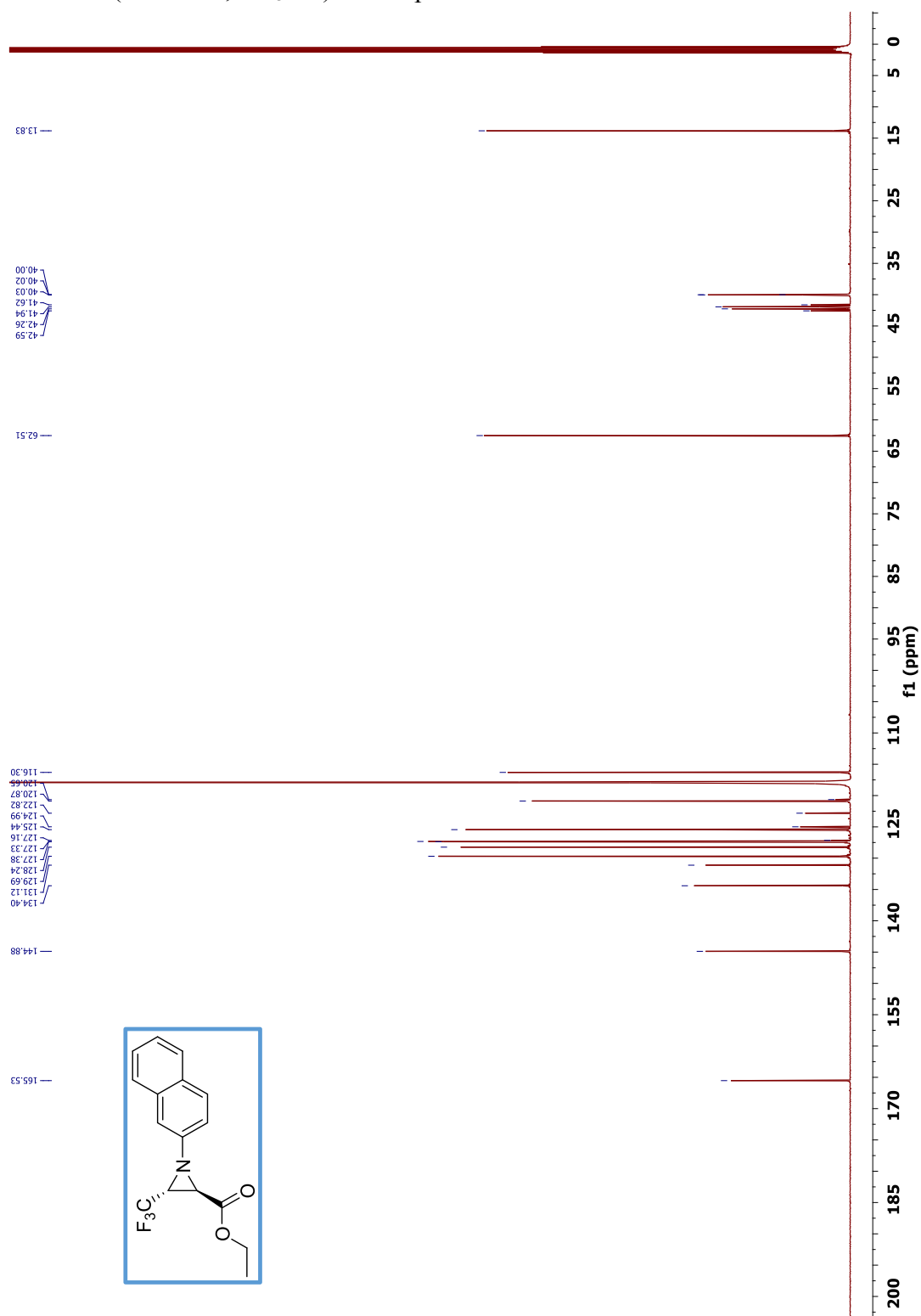
^1H NMR (500 MHz, CD_3CN) of compound *cis*-4A.



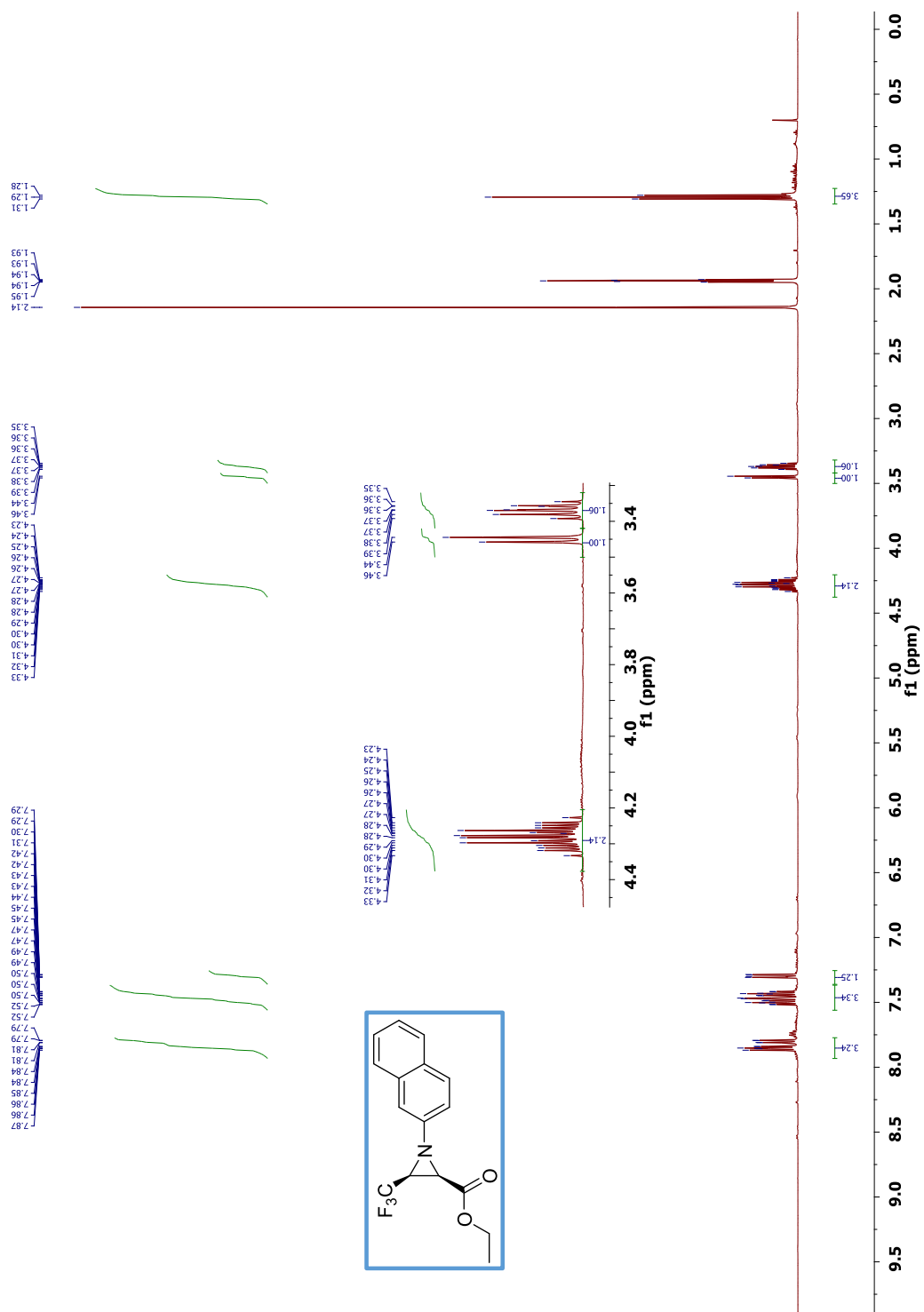
^{13}C NMR (126 MHz, CD_3CN) of compound *cis*-4A.



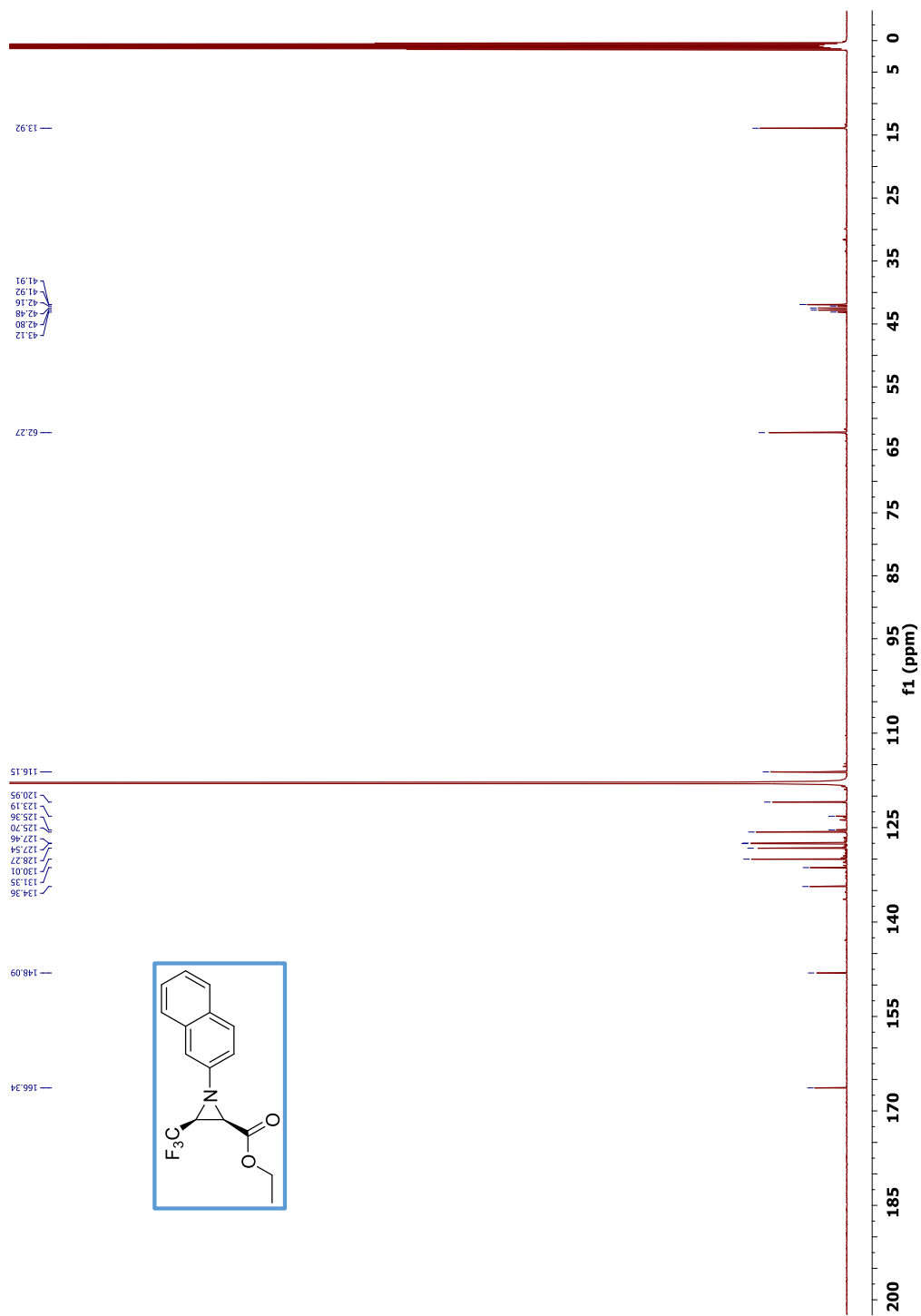
^{13}C NMR (126 MHz, CD_3CN) of compound *trans*-4B.



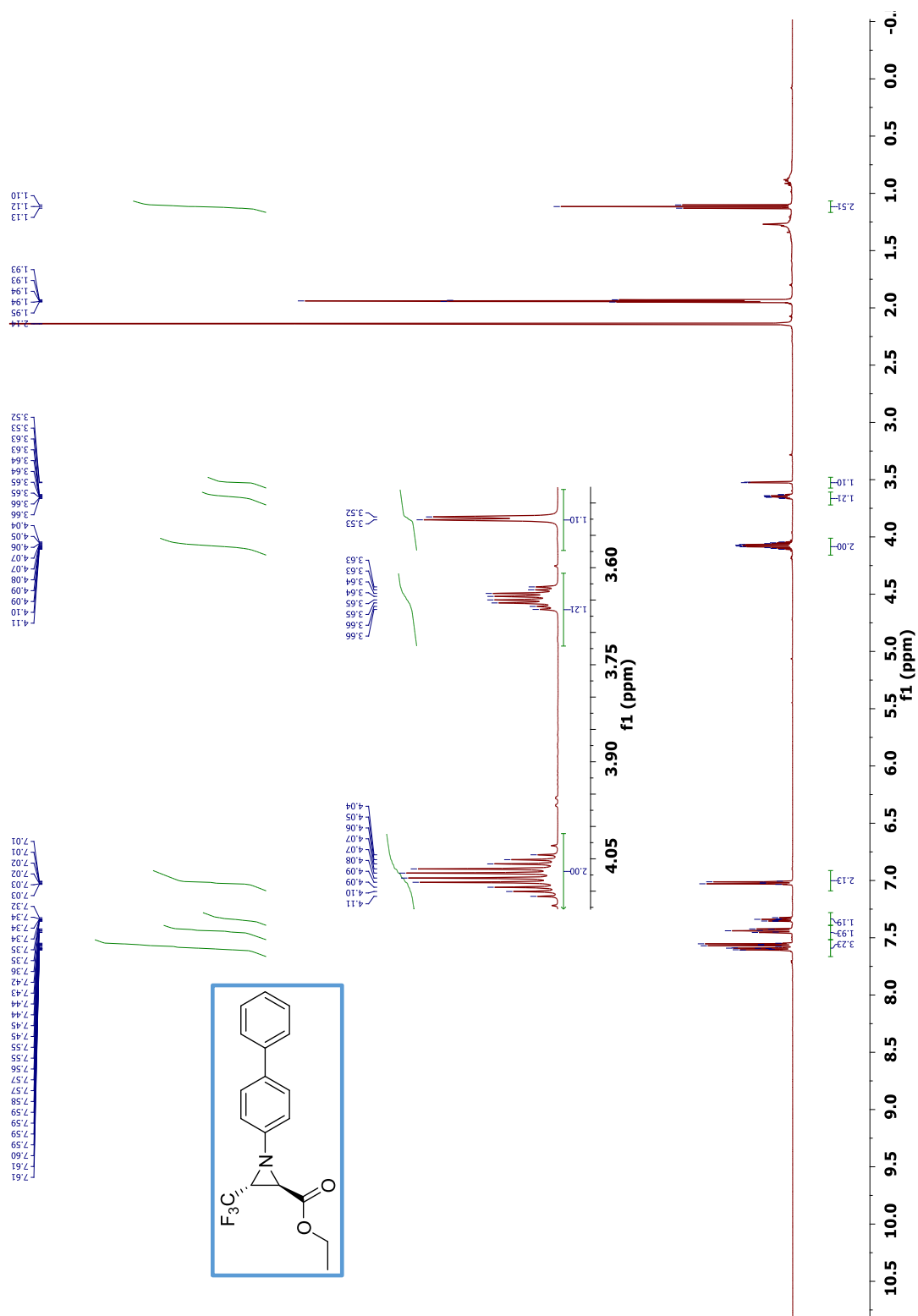
^1H NMR (500 MHz, CD_3CN) of compound *cis*-4B.



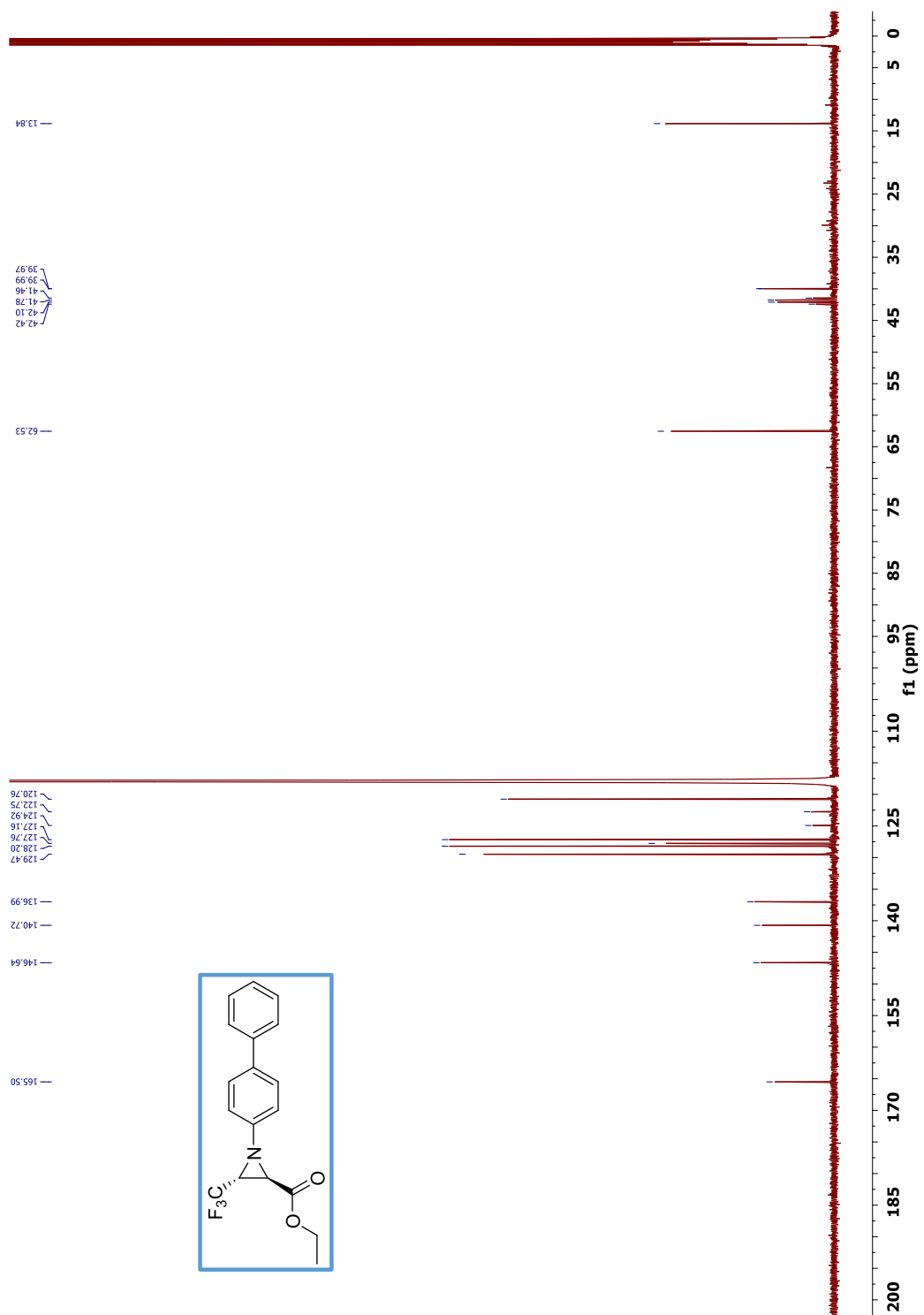
^{13}C NMR (126 MHz, CD_3CN) of compound *cis*-4B.



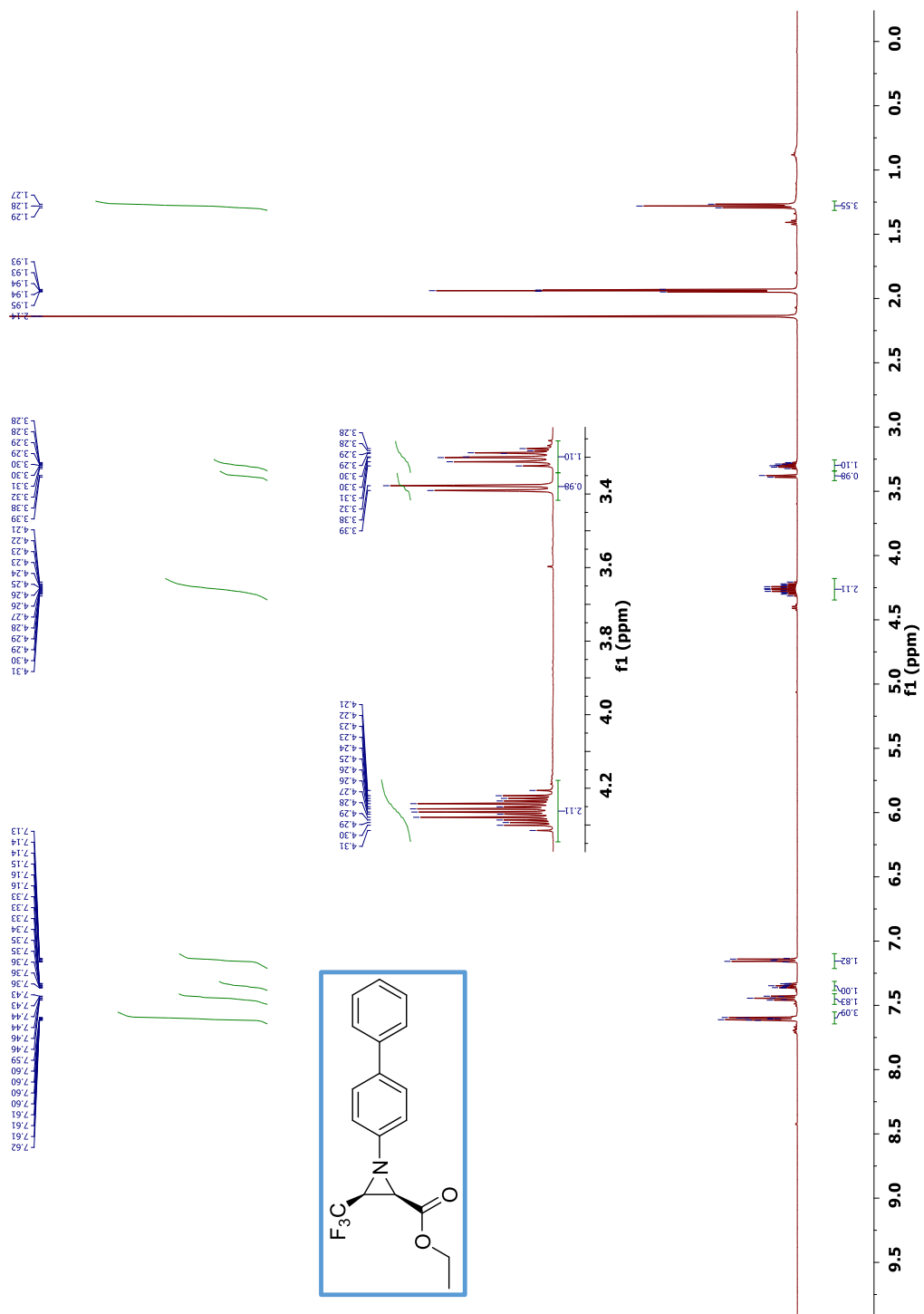
^1H NMR (500 MHz, CD_3CN) of compound *trans*-4C.



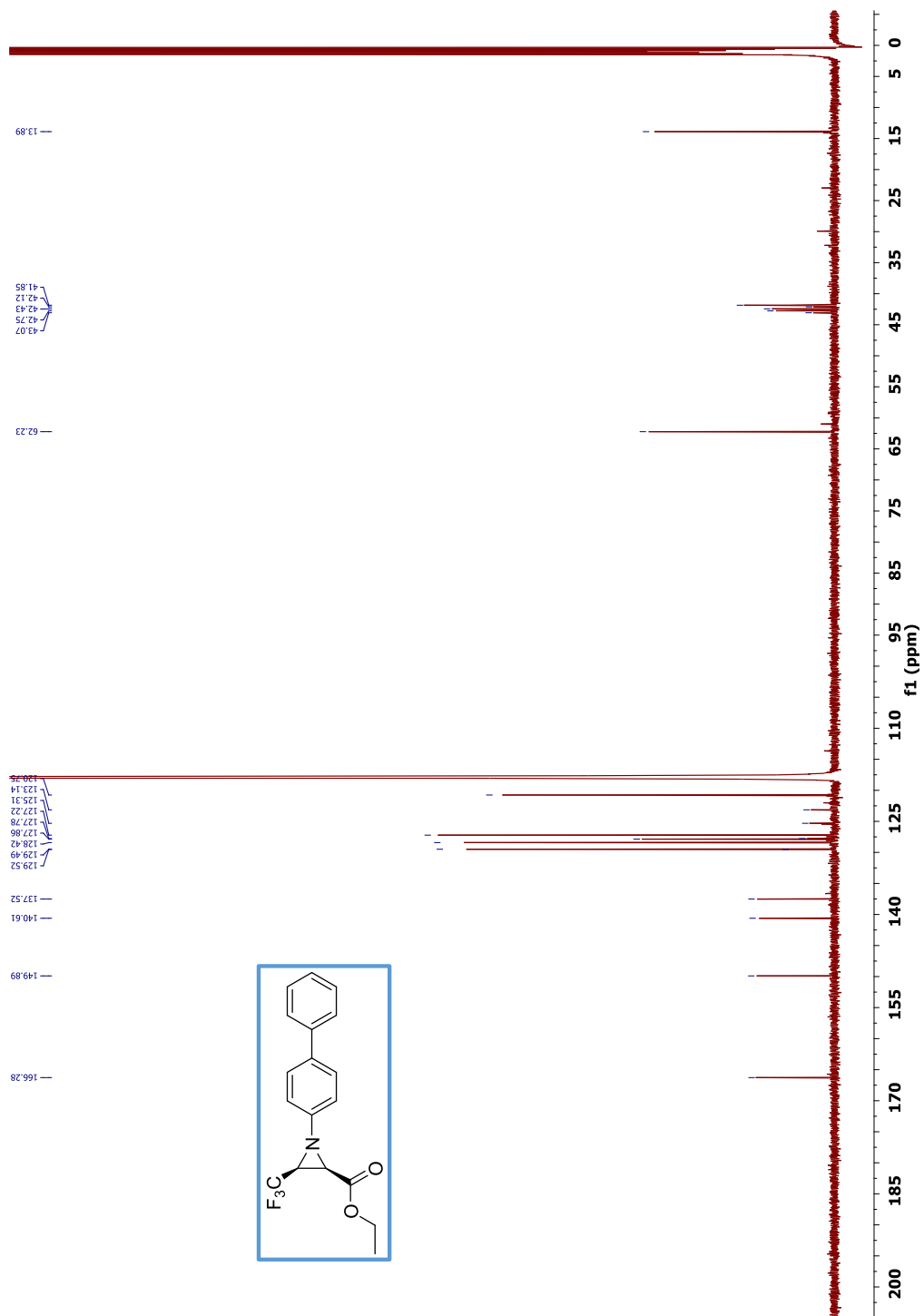
^{13}C NMR (126 MHz, CD_3CN) of compound *trans*-4C.



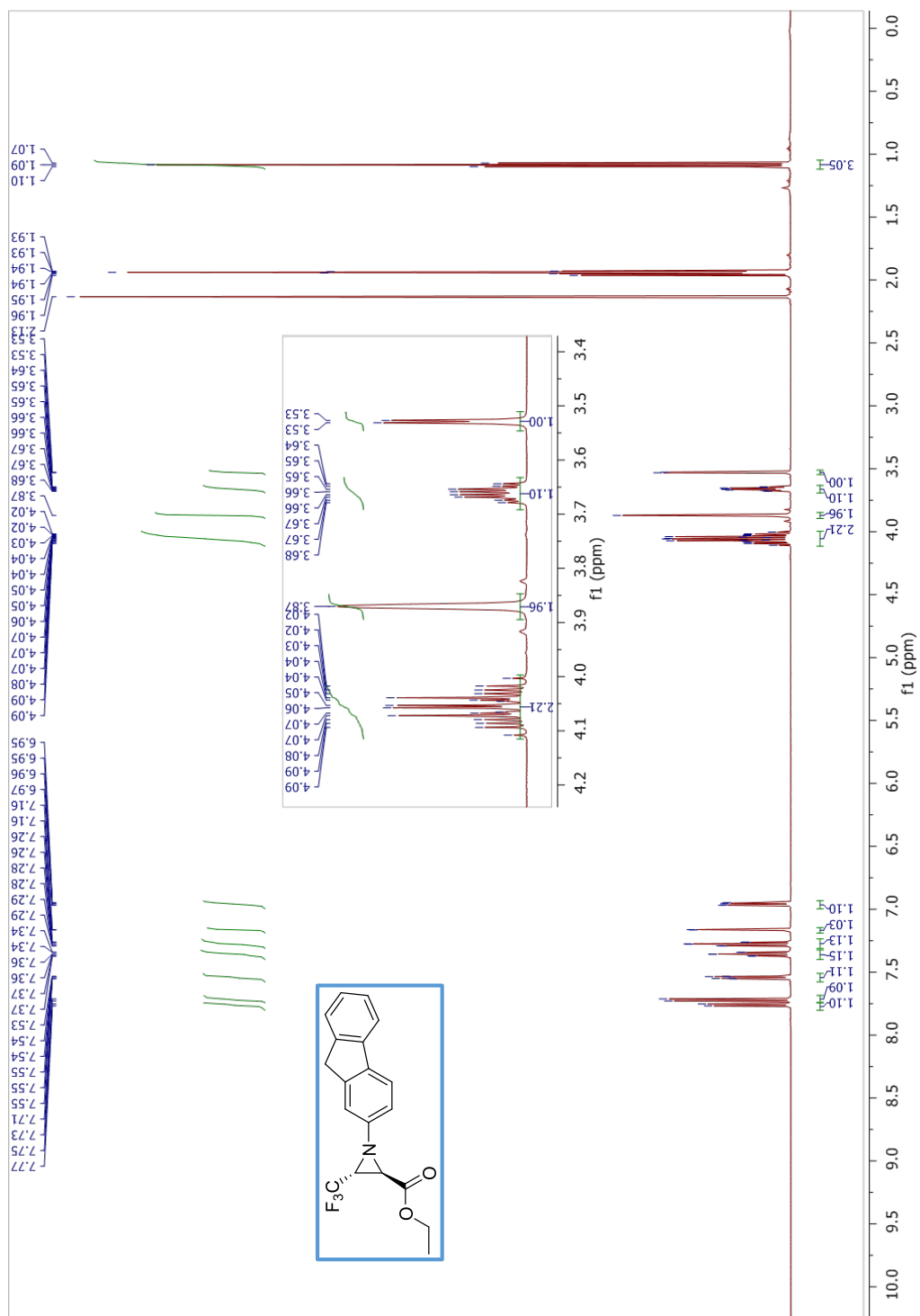
^1H NMR (500 MHz, CD_3CN) of compound *cis*-4C.



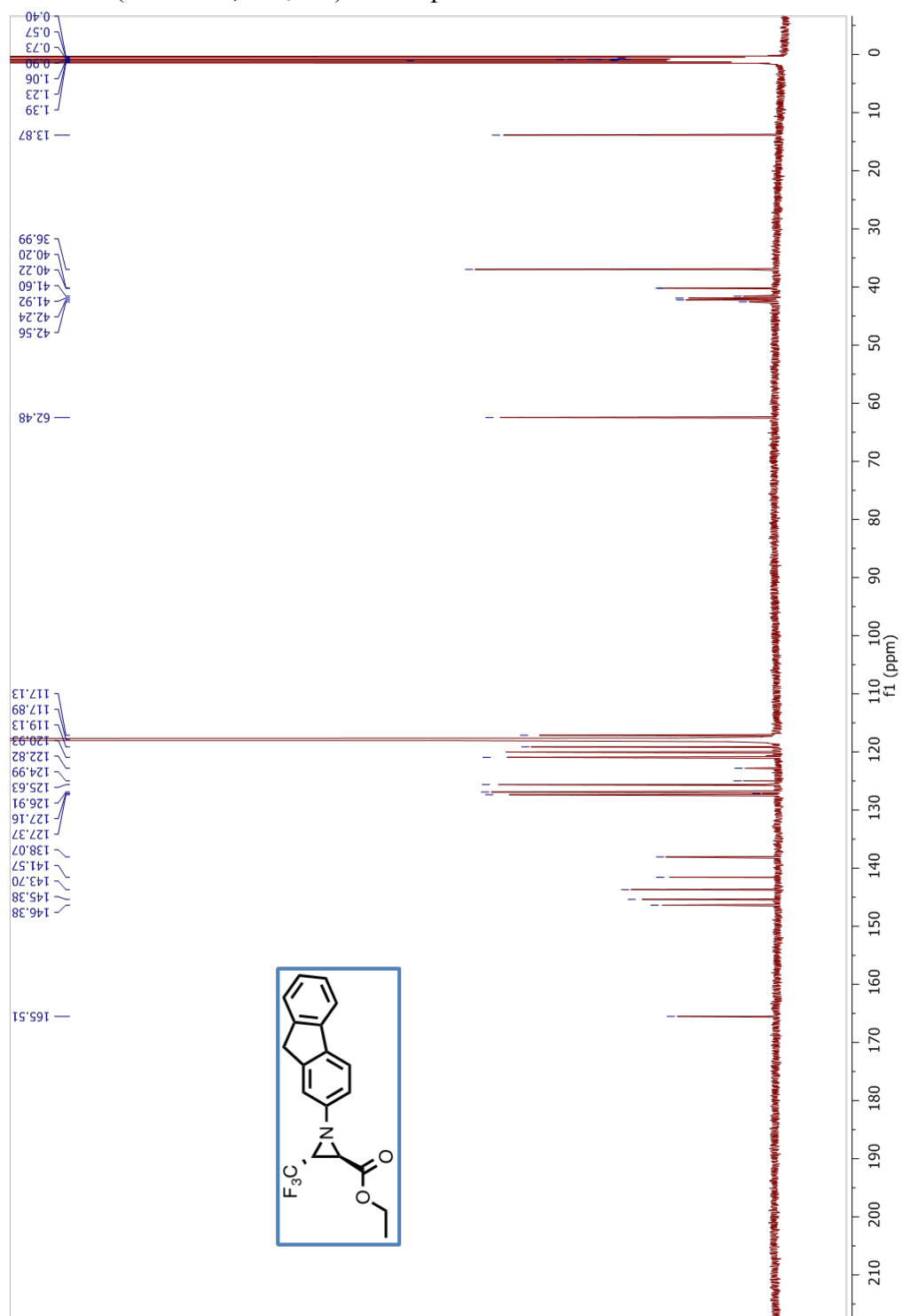
^{13}C NMR (126 MHz, CD_3CN) of compound *cis*-4C.



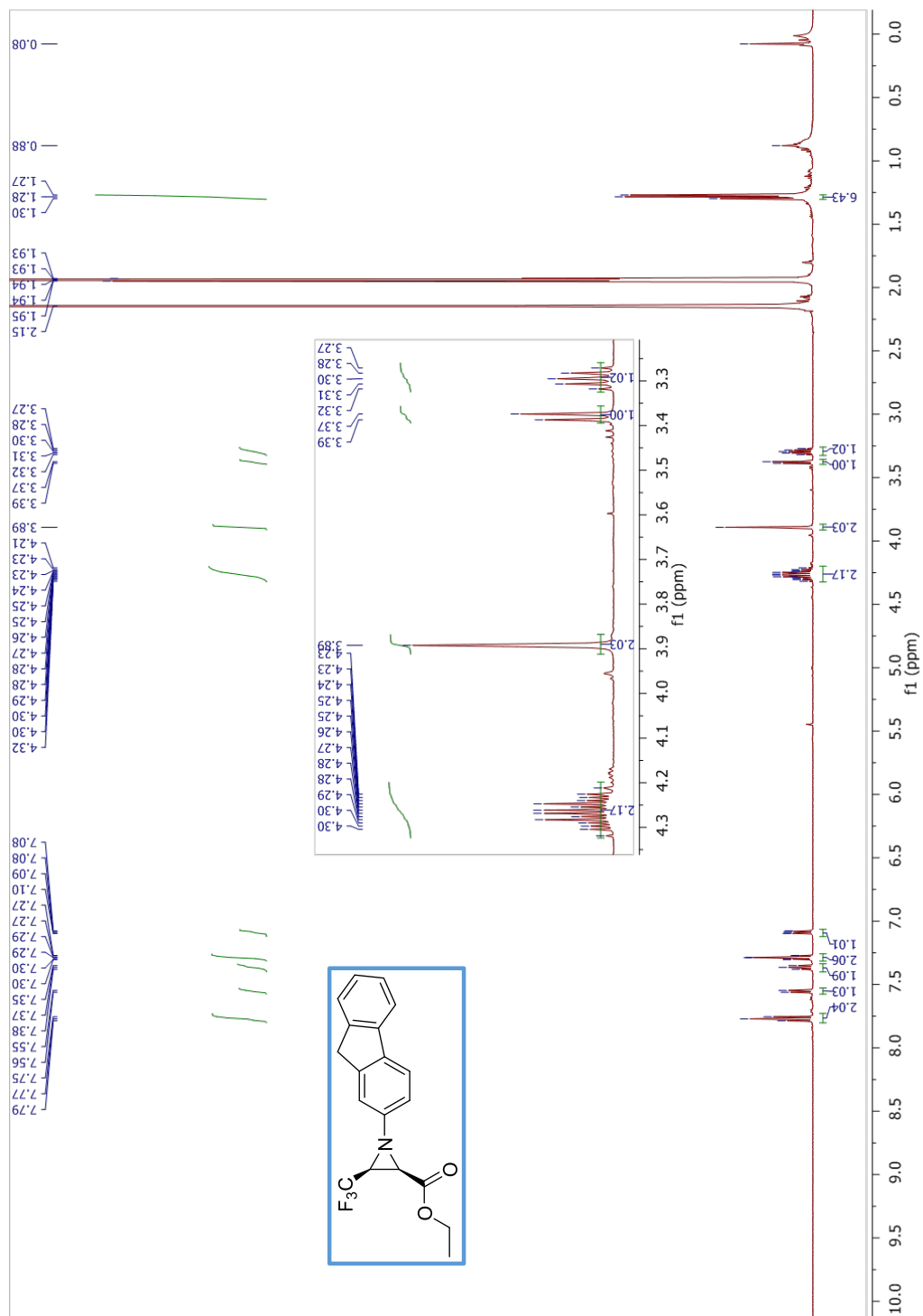
^1H NMR (500 MHz, CD_3CN) of compound *trans*-4D.



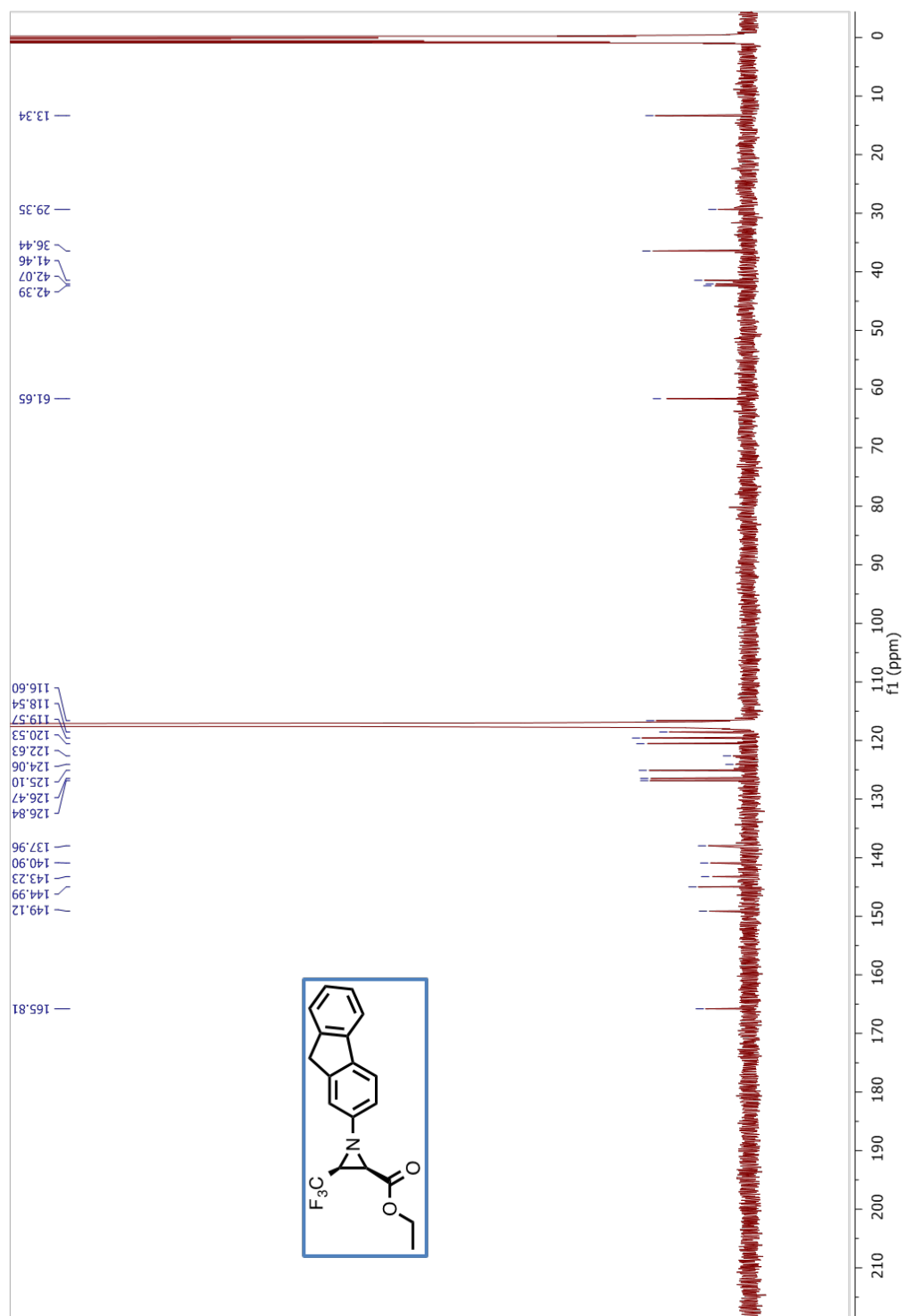
^{13}C NMR (126 MHz, CD_3CN) of compound *trans*-4D.



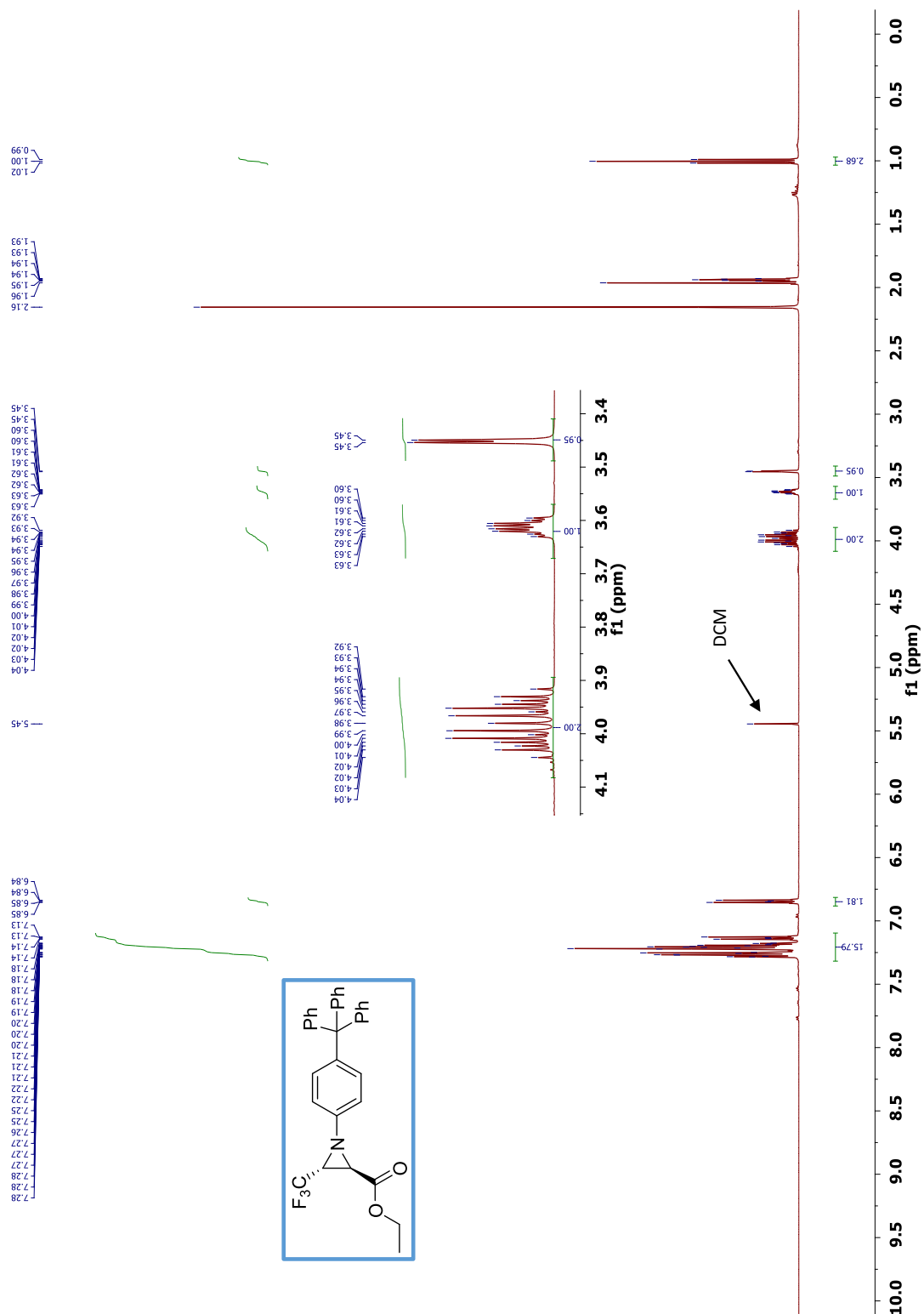
^1H NMR (500 MHz, CD_3CN) of compound *cis*-4D.



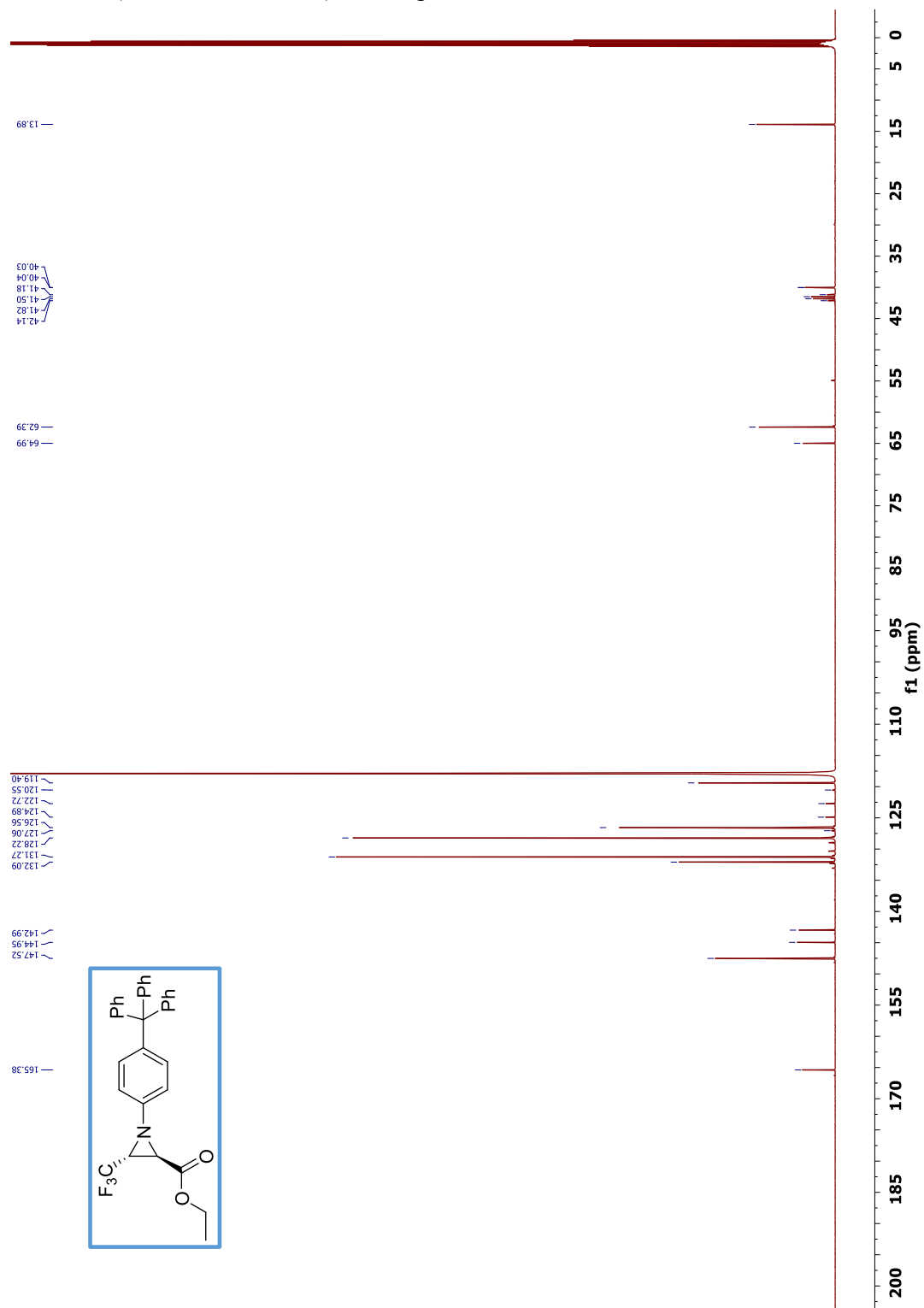
^{13}C NMR (126 MHz, CD_3CN) of compound *cis*-4D.



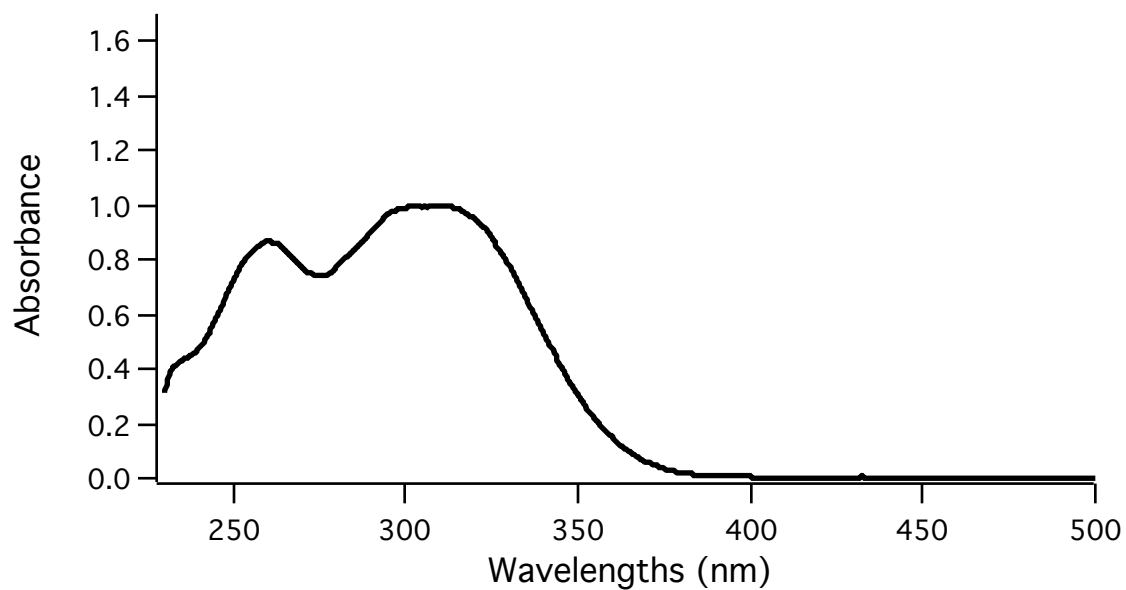
^1H NMR (500 MHz, CD_3CN) of compound *trans*-4E.



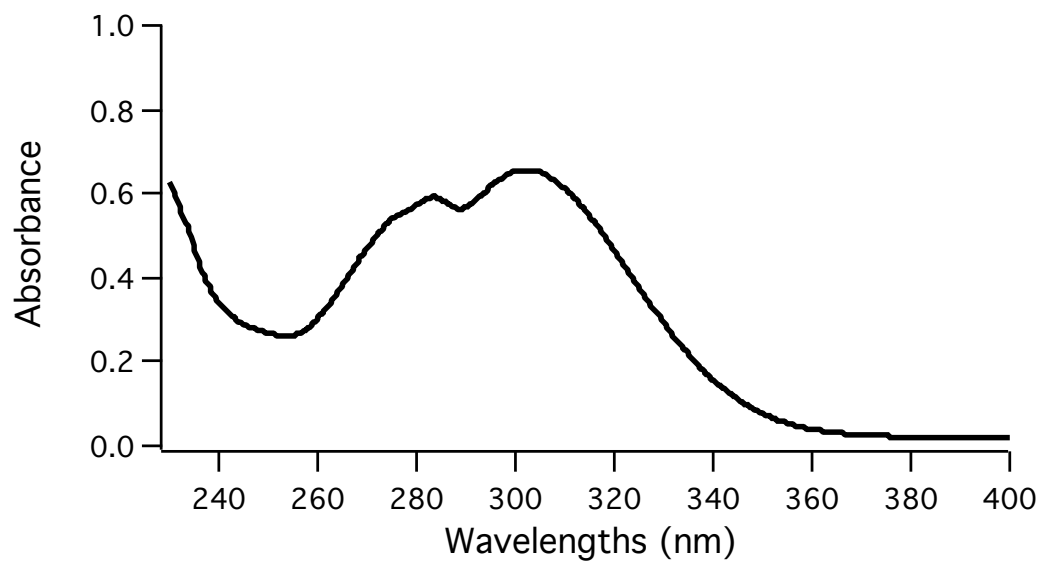
^{13}C NMR (126 MHz, CD_3CN) of compound *trans*-4E.



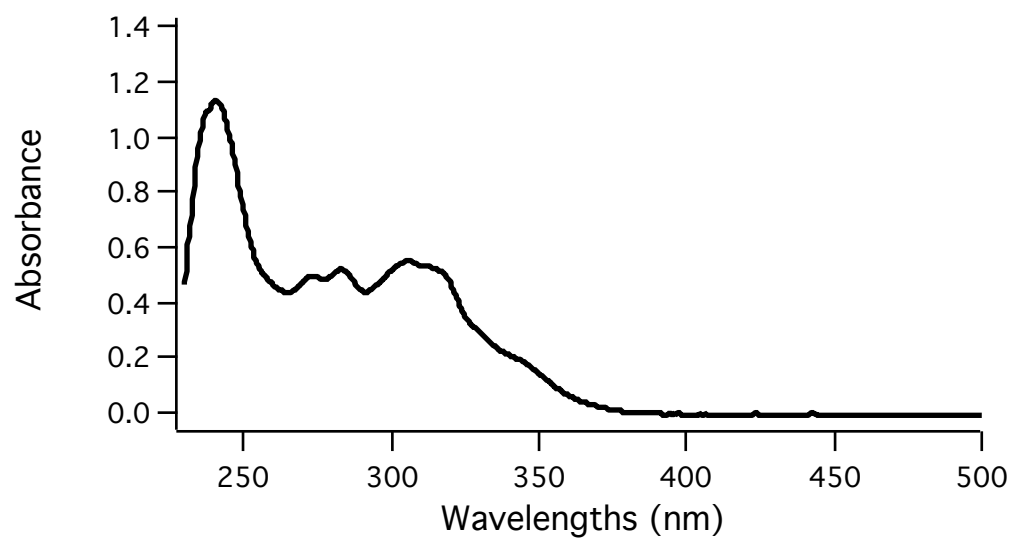
UV-Vis Spectrum of compound *trans*-3A in dichloromethane.



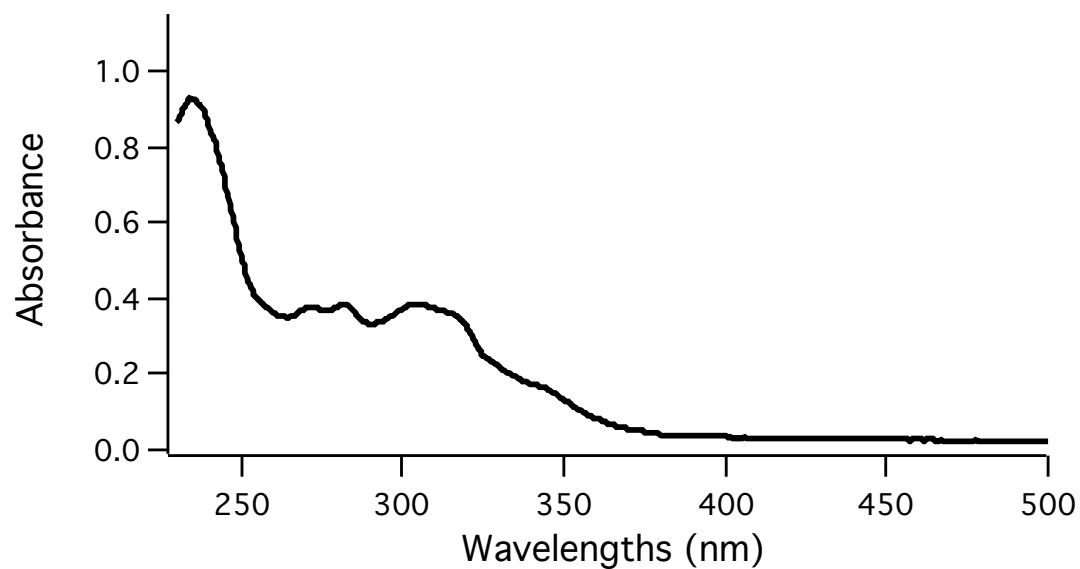
UV-Vis Spectrum of compound *cis*-3A in dichloromethane.



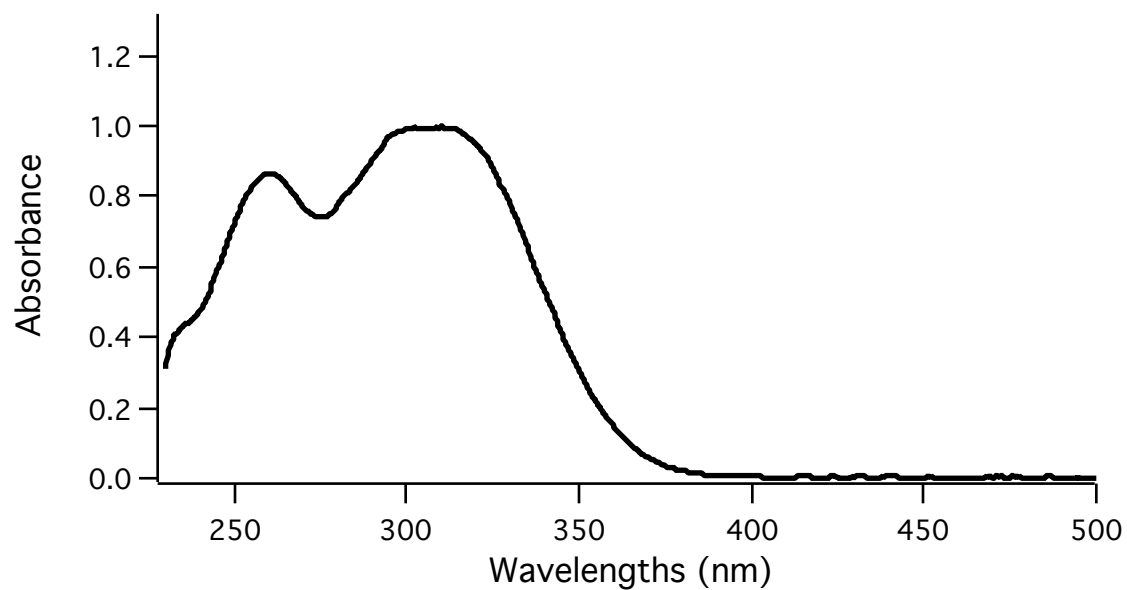
UV-Vis Spectrum of compound *trans*-**3B** in dichloromethane.



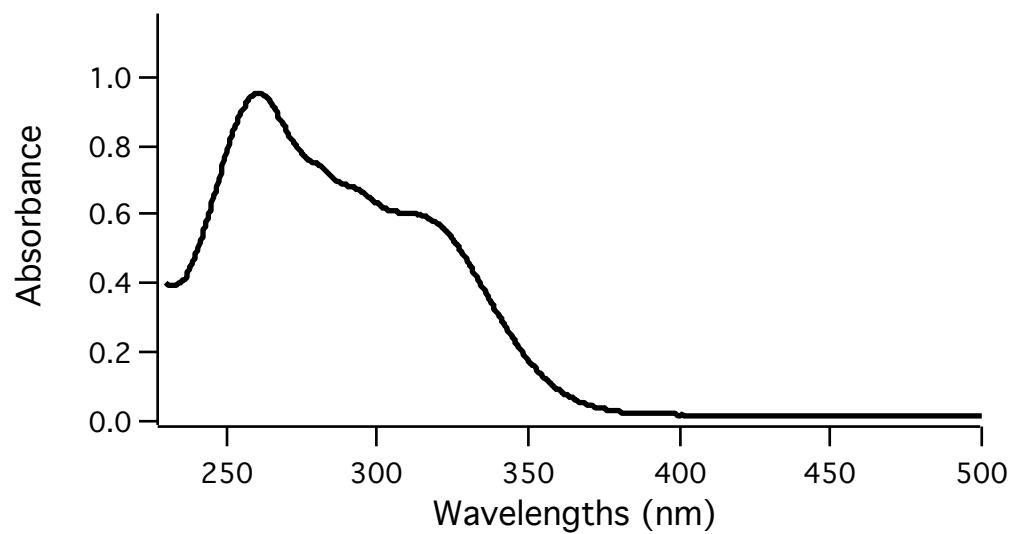
UV-Vis Spectrum of compound *cis*-**3B** in dichloromethane.



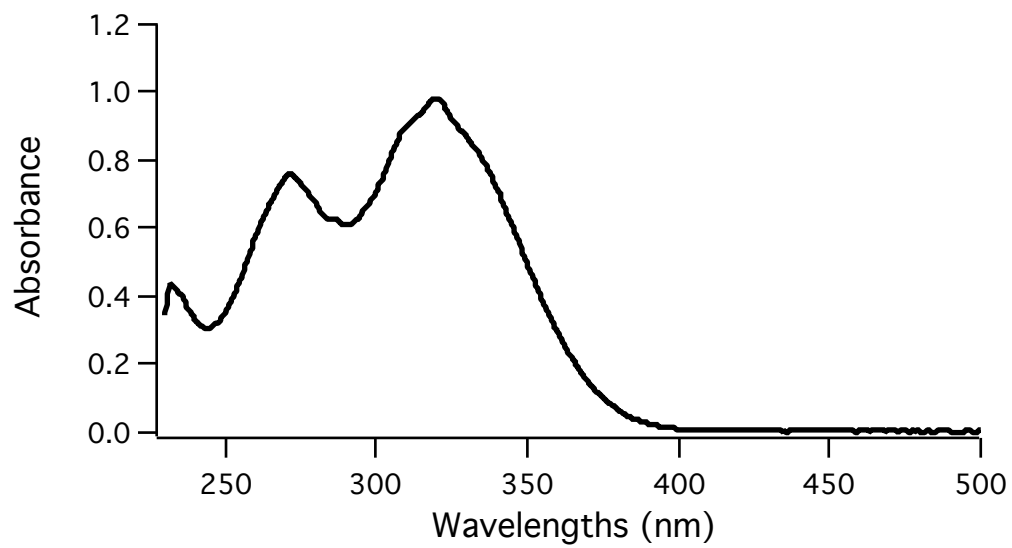
UV-Vis Spectrum of compound *trans*-3C in dichloromethane.



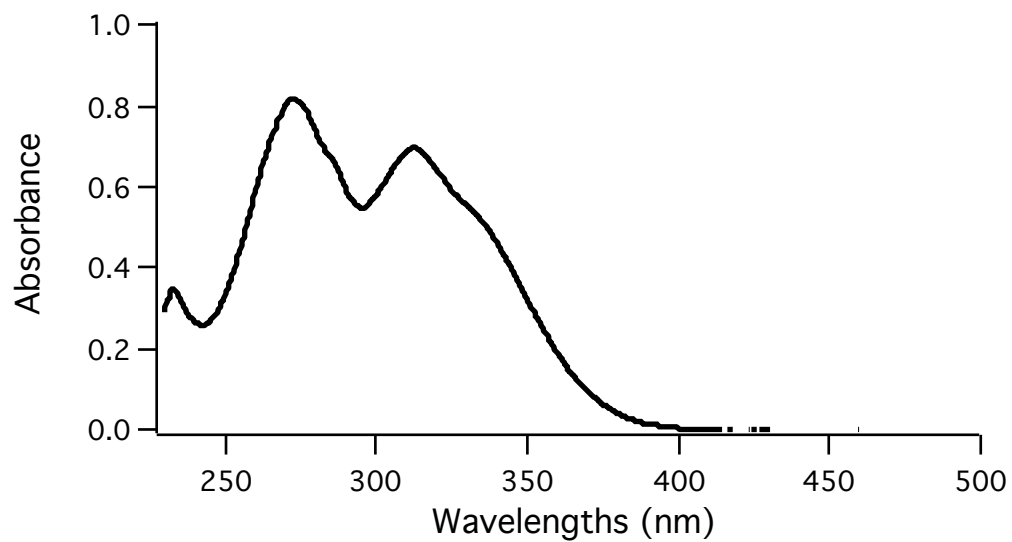
UV-Vis Spectrum of compound *cis*-3C in dichloromethane.



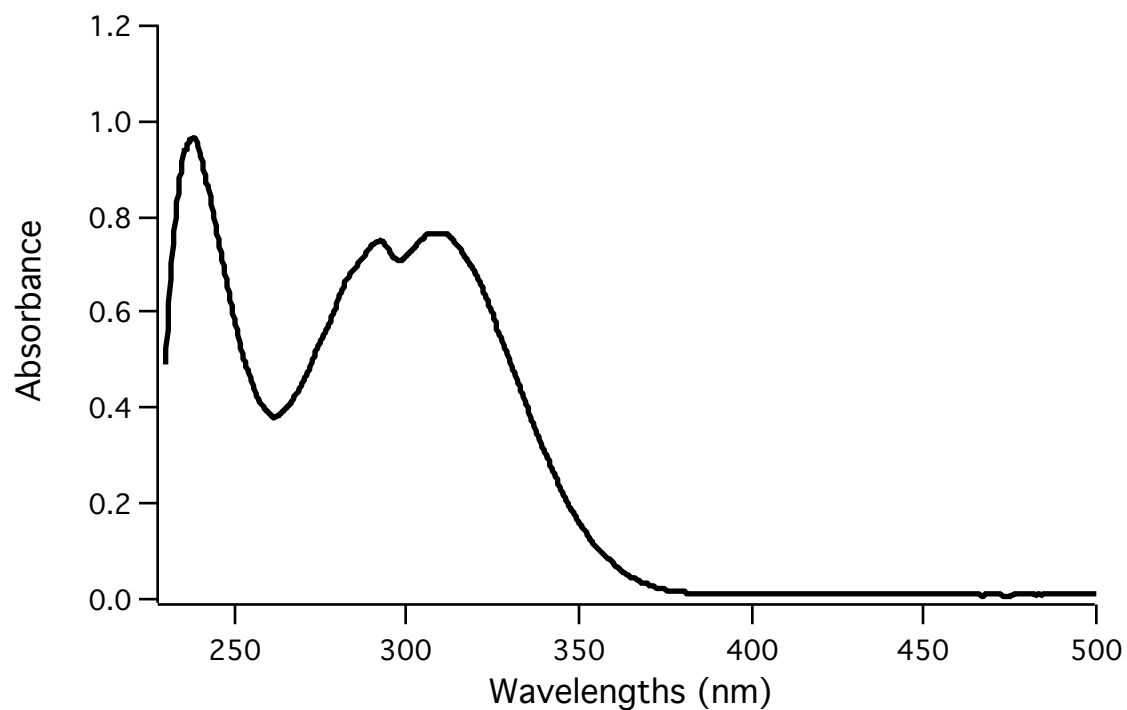
UV-Vis Spectrum of compound *trans*-**3D** in dichloromethane.



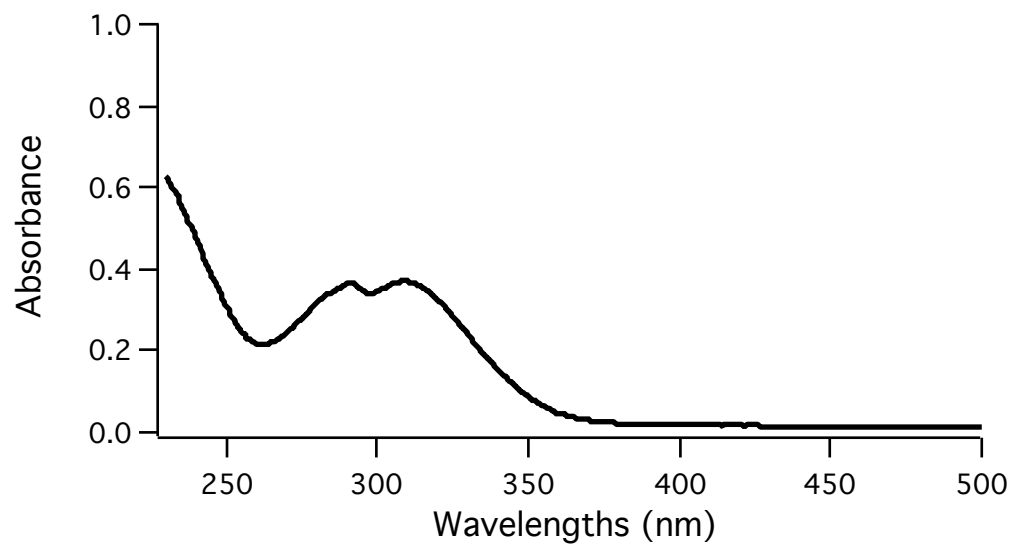
UV-Vis Spectrum of compound *cis*-**3D** in dichloromethane.



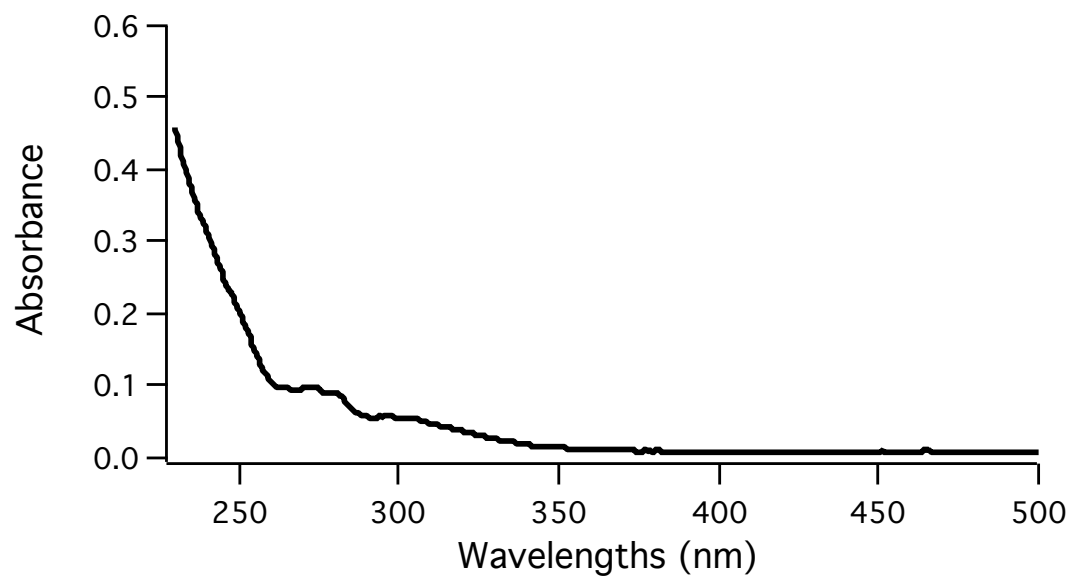
UV-Vis Spectrum of compound *trans*-3E in dichloromethane.



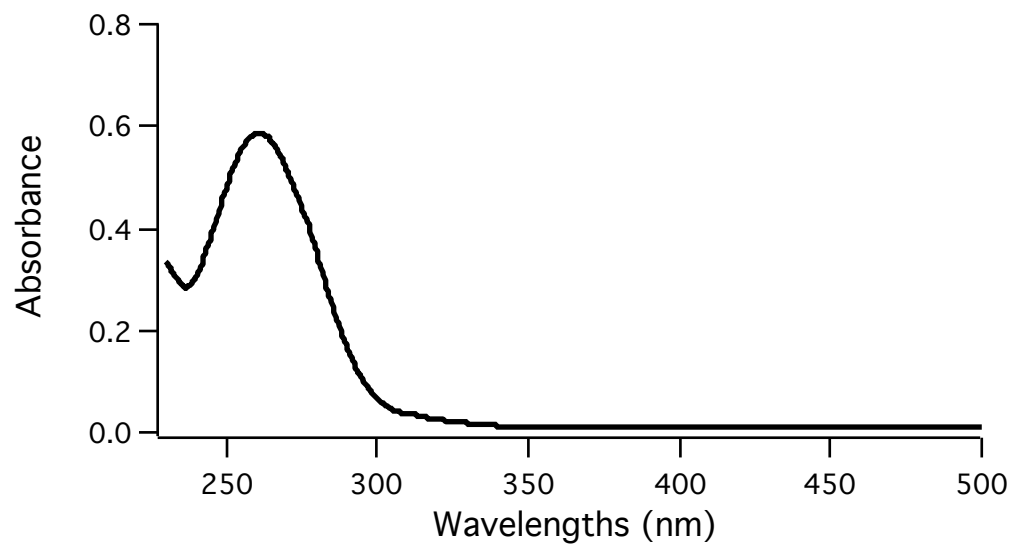
UV-Vis Spectrum of compound *cis*-3E in dichloromethane.



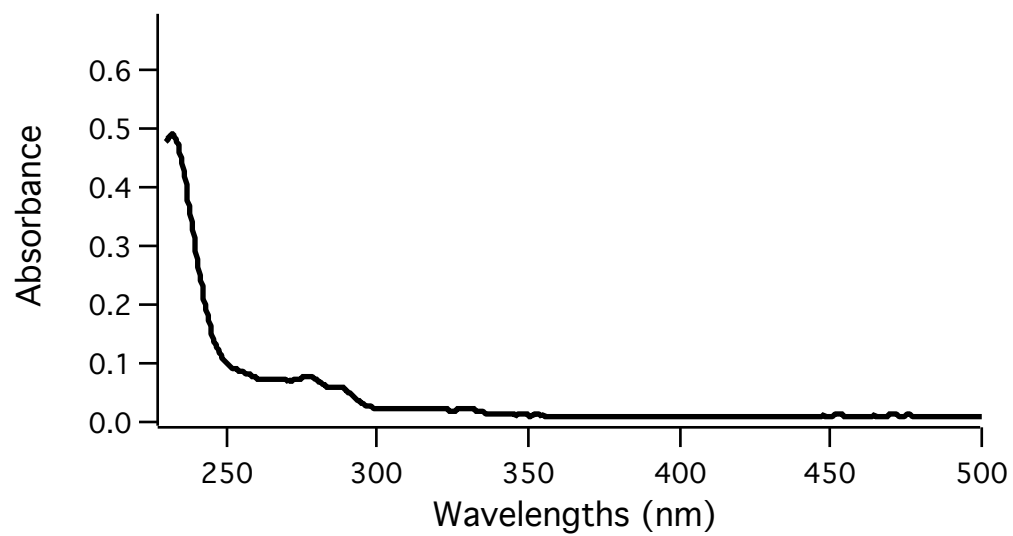
UV-Vis Spectrum of compound *trans*-4A in dichloromethane.



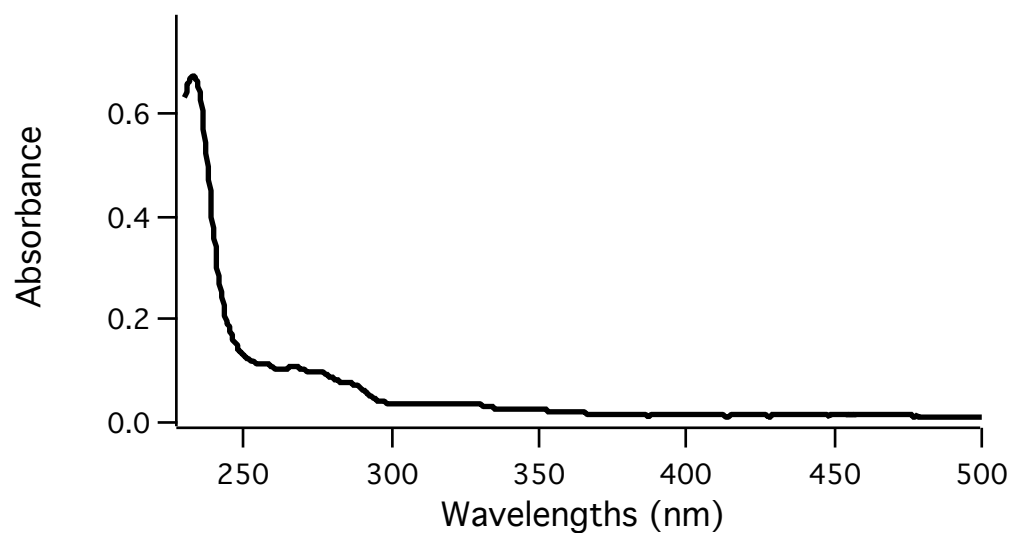
UV-Vis Spectrum of compound *cis*-4A in dichloromethane.



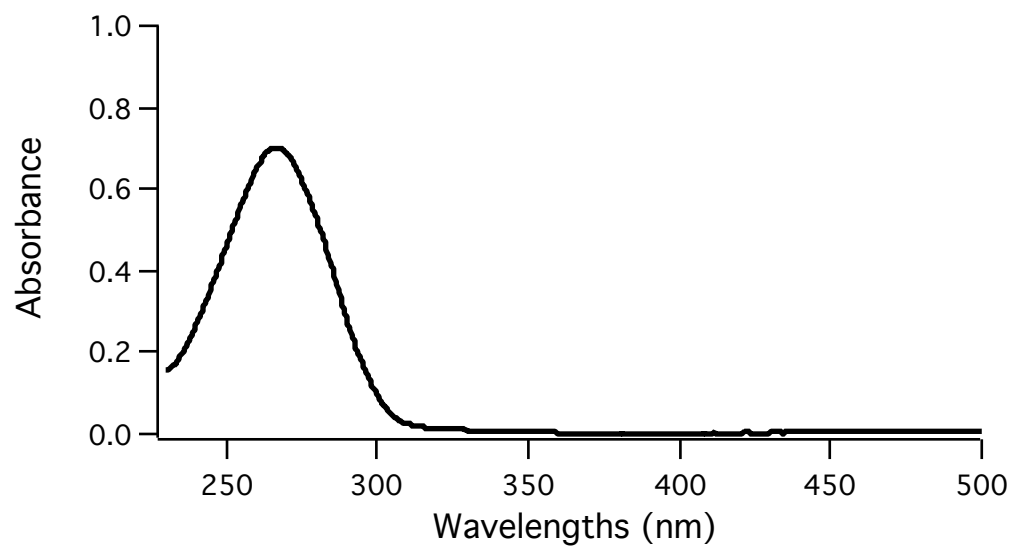
UV-Vis Spectrum of compound *trans*-**4B** in dichloromethane.



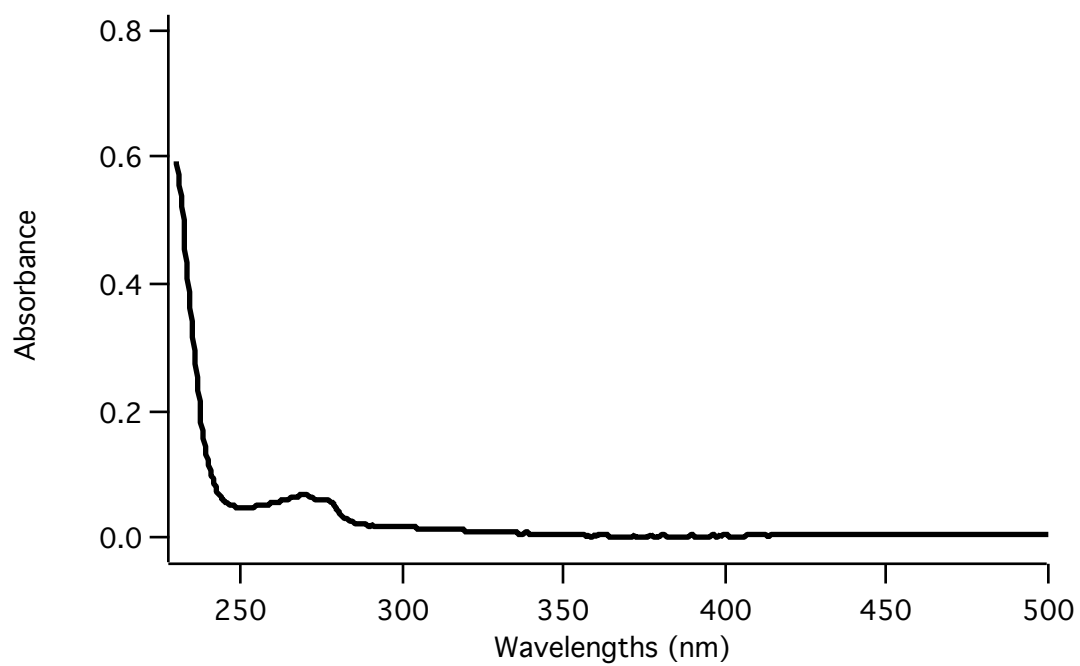
UV-Vis Spectrum of compound *cis*-**4B** in dichloromethane.



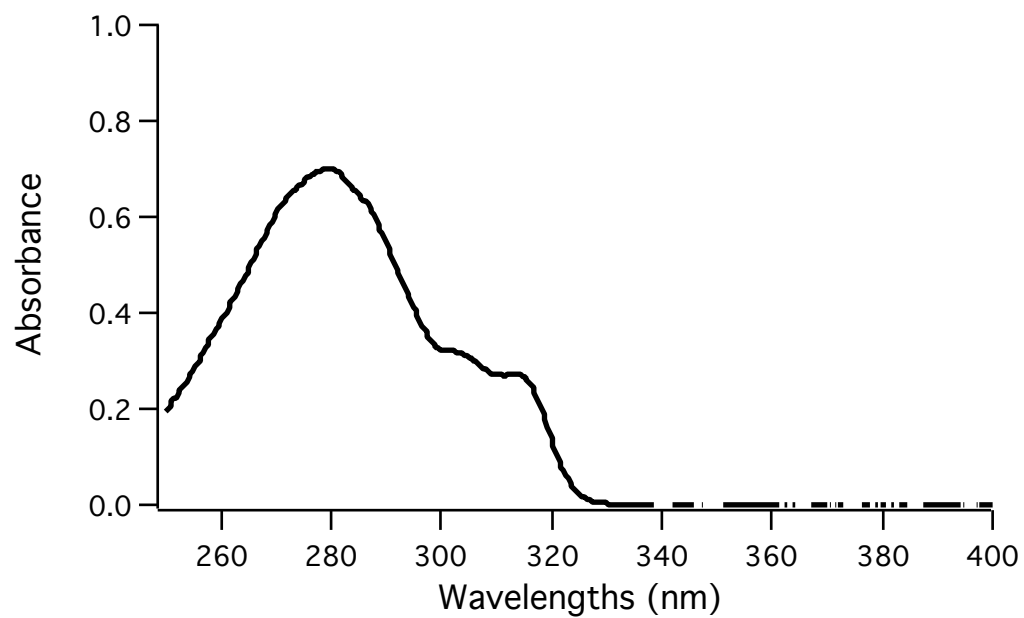
UV-Vis Spectrum of compound *trans*-4C in dichloromethane.



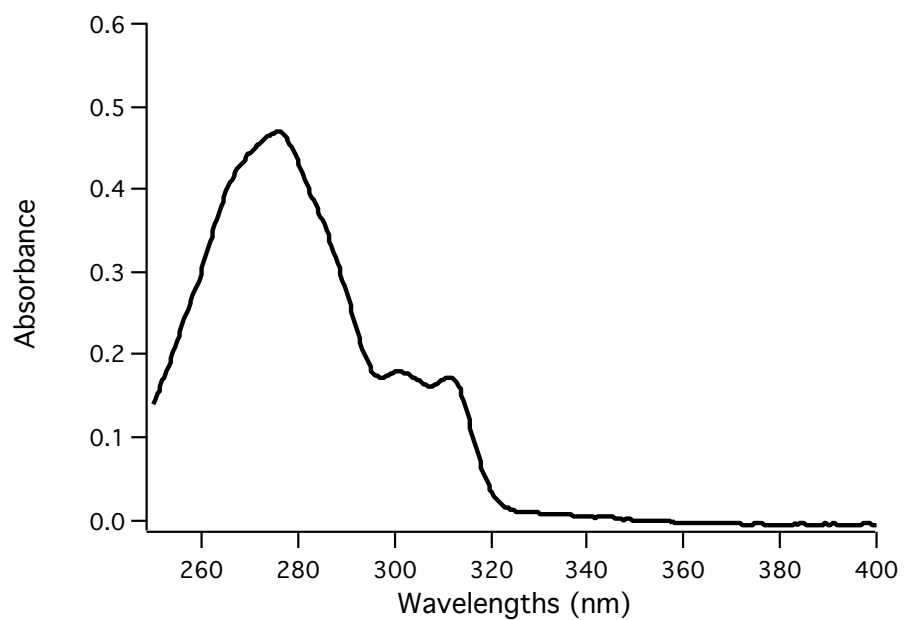
UV-Vis Spectrum of compound *cis*-4C in dichloromethane.



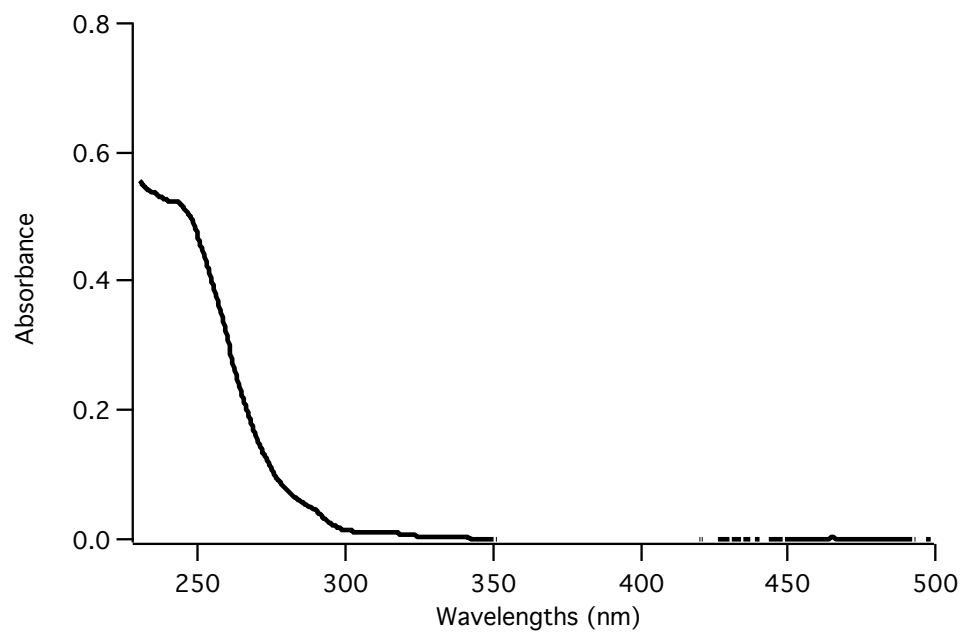
UV-Vis Spectrum of compound *trans*-**4D** in dichloromethane.



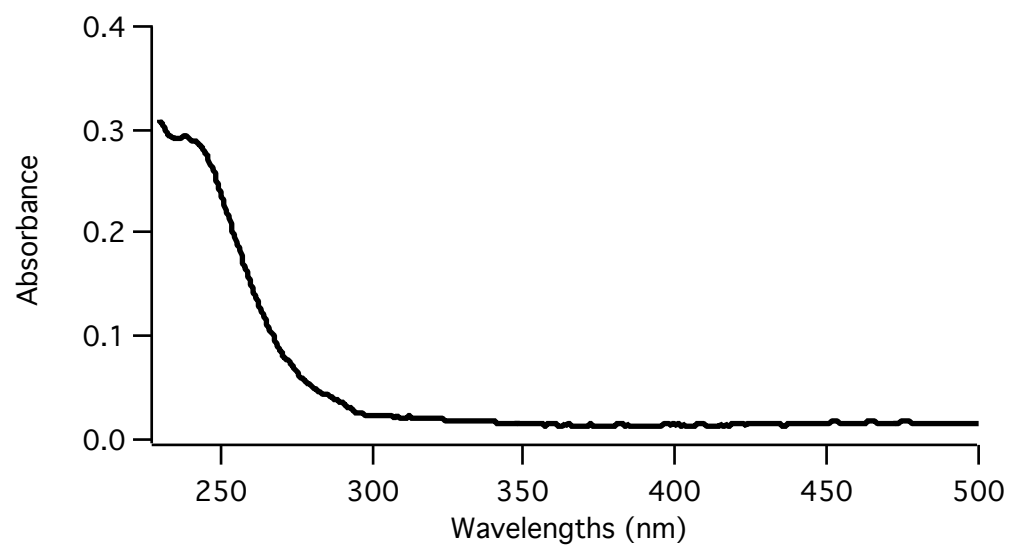
UV-Vis Spectrum of compound *cis*-**4D** in dichloromethane.



UV-Vis Spectrum of compound *trans*-4E in dichloromethane.



UV-Vis Spectrum of compound *cis*-4E in dichloromethane.



3.5.2 Computational Data

Computational analysis was performed using Spartan[®]16V1.1.0 on a PC computer. We calculated lowest energy conformer by Molecular Mechanics and subsequently submitted a B3LYP/6-31G* for the equilibrium geometry using the most stable conformation. The hartrees calculated from the output file was converted to kcals/mol to find the difference in ground state energies between the *trans*- and *cis*-aziridines. The calculations are shown below in the Table.

		<u>kcals/mol</u>	<u>Difference in Energies</u>
trans 4a	-969.205537 hartrees	-608185.7866	
cis 4a	-969.201410 hartrees	-608183.1969	-2.589732
trans 4b	-1122.849563 hartrees	-704598.8892	
cis 4b	-1122.839418 hartrees	-704592.5231	-6.366085
trans 4c	-1200.262929 hartrees	-753176.5201	
cis 4c	-1200.259202 hartrees	-753174.1814	-2.3387283
trans 4d	-1238.379969 hartrees	-777095.3289	
cis 4d	-1238.370067 hartrees	-777089.1153	-6.21360013

3.6 References

- 1 A. K. Yudin, *Aziridines and Epoxides in Organic Synthesis*, ed., Wiley-VCH, Weinheim, Germany, 2006
- 2 I. D. G. Watson, L. Yu and A. Yudin, *Acc. Chem. Res.*, 2006, **39**, 194–206.
- 3 B. Zwanenburg and P. ten Holte, *Topics in Current Chemistry, in Stereoselective Heterocyclic Synthesis III*, ed. P. Metz, Springer, Berlin, 2001, vol. 216, pp. 93–124.
- 4 C. Botuha, F. Chemla, F. Ferreira, A. Perez-Luna, Aziridines in natural product synthesis. In *Heterocycles in Natural Product Synthesis*; 2011; p 3.
- 5 K. Harada, K. Tomita, K. Fujii, K. Masuda, Y. Mikami, K. Yazawa, H. Komaki, *J. Antibiot.*, 2004, **57**, 125-135.
- 6 T. Tsuchida, H. Iinuma, N. Kinoshita, T. Ikeda, T. Sawa, M. Hamada, T. Takeuchi, *J. Antibiot.*, **1995**, *48*, 217-221.
- 7 See references within: L. Degennaro, P. Trinchera, R. Luisi, *Chem. Rev.*, 2014, **114**, 7881-7929.
- 8 T. S. Chung, S. A. Lopes, K. N. Houk, M. A. Garcia-Garibay, *Org. Lett.*, 2015, **17**, 4568-4571.
- 9 M. G. Hernandez-Linares, G. Guerrero-Luna, S. Perez-Estrada, M. Ellison, M. Ortin, M. A. Garcia-Garibay, *J. Am. Chem. Soc.*, 2015, **137**, 1679-1684.
- 10 S. Shiraki, C. S. Vogelsberg, M. A. Garcia-Garibay, *Photochem. Photobiol. Sci.*, 2012, **11**, 1929-1937.
- 11 A. Natarajan, D. Ng, Z. Yang, M. A. Garcia-Garibay, *Angew. Chem. Int. Ed.*, 2007, **46**, 6485-6487.
- 12 D. de Loera, M. A. Garcia-Garibay, *Org. Lett.*, 2012, **14**, 3874–3877.

- 13 P. Crews, J. Rodriguez, M. Jaspars, *Organic Structure Analysis*, 2nd ed.; Oxford University Press: New York, 2010.
- 14 A. G. Griesbeck, H. Mauder, S. Stadtmueller, *Acc. Chem. Res.* 1994, **27**, 70-75.
- 15 D. Andrew, A. C. Weedon, *J. Am. Chem. Soc.* 1995, **117**, 5647-5663.
- 16 J. C. Scaiano, *Tetrahedron* 1980, **36**, 819-824.
- 17 P. S. Engle, *Chem. Rev.* 1980, **80**, 99-150.
- 18 C. Reichardt, and T. Welton. *Solvents and Solvent Effects in Organic Chemistry*. Weinheim: Wiley VCH, 2011. Print.
- 19 E. V. Anslyn and D. A. Dougherty. *Modern Physical Organic Chemistry*. Sausalito, CA: U Science, 2008.

Chapter 4

Kinetics and Mechanism of Photochemistry of Δ^2 -1,2,3-Triazolines to form Aziridines in Solution and in Solid-State: Observation of 1,3-Biradical Intermediate by Pump-Probe Spectroscopy.

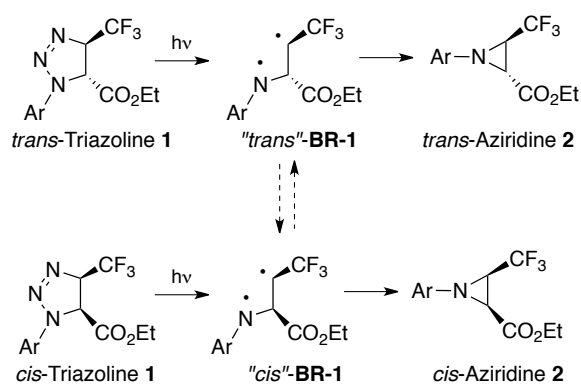
4.1 Introduction

One of the long-standing challenges in solid state photochemistry is the correlation of structural information with mechanistic models based on absolute kinetics of excited states and reactive intermediates. While transmission spectroscopy using laser pump-probe methods has been essential in the development of mechanistic models in solution, it is well known that bulk powders and large crystals display complex and heterogeneous kinetics due to their high optical densities, intense light scattering, and interference by accumulated photo-products.¹ Up to now, most mechanistic aspects of solid-state photochemistry rely on the correlation of reactant and product structures to infer their reaction trajectories.^{2,3} One may expect that faster progress will occur as operationally simple methods become available to measure absolute kinetics in crystalline solids. To that effect we have shown that crystals in the 50-200 nm size range (nanocrystals) can be suspended in water and may be viewed as a state in transition between large supramolecular entities and bulk solids, such that conventional transmission methods may be used to study them.⁴ ⁸ In this letter, we take advantage of this method to investigate the detection of the 1,3-alkyl-aminyll biradicals **BR** as intermediates in the photodenitrogenation of Δ^2 -1,2,3-triazolines (Scheme 1).

As illustrated in Scheme 1, we recently reported that ultraviolet light excitation of *trans*- and *cis*- Δ^2 -1,2,3-triazolines **1** (Ar=2-fluorenyl) in the crystalline solid state leads to stereospecific chemical reactions, with crystals of each diastereomer enhancing the selectivity of the corresponding starting material as compared to the results obtained in acetonitrile solution.⁹ Reactions carried out in MeCN with *trans*-**1** led to aziridine **2** with a *trans*:*cis* ratio of 76:24, suggesting that a short lived “*trans*” singlet biradical is not able to equilibrate. Similarly, when *cis*-**1** was irradiated in the same solvent a *trans*:*cis* aziridine ratio of 32:68 confirmed a non-fully equilibrating “*cis*” biradical, suggesting that direct irradiation in solution proceeds under kinetic

control via the singlet state. This hypothesis was supported by results from experiments carried out with either *trans*-**1** or *cis*-**1** using acetone as a solvent and triplet sensitizer. Under those conditions only *trans*-**2** was formed, suggesting that the triplet biradical lives long enough for conformational equilibration to occur and the reaction proceeds through the “*trans*”-biradical species.

Scheme 4.1.1



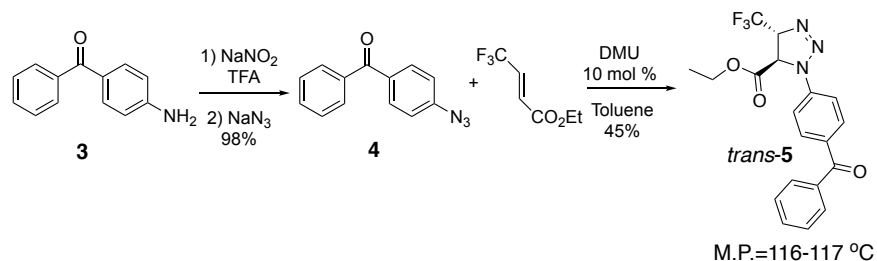
Triazoline	<i>trans</i> - 2 : <i>cis</i> - 2	<i>trans</i> - 2 : <i>cis</i> - 2	<i>trans</i> - 2 : <i>cis</i> - 2
Ar=2-fluorene	MeCN	Acetone	Crystals
<i>trans</i> - 1	76:24	>99:1	83:17
<i>cis</i> - 1	32:68	>99:1	10:90

Based on those observations, we recognized that we had an opportunity to detect the postulated triplet 1,3-alkyl-aminyl biradical and learn more about the reaction mechanism in solution and in the solid state. To facilitate our goal, instead of using external sensitizers we prepared triazoline *trans*-**5** with a benzophenone group linked at the N-aryl position, so that intramolecular triplet sensitization may take place (Scheme 2).¹⁰

4.2 Results and Discussion

4.2.1 Synthesis and Characterization

Scheme 4.2.1



Triazoline *trans*-**5** was prepared from commercially available 4-aminobenzophenone **3**, which was transformed in nearly quantitative yield to the corresponding aryl azide **4** by standard diazotization.⁹ Samples of 4-azidobenzophenone **4** displayed the characteristic IR stretch at ca. 2200 cm⁻¹ for the azido functional group, and its ¹H and ¹³C NMR spectra matched the literature data (See SI).¹¹ Triazoline *trans*-**5** was obtained in modest yield (45%) by a 1,3-dipolar cycloaddition with azide **4** and the *trans*-3-trifluoromethylcrotonate. The reaction was carried out in the presence of 10 mol% dimethyl urea, which served as a hydrogen bond donor catalyst. The identity of triazoline *trans*-**5** was confirmed by ¹H and ¹³C NMR spectra. A notable feature in the ¹H NMR is the vicinal coupling constant of the two ring hydrogen with $J_{trans} \approx 8$ Hz, which matched that of previous reports on similar *trans*-triazolines.⁹ Irradiating triazoline *trans*-**5** in acetonitrile with a medium pressure 450 W Hanovia Hg arc lamp equipped with a Pyrex filter (cutoff of $\lambda \leq 290$ nm) afforded exclusively the *trans* aziridine product, suggesting that triazoline *trans*-**5** undergoes efficient triplet sensitization from the benzophenone moiety.

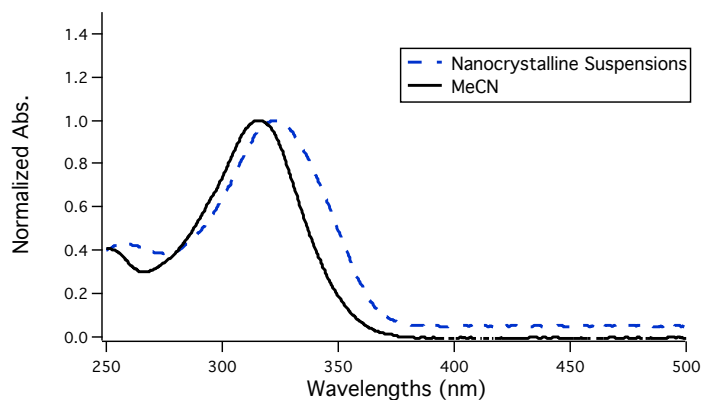


Figure 4.2.1 UV-Vis absorption spectra of triazoline *trans*-5 in acetonitrile (black solid line) and in nanocrystalline suspension (blue dotted line).

In order to carry out the sought-after pump-probe spectroscopic measurements we analyzed formation and stability of nanocrystalline suspension. As in previous studies, aqueous nanocrystalline suspensions were prepared by the solvent shift or reprecipitation method¹² and their formation was established by several methods, including powder X-ray diffraction and dynamic light scattering. As shown in Figure 1, we recorded powder X-ray diffraction (PXRD) of triazoline *trans*-5 both with bulk powder and with crystals acquired from nanocrystalline suspension obtained from centrifugation and air-drying. It is apparent that the two diffractograms have very similar patterns and peak positions, suggesting that both belong to same crystal polymorph. However, some differences in peak intensities suggest that nanocrystals collected by centrifugation tend to adopt specific crystallite alignments as compared to those in the bulk powder. Crystal sizes of triazoline *trans*-5 were analyzed by dynamic light scattering, which revealed an average value of ca. 186 nm in three distinct DLS experiments (see SI). The fact that nanocrystals of *trans*-5 are smaller than the wavelength of light used for excitation results in strongly diminished scattering, birefringence and dichroism, such that their optical properties should be suitable for transmission spectroscopy. This was confirmed by the excellent quality of the UV spectra obtained

with nanocrystalline suspension of *trans*-**5** (Figure 2, blue dotted line), which compare remarkably well with those obtained in acetonitrile solutions (black solid line). The only significant difference between that two is the ca. 5 nm red shift in the solid state compared to the $\lambda_{\text{max}} = 320$ nm measured in solution.

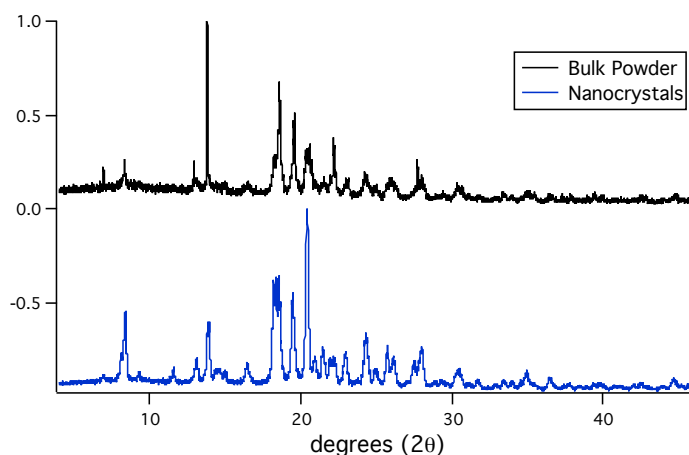


Figure 4.2.2 Powder X-Ray Diffraction (PXRD) patterns of bulk powder (black line) and nanocrystals (blue line) of triazoline *trans*-**5**.

4.2.2 Laser Flash Photolysis

The laser flash photolysis experiments with *trans*-**5** were performed with a Nd:YAG laser setup working at 355 nm with a pulse width of ca. 8 ns using a 1 cm quartz flow cell mounted on a home-built sample holder at the crossing path of the incident laser pump and white light probe beams. A continuous flow of argon gas was used to purge both the acetonitrile solutions and the aqueous crystalline suspension reservoirs, which were flown through the cell to ensure that unreacted sample was analyzed at every laser pulse working at a repetition rate of 1 Hz. Figure 3a depicts the transient absorption spectrum of triazoline *trans*-**5** in acetonitrile immediately after the laser pulse showing a broad band from 400-500 nm and a sharp strong absorption with a $\lambda_{\text{max}} \approx 570$ nm. The spectrum was shown to decrease in a homogeneous manner within ca. 300 ns and a kinetic

trace at 570 nm revealed a monoexponential decay with a lifetime of 70 ns (Figure 3b). Figure 3c depicts the transient absorption spectrum of *trans*-**5** in nanocrystalline suspensions obtained with the same experimental setup. At the end-of-pulse spectrum we observed a broad spectrum from ca. 400-480 nm and a broad band with a $\lambda_{\text{max}} \approx 510$ nm. We recorded kinetic decay at 510 nm in nanocrystalline suspensions and observed a monoexponential growth with a time constant of 63 ns and a monoexponential decay of 260 ns (Figure 3d). In order to explain the residual offset shown in Figure 3d, we initially thought the baseline offset was a second long-lived transient species, however, extending the time window to 100 μs revealed a consistent flat residual offset, ruling out the possibility of a second transient species. We have also attempted to change the laser intensity, as high laser power can change the temperature of the sample solution, thereby changing the index of refraction which may result in providing excess light into the probe. However, the residual offset proved to be impervious to laser intensity. Another possibility of the baseline offset in Figure 3d may be from absorption of a small amount of byproduct, which absorbs in the 510 nm region. We recorded UV-Vis of a freshly laser-pulsed sample and observed no absorption in this region, additionally knowing that the aziridine product has a UV profile which cuts off at 380 nm, we ruled out the possibility of the residual from product (or byproduct) absorption. We also ruled out the possibility of an impurity in our Millipore water used to make nanocrystalline suspensions, as laser flash photolysis experiment of just the water displayed no residual offset in the 510 nm region. We speculate that the high residual offset in the baseline in Figure 3d is the result of scattering of the nanocrystals. We observed aggregation of nanocrystals as indicated from DLS experiments before and after laser flash experiments. The post-laser flash nanocrystalline sample displayed an increase in particle size from 186 to 441 nm by dynamic light scattering. In fact, a fresh 50 mL nanocrystalline sample had to be added to the reservoir at 15 minute intervals

to ensure transient detection. It is worth noting that the kinetics of the solid-state photoreaction for triazoline *trans-5* seem to be much slower than those in solution, which is why we observe a growth of the triplet biradical and a subsequent decay in nanocrystals. The fact that the triplet biradical has a decay lifetime of 70 ns and 260 ns in acetonitrile and in nanocrystalline suspensions, respectively, would allow time for rotational equilibrium to provide the more thermodynamic *trans* azidirine product we observed previously. We have also attempted to detect transient kinetics for triazoline *trans-1*, however we were unable to detect any transients, presumably because *trans-1* undergoes denitrogenation in a singlet manifold, so that the biradical will be able to form the product in a time scale that is too fast for our 8 ns pump-probe experiment.

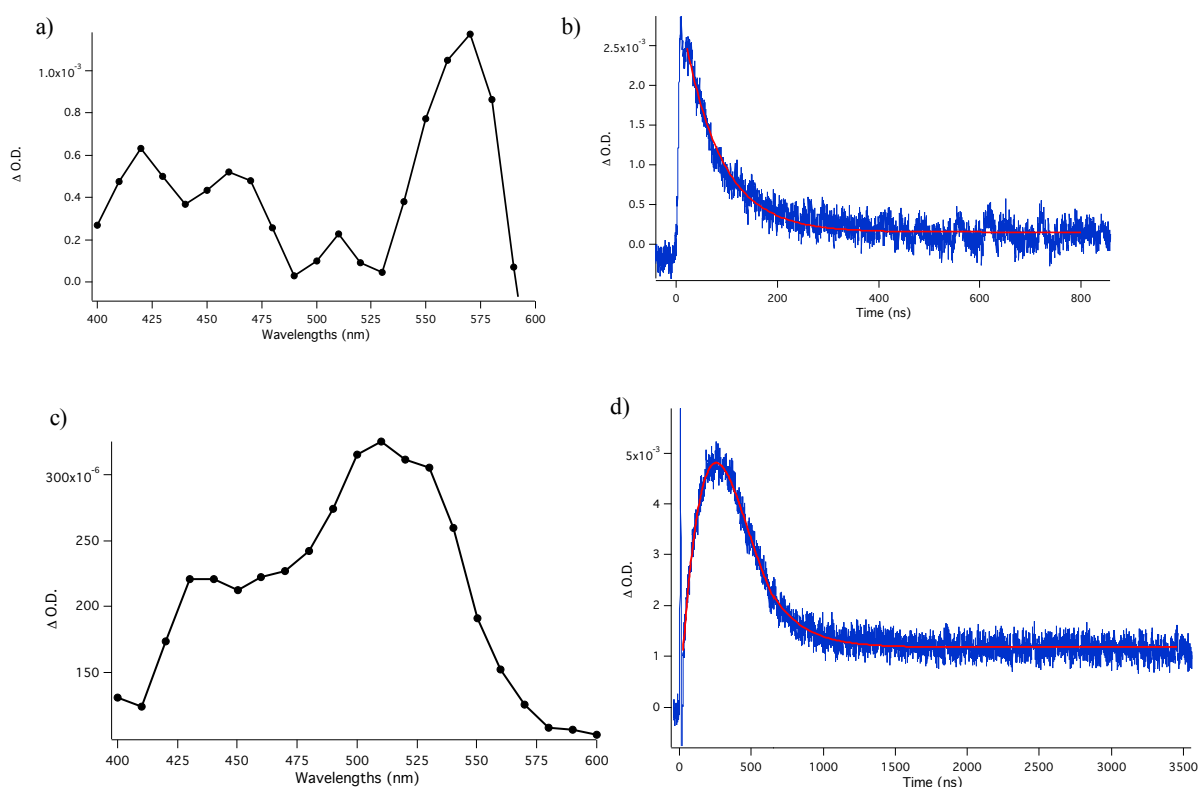
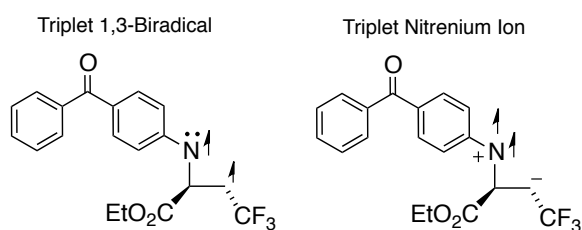


Figure 4.2.3 a) Transient absorption spectrum of triazoline *trans-5* sliced at various time points in acetonitrile, c) transient decay of triazoline *trans-5* in acetonitrile detected at 570 nm, c) transient absorption spectrum of triazoline *trans-5* sliced at various time points in nanocrystalline

suspension, d) transient decay of triazolone *trans*-5 in nanocrystalline suspension detected at 510 nm.

In order to assign the transient species observed in our experiments, we considered that the loss of nitrogen from the triplet excited state may occur via homolytic or heterolytic pathways (Scheme 3). While homolytic cleavage would result in formation of a triplet 1,3-biradical with the conjugated aryl aminyl radical center being the chromophore most likely to be observed in our experiment, heterolytic cleavage (or fast intramolecular electron transfer) would lead to the formation of a triplet aryl nitrenium species along with a CF₃-stabilized a carbanion center, with the conjugated benzophenone unit also being the most likely UV-Vis absorber.

Scheme 4.2.2



A literature search revealed that phenyl substitution in the simple species gives rise to absorptions at ca. 400 nm for the radical and ca. 500 nm for the electron-deficient the nitrenium ion intermediate.^{13,14} To address the different aryl substituent in our experiments and have a better standard for spectral comparison, we generated the 4- benzophenone aminyl radical (Figure 4) following a reported protocol by Platz and Wirz by performing laser flash photolysis experiments with 4-amino benzophenone **3** in the presence of di-tertbutyl peroxide (DTBP).

Figure 4 shows the end-of-pulse spectrum of 4-aminy benzophenone radical **4**, which shows a broad absorption at ca. 400-460 nm, and a large and sharp λ_{max} at 560 nm. The features

of the transient spectrum of the 4-aminy benzophenone radical **4** in Figure 4 are in good accord with the end-of-pulse spectrum of triazoline *trans*-**5** in acetonitrile (Figure 3a). Indeed, both show a broad absorption from ca. 400-460 nm and a sharp band with a $\lambda_{\text{max}} \approx 560$ -570 nm. Attempts to probe the formation a nitrenium ion resulted in negative results. For example, we reasoned that formation of a nitrenium ion could be demonstrated by taking advantage of reaction with a diffusion-controlled trapping agent, such as acetic acid, which would immediately protonate the carbanion center while the conjugate acetate base would bond to the electron deficient nitrogen after intersystem crossing. However, photochemical experiments carried out with *trans*-**5** in neat acetic acid led to the exclusive formation of azidirine *trans*-**7**, with no indication of the acetylated hydroxyl amine trapping product (Scheme 4).

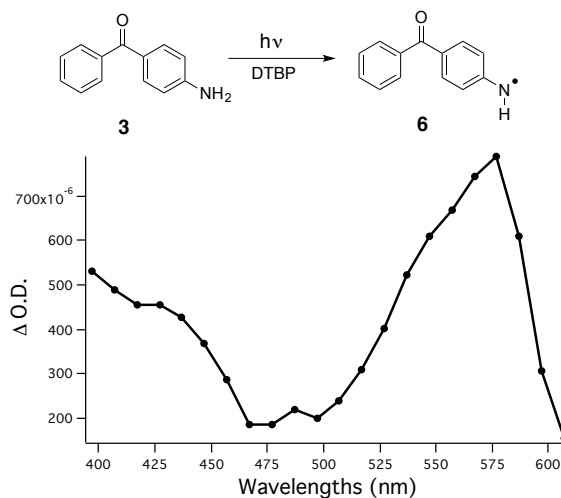
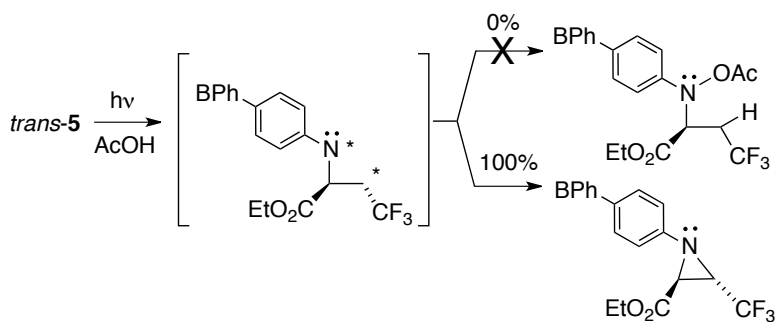


Figure 4.2.4 End-of-pulse transient absorption spectrum of 4-aminy benzophenone radical **4** by performing LFP studies with 4-amino benzophenone **3** in the presence of di-tertbutyl peroxide (DTBP).

We also attempted to generate and detect the benzophenone-linked nitrenium ion by performing LFP experiments with 4-azidobenzophenone in ethanol and acetic acid as solvents. It

was hoped that generation of nitrene from denitrogenation followed by rapid protonation of a nitrene might lead to the formation of the nitrenium ions, but unfortunately we were unable to detect any transient species. Considering that phenyl nitrenium ion is known to have a lifetime of ca. 110 ps in solution, it is reasonable to conclude that a benzophenone-substituted nitrenium ion would also have a lifetime that is much faster than the ca. 8 ns time resolution of our instrument.¹⁴ Considering that the observed transient has decay lifetime of 70 ns and 260 ns in acetonitrile and in nanocrystalline suspensions, respectively, it is more consistent with the triplet biradical. Furthermore, its relatively long lifetime allows for conformational equilibrium to provide the more stable *trans*-aziridine product (Scheme 1).

Scheme 4.2.3



4.3 Conclusions

In conclusion, we have synthesized a Δ^2 -1,2,3-triazoline with a benzophenone moiety as an internal triplet sensitizer and observed its kinetics by transient pump-probe spectroscopy in solution and in nanocrystals. Our results are consistent with the transient chromophore observed for this process which is the 4-aminy benzophenone radical which has a decay lifetime of 70 ns and 260 ns in acetonitrile and in nanocrystalline suspensions, respectively. We also observed the transient absorption spectrum for the 4-aminy benzophenone radical by irradiating 4-amino benzophenone in the presence of di-tert butyl peroxide, which is in good agreement with the

transient absorption spectrum observed for triazoline *trans*-**5** in solution. Additionally, we performed product analysis studies on triazoline *trans*-**5** in the presence of acetic acid as the solvent and only observed the aziridine *trans*-**7**, further providing evidence that the main intermediate in this process is in fact the 1,3-alkyl aminyl biradical. The fact that the triplet biradical has a decay lifetime in the range of 70-260 ns in solution and in nanocrystals, respectively, would provide necessary time for rotational equilibrium to solely provide the thermodynamic *trans* aziridine product.

4.4 Experimental

Synthesis of 2-azido benzophenone (compound **4**):

4-amino benzophenone was commercially available and was used without further purification.

Compound **4** was synthesized according to reported procedure in literature¹ from 2- amino benzophenone. Crude product from the reaction was purified by silica gel chromatography (eluent: EtOAc/Hexanes 20/80). Yield 98%, slightly yellow solid, R_f 0.85. IR (ATR cm^{-1}): 3067, 2126, 2095, 1660, 1651, 1593, 1271, 697. ^1H NMR (500 MHz, CDCl_3) δ 7.88 – 7.79 (m, 2H), 7.79 – 7.71 (m, 2H), 7.62 – 7.55 (m, 1H), 7.53 – 7.44 (m, 2H), 7.15 – 7.07 (m, 2H). ^{13}C NMR (126 MHz, CDCl_3) δ 195.29, 144.46, 137.60, 134.05, 132.41, 132.12, 129.85, 128.36, 118.78. Compound spectra have been matched with reported literature values.²

Synthesis of ethyl (4*R*,5*R*)-1-(4-benzoylphenyl)-4-(trifluoromethyl)-4,5-dihydro-1*H*-1,2,3-triazole-5-carboxylate (compound *trans*-**5**):

Commercially available ethyl 4,4,4-trifluorocrotonate (0.3 mmol), **4** (0.3 mmol), and $\text{N,N}'$ -dimethylurea (0.03 mmol) was dissolved in 1.5mL of dry toluene the reaction was stirred for 32 hours at 60⁰C under argon atmosphere. After the initial 32 hours, an additional 0.3 mmol of ethyl

4,4,4-trifluorocrotonate was added to the solution. After 33 more hours of heating, the reaction was cooled when the disappearance of azide by TLC was observed. The product mixture was purified by two separate silica gel column chromatography. First purification was performed with (eluent 10/60 EtOAc/Hexanes) R_f 0.39 and second column chromatography was performed with 100% DCM R_f 0.65 to obtain *trans*-**5** with yield 45% as a white solid. IR (ATR): 2972, 1754, 1651, 1599, 1239, 1223, 1134, 700 cm^{-1} . ^1H NMR (500 MHz, CD_3CN) δ 7.94 – 7.80 (m, 2H), 7.80 – 7.70 (m, 2H), 7.71 – 7.58 (m, 1H), 7.60 – 7.49 (m, 2H), 7.49 – 7.35 (m, 2H), 5.74 – 5.57 (m, 1H), 5.04 (d, $J = 6.9$ Hz, 1H), 4.23 (q, $J = 7.1$ Hz, 2H), 1.22 (t, $J = 7.1$ Hz, 3H). ^{13}C NMR (126 MHz, CD_3CN) δ 194.85, 167.04, 142.11, 137.81, 132.76, 132.29, 131.91, 129.56, 128.40, 123.93, 121.71, 119.49, 114.67, 82.09, 81.85, 81.62, 81.38, 63.10, 55.61, 13.17. Melting Point: 116-117°C.

Synthesis of ethyl (2*R*,3*R*)-1-(4-benzoylphenyl)-3-(trifluoromethyl)aziridine-2-carboxylate (compound *trans*-**7**):

For solid-state photolysis:

Triazoline *trans*-**5** (5-8 mg) was crushed between two microscope slides and photolyzed using a medium-pressure Hg Hanovia lamp with a pyrex emersion well filter with cutoff of $\lambda \leq 290$ nm.

The reaction was monitored by ^1H NMR and was completed in ca. one hour.

For solution-state photolysis:

Triazoline (5-8mg) was dissolved in deuterated acetonitrile in an NMR tube and the solution was freeze-pump-thawed for 3 cycles to ensure no gas was present in the photoreaction. The NMR tube was irradiated using a medium-pressure Hg Hanovia lamp with a pyrex emersion well filter with cutoff of $\lambda \leq 290$ nm. The reactions were monitored by ^1H NMR and showed completion in less than one hour.

IR (ATR): 2983, 1737, 1654, 1598, 1336, 1273, 1144, 699, 658 cm^{-1} . ^1H NMR (500 MHz, CD_3CN) δ 7.79 – 7.68 (m, 4H), 7.68 – 7.57 (m, 1H), 7.57 – 7.45 (m, 2H), 7.11 – 6.97 (m, 2H), 4.20 – 3.97 (m, 2H), 3.69 (qd, $J = 5.0, 2.3$ Hz, 1H), 3.59 (d, $J = 2.3$ Hz, 1H), 1.12 (t, $J = 7.1$ Hz, 3H). ^{13}C NMR (126 MHz, CD_3CN) δ 195.65, 165.35, 151.31, 138.45, 133.51, 132.79, 132.00, 130.08, 128.93, 126.88, 124.71, 122.53, 120.36, 120.08, 117.90, 62.72, 42.47, 42.15, 41.83, 41.51, 39.91, 39.89, 13.85. White solid, melting Point: 95-96°C.

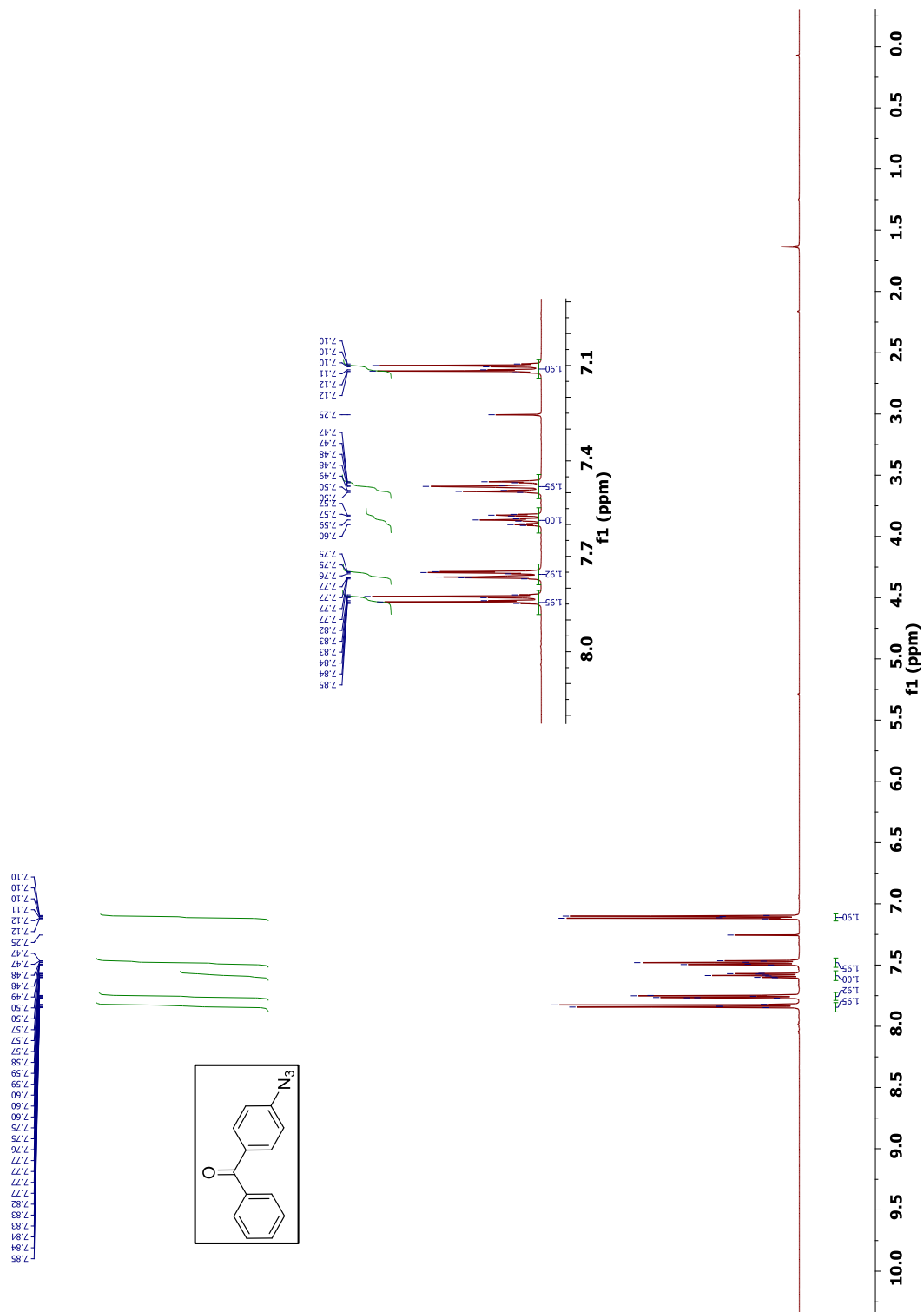
4.5 Appendix

Characterization for Chapter 4

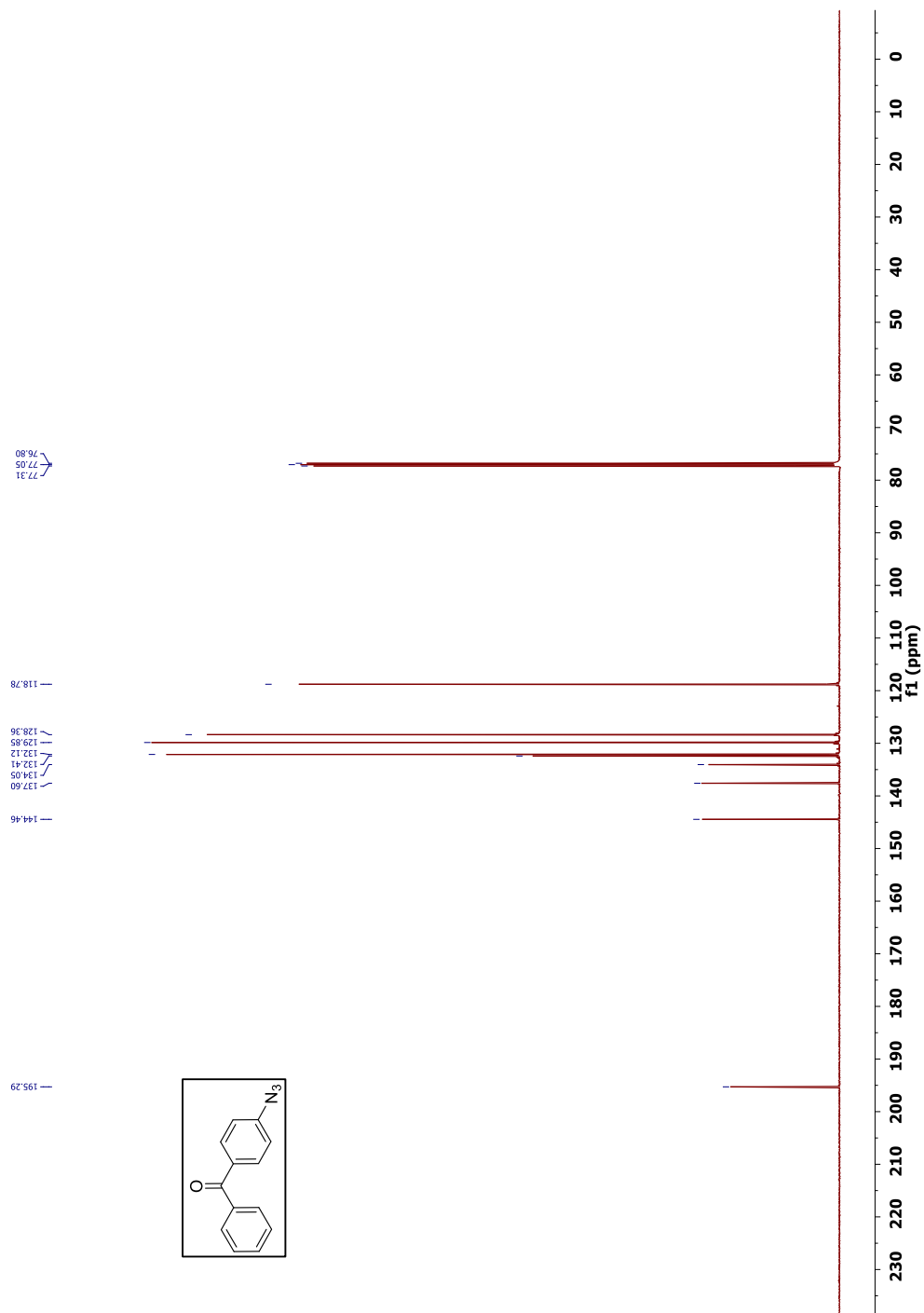
4.5.1	Compound Spectra (^1H NMR, ^{13}C NMR, UV-Vis).....	6
4.5.2	Dynamic Light Scattering.....	13
4.5.3	Laser Flash Photolysis.....	14

4.5.1 Compound Spectra (^1H NMR, ^{13}C NMR, UV-Vis)

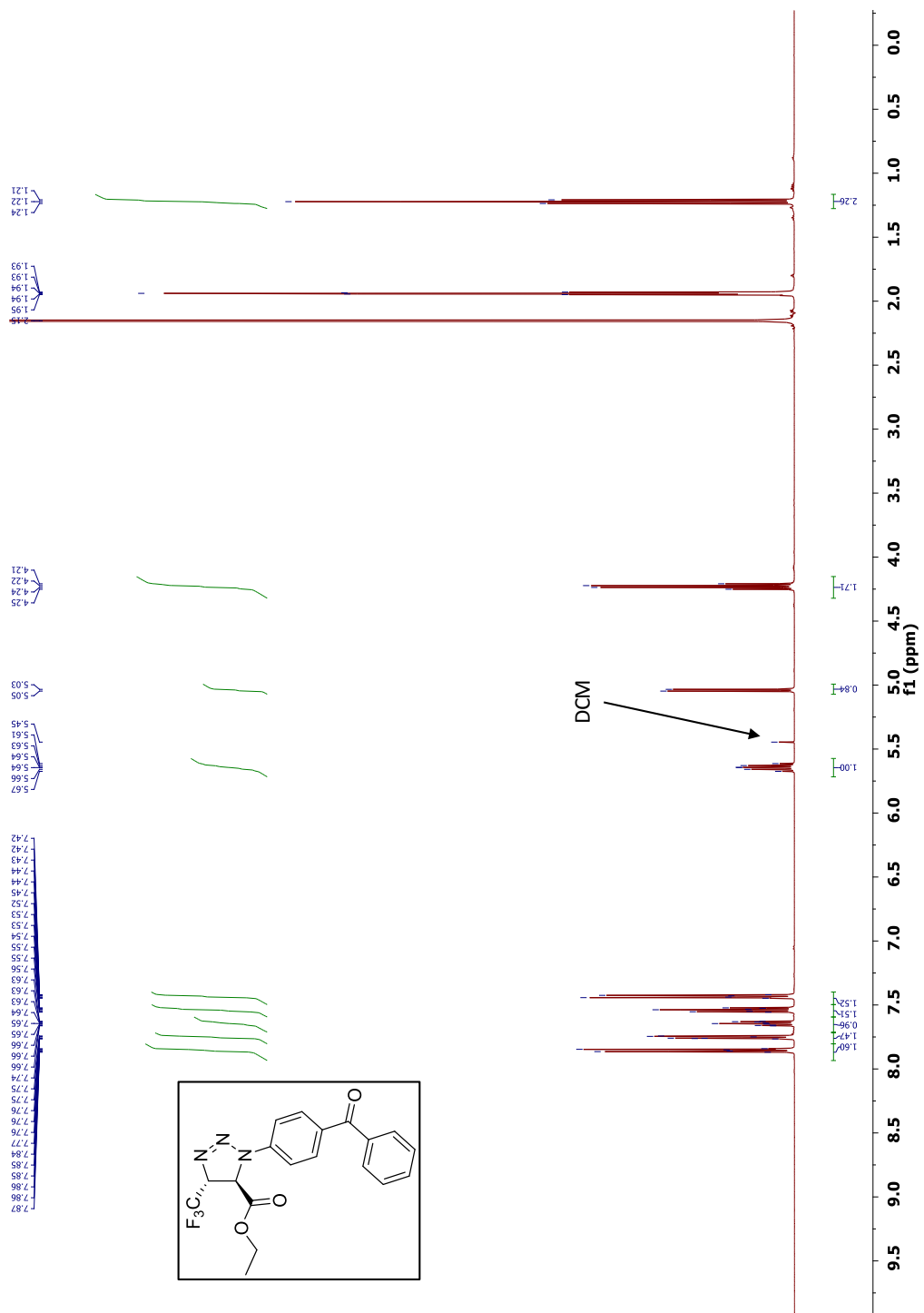
^1H NMR (CDCl_3 , 500 MHz) spectrum of compound 4.



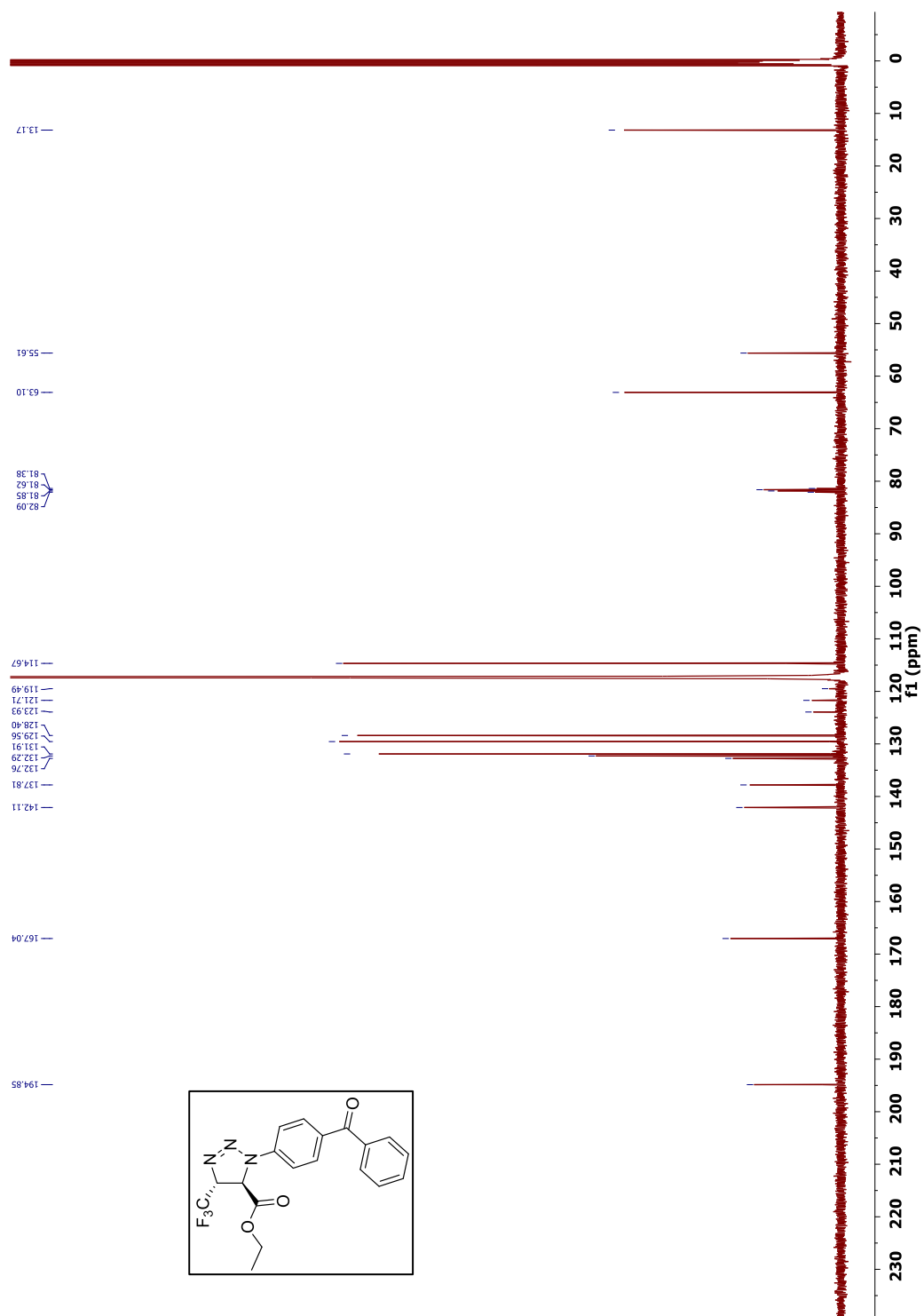
^{13}C NMR (CDCl_3 , 125 MHz) spectrum of compound 4.



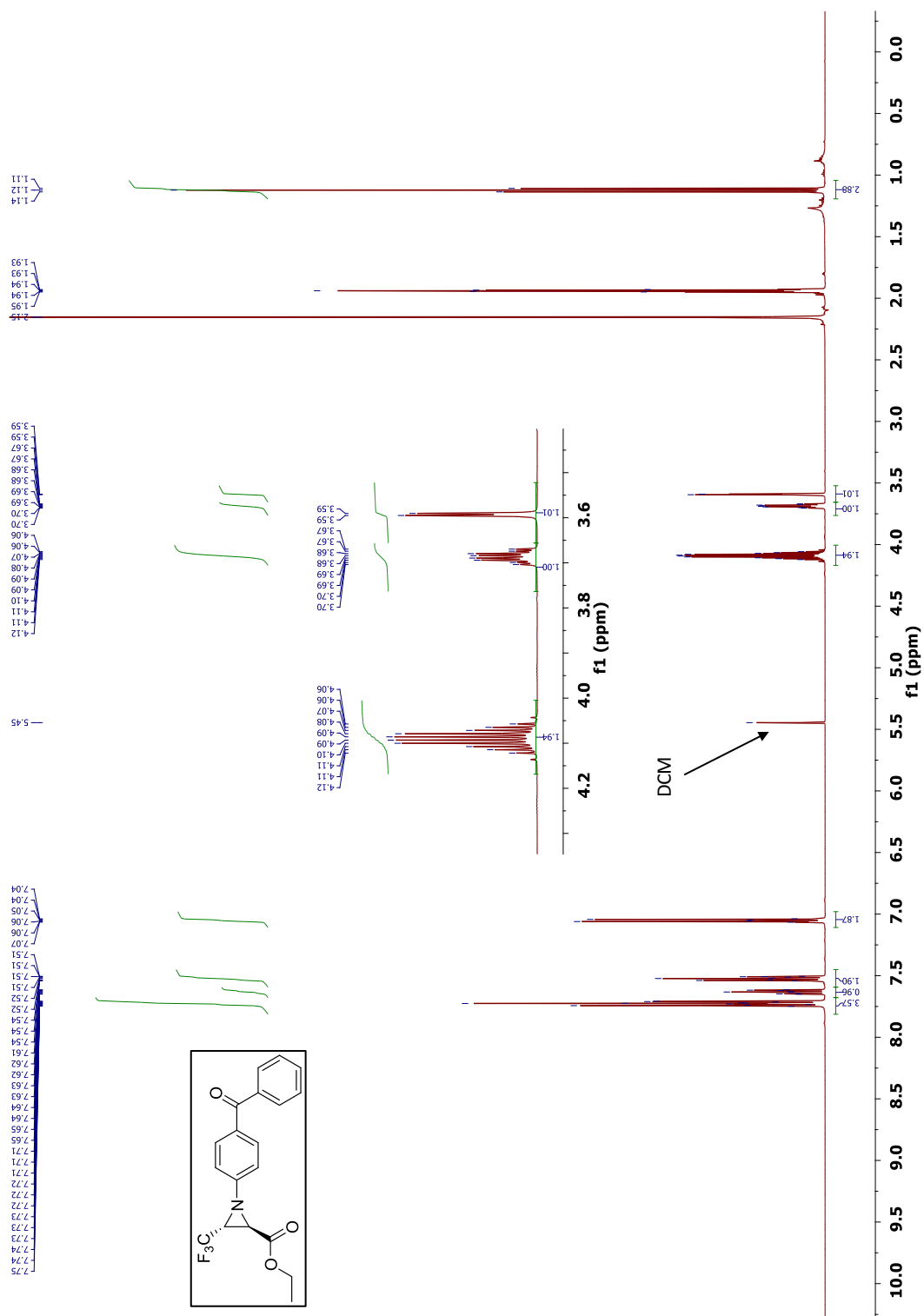
^1H NMR (500 MHz, CD_3CN) of compound *trans*-5.



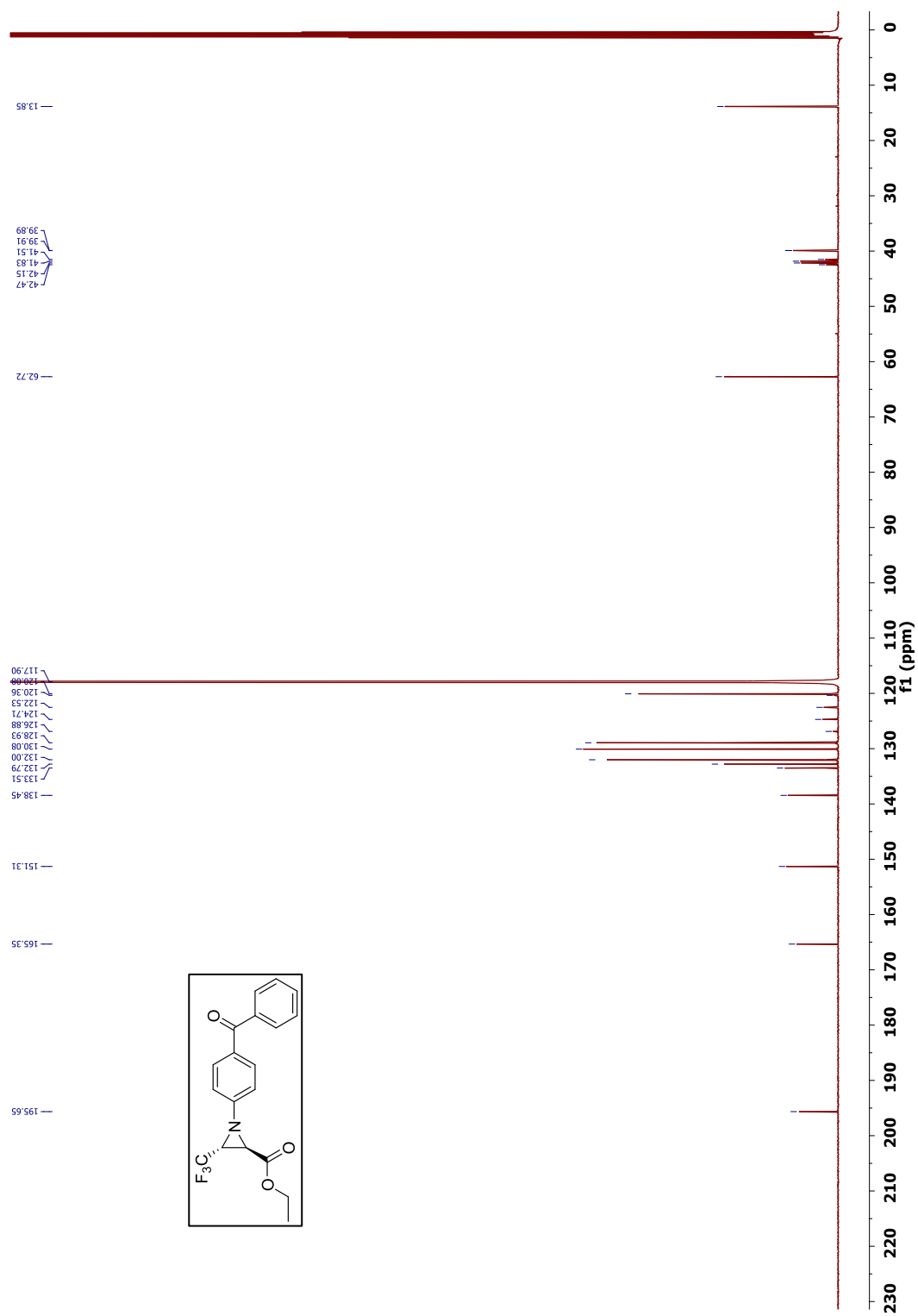
^{13}C NMR (126 MHz, CD_3CN) of compound *trans*-5.



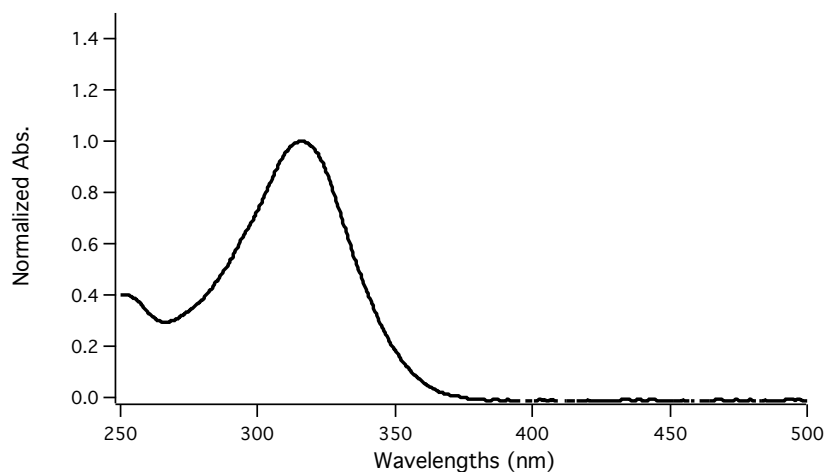
^1H NMR (500 MHz, CD_3CN) of compound *trans*-7.



^{13}C NMR (126 MHz, CD_3CN) of compound *trans*-7.

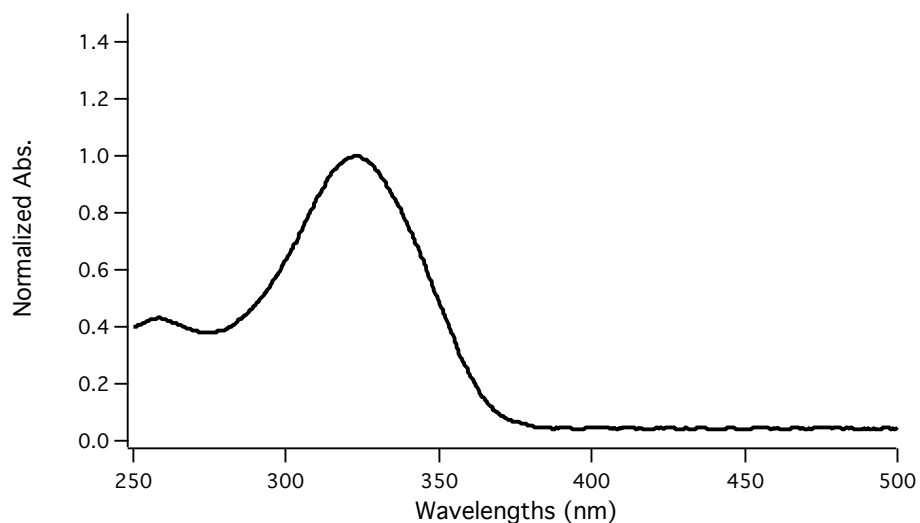


UV-Vis Spectrum of compound *trans-5* in acetonitrile.

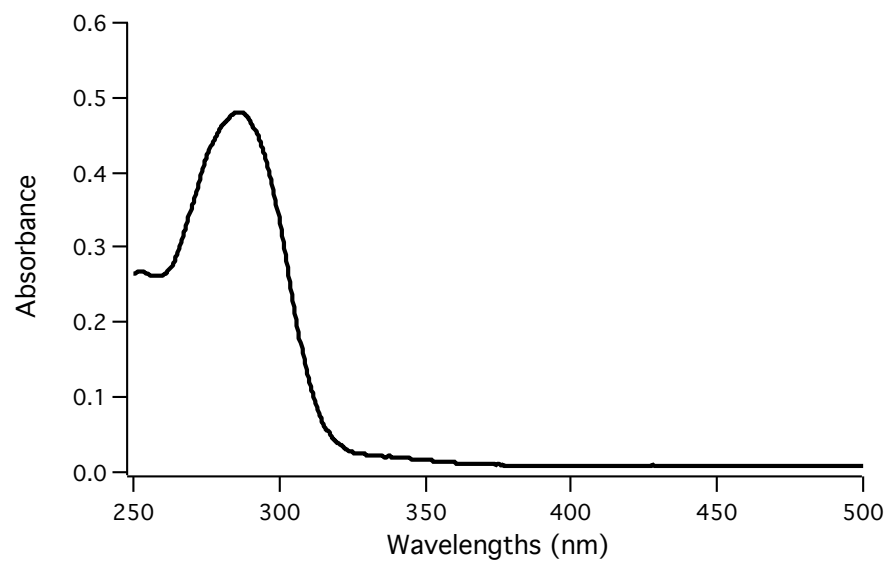


UV-Vis Spectrum of compound *trans-5* in nanocrystalline suspension in water.

Stable nanocrystalline suspensions were using the reprecipitation method,³ pouring concentrated acetonitrile solutions (20 mg/10mL) of the triazoline into (60 mL) of rapidly vortexing water with submicellar concentrations of cetyltrimethylammonium bromide (CTAB) to passivate the surface of the nanocrystals and prevents aggregation.



UV-Vis Spectrum of compound *trans*-7 in acetonitrile.

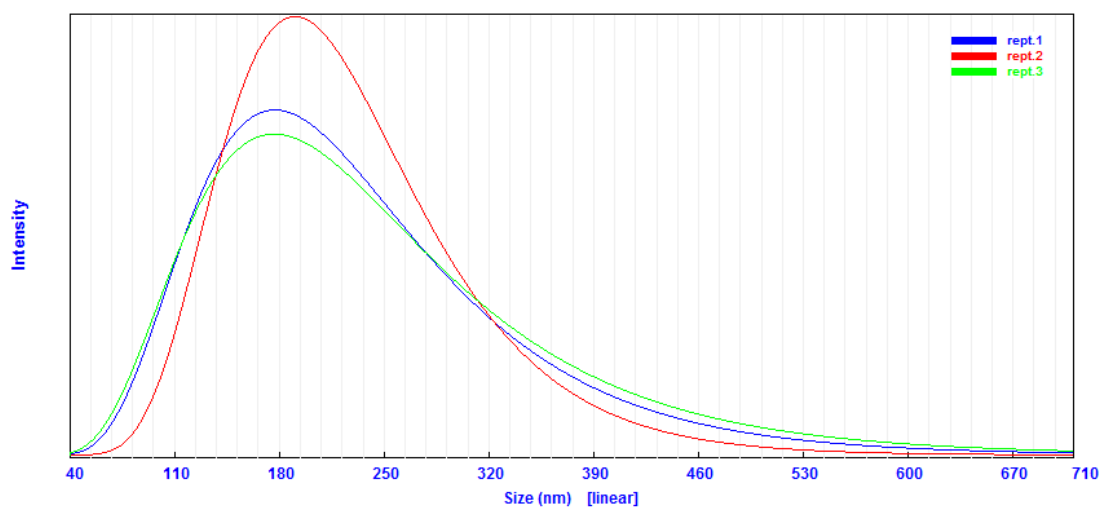


4.5.2 Dynamic Light Scattering

Average Dynamic Light Scattering (DLS) of nanocrystalline suspension of *trans*-5 for three distinct average runs.

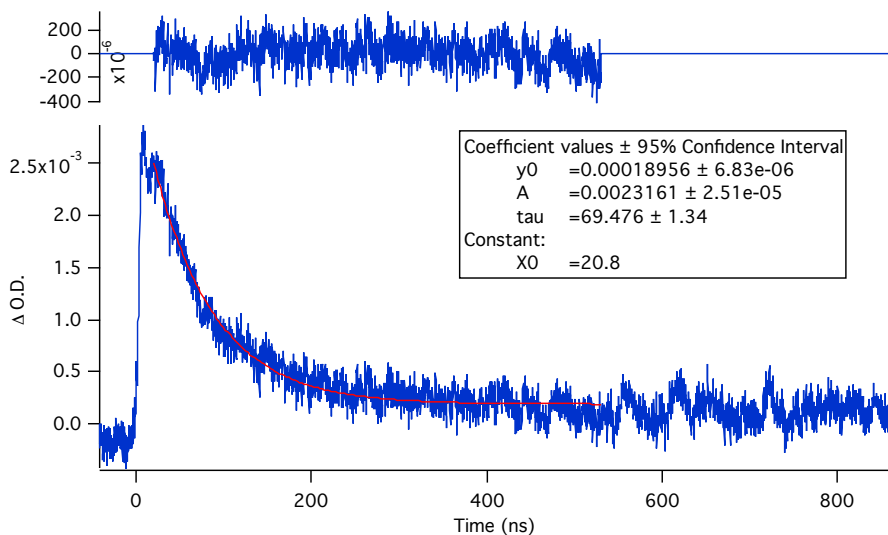
Unimodal Results Summary

Rept.#	Mean (nm)	Std.Dev (nm)	Baseline Error	P.I.	Counts/s	Diff.Coeff (m ² /s)	Overflow
Rept.1	183.2	66.4	0.01%	0.139	2.47e+05	2.47e-12	0
Rept.2	189.5	52.1	0.01%	0.054	2.53e+05	2.39e-12	0
Rept.3	186.4	73.9	0.01%	0.211	2.59e+05	2.43e-12	0
Average	186.4	64.14		0.135			

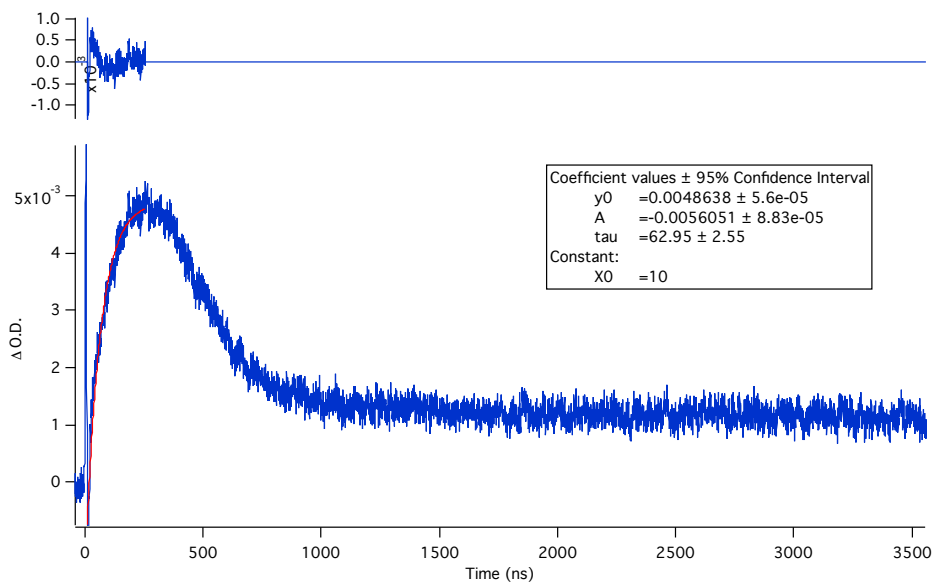


4.5.3 Laser Flash Photolysis

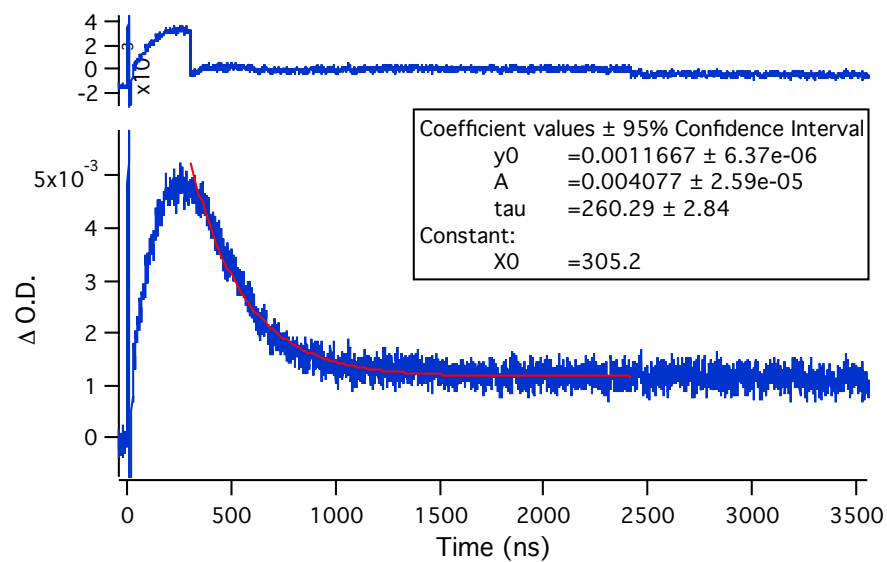
Transient decay of *trans*-5 in acetonitrile probed at 550 nm.



Transient growth of *trans*-5 in nanocrystalline suspension probed at 530 nm.



Transient decay of *trans*-5 in nanocrystalline suspension probed at 530 nm.



4.6 References

- (1) Wilkinson, F.; Kelly, G., CRC Press: Boca Raton, 1989; Vol. 1; (b) Kessler, R. W.; Krabichler, G.; Uhl, S.; Oelkrug, D.; Hagan, W. P.; Hyslop, J.; Wilkinson, F. *Optica. Acta.* **1983**, *30*, 1099.
- (2) Campos, L. M.; Garcia-Garibay, M. A. Reactive Intermediates in Crystals: Form and Function, in *Reactive Intermediates*; Platz, M. S., Jones, M., Moss, R., Eds.; Hoboken, NJ, 2007.
- (3) Scheffer, J. R.; Scott, C. in *CRC Handbook of Organic Photochemistry and Photobiology*, Second Edition, Lenci, F.; Horspool, W. Eds. Volumes 1 & 2, Ch. 54, CRC Press, Boca Raton FL, 2003.
- (4) Chin, K. K.; Natarajan, A.; Gard, M. N.; Campos, L. M.; Johansson, E.; Shepherd, H.; Garcia-Garibay, M. A. *Chem. Commun.* **2007**, *41*, 4266-4268.
- (5) Kuzmanich, G.; Simoncelli, S.; Gard, M.N.; Spänig, F.; Hoekstra, R.; Guldi, D. M.; Garcia-Garibay, M. A. *J. Am. Chem. Soc.* **2011**, *133*, 17296-17306.
- (6) Doan, S. C.; Kuzmanich, G.; Gard, M. N.; Garcia-Garibay, M. A.; Schwartz, B. J. *J. Phys. Chem. Lett.* **2012**, *3*, 81-86.
- (7) Kuzmanich, G.; Vogelsberg C. S.; Maverick, E. F.; Netto-Ferreira, J. C.; Scaiano, J. C.; Garcia-Garibay, M. A. *J. Am. Chem. Soc.* **2012**, *134*, 1115-1123.
- (8) Ayitou, A. J.-L.; Flynn, K.; Jockusch, S.; Khan, S. I.; Garcia-Garibay, M. A. *J. Am. Chem. Soc.* **2016**, *138*, 2644-2648.
- (9) Chung, T.S.; Lopez, S.A.; Houk, K.N.; Garcia-Garibay, M.A. *Org. Lett.* **2015**, *17*, 4568-4571.

- (10) Turro, Nicholas J., V. Ramamurthy, and J. C. Scaiano. *Modern Molecular Photochemistry of Organic Molecules*. Sausalito, CA: U Science, 2010. Print.
- (11) Mori, A.; Mizusaki, T.; Kawase, M.; Maegawa, T.; Monguchi, Y.; Takao, S.; Takagi, Y.; Sajiki, H. *Adv. Synth. Catal.* **2008**, *350*, 406 – 410.
- (12) Kasai, H.; Nalwa, H. S.; Oikawa, H.; Okada, S.; Matsuda, H.; Minami, N.; Kuakuta, A.; Ono, K.; Mukoh, A.; Nakanishi, H. *Jpn. J. Appl. Phys.*, **1992**, *31*, 1132-1134.
- (13) Levya, E.; Platz, M. S.; Niu, B.; Wirz, J. *J. Phys. Chem.* **1987**, *91*, 2293.
- (14) Wang, J.; Kubicki, J.; Platz, M. S. *Org. Lett.* **2007**, *9*, 3973–3976.

Chapter 5

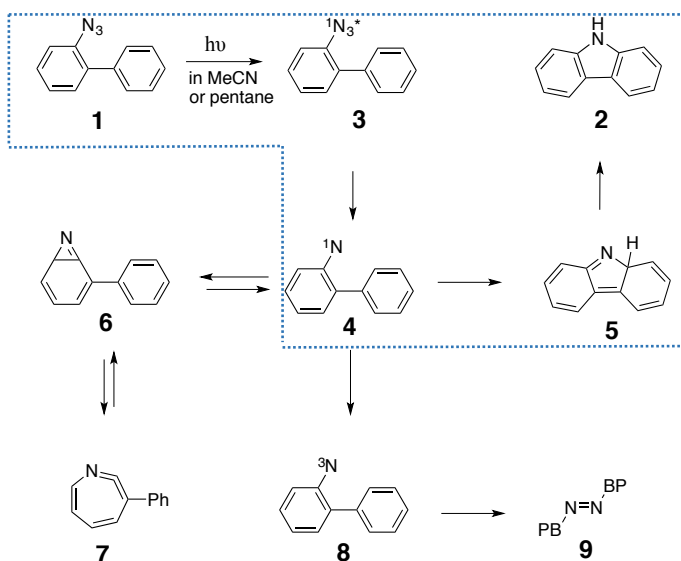
Photochemistry and Transmission Pump-Probe Spectroscopy of 2-Azidobiphenyls in Aqueous Nanocrystalline Suspensions: Simplified Kinetics in Crystalline Solids

5.1 Introduction

While there are an increasing number of solid-state photochemical reactions shown to display high synthetic¹ and materials science² potential, the detailed elucidation of their excited states, reaction mechanisms, and kinetics remains a major challenge in the field. Most mechanistic studies reported to date are based on product analysis combined with single crystal X-ray diffraction of the reactant, which provide information to correlate the structures of the reactant and the product in order to rationalize the observed reaction trajectory.³ A few examples report the use of single crystal electron paramagnetic resonance⁴ and infrared spectroscopy⁵ to detect the formation and fate of intermediate species. Finally, one of the most elegant but limited strategies involves the use of pulsed laser excitation combined with single crystal X-ray diffraction to detect reversible reactions occurring upon formation of excited states, reactive intermediates and photoproducts.⁶ Further progress in the field would benefit strongly from a more general and widely applicable analytical method to study the formation of reactive intermediates and kinetics of reactions in crystals. However, it is known that the spectroscopic analyses of crystals and bulk powders is complicated by their high optical densities, strong light scattering, and the potential interference by the accumulation of photoproducts. To address these challenges, our group has developed a flow method that uses nanocrystals suspended in a non-dissolving fluid such as water.⁷ We have shown that low loading suspensions of crystals in the ca. 50-500 nm size range are suitable for transmission spectroscopy due to their homogeneous illumination and reduced light scattering. One may view nanocrystals as a state in transition between supramolecular systems and bulk solids. In this letter, we explore the use of this method to compare the solution and solid state spectroscopy and kinetics of several 2-azidobiphenyls (**1**, Scheme 1). Knowing that reactions

in crystals of **1** are confined to the pathway shown within the dotted lines in Scheme 1,⁸ which leads to the exclusive formation of carbazoles **2**, we set out to confirm that the same will be observed when measuring their nanosecond spectroscopy and kinetics in the crystalline state.

Scheme 5.1.1.



We selected 2-azidobiphenyl knowing that Platz and co-workers have thoroughly investigated the relatively complex kinetic scheme in solution using laser flash photolysis.^{9,10} As shown in Scheme 1, 2-azidobiphenyl **1** undergoes a photoinduced denitrogenation to generate the singlet nitrene **4** with a time constant of ca. 280 fs.¹¹ The singlet nitrene **4** in solution can select between 3 different reaction pathways. Within 16 ps it decays by inserting into the aromatic ring to generate the azirine **6**, which either undergoes a ring expansion to generate the ketene imine **7** or inserts into the neighboring aromatic *ortho*-C-H bond to generate the isocarbazole **5**.^{9,10} The latter displays a broad absorption at ca. 400-500 nm.¹⁰ It was shown that the isocarbazole **5** undergoes a 1,5-H shift within 70 ns to produce the final carbazole product **2**, which has a strong absorption with a $\lambda_{\text{max}} \approx 290$ nm and a smaller shoulder in the range of ca. 320-340 nm. Platz and co-workers also

showed that under cryogenic conditions the singlet nitrene can intersystem cross to generate the triplet nitrene **8**, which dimerizes to yield the azo species **9**.¹⁰

The photochemistry of 2-azidobiphenyl in the crystalline solid-state was reported by Sugawara and co-workers who demonstrated the exclusive formation of carbazole **2**⁸ and later showed that intersystem crossing of singlet nitrene **4** to triplet **8** occurs in the solid under cryogenic conditions to afford the azo-species **9**.¹² Taking advantage of this information, we set out to explore the transient kinetics of a set of 2-azido-1,1'-biphenyls using aqueous nanocrystalline suspensions. The compounds selected for this study included the unsubstituted 2-azido-1,1'-biphenyl **1A** plus derivatives 4'-methoxy-1,1'-biphenyl **1B**, 4'-fluoro-1,1'-biphenyl **1C**, 4'-trifluoromethyl-1,1'-biphenyl **1D**, 3',5'-difluoro-1,1'-biphenyl **1E**, and 3',5'-bis(trifluoromethyl)-1,1'-biphenyl **1F** groups (Scheme 2 and Table 1).

Scheme 5.1.2.

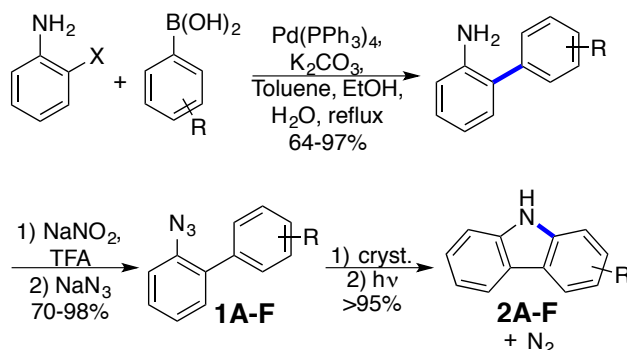


Table 5.1.1. Various substituents on 2-azidobiphenyl derivatives listed with their corresponding melting points and particle sizes.

Compound	R	M.P. (°C)	DLS (nm)
1A	H	52-53 ¹⁵	440
1B	4-OMe	35-36 ¹³	400
1C	4-F	31-32 ¹³	350
1D^a	4-CF ₃	N.A.	N.A.

1E	3,5-F	53-55	400
1F	3,5-CF ₃	45-46 ¹⁶	250

^aLiquid at 298 K.

5.2 Results and Discussion

5.2.1 Synthesis and Characterization

Using compounds bearing substituents with electron-donating and electron-withdrawing capabilities we set out to determine (1) the scope of the solid-state reaction, (2) the generality of the analytical method, and (3) the reaction sensitivity to electronic effects, both in solution and in the solid-state. We synthesized the 2-azidobiphenyls shown in Scheme 2 and Table 1 with commercially available *ortho*-iodoaniline and substituted phenyl boronic acids using a standard Suzuki coupling reaction.¹³ The 2-aminobiphenyl derivatives were converted to the corresponding azides using standard diazotization conditions.¹ The identity of all compounds was established by ¹H NMR, ¹³C NMR and FTIR spectra, which matched reported data from all the known compounds. Subsequent recrystallization from acetonitrile yielded crystalline solids in all cases except for **1D**, which is a liquid at ambient temperature (Table 1). Stable nanocrystalline suspensions were obtained for all crystalline compounds using the reprecipitation method,¹⁴ pouring concentrated acetonitrile solutions (20 mg/10mL) of the azide into (60 mL) of rapidly vortexing water with submicellar concentrations of cetyltrimethylammonium bromide (CTAB) to passivate the surface of the nanocrystals and prevents aggregation.

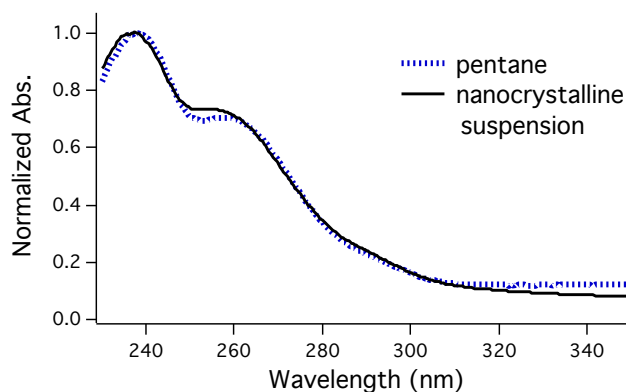


Figure 5.2.1. UV-Vis absorption spectra of 2-azidobiphenyl in pentane (blue dotted line) and in nanocrystalline suspension (black solid line).

The formation of stable nanocrystalline suspensions was analyzed by UV-Vis spectroscopy by monitoring the amount of scattering and precipitation, which are observed by the appearance of a high baseline followed spectral disappearance. The UV-Vis spectrum of 2-azidobiphenyl in pentane (Figure 1 dotted blue line) is very similar to that of the nanocrystalline suspension (solid black line), with a λ_{\max} at ca. 236 nm and a shoulder at ca. 260 nm. Crystal sizes were revealed in the range of 250- 440 nm by dynamic light scattering (DLS, Table 1).

In order to confirm the crystallinity of the particles, we compared powder X-ray diffraction (PXRD) data acquired with nanocrystalline samples collected by centrifugation and air-drying with those from bulk powders obtained from single crystals. Figure 2 illustrates the PXRD from the two solid forms of 2-azidobiphenyl (others are included in the SI section). One can appreciate that the two diffractograms have similar patterns and peak positions, suggesting that the nanocrystals are indeed crystalline and belong to same polymorph. However, clear differences in intensities suggest that nanocrystals collected by centrifugation tend to adopt specific crystallite alignments.

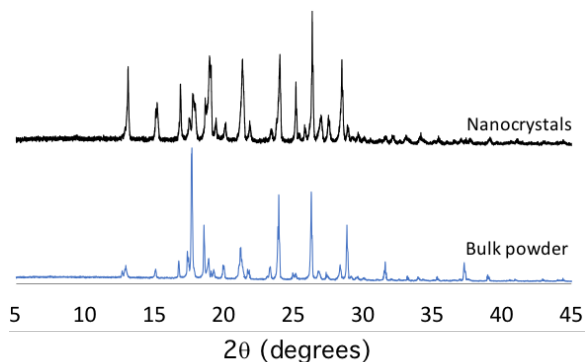


Figure 5.2.2. Powder X-Ray Diffraction (PXRD) patterns of bulk powder and nanocrystals of 2-azidobiphenyl (**1A**).

Having determined the formation of nanocrystals we set out to confirm that all azidobiphenyls react in the solid-state upon UV light irradiation. After showing that all samples react in pentane to yield the corresponding carbazoles as the major products (ca. 70%),¹⁰ experiments carried with dry powders and nanocrystalline suspension of **1A-1C** and **1E-1F** afforded the corresponding carbazoles in essentially quantitative yields (>95%). Solid state reactions analyzed by PXRD showed that the reactant transforms into the stable form of the carbazole product, indicating that reaction proceeds by a reconstructive phase transition mechanism (Figure 3).¹⁷ The PXRD of the carbazole recrystallized from acetonitrile is essentially identical to the one formed *in situ* during the solid-state photoreaction, indicating that the most stable form of the carbazole is produced in the reaction. It is worth noting that the melting points of the carbazoles are above 100 °C, which may be an important factor for the reaction to proceed without melting despite the relatively low melting points of the reactants (Table 1).

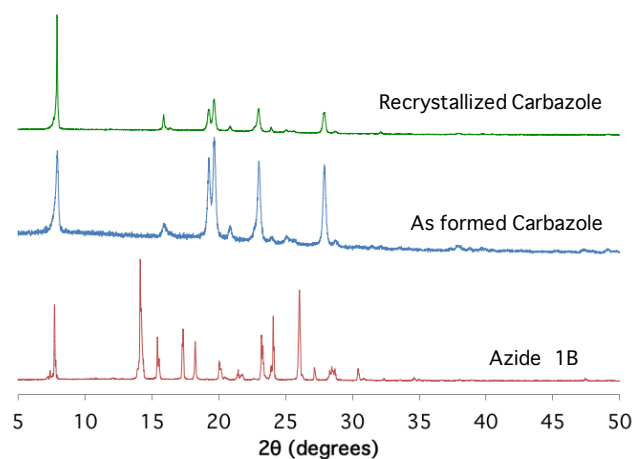


Figure 5.2.3. Powder X-Ray Diffraction (PXRD) patterns of starting azide **1B** (in bottom red), as formed carbazole **2B** (middle blue), and recrystallized carbazole product **2B** (top green).

5.2.2 Laser Flash Photolysis

For fast kinetic measurements we were limited by our Nd:YAG laser setup working at 266 nm with a laser pulse of ca. 8 ns, such that the expected transient for us to probe was isocarbazole **5** and its decay to carbazole **2**. Experiments carried out in pentane solution revealed end-of-pulse spectra with a strong signal near 300 nm with other components that extend from 380–500 nm, which are consistent with data reported by Platz et al.¹⁰ While overlapping contribution from ring **7** is expected in pentane, it has been shown that isocarbazole absorption occurs in the range of 400–500 nm. A strong signal near 300 nm with shoulders at ca. 340 nm is assigned to overlapping contributions from carbazole **2**. Figure 4a illustrates the transient absorption spectra at various time delays after the laser pulse for azide **1B** in pentane. Spectra were taken 10 ns, 350 ns and 650 ns after the initial excitation. One can observe the isocarbazole species at the earliest times, as indicated by a broad absorption from 380–500 nm. As the isocarbazole signal gradually decreases one can observe contributions assigned to carbazole, characterized by a peak near ca. 300 nm with additional components in the range of 370–390 nm, which following the work of Platz and co-

workers may be assign to the ketene imine **7**. Figure 4b depicts analogous measurements using a nanocrystalline suspension in a flow cell setup showing a broad absorption from 400-500 nm, which we assign to isocarbazole. As in solution, disappearance of the isocarbazole peak at a longer time scales is accompanied by the growth of the carbazole absorption near ca. 290 nm. By contrast, nanocrystalline samples do not give rise to the signal in the 370-450 nm range as expected from the absence of the ketene imine **7**. Measurements carried out with other azidobiphenyls are similar to the ones obtained with **1B**. The primary data are included in the SI and the kinetics information disclosed in Tables 2 and 3.

With respect to the kinetics of the reaction, Platz and co-workers reported the decay of isocarbazole **5** at 430 nm and the growth of carbazole **2** at 290 nm to occur in a correlated fashion with a time constant of ca. 70 ns in pentane. Additionally, Platz and co-workers reported the formation of carbazole product is not single exponential. Our own measurements with excitation at 266 nm revealed a time constant of ca. 200 ns and 1 μ s in the same solvent (See SI). Although the time constants are different, the growth and decay features are consistent with those reported earlier. Analogous measurements with nanocrystals of **1A** measured at 460 nm revealed a decay with a time constant of 480 ns. Figure 4c illustrates the transient decays of azide **1B** in both pentane and in nanocrystals. The decay in solution probed at 430 nm was shown to be a double exponential with time constant of 200 ns and 530 ns. The decay in nanocrystals probed at 460 nm exhibited single exponential kinetics with a time constant of 500 ns. The single exponential decay of the nanocrystalline sample is consistent with the exclusive formation of carbazole, which results in kinetics that are simpler than those observed in solution.

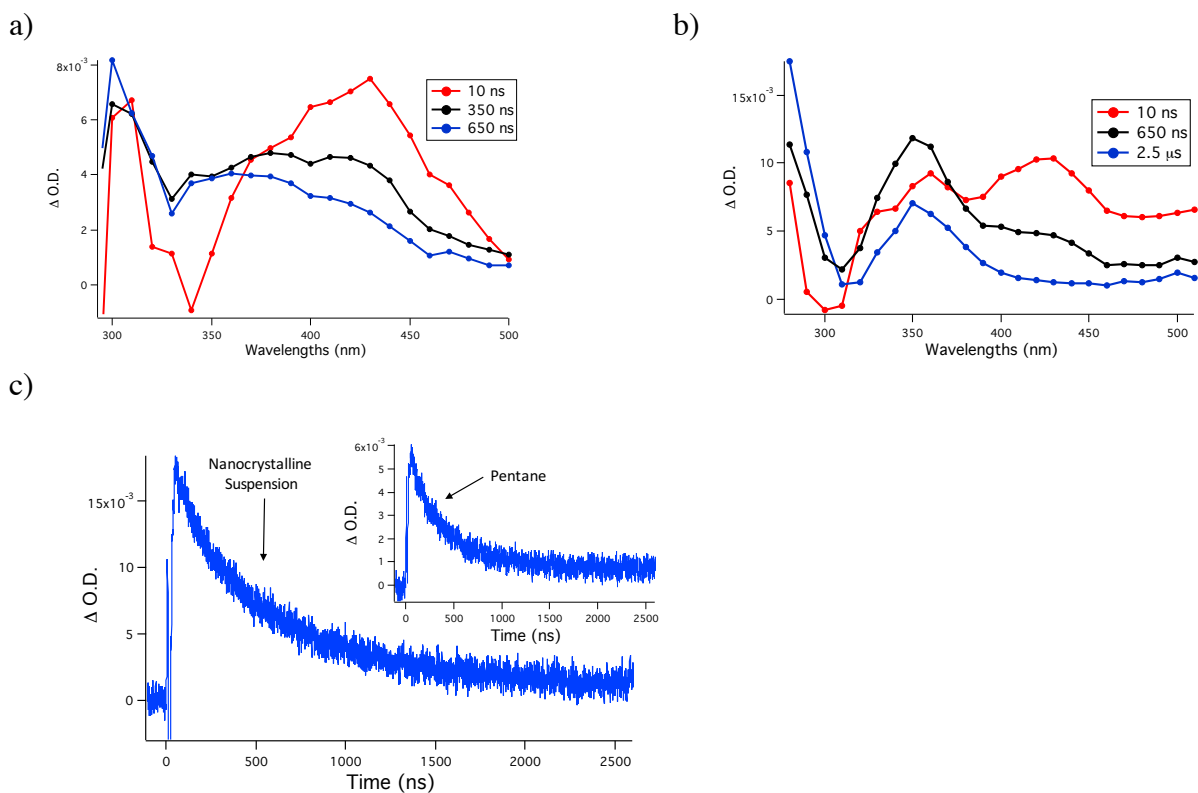
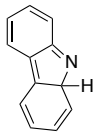
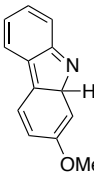
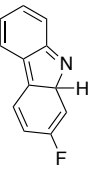
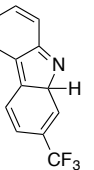


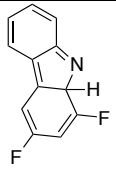
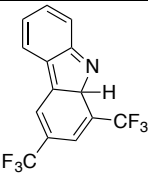
Figure 5.2.4. a) Transient absorption spectrum of azide **1B** sliced at various time points in pentane, b) transient absorption spectrum of azide **1B** sliced at various time points in nanocrystalline suspension c) LFP decays in both pentane and in NC suspensions of azide **1B** at 430 nm and 460 nm, respectively.

Table 5.2.1. Transient decay lifetimes of various isocarbazoles to form carbazoles of various 2-azidobiphenyl derivatives with substituents in the 4'-biphenyl position.

				
Pentane, τ_1	200 ns (32%)	200 ns (23%)	100 ns (4%)	110 ns (2%)
Pentane, τ_2	1 μ s (68%)	530 ns (77%)	530 ns (96%)	680 ns (98%)
Nanocrystals	480 ns	500 ns	560 ns	N/A

The data shown in Table 2 includes the lifetimes of the various isocarbazole derivatives in solution and in nanocrystalline suspensions. While the isocarbazole decay lifetimes in pentane solution occur in the range of 100 ns to 1 μ s, nanocrystalline suspensions leads to values that range from 480 ns to 560 ns. We proposed that solution lifetimes are not a simple exponential as the result of having isocarbazole **2**, and ketene imine **7** transients overlapping in the 430 nm region. This hypothesis is supported by observing a relatively clean monoexponential decay in nanocrystalline suspensions, consistent with a very clean solid-state photoreaction.

Table 5.2.2. Transient decay lifetimes of isocarbazoles to carbazoles from 3',5'-disubstituted 2-azidobiphenyls.

		
Pentane, τ_1	70 ns (6%)	920 ns
Pentane, τ_2	350 ns (94%)	n.a.
Nanocrystals	120 ns	750 μ s

While the data set is limited, in solution one may appreciate a slower decay for the 1,5-H shift when there are electron-withdrawing groups on 4'-biphenyl position. One can also see that decays in the nanocrystalline suspension display decay rates that are slower than those measured in solution, which can be attributed to the fact that nanocrystalline solids have a more rigid chemical environment. We also note an even smaller dependence of the 1,5-H shift reaction on the nature of the substituent, suggesting that steric effects in the solid state may play a more important role.

Searching for additional insight we analyzed the photochemistry and kinetics of the 3',5'-disubstituted-2-azidobiphenyl derivatives **1E** and **1F** shown in Table 3. Azide **1E** with 3',5'-difluoro- substituents showed a biexponential decay in solution with time constants of 70 ns and 330 ns. Azide **1F** with 3'-5'-trifluoromethyl-substituents showed a single exponential decay with a time constant of 920 ns in pentane. The nanocrystalline suspensions showed monoexponential decays of 120 ns to 750 μ s for **1E** and **1F**, respectively, suggesting that the long lifetime of **1F** may be due to steric factors associated with the relatively large size of the trifluoromethyl group.

Taken together, the data shown in Tables 2 and 3 indicate that electronic effects play a relatively minor role on the rate of the 1,5-shift of the isocarbazole to carbazole reaction.

5.3 Conclusions

In conclusion, we have synthesized several 2-azidobiphenyls with varying substituents on the 4' and 3',5'-biphenyl positions and investigated their nanosecond spectroscopy and kinetics in solution and in nanocrystals. The main process observed in these experiments is the formal 1,5-H shift that transforms an unstable isocarbazole into the stable carbazole product. It is worth mentioning that decay kinetics in solution are at least biexponential, in agreement with the formation of various overlapping transients from the highly reactive nitrene. By contrast, the decay kinetics in the solid-state are single exponential, consistent with the formation of a single product by a simple, least motion reaction pathway. Furthermore, results obtained with compounds that have a range of electron-withdrawing substituents indicate that electronic effects play a relatively minor role on the kinetics of the 1,5-H reaction both in solution and in the solid-state. Finally, PXRD studies before and after reactions indicate that the crystalline 2-azidobiphenyls transform into the crystalline carbazole products by a reconstructive phase transition mechanism. Taken together, these observations indicate that the use of nanocrystals suspended in water provides a promising avenue for the use of transmission spectroscopy and kinetics for the study solid-state photochemical reactions.

Author's note. Chapter 5 is adapted from the following publication: Chung, T. S.; Ayitou, A. J.-L.; Park, J.; Breslin, V. M.; Garcia-Garibay, M.A. "Photochemistry and Transmission Pump–Probe Spectroscopy of 2-Azidobiphenyls in Aqueous Nanocrystalline Suspensions: Simplified Kinetics in Crystalline Solids" *J. Phys. Chem. Lett.*, **2017**, *8*, 1845–1850. Park,

Breslin, Ayitou, and I were part of a team working with nanocrystals and the co-authors aided in fruitful discussions.

5.4 Experimental

Unless stated otherwise, all of the 2-aminobiaryls were synthesized using standard Suzuki coupling protocols from commercially available starting materials. Unless stated otherwise, all of the 2-azidobiphenyls (**1A-F**) were synthesized using standard protocols. Unless stated otherwise, all of the carbazole products (**2A-F**) were synthesized using solid-state photochemistry. All of the solid 2-azidobiphenyls (5-8 mg) were crushed between two microscope slides and photolyzed using a medium-pressure Hg Hanovia lamp with a quartz immersion well filter with cutoff of $\lambda \leq 220$ nm. The reaction was monitored by ^1H NMR and was completed in ca. 2 hours.

Synthesis of 2-azido biphenyl (compound **1A**):

2-aminobiphenyl was commercially available and was used without further purification.

Compound **2** was synthesized according to reported procedure in literature from 2-Aminobiphenyl. Crude product from the reaction was purified by silica gel chromatography (eluent: EtOAc/Hexanes 20/80). Yield 92%, slightly yellow solid, R_f 0.89. IR (ATR cm^{-1}): 3060, 2435, 2120, 2086, 1580, 1501, 1479, 1431, 1285, 1257. ^1H NMR (500 MHz, CDCl_3) δ 7.48 – 7.31 (m, 7H), 7.29 – 7.24 (m, 1H), 7.22 (dd, $J = 7.5, 1.1$ Hz, 1H). ^{13}C NMR (126 MHz, CDCl_3) δ 138.16, 137.13, 133.79, 131.27, 129.47, 128.72, 128.15, 127.56, 124.95, 118.78. Melting Point: 52.2-53.1 °C. Compound spectra have been matched with reported literature values.

Synthesis of 2-azido-4'-methoxy-1,1'-biphenyl (compound **1B**):

The general procedure was followed with 200 mg of 4'-methoxy-[1,1'-biphenyl]-2-amine (1.68 mmol), 579 mg of NaNO₂ (8.4 mmol), and 546 mg of NaN₃ (8.4 mmol) in .7 mL of trifluoroacetic acid and 8.4 mL of H₂O. Crude product from the reaction was purified by silica gel chromatography (eluent: EtOAc/Hexanes 30/70). Yield 98%, slightly yellow solid, R_f 0.65. IR (ATR cm⁻¹): 3063, 3023, 2958, 2838, 2118, 2084, 1610, 1569, 1515, 1467, 1480. ¹H NMR (500 MHz, CDCl₃) δ 7.42 – 7.37 (m, 1H), 7.37 – 7.34 (m, 3H), 7.32 (dd, *J* = 7.6, 1.4 Hz, 1H), 7.24 (dd, *J* = 8.0, 0.9 Hz, 1H), 7.19 (td, *J* = 7.5, 1.2 Hz, 1H), 7.01 – 6.94 (m, 2H), 3.85 (s, 3H). ¹³C NMR (126 MHz, CDCl₃) δ 159.11, 137.06, 133.45, 131.16, 130.59, 130.51, 128.33, 124.93, 118.74, 113.63, 55.31. Melting Point: 35.4-36.1 °C. Compound spectra have been matched with reported literature values.

Synthesis of 2-azido-4'-fluoro-1,1'-biphenyl (compound **1C**):

The general procedure was followed with 146 mg of 4'-fluoro-[1,1'-biphenyl]-2-amine (0.779 mmol), 268 mg of NaNO₂ (3.89 mmol), and 252 mg of NaN₃ (3.89 mmol) in .35 mL of trifluoroacetic acid and 2 mL of H₂O. Crude product from the reaction was purified by silica gel chromatography (eluent: EtOAc/Hexanes 1:7). Yield 87%, slightly yellow solid, R_f 0.88. IR (ATR cm⁻¹): 2123, 2091, 1609, 1596, 1515, 1481, 1443. ¹H NMR (500 MHz, CDCl₃) δ 7.46 – 7.36 (m, 1H), 7.31 (dd, *J* = 7.6, 1.5 Hz, 1H), 7.28 – 7.22 (m, 1H), 7.22 – 7.18 (m, 1H), 7.16 – 7.07 (m, 1H). ¹³C NMR (126 MHz, CDCl₃) δ 163.32, 161.35, 137.14, 134.09, 134.07, 132.71, 131.19, 131.16, 131.10, 128.86, 125.00, 118.79, 115.19, 115.02. Melting Point: 31.2-32.6 °C. Compound spectra have been matched with reported literature values.

Synthesis of 2-azido-4'-(trifluoromethyl)-1,1'-biphenyl (Compound **1D**):

The general procedure was followed with 207 mg of 4'-(trifluoromethyl)-[1,1'-biphenyl]-2-amine (0.873 mmol), 301 mg of NaNO₂ (4.36 mmol), and 283 mg of NaN₃ (4.36 mmol) in 597mg of trifluoroacetic acid and 4 mL of H₂O. Crude product from the reaction was purified by silica gel chromatography (eluent: EtOAc/Hexanes 1:7). Yield 84%, slightly yellow liquid, R_f 0.79.

IR (ATR cm⁻¹): 2123, 2093, 1618, 1582, 1485, 1322, 1162. ¹H NMR (500 MHz, CDCl₃) δ 7.69 (d, *J* = 8.1 Hz, 2H), 7.57 (dd, *J* = 8.6, 0.6 Hz, 2H), 7.45 (ddd, *J* = 8.0, 7.4, 1.6 Hz, 1H), 7.34 (dd, *J* = 7.7, 1.5 Hz, 1H), 7.29 (dd, *J* = 8.1, 0.9 Hz, 1H), 7.27 – 7.21 (m, 1H). ¹³C NMR (126 MHz, CDCl₃) δ 141.78, 141.77, 137.25, 132.22, 131.14, 129.99, 129.86, 129.73, 129.52, 129.47, 129.21, 127.47, 125.31, 125.12, 125.09, 125.06, 125.03, 123.15, 120.98, 118.85.

Synthesis of 2-azido-3',5'-difluoro-1,1'-biphenyl (Compound **1E**):

The general procedure was followed with 174 mg of 3',5'-difluoro-[1,1'-biphenyl]-2-amine (0.848 mmol), 292 mg of NaNO₂ (4.24 mmol), and 275 mg of NaN₃ (4.24 mmol) in .39 mL of trifluoroacetic acid and 4.2 mL of H₂O. Crude product from the reaction was purified by silica gel chromatography (eluent: EtOAc/Hexanes 30/70). Yield 70%, white solid, R_f 0.75. IR (ATR cm⁻¹): 3081, 2135, 2091, 1626, 1596, 1416, 1306, 1114, 986. ¹H NMR (500 MHz, CDCl₃) δ 7.43 (ddd, *J* = 8.1, 7.4, 1.6 Hz, 1H), 7.31 (dd, *J* = 7.7, 1.4 Hz, 1H), 7.27 (d, *J* = 0.8 Hz, 1H), 7.21 (td, *J* = 7.5, 1.1 Hz, 1H), 7.02 – 6.94 (m, 2H), 6.81 (tt, *J* = 9.0, 2.3 Hz, 1H). ¹³C NMR (126 MHz, CDCl₃) δ 163.66, 163.55, 161.69, 161.58, 141.25, 141.17, 141.09, 137.17, 131.30, 130.94, 129.66, 125.09, 118.91, 112.63, 112.58, 112.47, 112.42, 103.08, 102.88, 102.68. Melting Point: 53.3-54.6 °C.

Synthesis of 2-azido-3',5'-bis(trifluoromethyl)-1,1'-biphenyl (Compound **1F**):

The general procedure was followed with 200 mg of 3',5'-bis(trifluoromethyl)-[1,1'-biphenyl]-2-amine (0.656 mmol), 226 mg of NaNO₂ (3.28 mmol), and 213 mg of NaN₃ (3.28 mmol) in .3 mL of trifluoroacetic acid and 3.2 mL of H₂O. Crude product from the reaction was purified by silica gel chromatography (eluent: EtOAc/Hexanes 30/70). Yield 96%, white solid, R_f 0.75. IR (ATR cm⁻¹): 3099, 2121, 2089, 1577, 1497, 1467, 1376, 1108. ¹H NMR (500 MHz, CDCl₃) δ 7.91 (s, 2H), 7.87 (s, 1H), 7.49 (ddd, *J* = 8.1, 7.4, 1.6 Hz, 1H), 7.35 (dd, *J* = 7.7, 1.5 Hz, 1H), 7.31 (dd, *J* = 8.1, 0.8 Hz, 1H), 7.26 (td, *J* = 7.5, 1.1 Hz, 1H). ¹³C NMR (126 MHz, CDCl₃) δ 140.09, 137.40, 131.84, 131.57, 131.31, 131.07, 131.05, 130.45, 130.21, 129.71, 129.69, 126.61, 125.30, 124.44, 122.27, 121.31, 121.28, 121.25, 121.21, 121.18, 120.10, 118.89. Melting Point: 45.5-46.2 °C.

Synthesis of 4'-Methoxy-2-biphenylamine:

The general procedure of Suzuki coupling was followed with 250 mg of 2-iodoaniline (1.14 mmol), 225 mg of 4-methoxyphenylboronic acid (1.48 mmol), 131 mg of Pd(PPh₃)₄ (0.114 mmol), and 630 mg of K₂CO₃ (4.56 mmol) in 4 mL of toluene, 2 mL of ethanol, and 3 mL of H₂O. The mixture was refluxed overnight for 14 hours. After cooling, the biphasic solution was diluted with saturated aqueous NH₄Cl and H₂O. The mixture was extracted with DCM three times. The organic layer was dried, evaporated, and was purified by column chromatography using ethyl acetate and hexanes (1:4; R_f = 0.4). We obtained the aniline as a pale yellow oil (200 mg, 97%). ¹H NMR (500 MHz, CDCl₃) δ 7.47 – 7.33 (m, 2H), 7.18 – 7.05 (m, 2H), 7.02 – 6.92 (m, 2H), 6.81 (td, *J* = 7.4, 1.2 Hz, 1H), 6.77 – 6.70 (m, 1H), 3.85 (s, 3H), 3.76 (s, 2H).

^{13}C NMR (126 MHz, CDCl_3) δ 158.77, 143.66, 131.77, 130.49, 130.20, 128.19, 127.37, 118.64, 115.51, 114.21, 55.33. IR (ATR cm^{-1}): 3455, 3369, 3030, 2935, 2835, 1610, 1512, 1487, 1451.

Compound spectra have been matched with reported literature values.

Synthesis of 4'-fluoro-[1,1'-biphenyl]-2-amine:

The general procedure of Suzuki coupling was followed with 250 mg of 2-iodoaniline (1.14 mmol), 207 mg of 34-fluorophenylboronic acid (1.48 mmol), 131 mg of $\text{Pd}(\text{PPh}_3)_4$ (0.114 mmol), and 630 mg of K_2CO_3 (4.56 mmol) in 4 mL of toluene, 2 mL of ethanol, and 3 mL of H_2O . The mixture was refluxed overnight for 14 hours. After cooling, the biphasic solution was diluted with saturated aqueous NH_4Cl and H_2O . The mixture was extracted with DCM three times. The organic layer was dried, evaporated, and was purified by column chromatography using ethyl acetate and hexanes (1:6; $R_f = 0.48$). We obtained the aniline as a pale yellow oil (156 mg, 73%). ^1H NMR (500 MHz, CDCl_3) δ 7.47 – 7.37 (m, 1H), 7.20 – 7.07 (m, 2H), 6.83 (td, $J = 7.5, 1.2$ Hz, 1H), 6.78 (dd, $J = 8.0, 0.9$ Hz, 1H), 3.80 (s, 2H). ^{13}C NMR (126 MHz, CDCl_3) δ 163.05, 161.09, 143.26, 135.34, 135.31, 130.80, 130.74, 130.48, 128.66, 126.78, 118.91, 115.80, 115.63. IR (ATR cm^{-1}): 3478, 3390, 3054, 2986, 736, 706. Compound spectra have been matched with reported literature values.

Synthesis of 4'-(trifluoromethyl)-[1,1'-biphenyl]-2-amine:

The general procedure of Suzuki coupling was followed with 250 mg of 2-iodoaniline (1.14 mmol), 281 mg of 4-trifluoromethyl phenylboronic acid (1.48 mmol), 131 mg of $\text{Pd}(\text{PPh}_3)_4$ (0.114 mmol), and 630 mg of K_2CO_3 (4.56 mmol) in 4mL of toluene, 2 mL of ethanol, and 3 mL of H_2O . The mixture was refluxed overnight for 14 hours. After cooling, the biphasic solution

was diluted with saturated aqueous NH_4Cl and H_2O . The mixture was extracted with DCM three times. The organic layer was dried, evaporated, and was purified by column chromatography using ethyl acetate and hexanes (1:6; $R_f = 0.41$). We obtained the aniline as a slightly tan oil (214 mg, 79%). ^1H NMR (500 MHz, CDCl_3) δ 7.69 (d, $J = 8.0$ Hz, 2H), 7.59 (d, $J = 7.9$ Hz, 2H), 7.22 (ddd, $J = 8.0, 7.5, 1.6$ Hz, 1H), 7.13 (dd, $J = 7.6, 1.5$ Hz, 1H), 6.90 (td, $J = 7.5, 0.9$ Hz, 1H), 6.85 (d, $J = 8.0$ Hz, 1H), 4.46 (s, 2H). ^{13}C NMR (126 MHz, CDCl_3) δ 143.01, 130.41, 129.52, 129.28, 125.81, 125.78, 125.75, 125.72, 125.27, 123.11, 119.77, 116.57. IR (ATR cm^{-1}): 3366, 1617, 1404, 1106, 848, 757. Compound spectra have been matched with reported literature values.

Synthesis of 3',5'-Difluoro-2-biphenylamine:

The general procedure of Suzuki coupling was followed with 300 mg of 2-iodoaniline (1.37 mmol), 229 mg of 3,5-difluorophenylboronic acid (1.78 mmol), 158 mg of $\text{Pd}(\text{PPh}_3)_4$ (0.137 mmol), and 757 mg of K_2CO_3 (5.49 mmol) in 4 mL of toluene, 2 mL of ethanol, and 3 mL of H_2O . The mixture was refluxed overnight for 14 hours. After cooling, the biphasic solution was diluted with saturated aqueous NH_4Cl and H_2O . The mixture was extracted with DCM three times. The organic layer was dried, evaporated, and was purified by column chromatography using ethyl acetate and hexanes (1:4; $R_f = 0.48$). We obtained the aniline as a pale yellow solid (181 mg, 64%). ^1H NMR (500 MHz, CDCl_3) δ 7.18 (ddd, $J = 8.0, 7.4, 1.6$ Hz, 1H), 7.09 (dd, $J = 7.6, 1.5$ Hz, 1H), 7.04 – 6.97 (m, 2H), 6.87 – 6.72 (m, 3H), 3.76 (s, 2H). ^{13}C NMR (126 MHz, CDCl_3) δ 164.30, 164.19, 162.32, 162.21, 143.27, 142.93, 142.86, 142.78, 130.15, 129.38, 125.17, 125.15, 118.80, 115.93, 112.09, 112.04, 111.93, 111.89, 102.79, 102.59, 102.39. IR (ATR cm^{-1}): 3468, 3370, 3079, 2923, 1622, 1594, 1502, 1464, 1424, 1338, 1117, 986, 750.

Synthesis of 3',5'-bis(trifluoromethyl)-[1,1'-biphenyl]-2-amine:

The general procedure of Suzuki coupling was followed with 500 mg of 2-iodoaniline (2.18 mmol), 732 mg of 3,5-bis(trifluoromethyl)phenylboronic acid (2.83 mmol), 252 mg of Pd(PPh₃)₄ (0.218 mmol), and 1.205 g of K₂CO₃ (8.72 mmol) in 8 mL of toluene, 3 mL of ethanol, and 5 mL of H₂O. The mixture was refluxed overnight for 14 hours. After cooling, the biphasic solution was diluted with saturated aqueous NH₄Cl and H₂O. The mixture was extracted with DCM three times. The organic layer was dried, evaporated, and was purified by column chromatography using ethyl acetate and hexanes (1:4; R_f = 0.45). We obtained the aniline as a pale yellow solid (480 mg, 72%). ¹H NMR (500 MHz, CDCl₃) δ 7.96 (s, 2H), 7.86 (s, 1H), 7.23 (td, *J* = 8.0, 1.5 Hz, 1H), 7.11 (dd, *J* = 7.6, 1.5 Hz, 1H), 6.87 (td, *J* = 7.5, 1.0 Hz, 1H), 6.80 (dd, *J* = 8.0, 0.7 Hz, 1H), 3.70 (s, 2H). ¹³C NMR (126 MHz, CDCl₃) δ 143.29, 141.76, 132.56, 132.29, 132.03, 131.76, 130.42, 129.94, 129.37, 129.34, 126.56, 124.40, 124.34, 122.23, 121.06, 121.03, 121.00, 120.97, 120.94, 120.06, 119.24, 116.23. IR (ATR cm⁻¹): 3482, 3391, 1620, 1577, 1501, 1466, 1436, 1379, 1275.

All of the following carbazole products were synthesized using solid-state photochemistry.

Approximately 5-8 mg of the corresponding azide were crushed using two microscope slides and the solid sample was irradiated for ca. 2 hours using medium pressure Hg Hanovia lamp with a quartz immersion well filter with cutoff of $\lambda \leq 220$ nm. All solid azides afforded the carbazole product in a spot to spot quantitative yields. For azide **1D** (which was not a solid), the sample was dissolved in acetonitrile, degassed and irradiated using the same lamp.

9H-carbazole (2A):

^1H NMR (500 MHz, CDCl_3) δ 8.09 (d, $J = 7.8$ Hz, 2H), 8.04 (s, 1H), 7.50 – 7.37 (m, 4H), 7.31 – 7.15 (m, 2H). ^{13}C NMR (126 MHz, CDCl_3) δ 139.47, 125.84, 123.35, 120.34, 119.45, 110.58. IR (ATR cm^{-1}): 3053, 1450, 1256, 756, 735. Melting Point: 237-238 $^\circ\text{C}$

2-methoxy-9H-carbazole (2B):

^1H NMR (500 MHz, CDCl_3) δ 8.01 – 7.89 (m, 3H), 7.38 (m, 1H), 7.33 (ddd, $J = 8.1, 7.1, 1.1$ Hz, 1H), 7.23 – 7.17 (m, 1H), 6.91 (d, $J = 2.2$ Hz, 1H), 6.85 (dd, $J = 8.5, 2.3$ Hz, 1H), 3.90 (s, 3H). ^{13}C NMR (126 MHz, CDCl_3) δ 159.07, 140.80, 139.49, 124.55, 123.53, 121.05, 119.56, 119.49, 117.26, 110.30, 108.16, 94.70, 55.63. IR (ATR cm^{-1}): 3387, 2921, 2852, 1626, 1599, 1570, 1029, 746. Melting Point: 233-234 $^\circ\text{C}$

2-fluoro-9H-carbazole (2C):

^1H NMR (500 MHz, CDCl_3) δ 8.06 (s, 1H), 8.04 – 8.00 (m, 2H), 7.98 (dd, $J = 8.5, 5.4$ Hz, 2H), 7.45 – 7.36 (m, 3H), 7.28 – 7.19 (m, 3H), 7.10 (dd, $J = 9.5, 2.2$ Hz, 2H), 6.97 (ddd, $J = 9.5, 8.6, 2.3$ Hz, 2H). ^{13}C NMR (126 MHz, CDCl_3) δ 162.95, 161.03, 140.06, 139.96, 139.88, 139.87, 125.48, 122.98, 121.27, 121.18, 119.95, 119.92, 119.81, 119.80, 110.58, 107.79, 107.59, 97.50, 97.29. IR (ATR cm^{-1}): 3415, 2955, 2920, 2850, 1628, 1620, 1460, 1336, 756. Melting Point: 226-227 $^\circ\text{C}$

2-(trifluoromethyl)-9H-carbazole (2D):

^1H NMR (500 MHz, CDCl_3) δ 8.23 (s, 1H), 8.14 (dd, $J = 16.7, 8.0$ Hz, 2H), 7.70 (s, 1H), 7.50 – 7.44 (m, 3H), 7.29 (ddd, $J = 8.0, 5.8, 2.3$ Hz, 1H). ^{13}C NMR (126 MHz, CDCl_3) δ 140.36,

138.52, 127.80, 127.54, 127.18, 125.95, 123.76, 122.42, 120.96, 120.63, 120.16, 116.26, 116.23, 110.97, 107.91, 107.88, 107.85. IR (ATR cm^{-1}): 3424, 2922, 1610, 1504, 1459, 1443, 1102, 731. Melting Point: 207-208 °C

1,3-difluoro-9*H*-carbazole (**2E**):

^1H NMR (500 MHz, CDCl_3) δ 8.14 (s, 1H), 8.00 (dd, $J = 7.9, 0.6$ Hz, 1H), 7.53 (dd, $J = 8.5, 2.2$ Hz, 1H), 7.50 – 7.44 (m, 2H), 7.31 – 7.21 (m, 2H), 6.97 (ddd, $J = 10.7, 9.3, 2.2$ Hz, 1H). ^{13}C NMR (126 MHz, CDCl_3) δ 157.57, 157.49, 155.68, 155.60, 149.16, 149.06, 147.21, 147.10, 140.29, 127.16, 126.08, 126.03, 124.06, 123.97, 123.05, 120.79, 120.00, 111.33, 101.87, 101.84, 101.68, 101.65, 100.93, 100.77, 100.70, 100.53. IR (ATR cm^{-1}): 3393, 2920, 2851, 1640, 1588, 1454, 1085, 764. Melting Point: 120-121 °C

1,3-bis(trifluoromethyl)-9*H*-carbazole (**2F**):

^1H NMR (500 MHz, CDCl_3) δ 8.67 (s, 1H), 8.50 (s, 1H), 8.14 (dd, $J = 7.9, 0.7$ Hz, 1H), 7.91 (s, 1H), 7.61 – 7.55 (m, 2H), 7.40 – 7.33 (m, 1H). ^{13}C NMR (126 MHz, CDCl_3) δ 140.08, 136.77, 128.03, 125.52, 125.33, 125.19, 123.36, 123.17, 121.98, 121.71, 121.44, 121.30, 121.25, 120.75, 119.98, 119.95, 119.92, 113.01, 112.75, 111.42. IR (ATR cm^{-1}): 3493, 2921, 2851, 1611, 1457, 1382, 1270, 880. Melting Point: 109-110 °C

5.5 Appendix

Characterization for Chapter 5

5.5.1	General Methods.....	209
5.5.2	Compound Spectra (¹ H NMR, ¹³ C NMR, UV-Vis).....	211
5.5.3	Thermal Analysis.....	254
5.5.4	PXRD Analysis.....	256
5.5.5	Laser Flash Photolysis.....	259

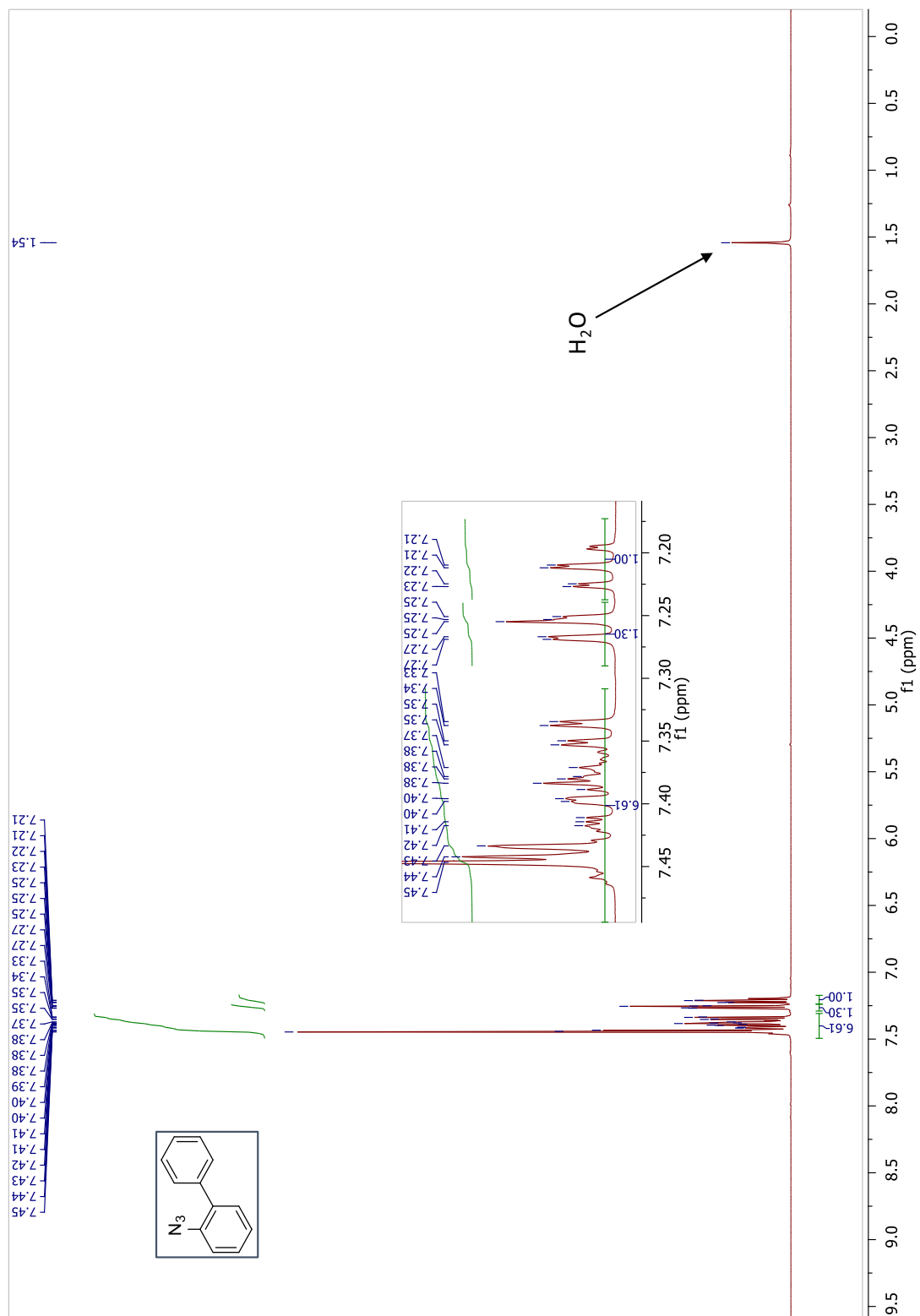
5.5.1 General Methods

All commercially obtained reagents/solvents were used as received without further purification. Unless stated otherwise, reactions were conducted in oven-dried glassware under argon atmosphere. Proton magnetic resonance spectra were recorded at 500 MHz, and carbon-13 magnetic resonance spectra were recorded at 125 MHz, respectively. All chemical shifts are reported in ppm on the δ -scale relative to TMS (δ 0.0) using residual solvent as reference (CDCl_3 δ 7.26 and δ 77.16 for proton and carbon, respectively, CD_3CN δ 1.94 and 1.32, 118.26 for proton and carbon respectively. Standard abbreviations indicating multiplicity were used as follows: s (singlet), b (broad), d (doublet), t (triplet), q (quartet), and m (multiplet). Data for ^{13}C NMR spectra are reported in terms of chemical shift (δ ppm). High-resolution mass spectrum data were recorded on a DART spectrometer in positive (ESI+) ion mode. UV-Vis absorption and transmission spectra were recorded on Ocean Optics spectrometer (DT-MINI-2-GS UV-VIS-NIR LightSource and USB2000+ using SpectraSuite software package). Dynamic Light Scattering (DLS) data were recorded using a Beckman-Coulter N4 Plus particle analyzer with a 10 mW helium-neon laser at 632.8 nm. The particle size was determined using the 62.6° detection angle and was calculated using the size distribution processor (SDP) analysis package provided by the manufacturer. Melting point values were recorded on a Melt-Point II[®] apparatus. Infra-Red spectra were recorded on a PerkinElmer[®] Spectrum Two spectrometer equipped with a universal ATR sampling accessory. Nanosecond transient absorption experiments were performed using Laser Flash Photolysis instrument from Edinburgh Instruments in conjunction with a Nd:YAG laser (Brilliant b, Quantel[®]) with 266-nm output, 4-6 ns pulse width and 36-40 mJ pulse energy. The optical detection is based on a pulsed Xenon arc lamp (450 W), a monochromator (TMS300, Czerny-Turner), a photomultiplier detector (Hamamatsu R928) and a digital oscilloscope (TDS3012C, 100

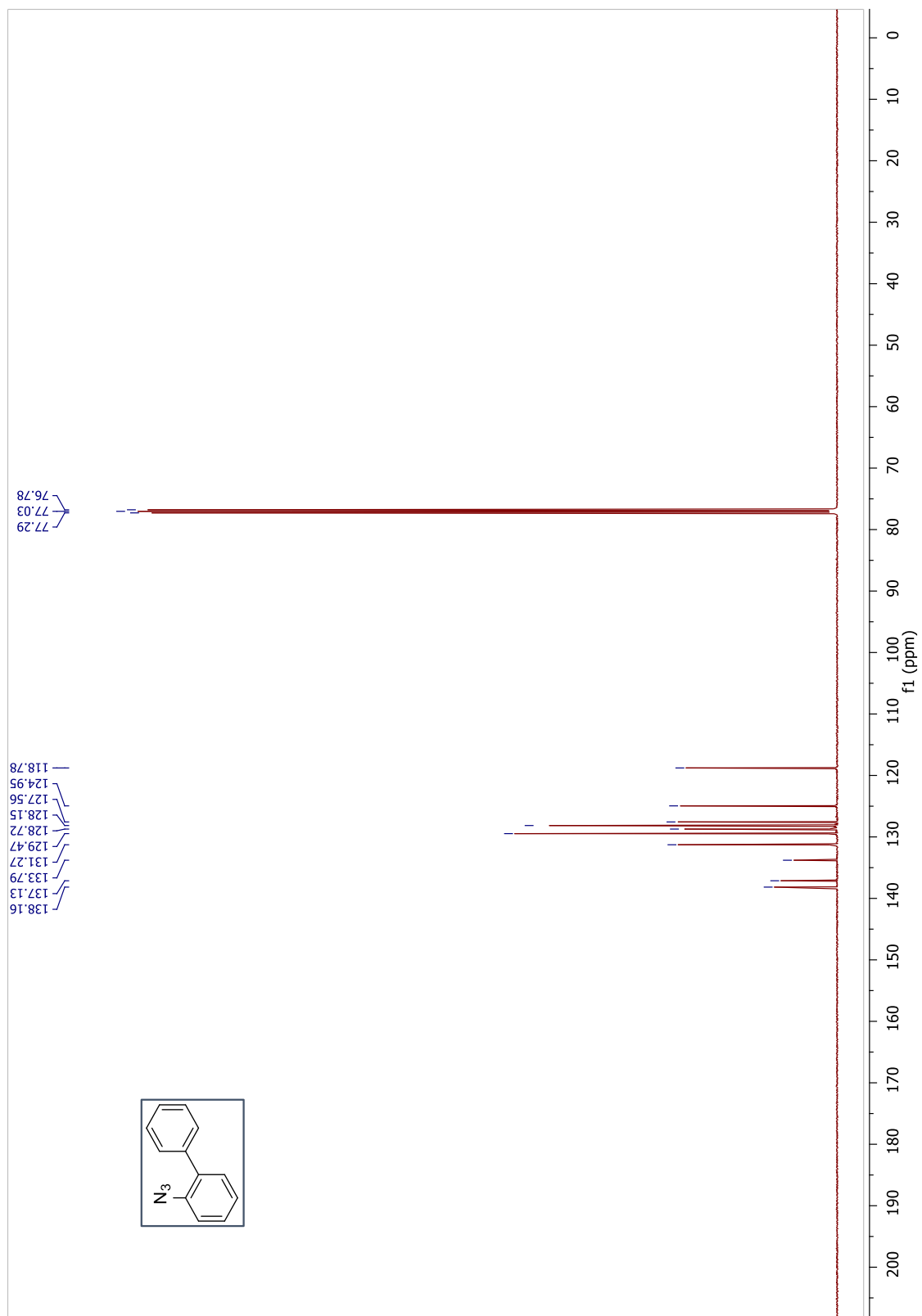
MHz and 1.25 GS/s from Tektronix). The laser flash photolysis experiments were performed with 1 cm quartz flow cell mounted on a home-built sample holder that is placed at the cross-section of the laser incident beam and the probe light. Continuously Argon gas purged acetonitrile solutions or crystalline suspensions of azides were flown through the quartz cell using a peristaltic pump (Masterflex L/S) at a rate of 2.5–4 mL/min. Time-resolved absorption maps were recorded with continuous flow of samples through the quartz cell. Lifetimes at λ_{max} for end-of-pulse spectra were reproducible and doubly verified/processed with Edinburgh Instruments L900 internal software and Igor Pro (version 6.34A, Wavemetrics) software.

5.5.2 Compound Spectra (^1H NMR, ^{13}C NMR, UV-Vis)

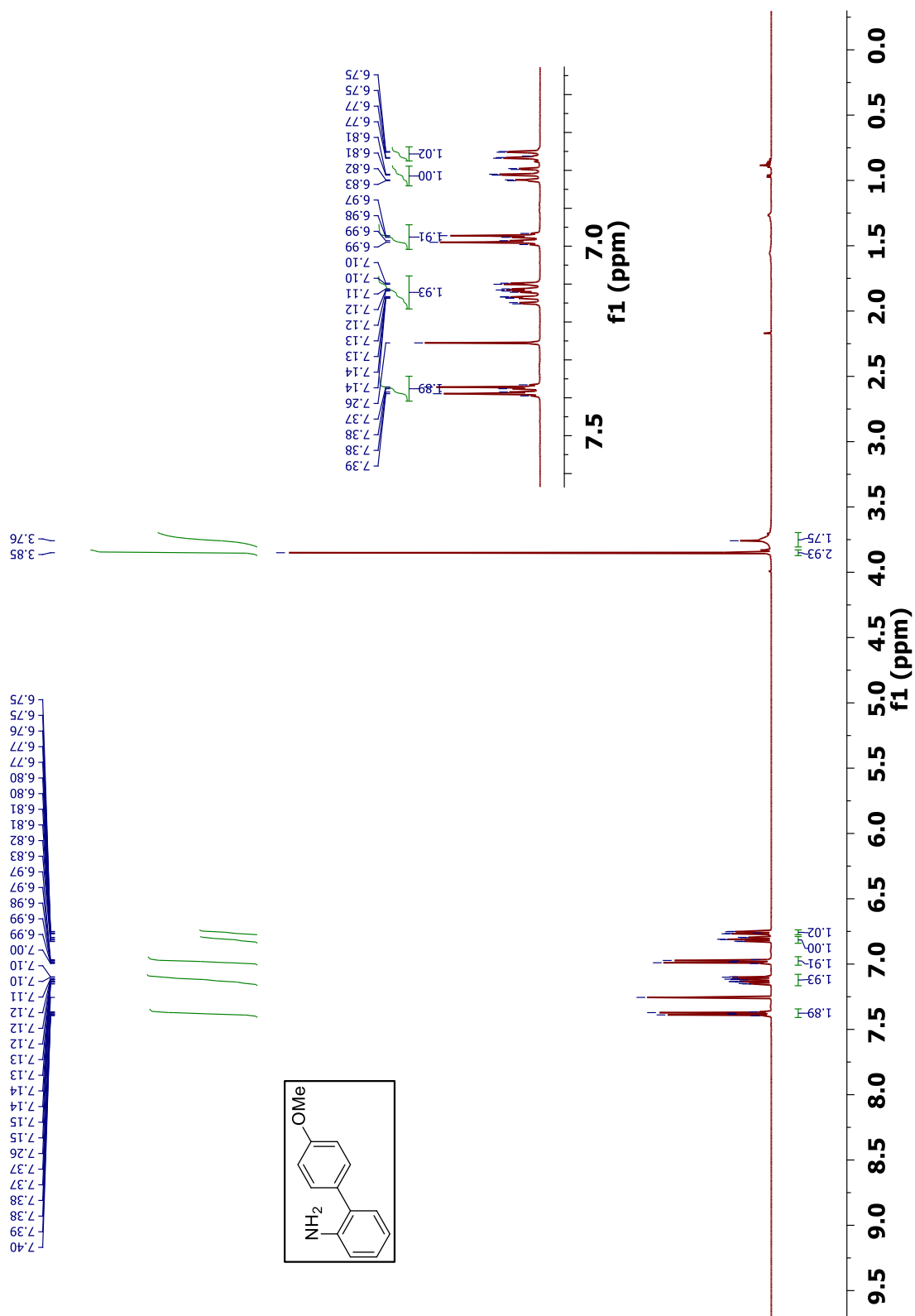
^1H NMR (CDCl_3 , 500 MHz) spectrum of compound 1A.



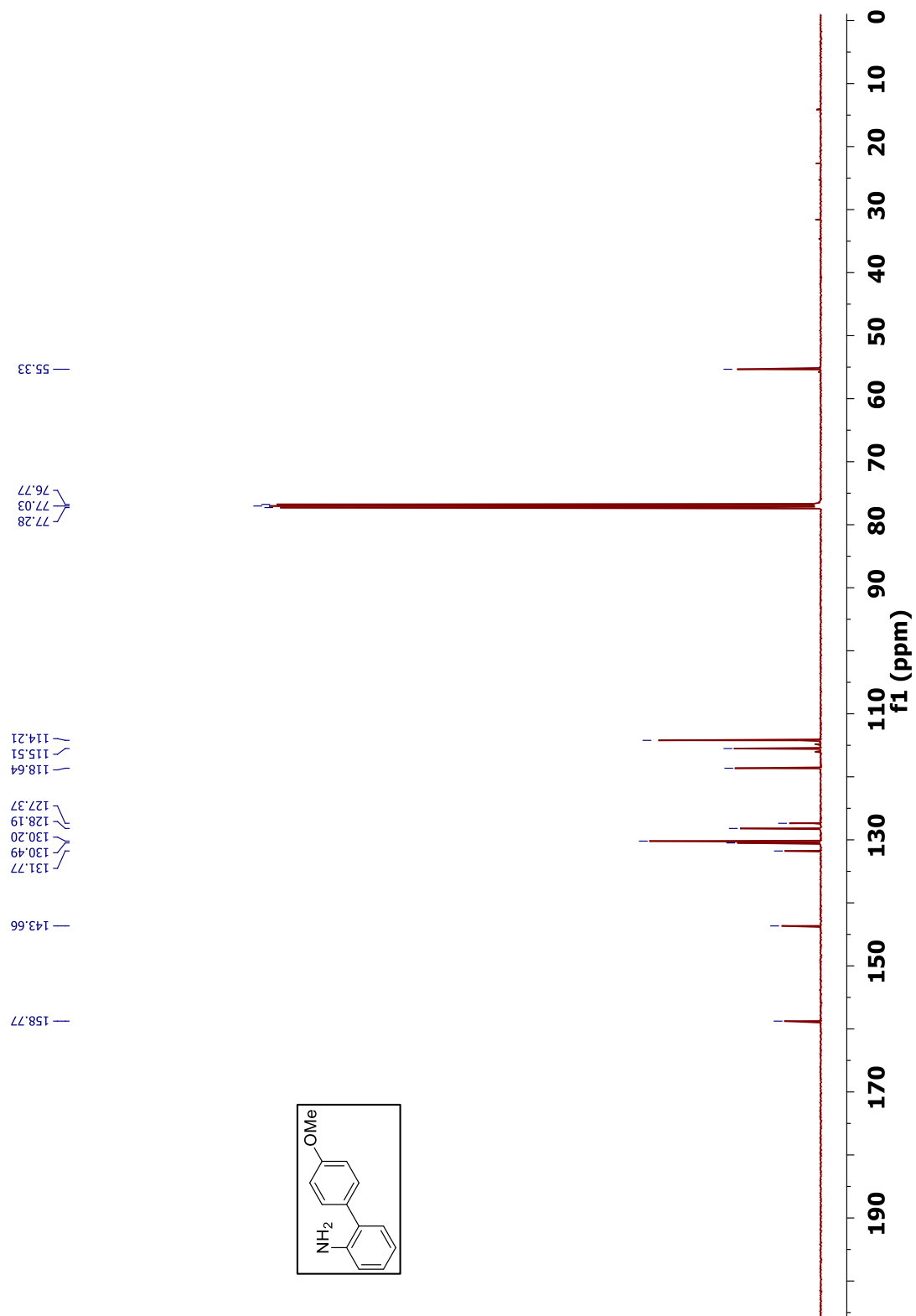
^{13}C NMR (CDCl_3 , 125 MHz) spectrum of compound 1A.



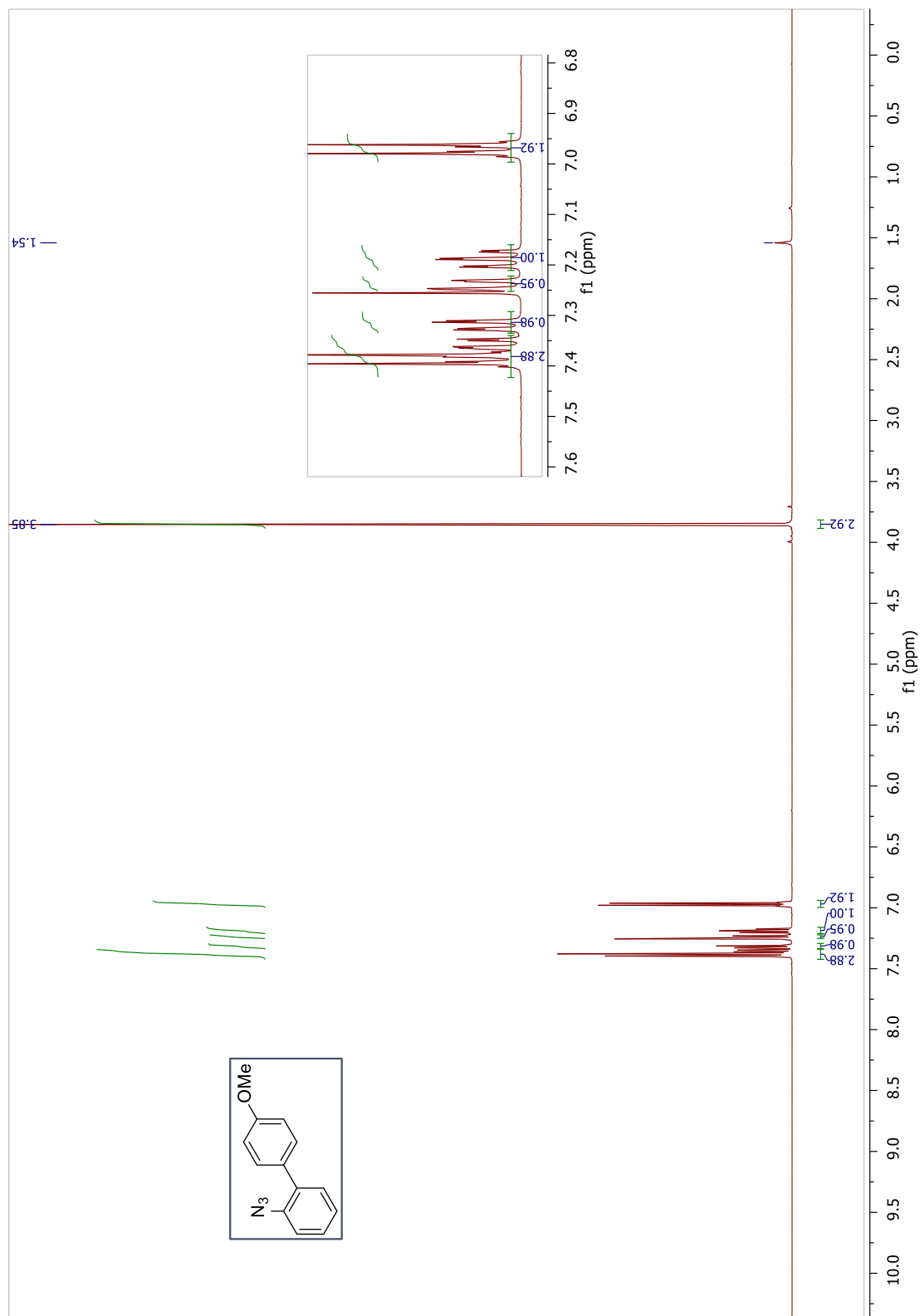
^1H NMR (CDCl_3 , 500 MHz) spectrum of 4'-Methoxy-2-biphenylamine.



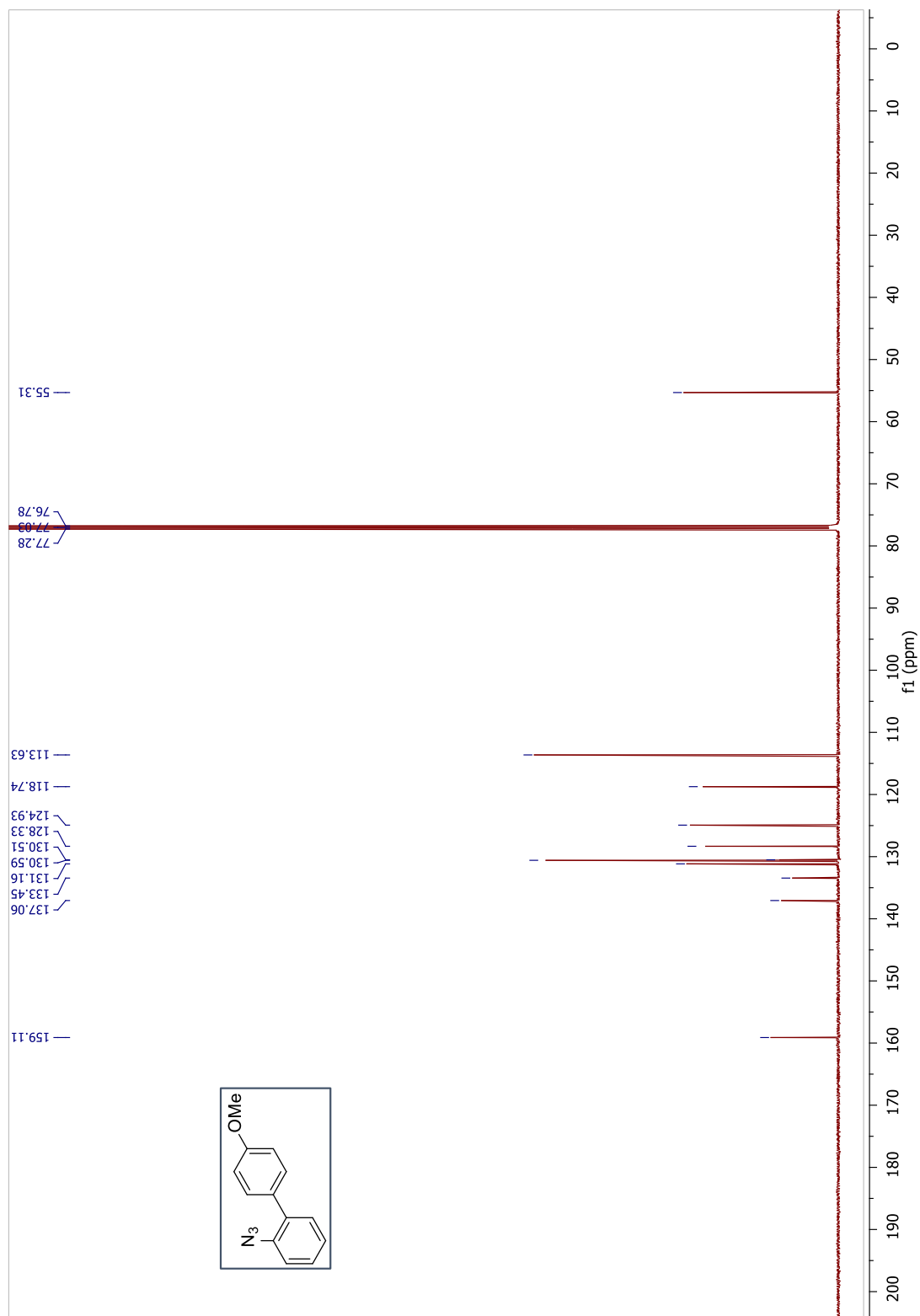
^{13}C NMR (CDCl_3 , 125 MHz) spectrum of 4'-Methoxy-2-biphenylamine.



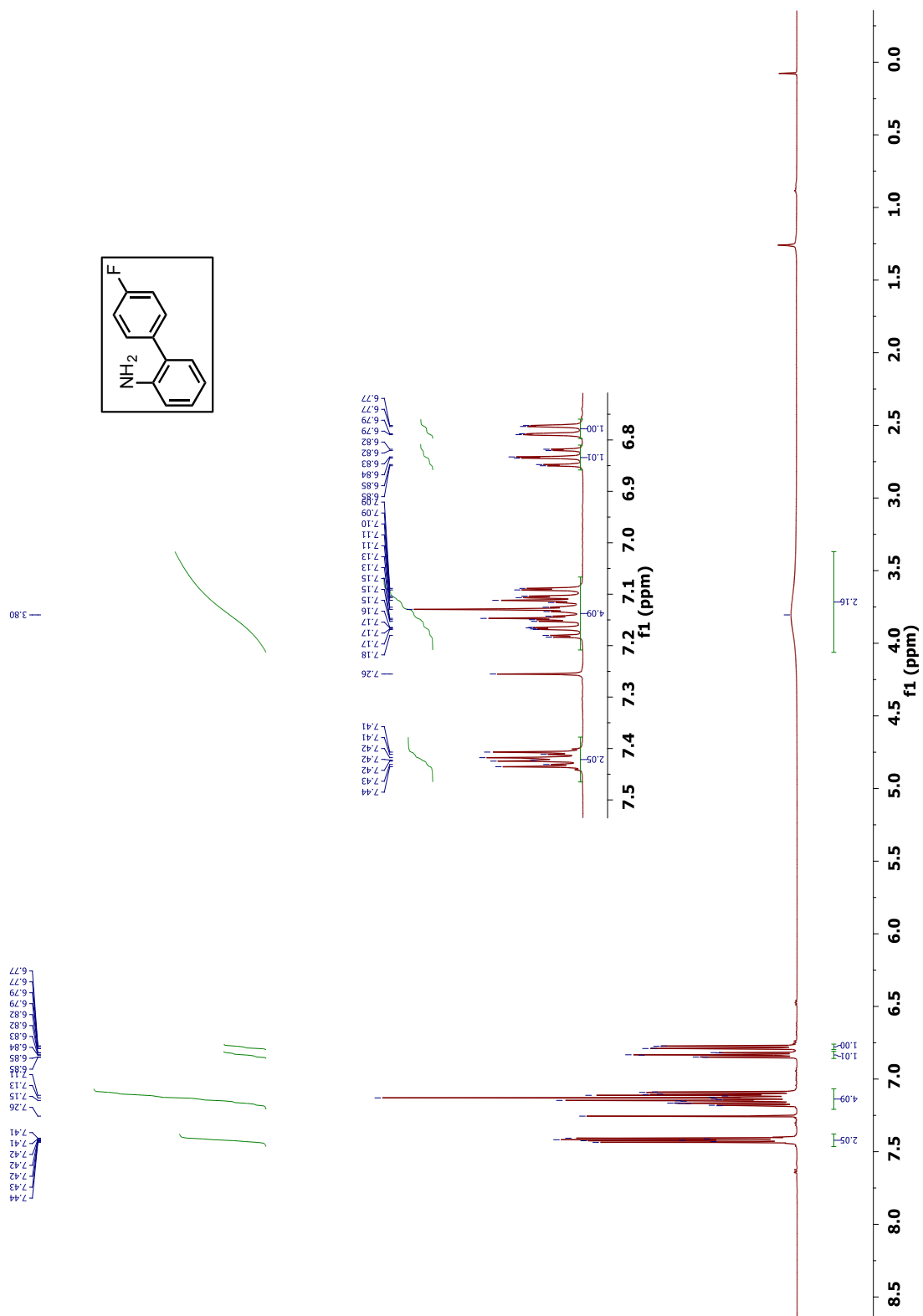
^1H NMR (CDCl_3 , 500 MHz) spectrum of compound 1B.



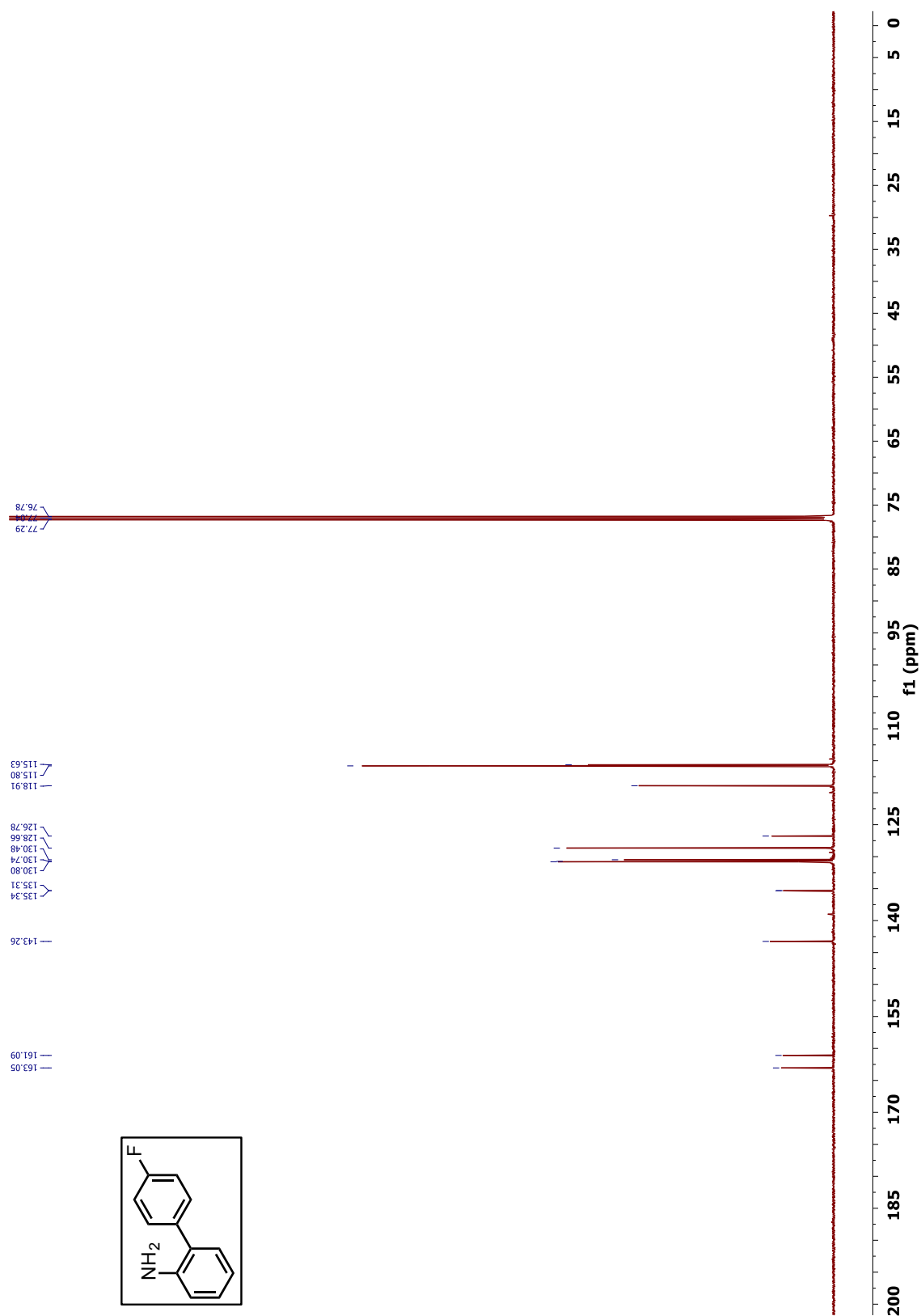
^{13}C NMR (CDCl_3 , 125 MHz) spectrum of compound 1B.



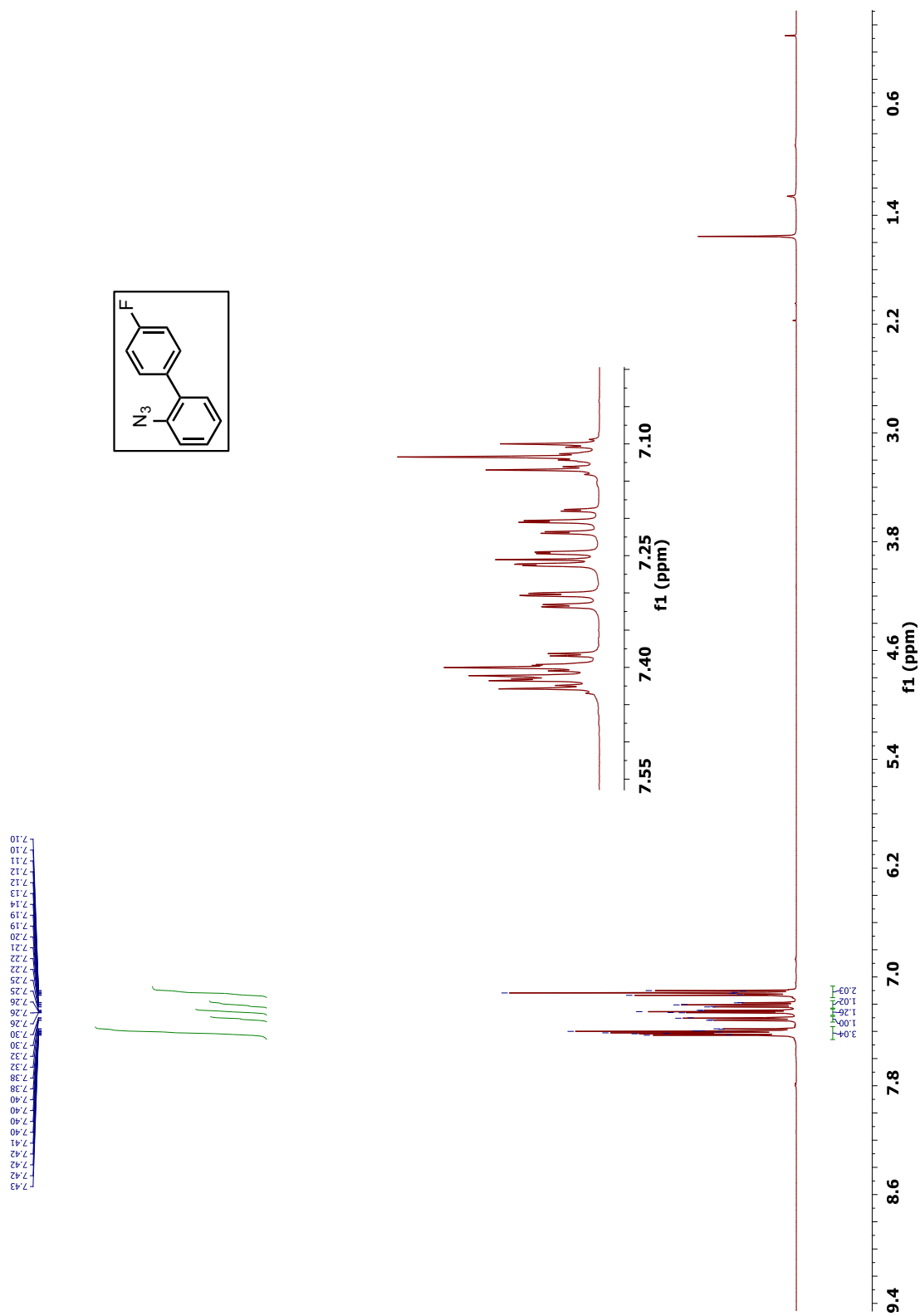
^1H NMR (CDCl_3 , 500 MHz) spectrum of 4'-fluoro-[1,1'-biphenyl]-2-amine.



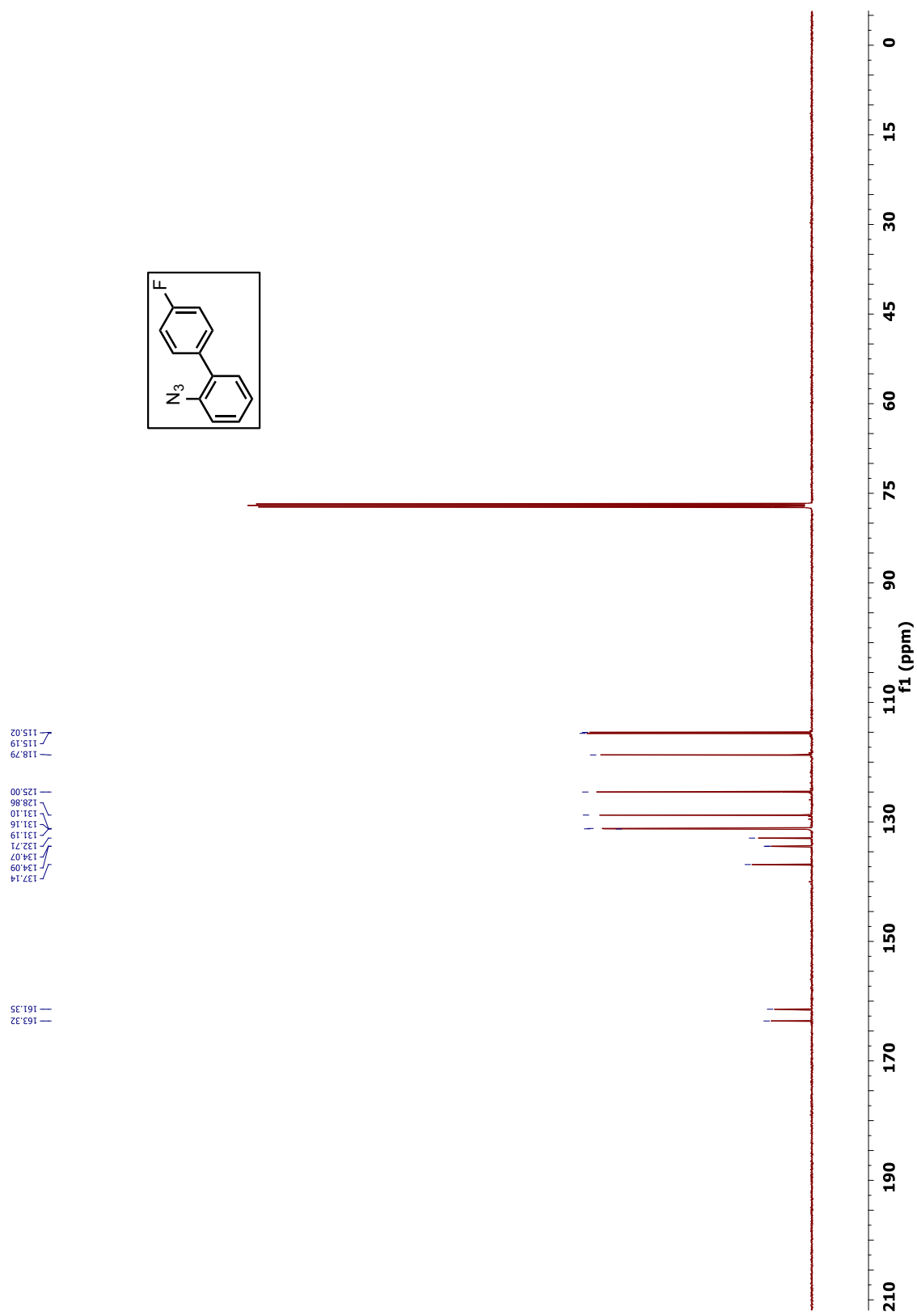
^{13}C NMR (CDCl_3 , 125 MHz) spectrum 4'-fluoro-[1,1'-biphenyl]-2-amine.



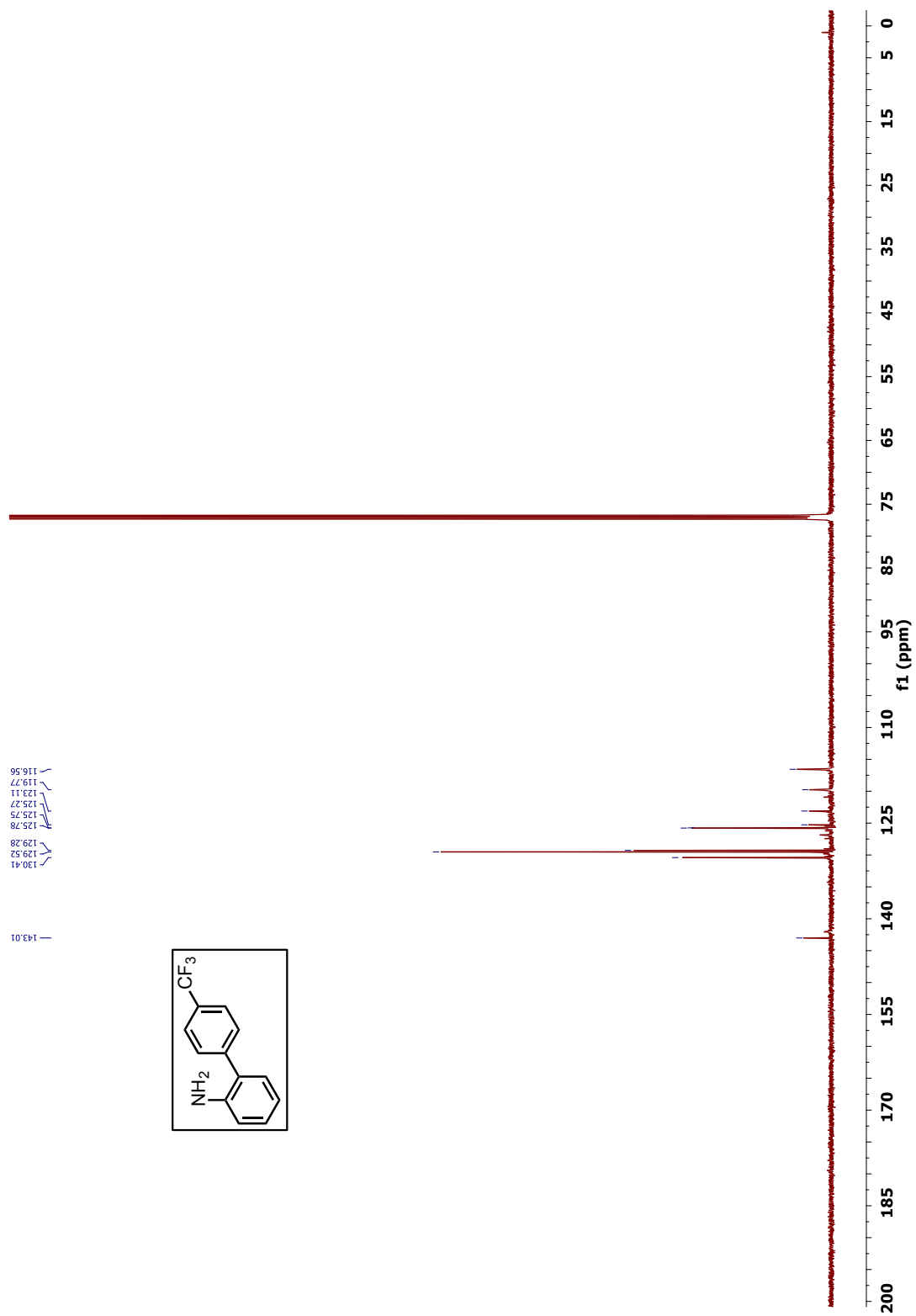
^1H NMR (CDCl_3 , 500 MHz) spectrum of compound 1C.



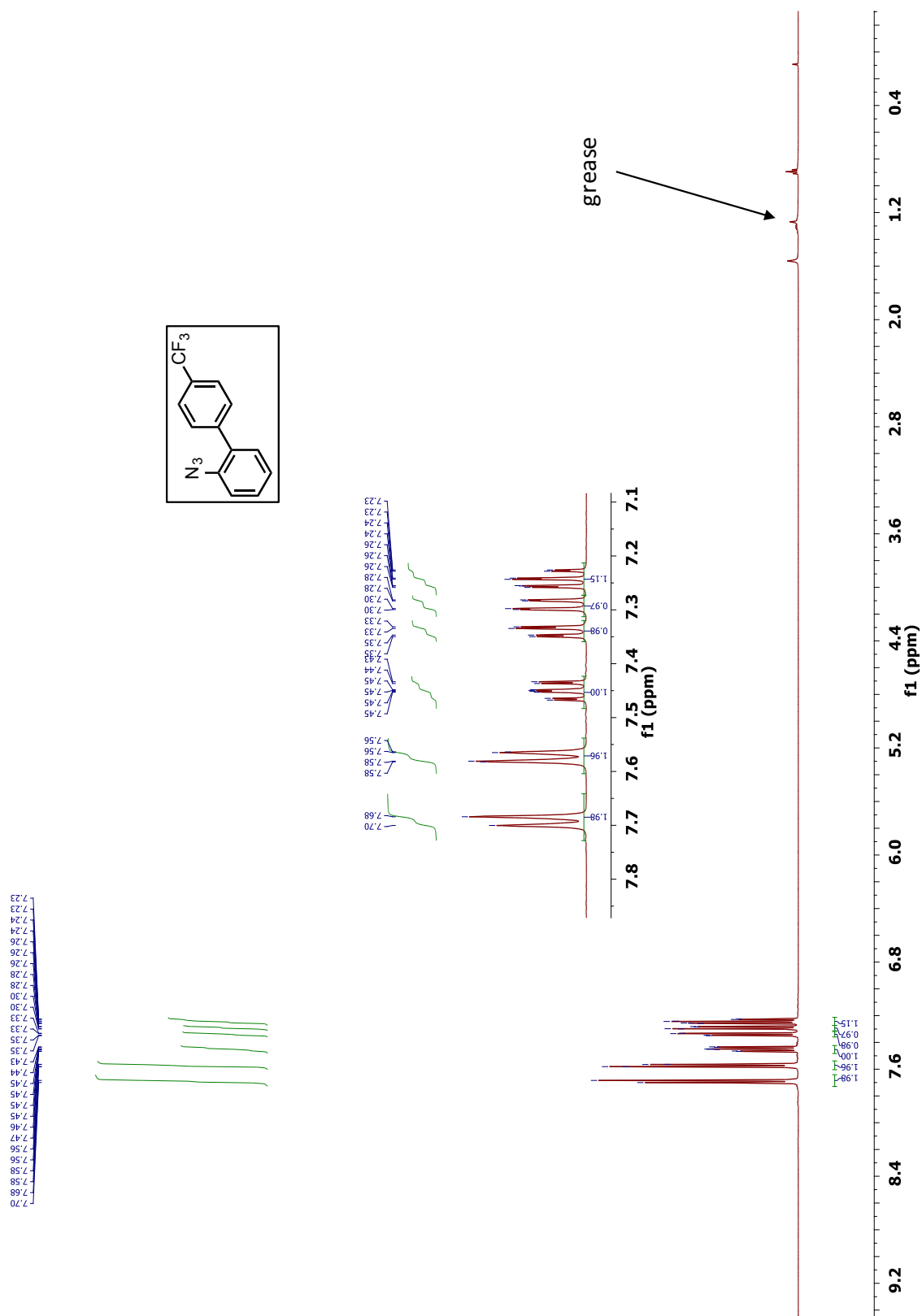
^{13}C NMR (CDCl_3 , 125 MHz) spectrum of compound 1C.



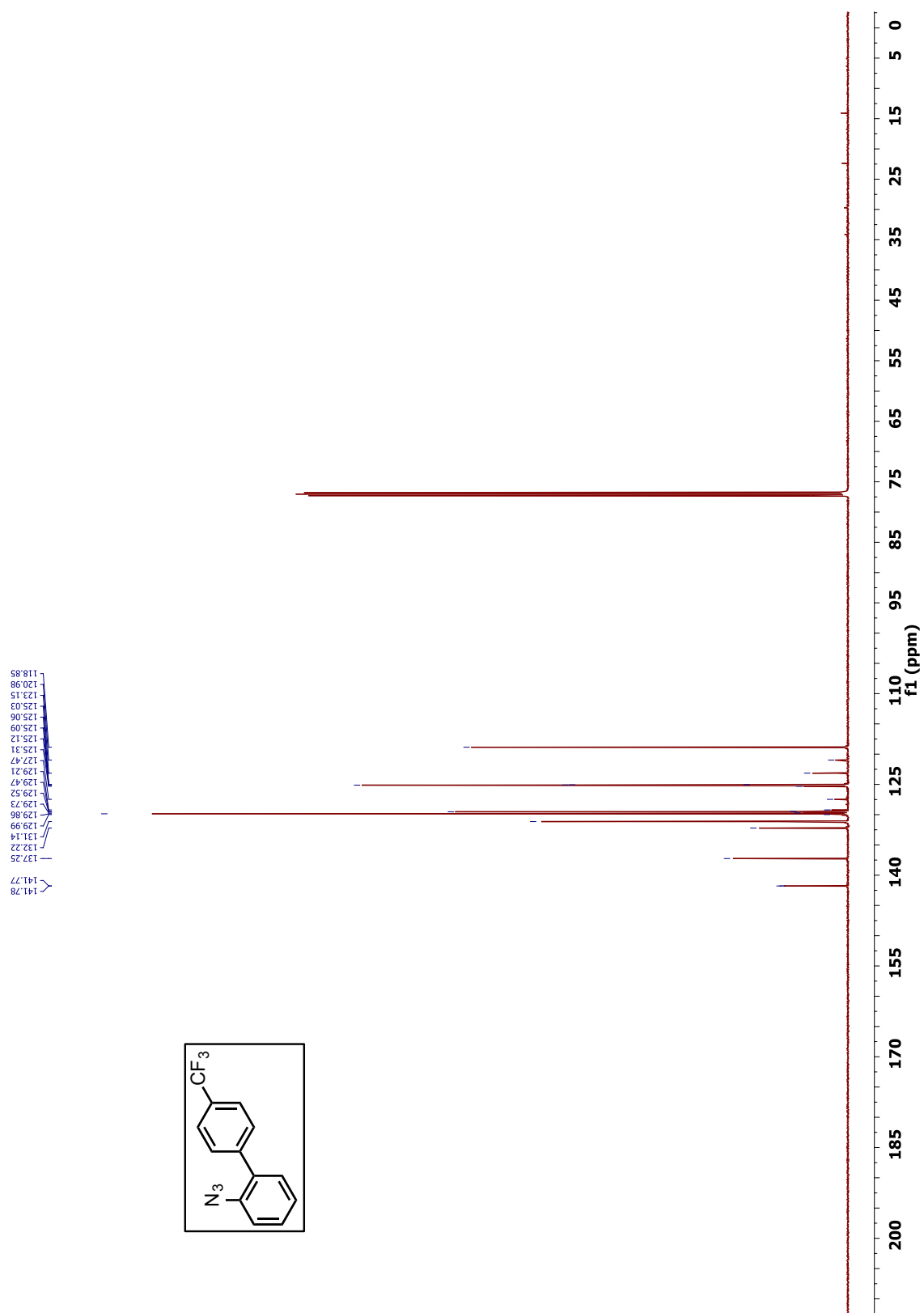
^{13}C NMR (CDCl_3 , 125 MHz) spectrum of 4'-(trifluoromethyl)-[1,1'-biphenyl]-2-amine.



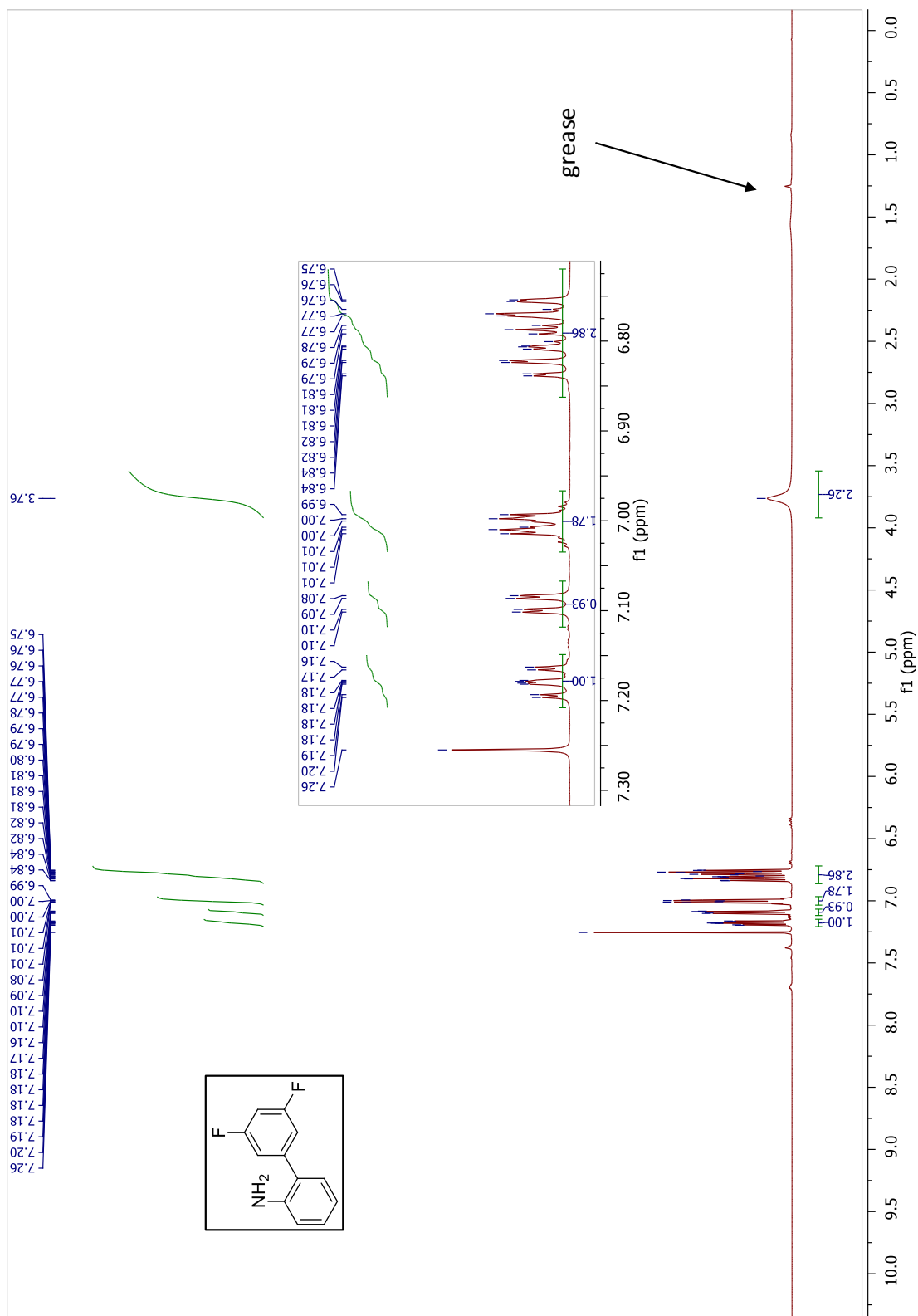
^1H NMR (CDCl_3 , 500 MHz) spectrum of compound 1D.



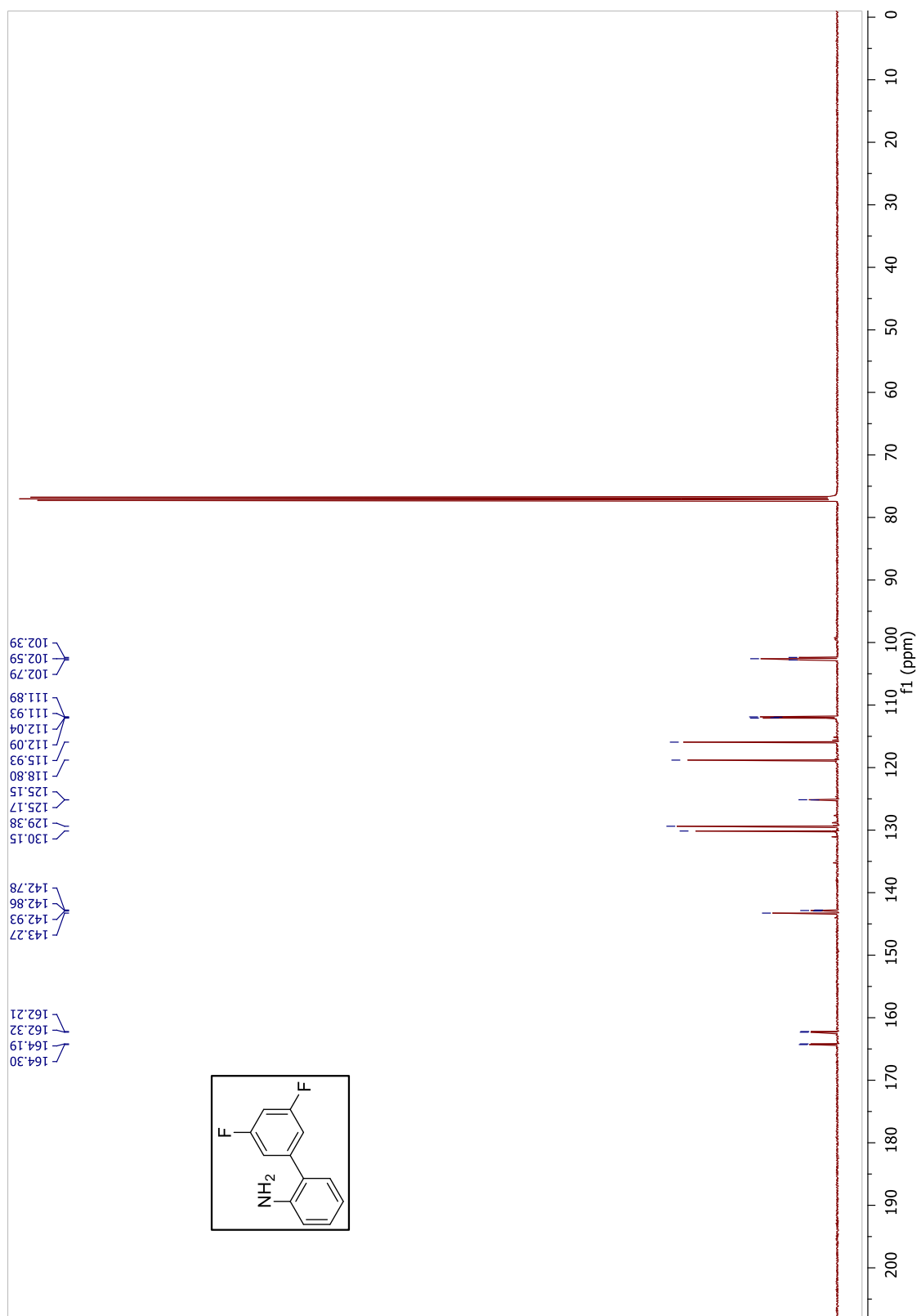
^{13}C NMR (CDCl_3 , 125 MHz) spectrum of compound 1D.



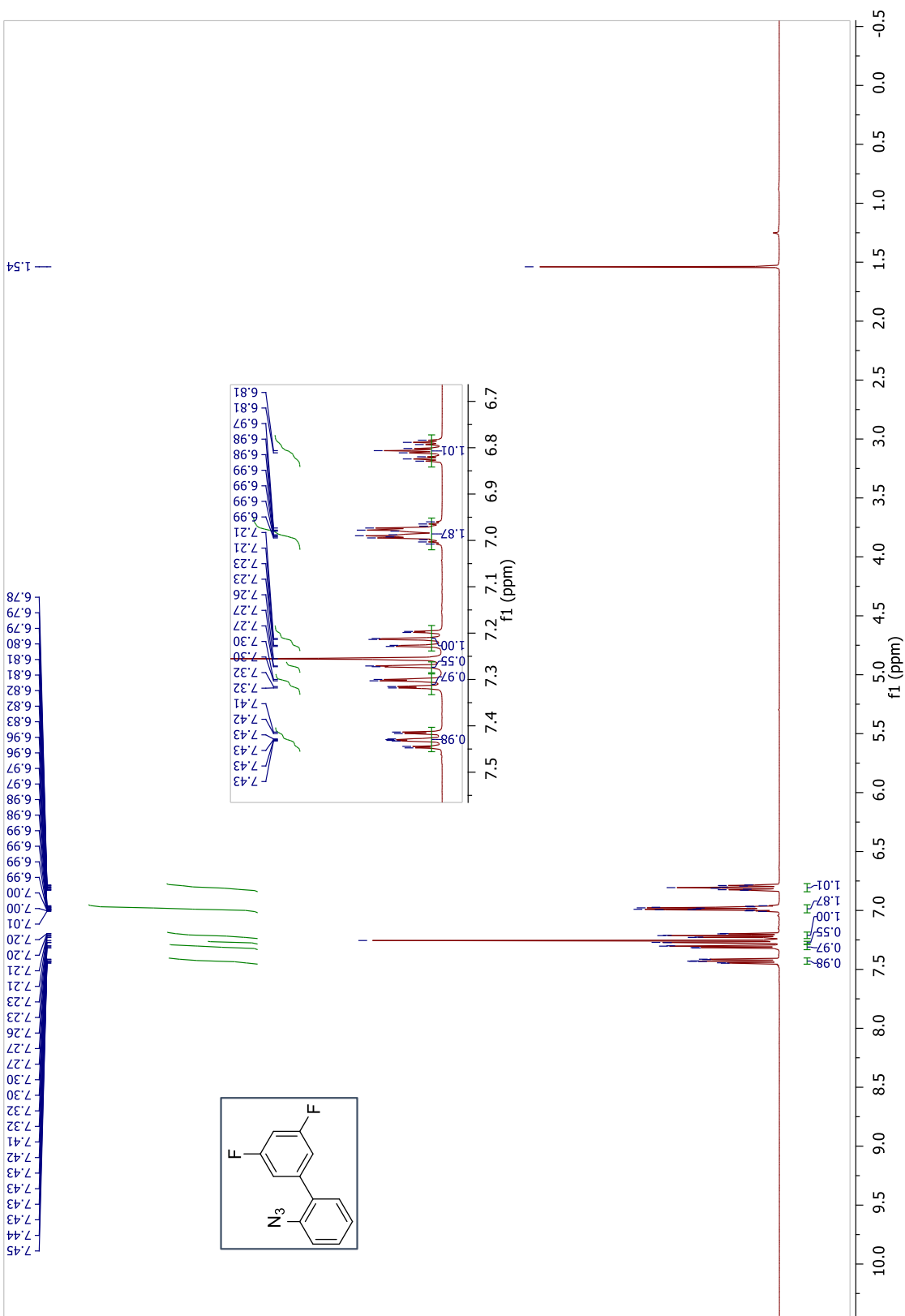
^1H NMR (CDCl_3 , 500 MHz) spectrum of 3',5'-Difluoro-2-biphenylamine.



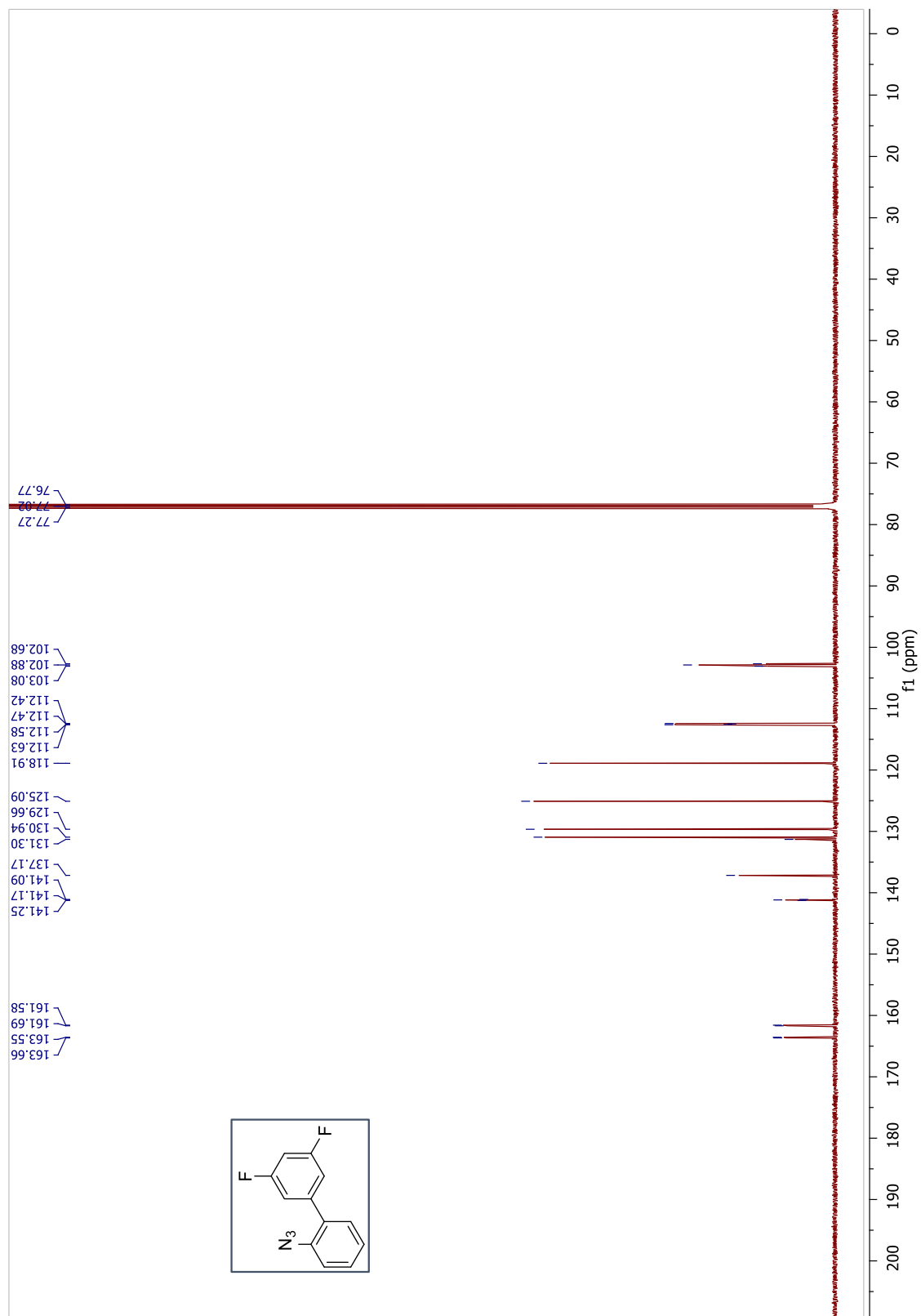
^{13}C NMR (CDCl_3 , 125 MHz) spectrum of 3',5'-Difluoro-2-biphenylamine.



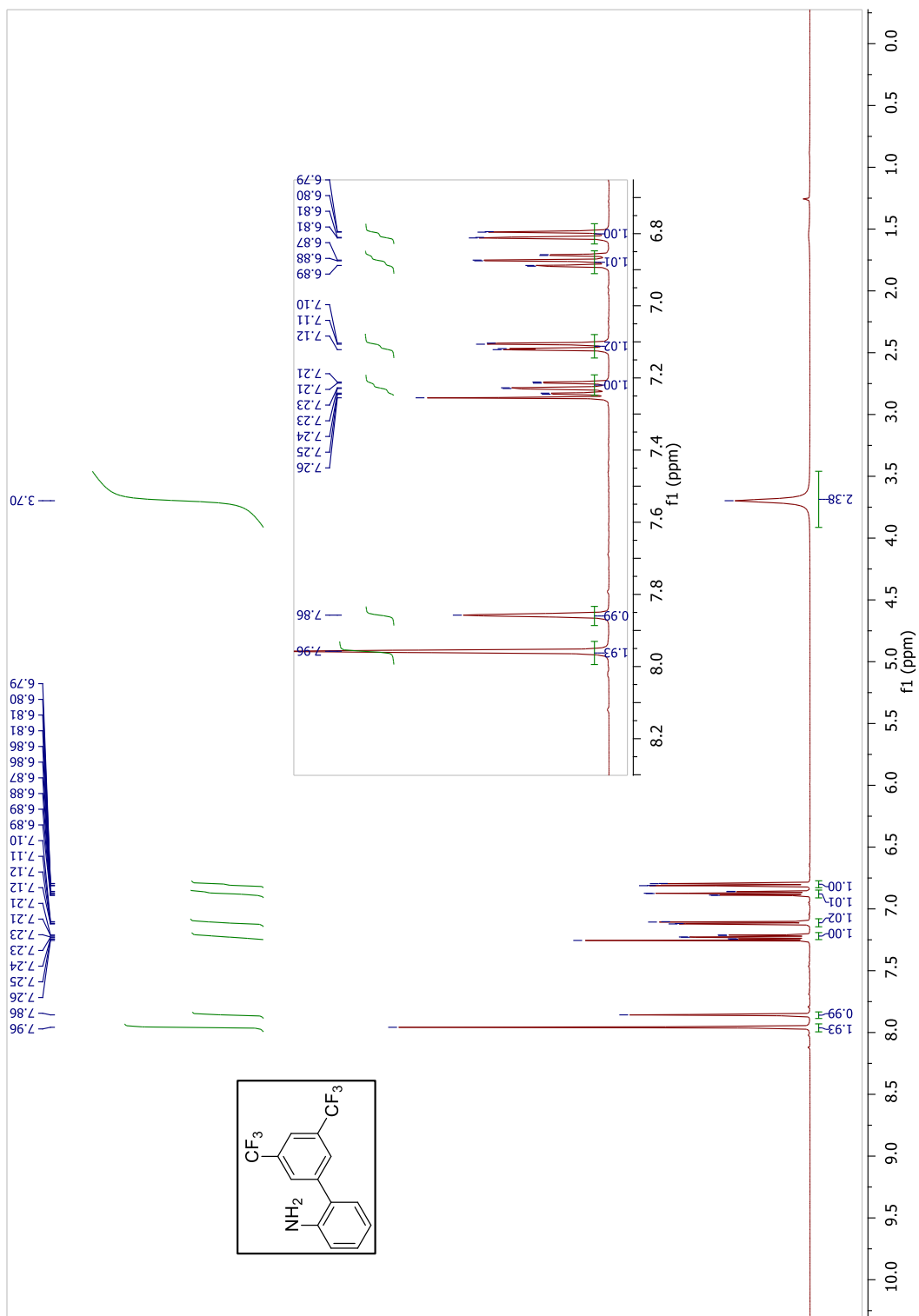
^1H NMR (CDCl_3 , 500 MHz) spectrum of compound 1E.



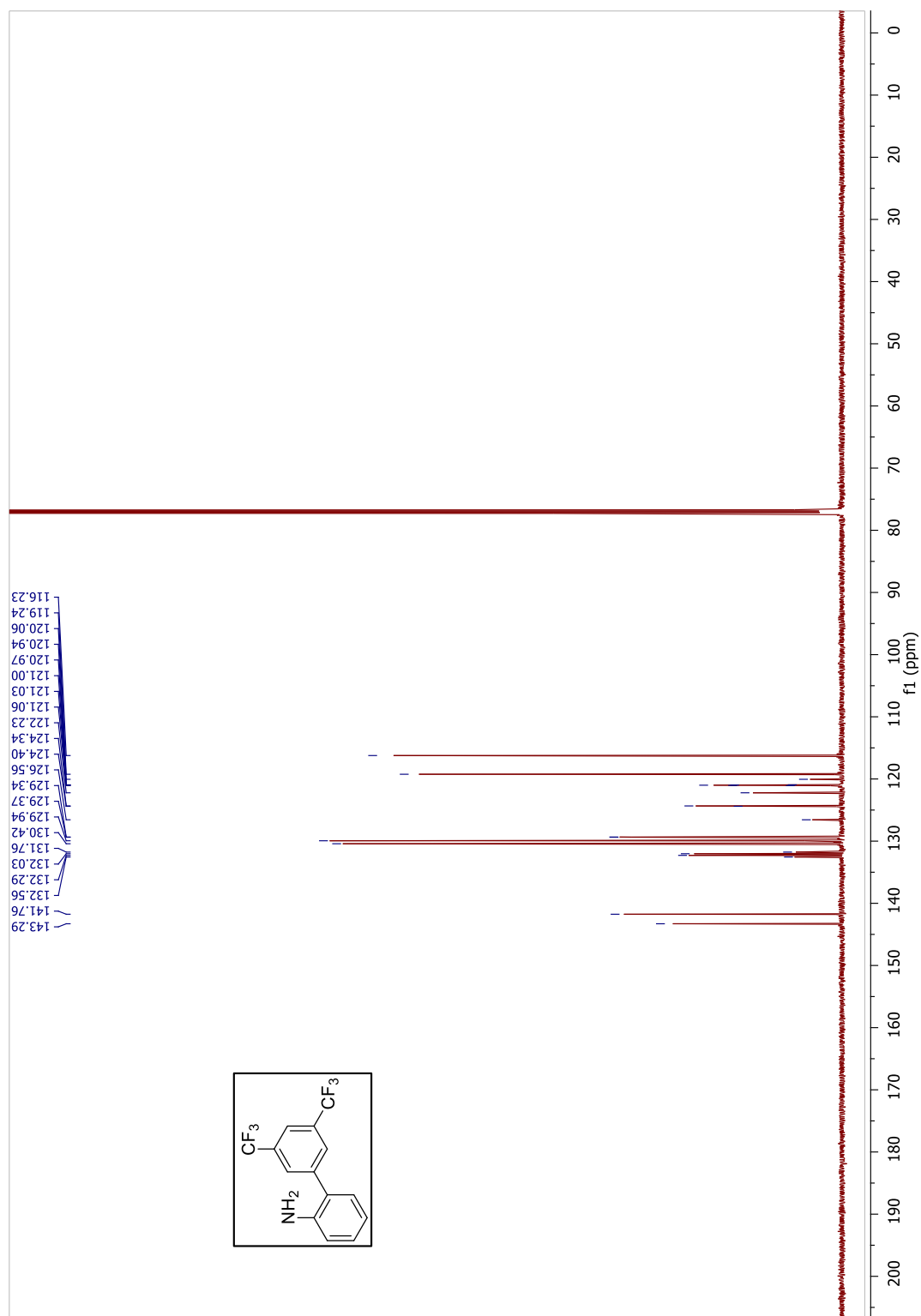
^{13}C NMR (CDCl_3 , 125 MHz) spectrum of compound 1E.



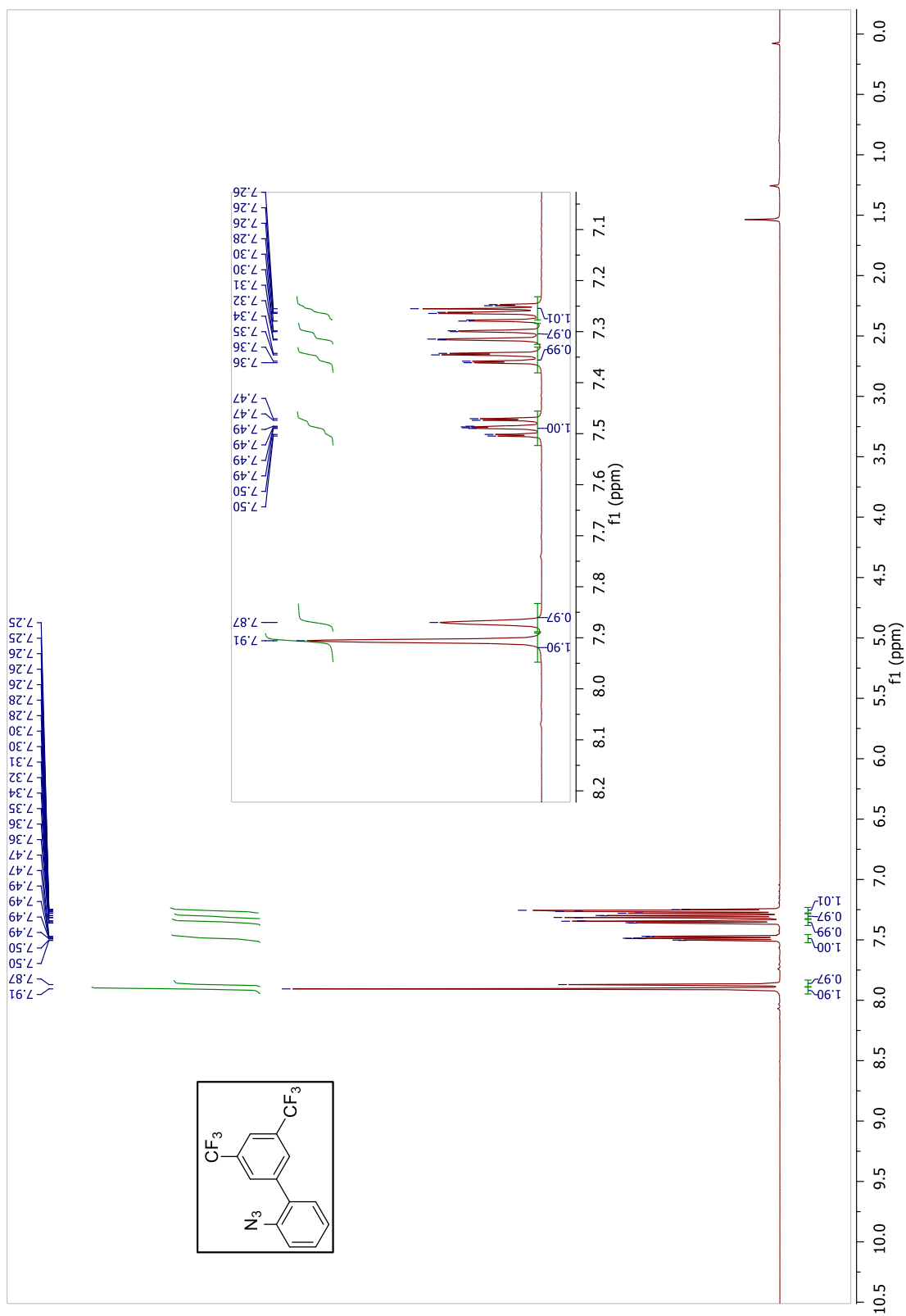
^1H NMR (CDCl_3 , 500 MHz) spectrum of 3',5'-bis(trifluoromethyl)-[1,1'-biphenyl]-2-amine.



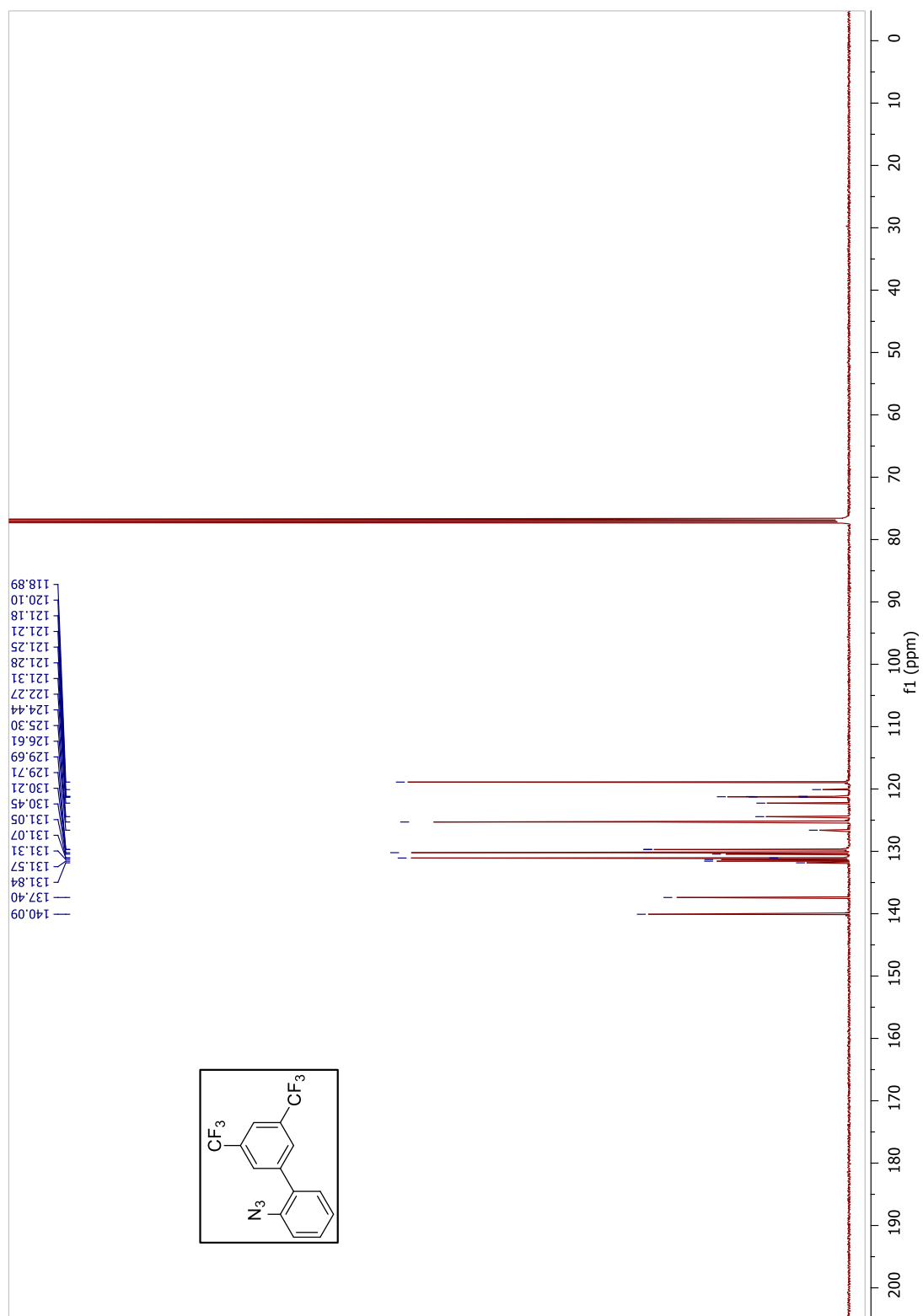
^{13}C NMR (CDCl_3 , 125 MHz) spectrum of 3',5'-bis(trifluoromethyl)-[1,1'-biphenyl]-2-amine.



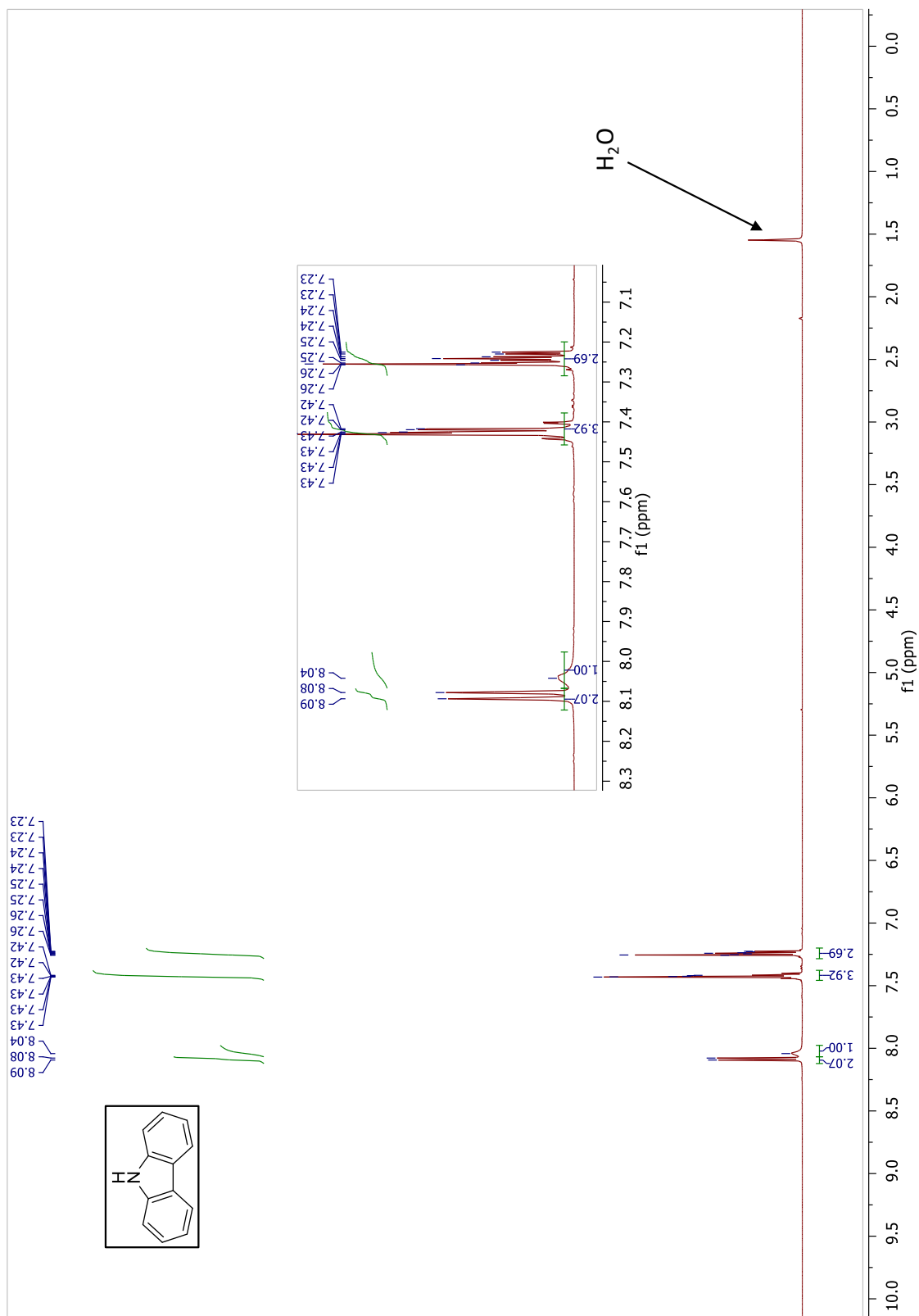
^1H NMR (CDCl_3 , 500 MHz) spectrum of compound 1F.



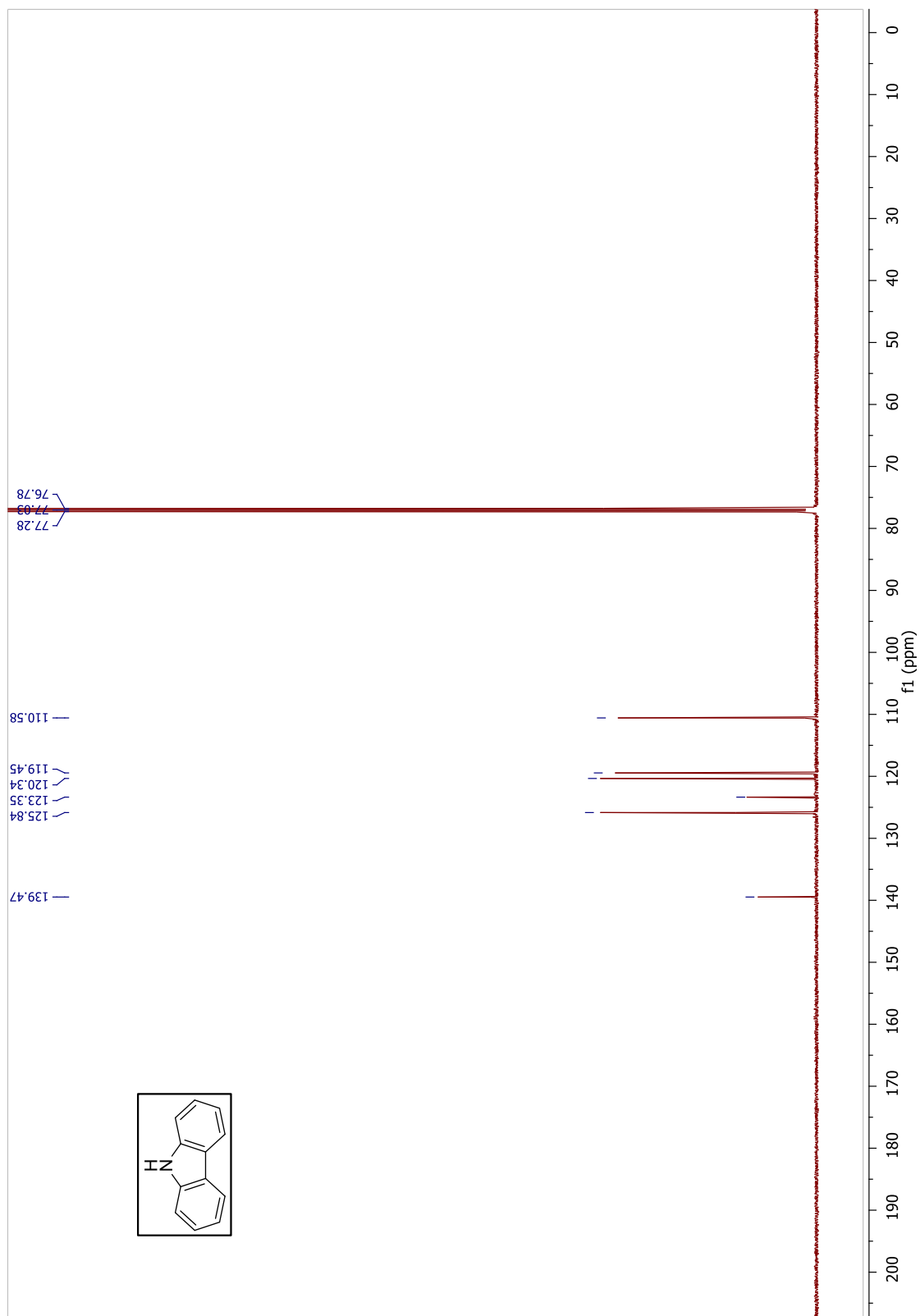
^{13}C NMR (CDCl_3 , 125 MHz) spectrum of compound 1F.



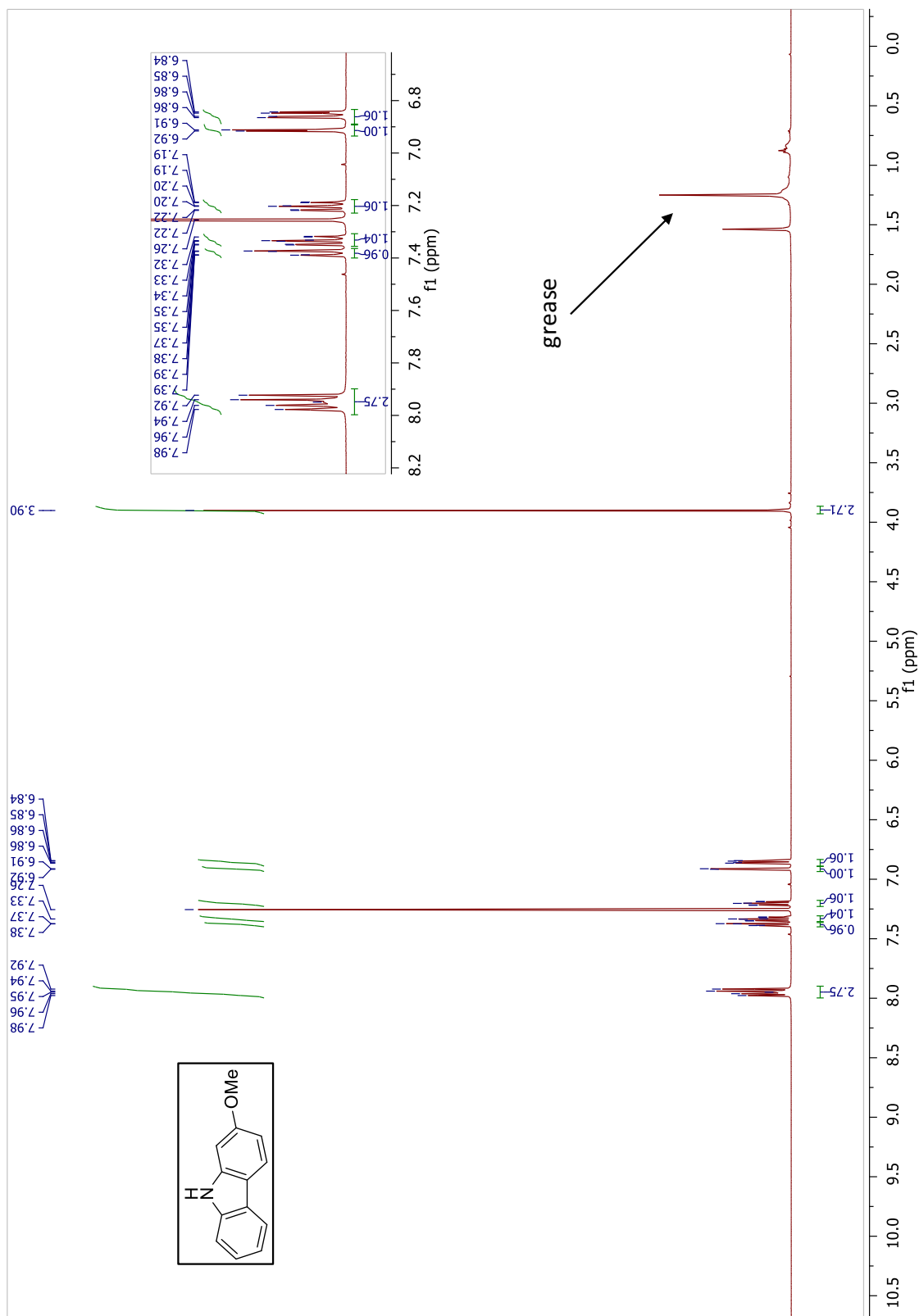
^1H NMR (CDCl_3 , 500 MHz) spectrum of compound 2A.



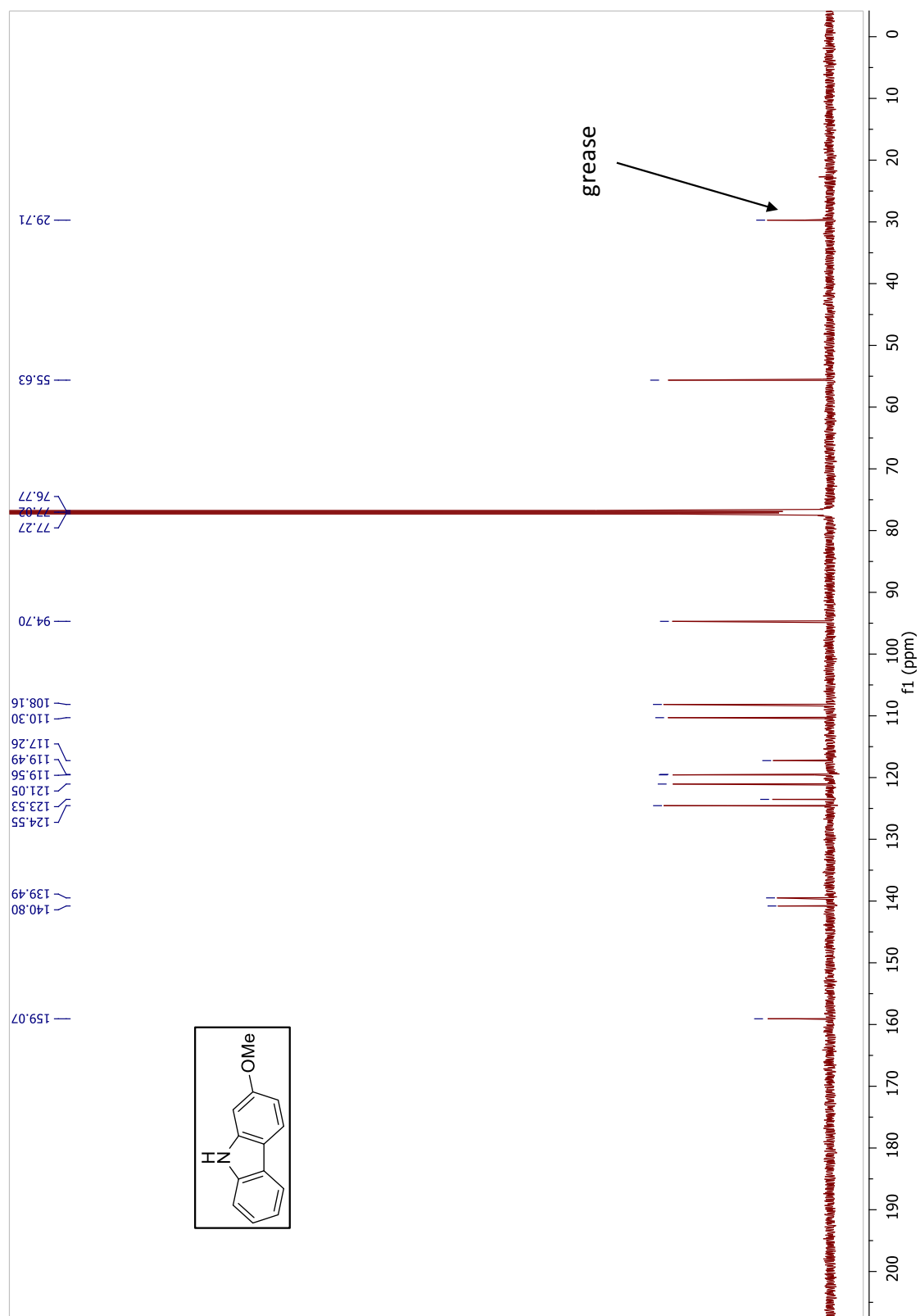
^{13}C NMR (CDCl_3 , 125 MHz) spectrum of compound 2A.



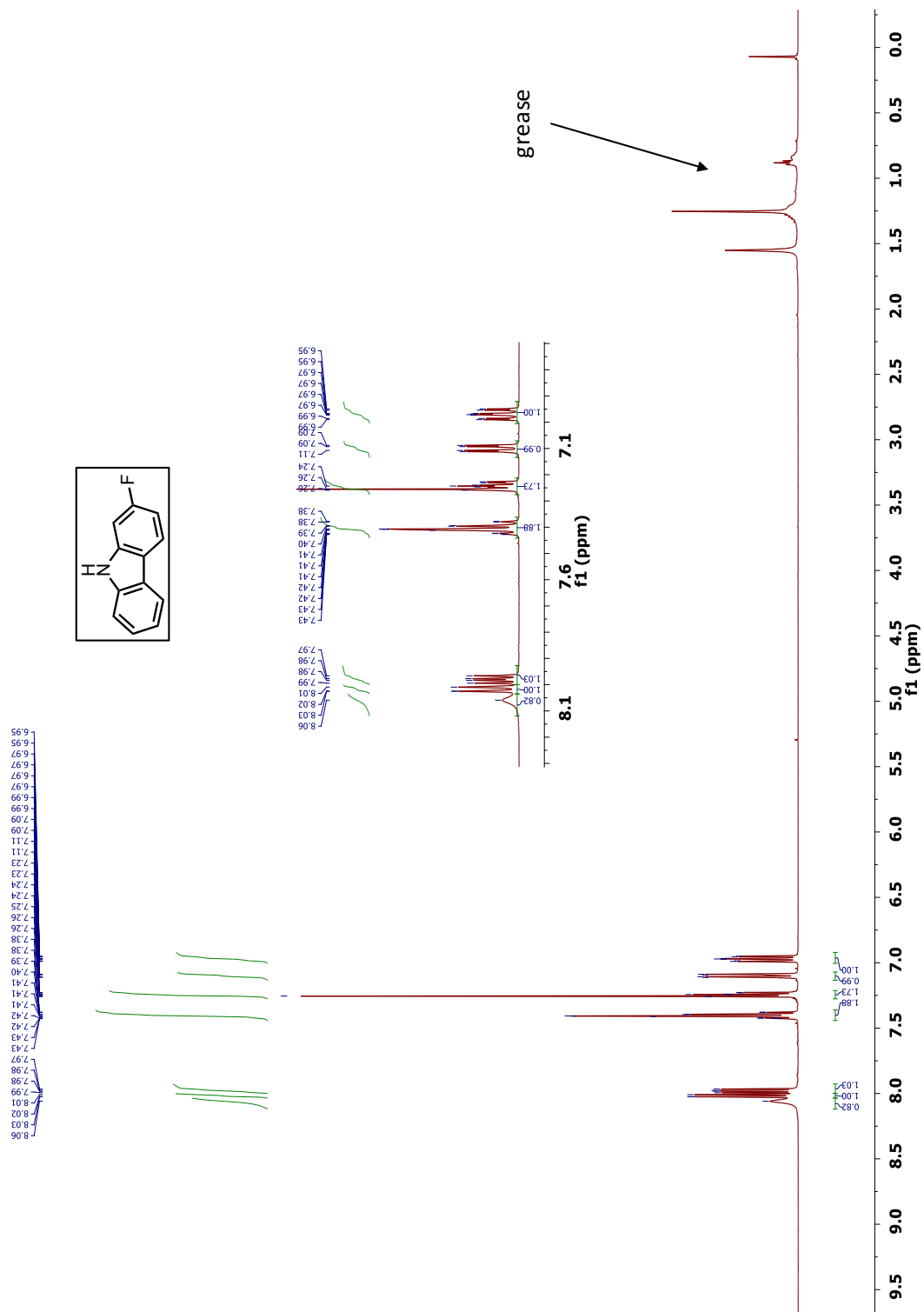
^1H NMR (CDCl_3 , 500 MHz) spectrum of compound 2B.



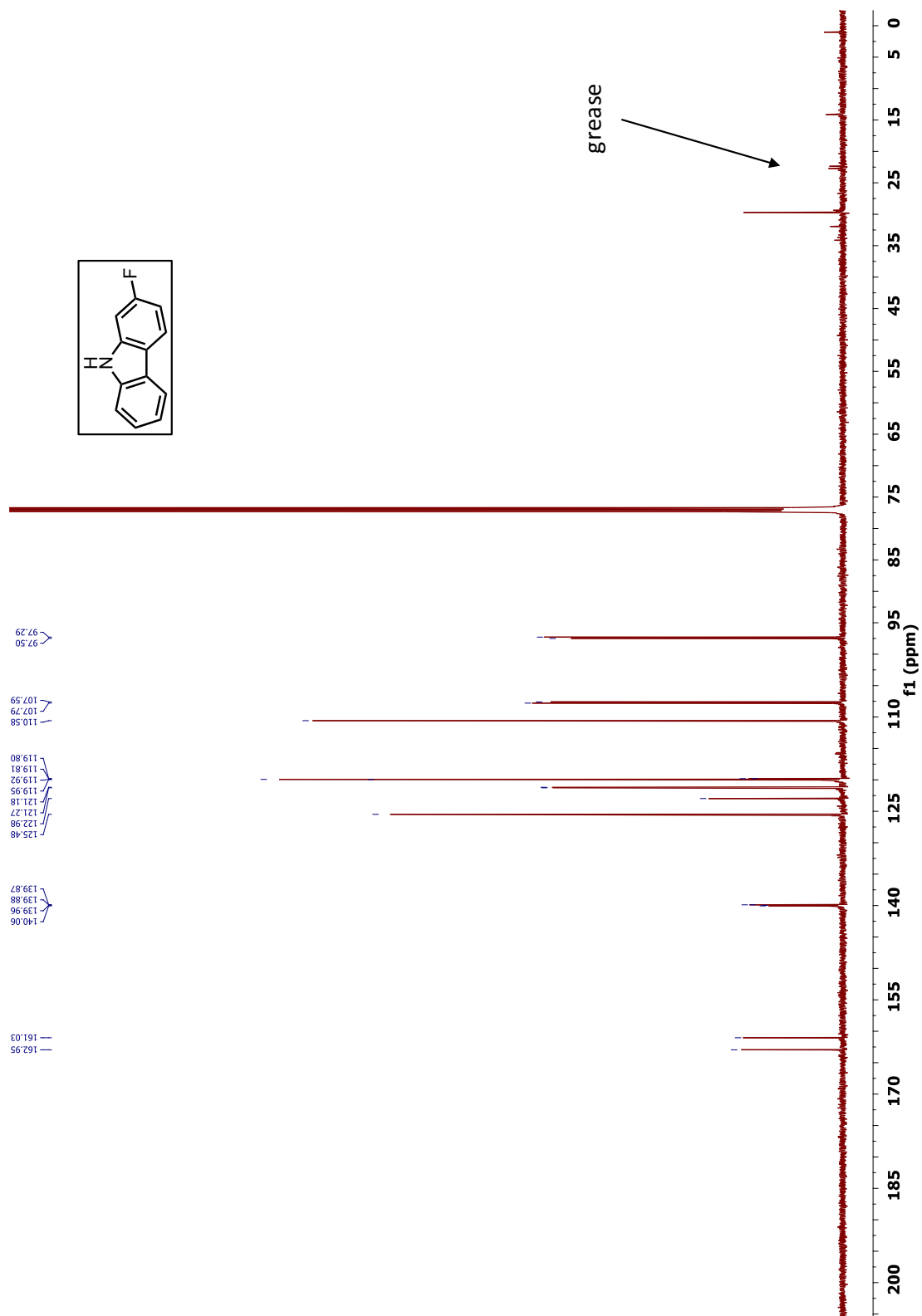
^{13}C NMR (CDCl_3 , 125 MHz) spectrum of compound 2B.



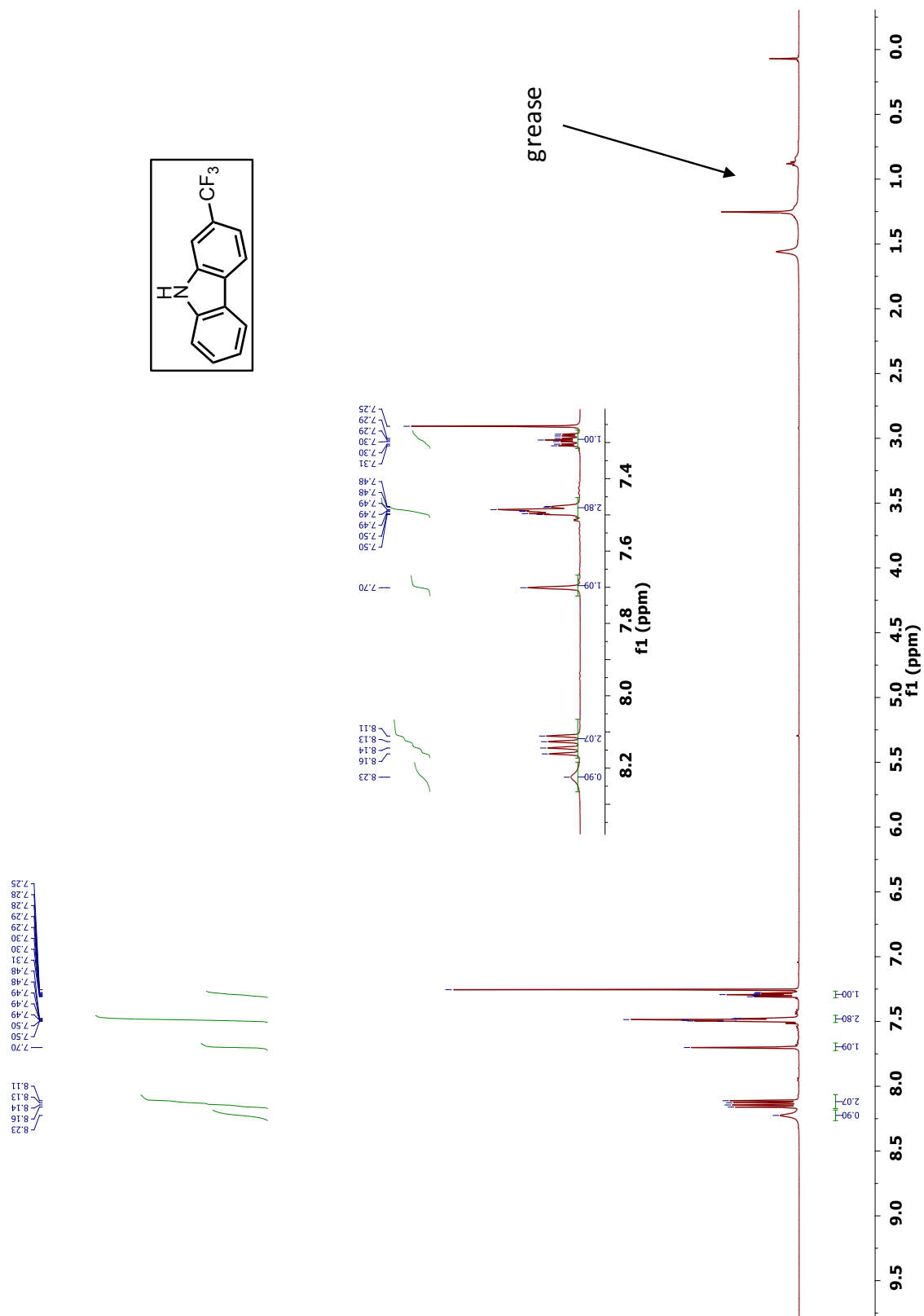
^1H NMR (CDCl_3 , 500 MHz) spectrum of compound 2C.



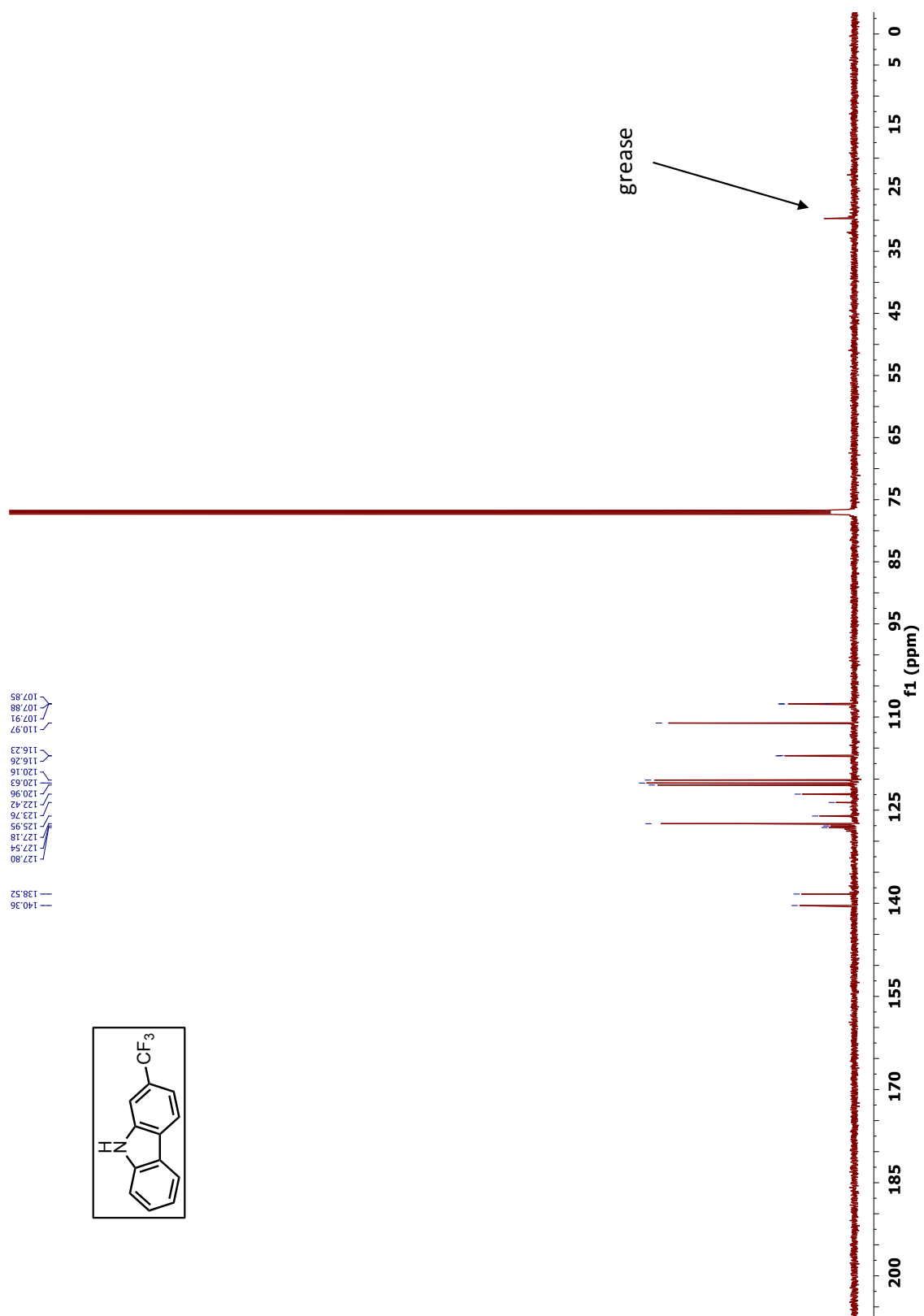
^{13}C NMR (CDCl_3 , 125 MHz) spectrum of compound 2C.



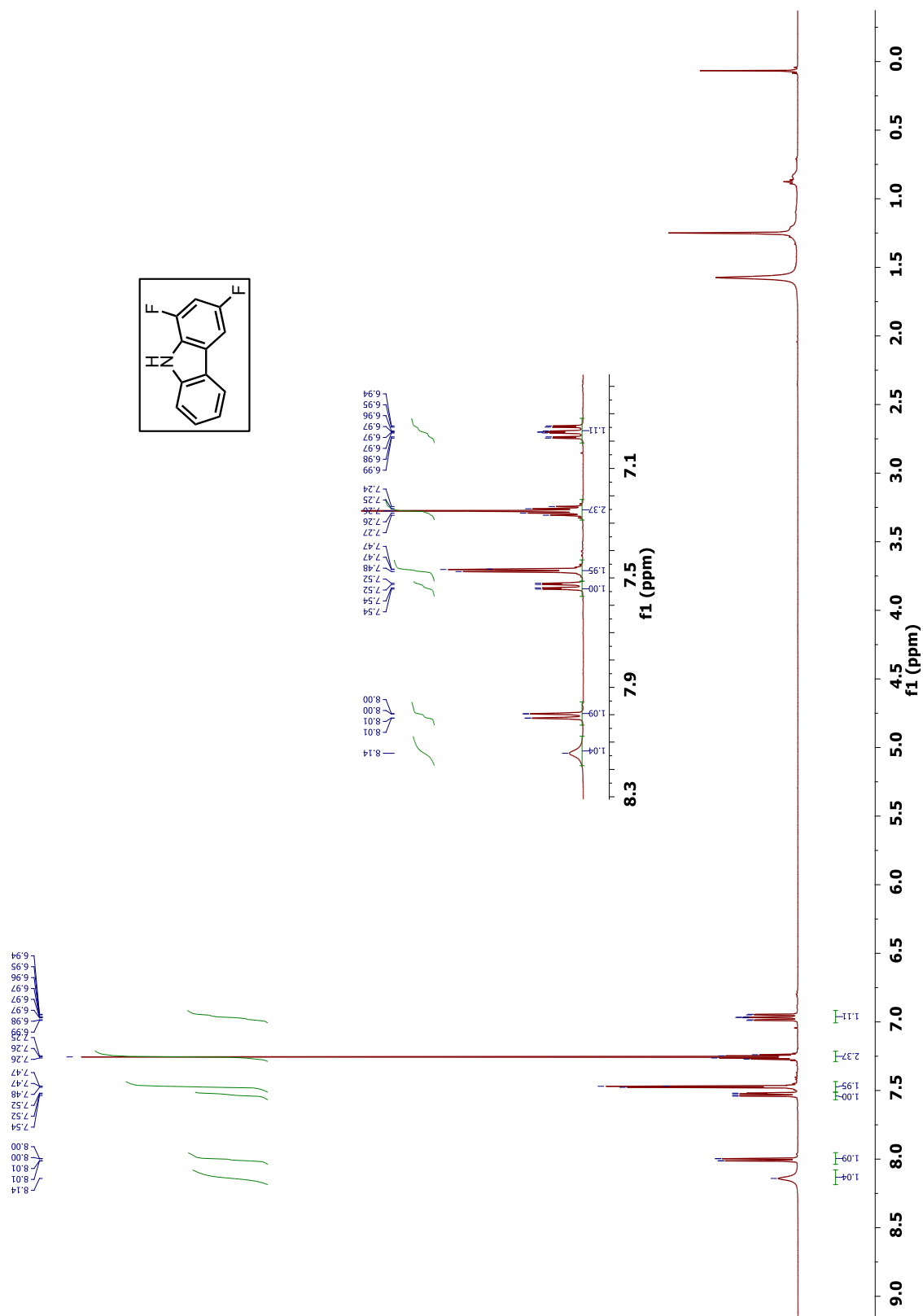
^1H NMR (CDCl_3 , 500 MHz) spectrum of compound 2D.



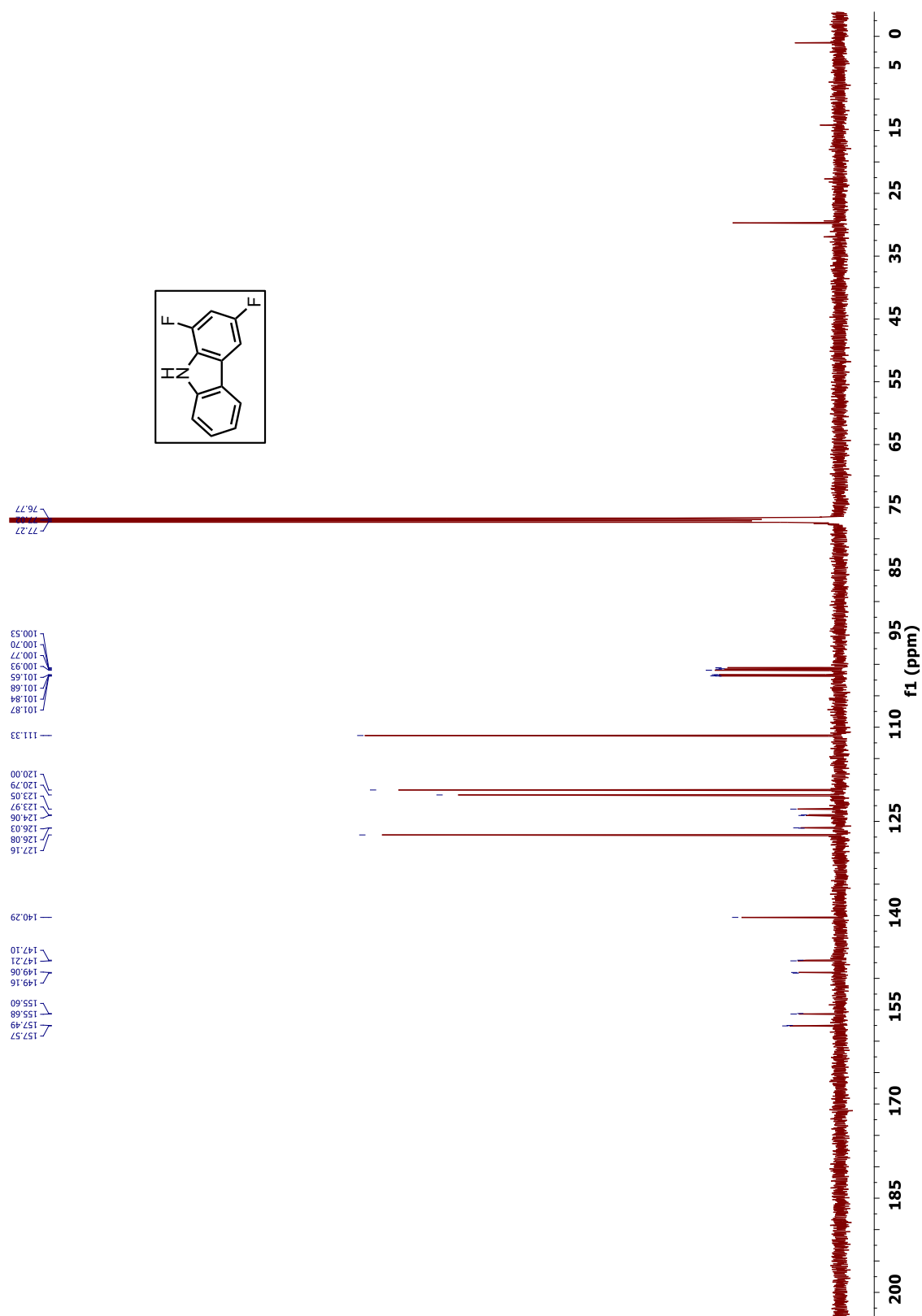
^{13}C NMR (CDCl_3 , 125 MHz) spectrum of compound 2D.



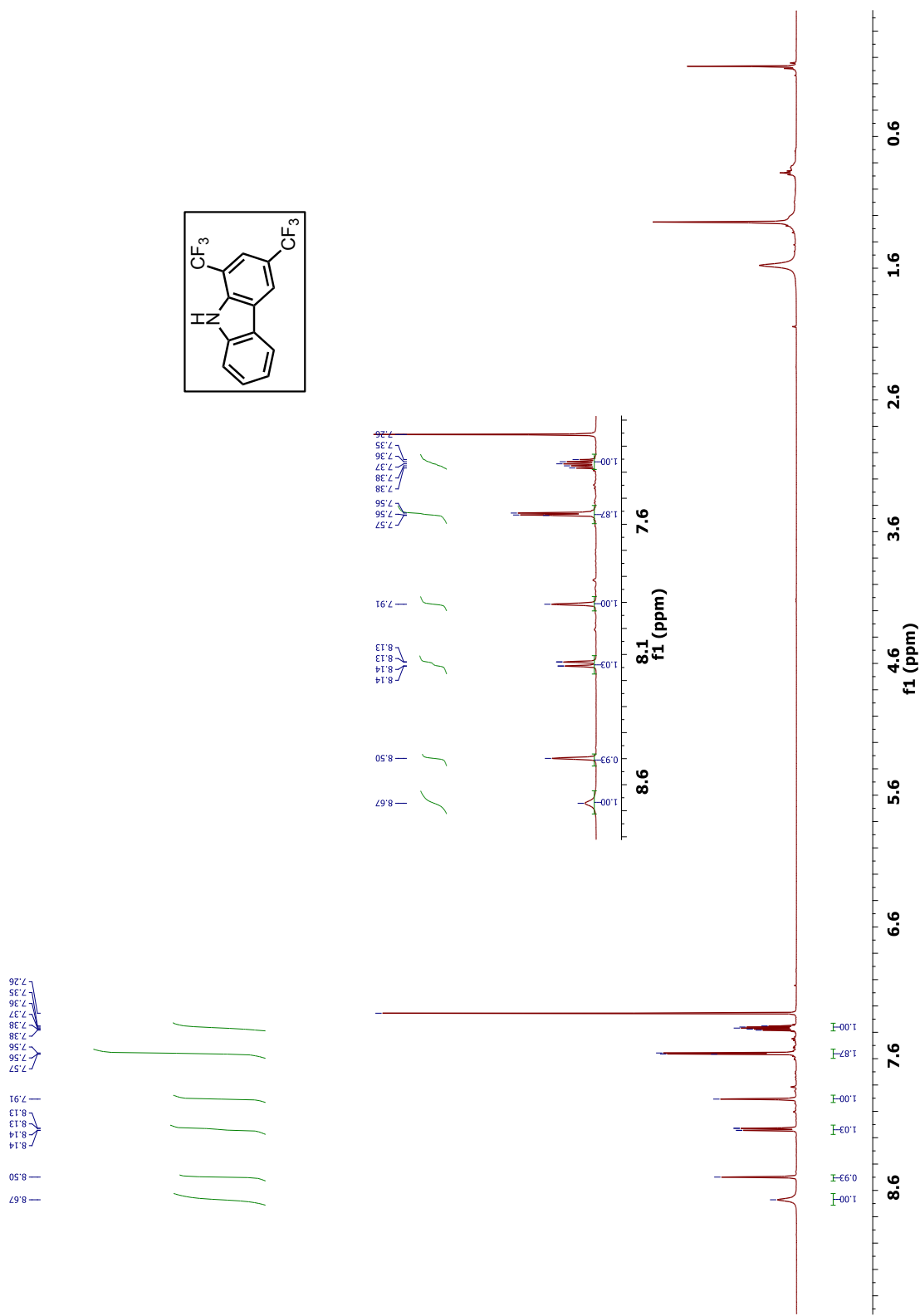
^1H NMR (CDCl_3 , 500 MHz) spectrum of compound 2E.



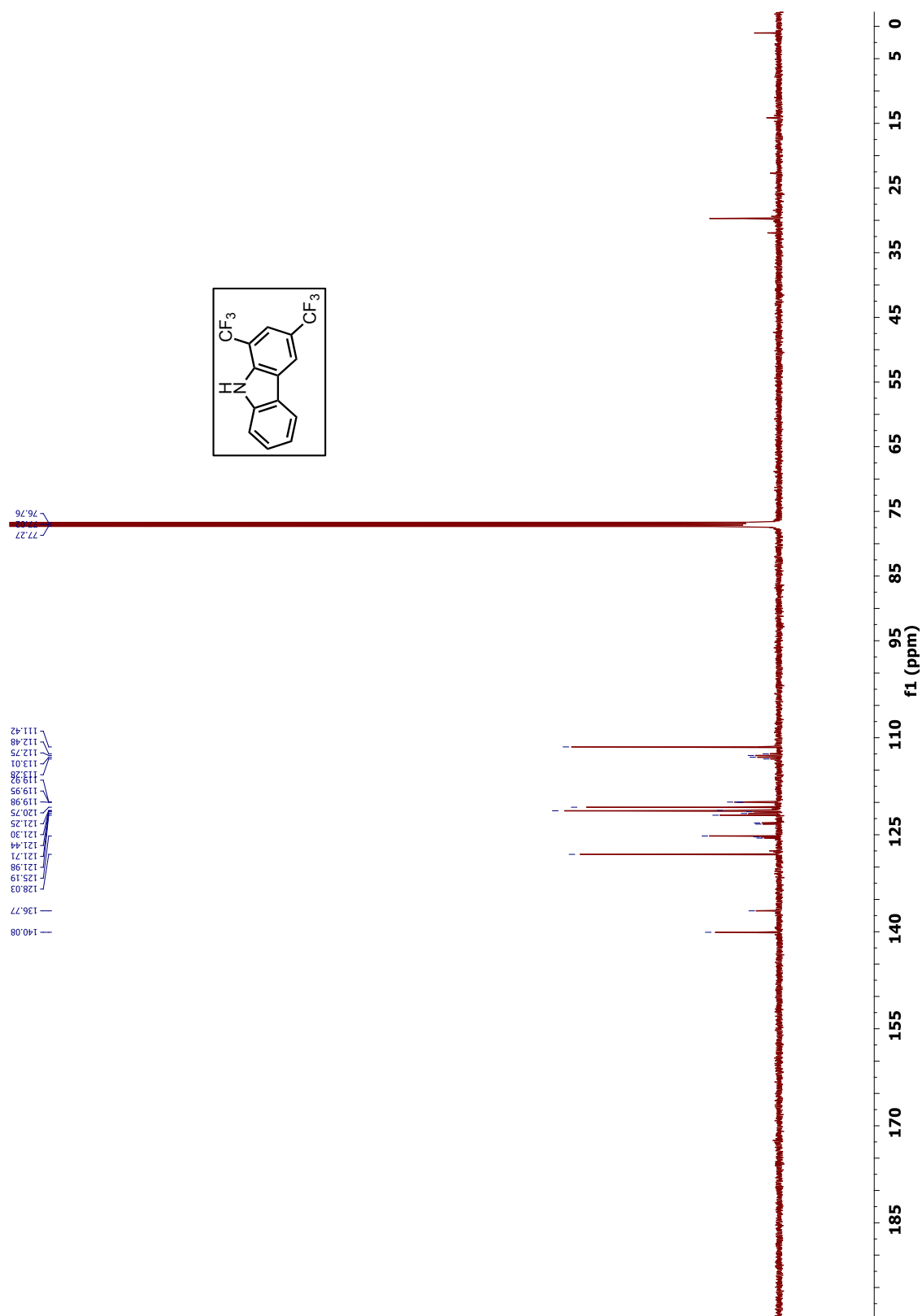
^{13}C NMR (CDCl_3 , 125 MHz) spectrum of compound 2E.



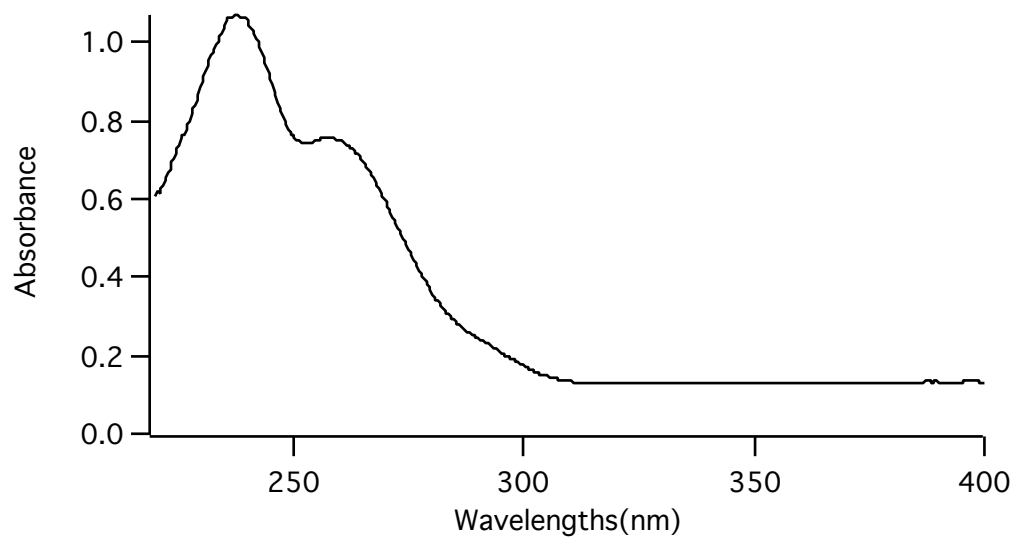
^1H NMR (CDCl_3 , 500 MHz) spectrum of compound 2F.



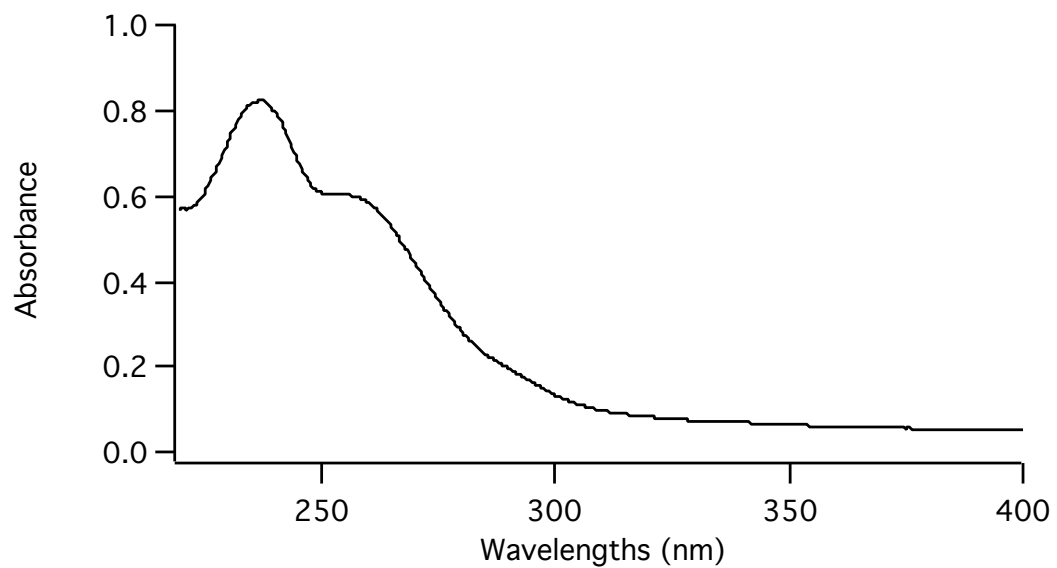
^{13}C NMR (CDCl_3 , 125 MHz) spectrum of compound 2F.



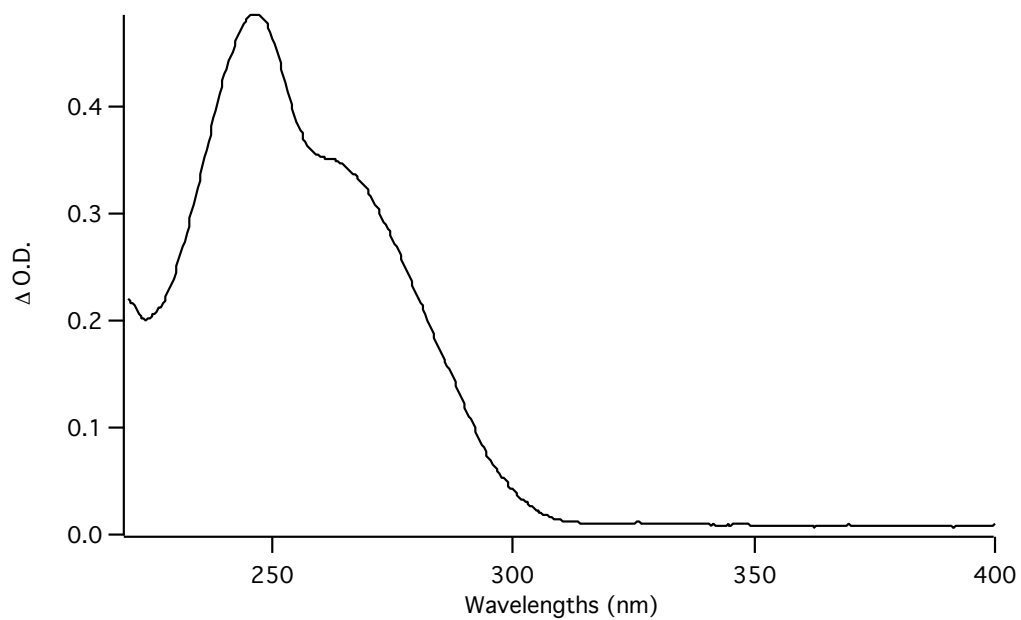
UV-Vis of compound 1A in pentane.



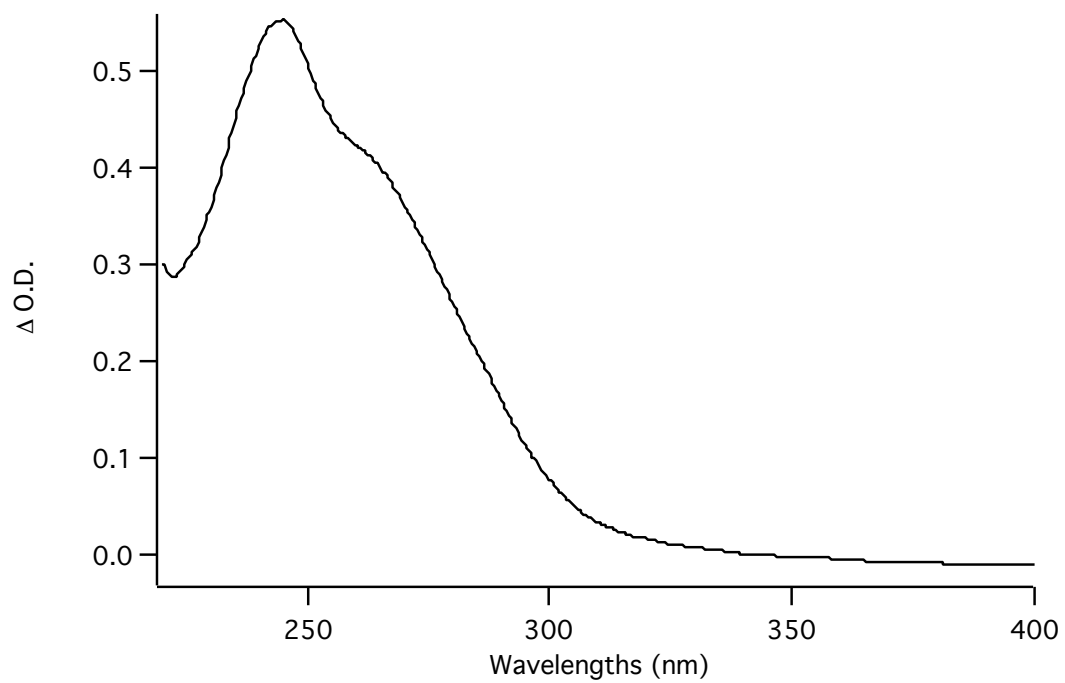
UV-Vis of compound 1A in aqueous nanocrystalline suspensions.



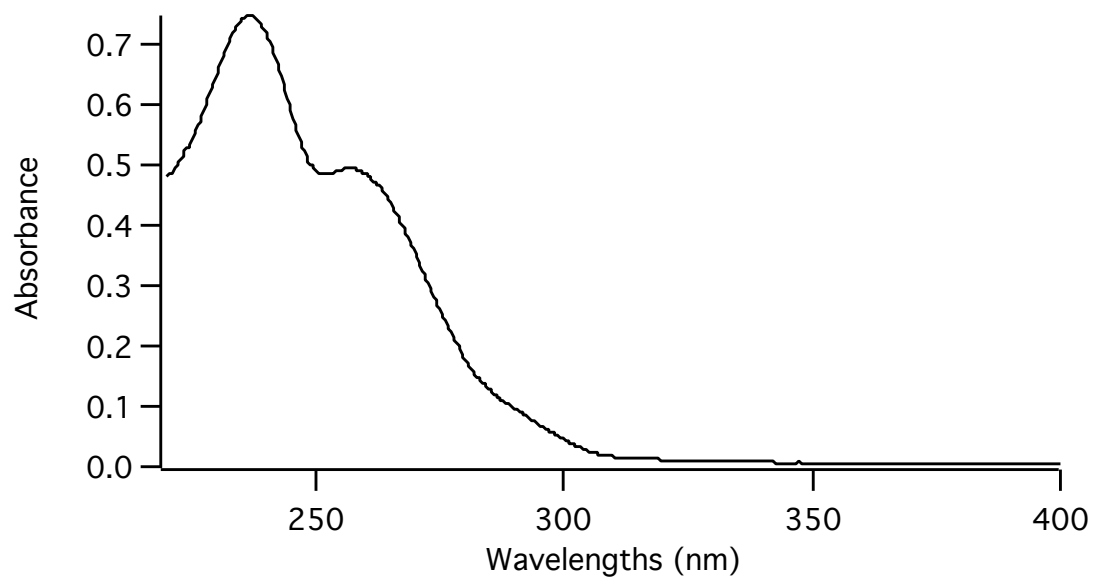
UV-Vis of compound 1B in pentane.



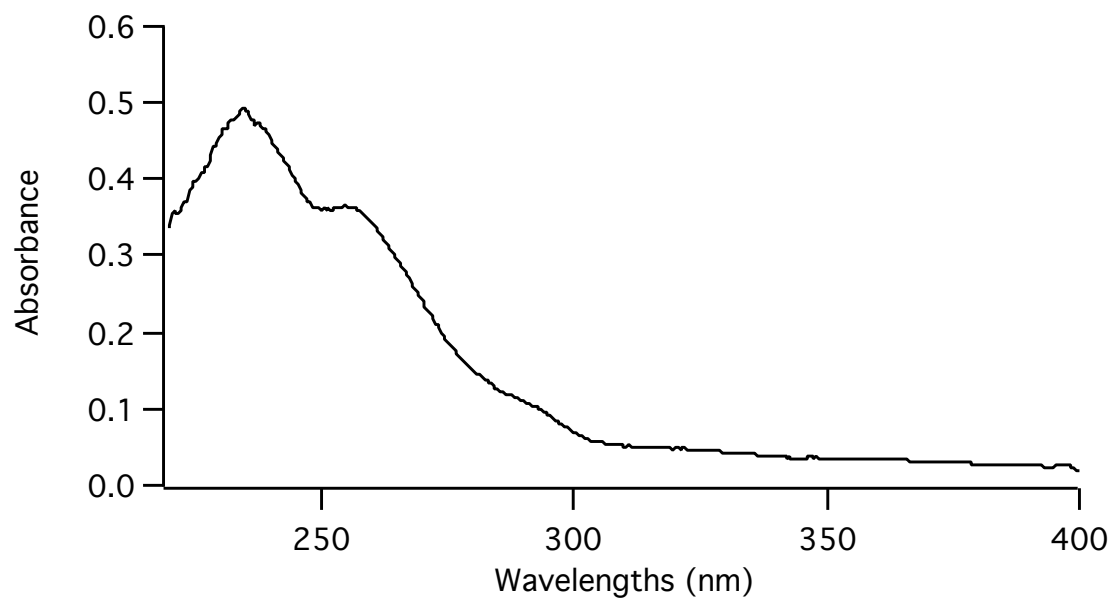
UV-Vis of compound 1B in aqueous nanocrystalline suspensions.



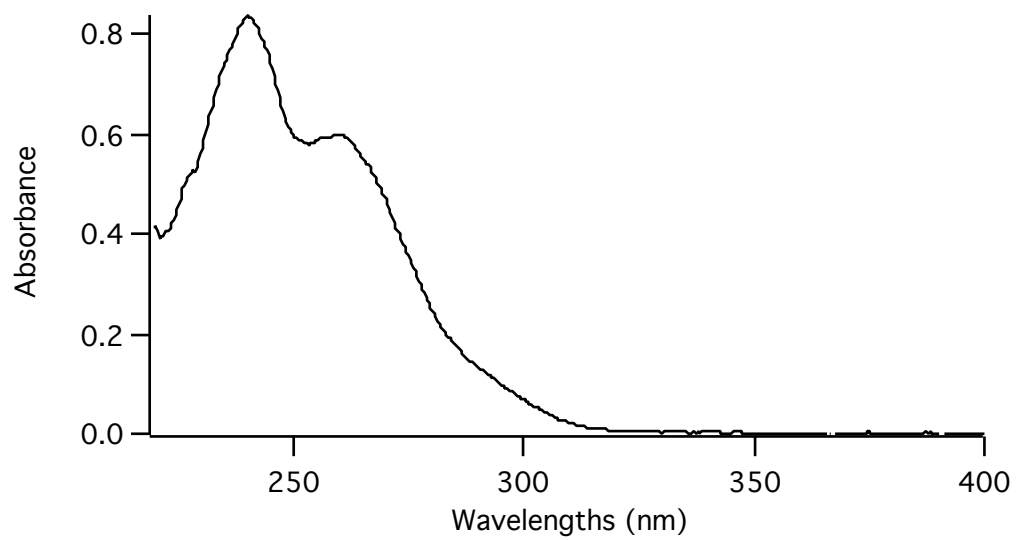
UV-Vis of compound 1C in pentane.



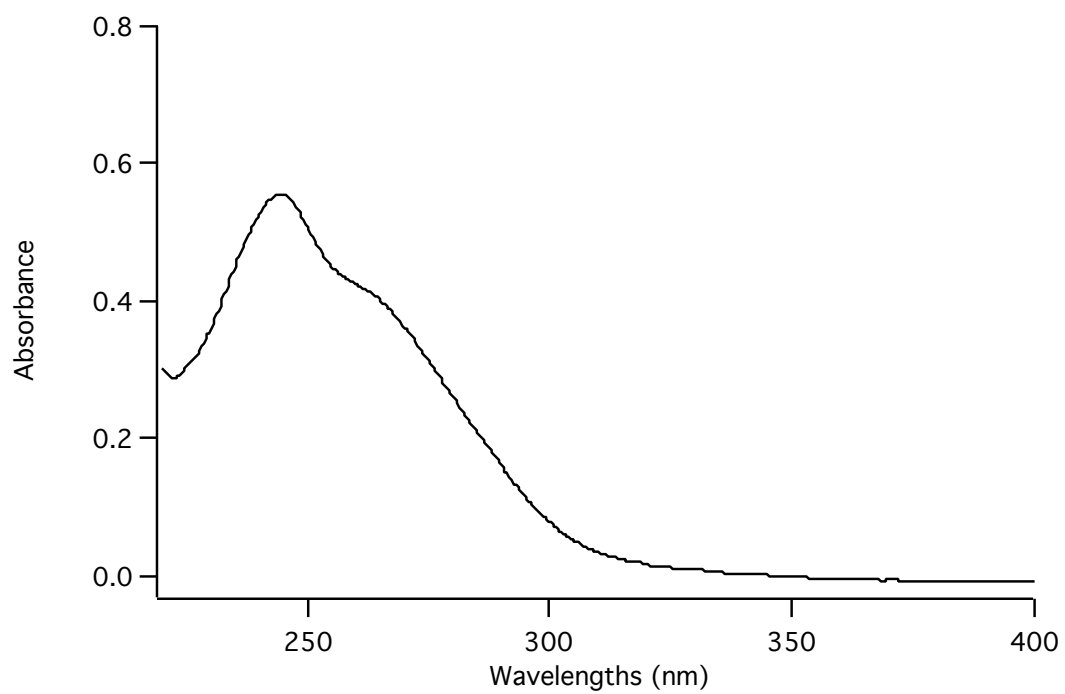
UV-Vis of compound 1C in aqueous nanocrystalline suspensions.



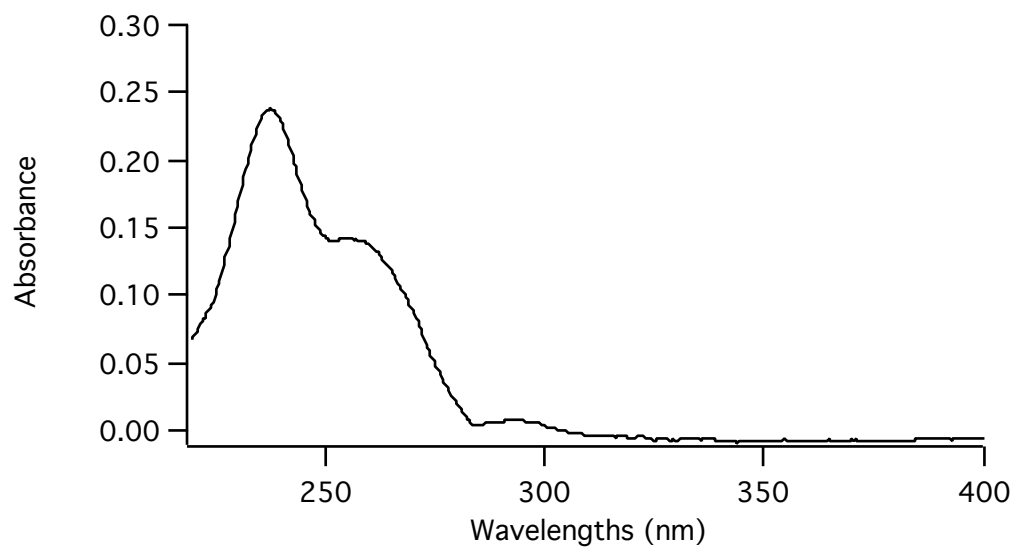
UV-Vis of compound 1D in pentane.



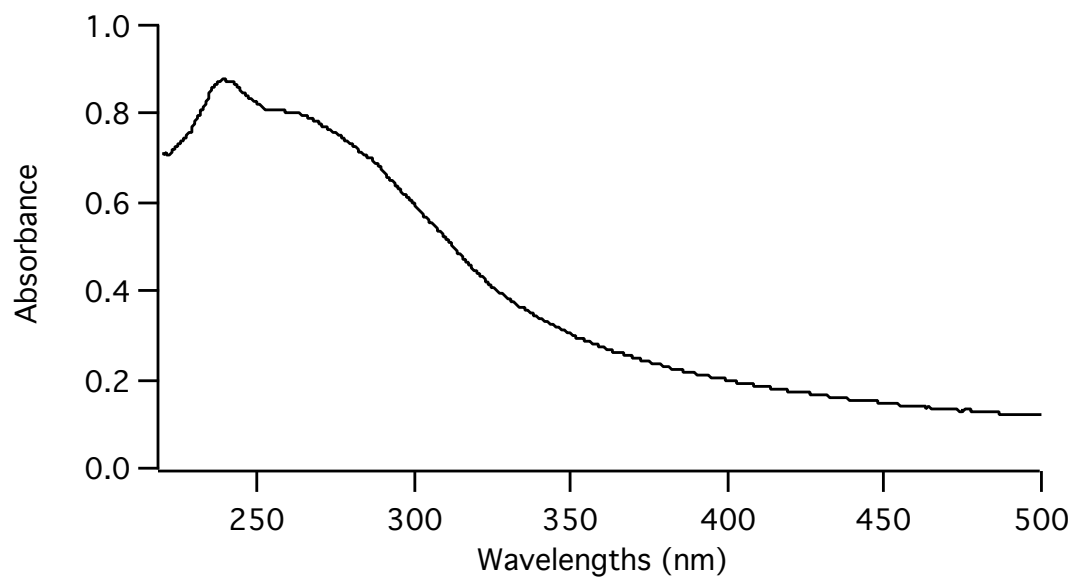
UV-Vis of compound 1D in aqueous nanocrystalline suspensions.



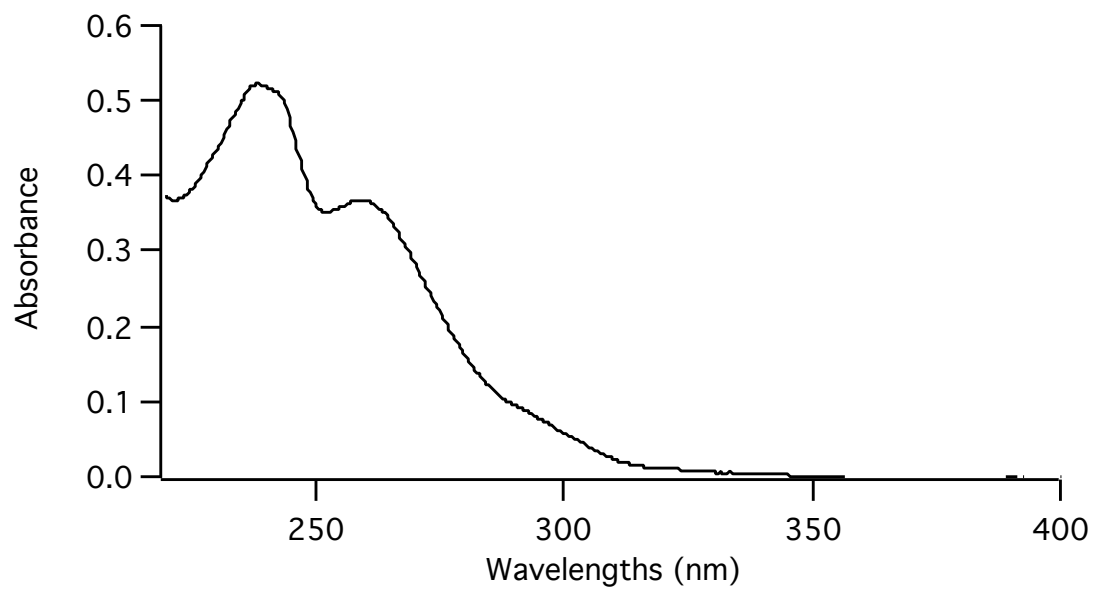
UV-Vis of compound 1E in pentane.



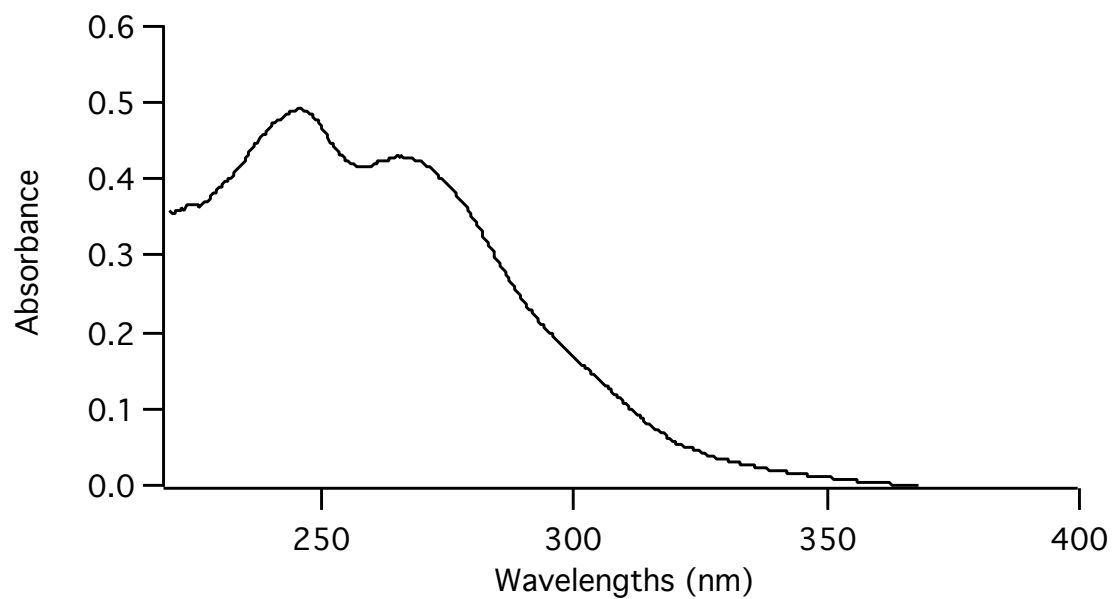
UV-Vis of compound 1E in aqueous nanocrystalline suspensions.



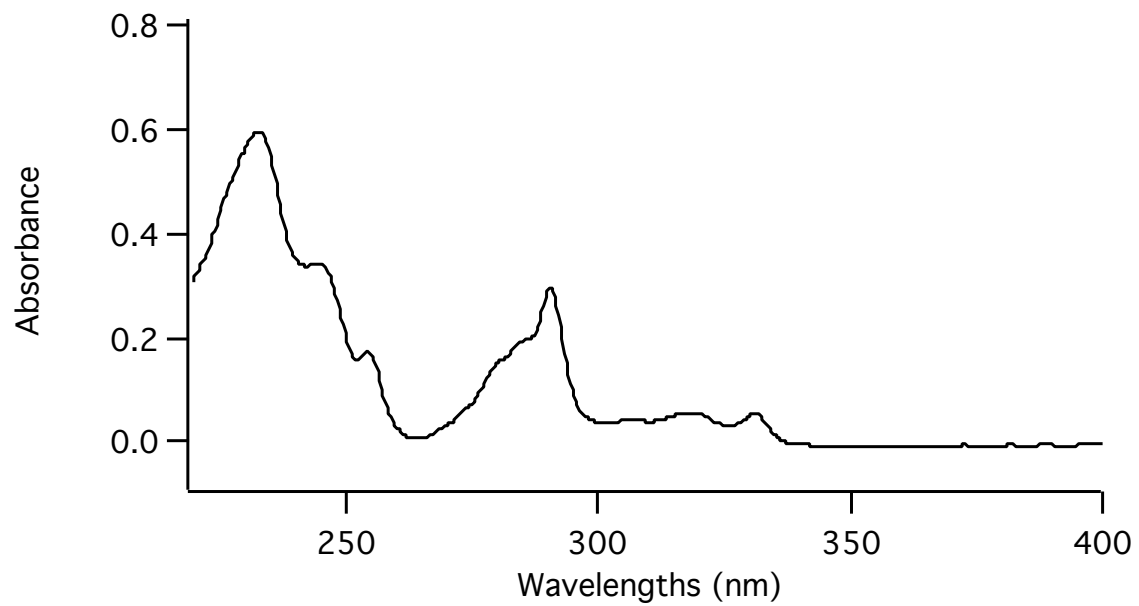
UV-Vis of compound 1F in pentane.



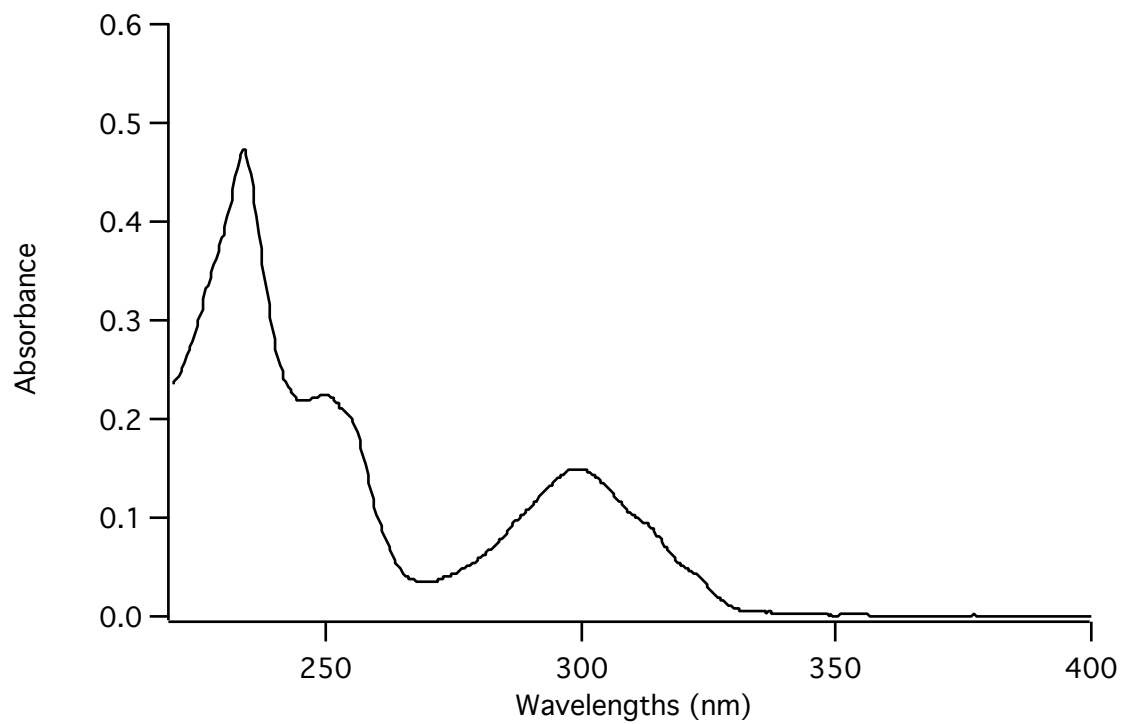
UV-Vis of compound 1F in aqueous nanocrystalline suspensions.



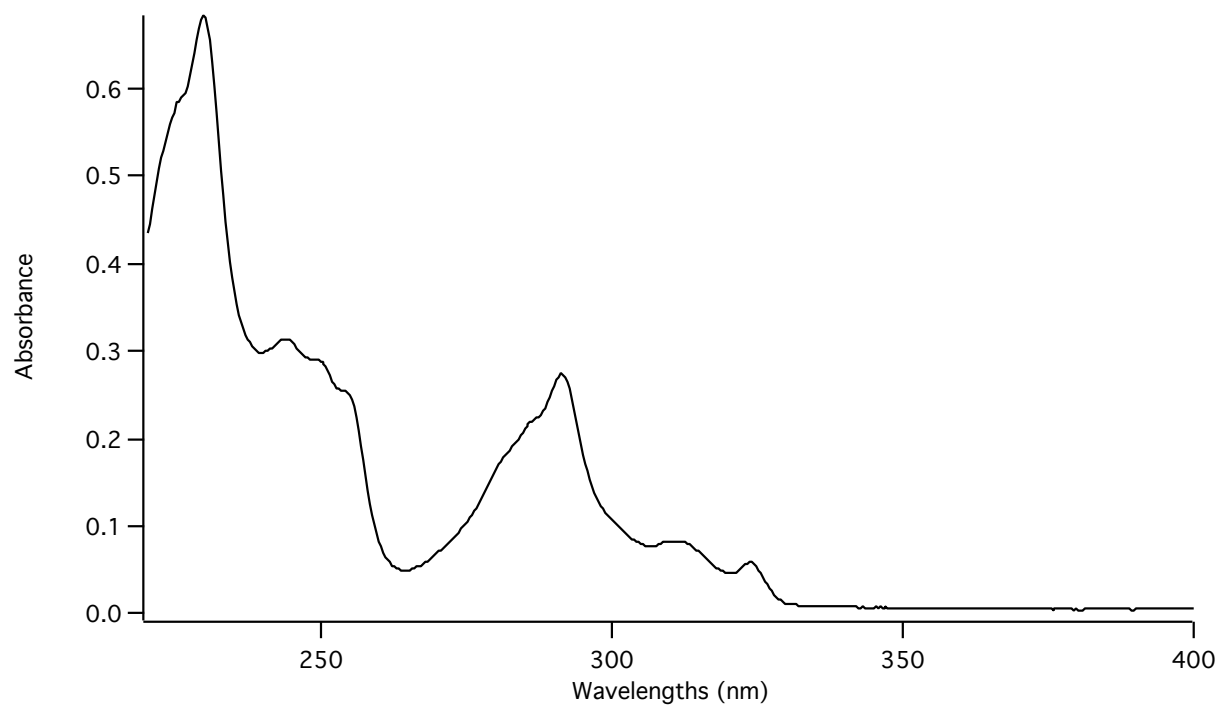
UV-Vis of compound 2A in pentane.



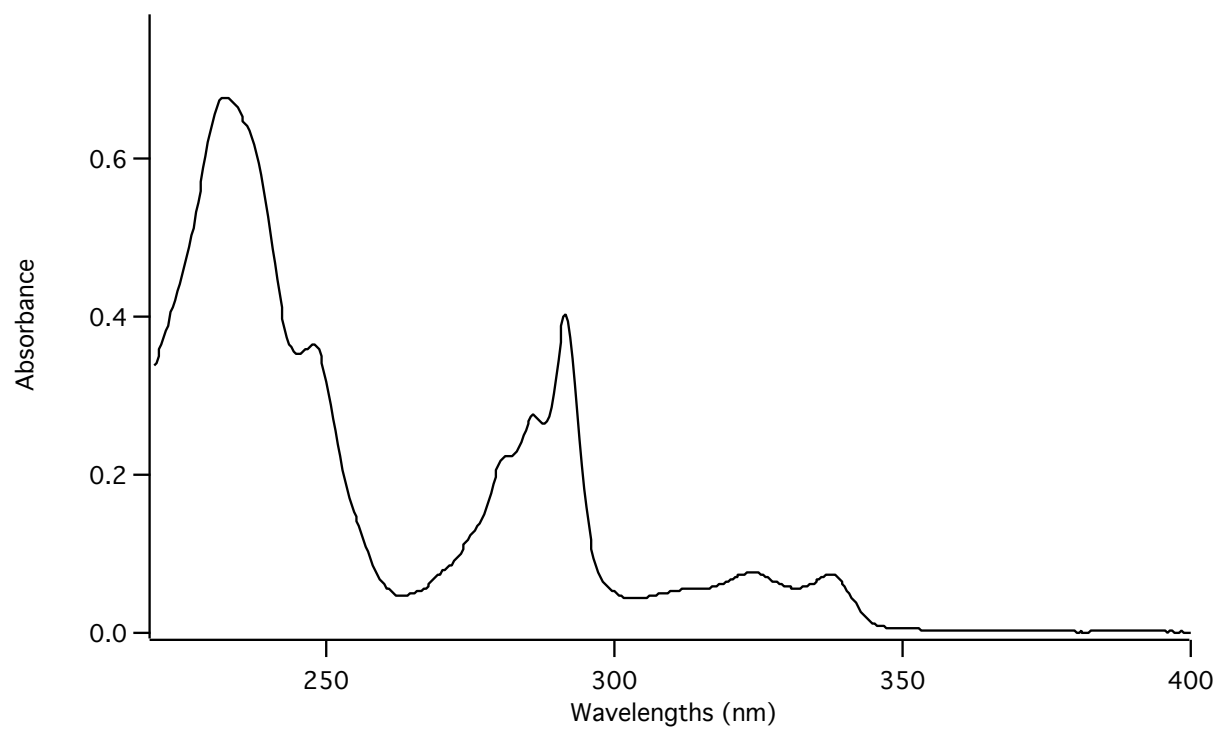
UV-Vis of compound 2B in pentane.



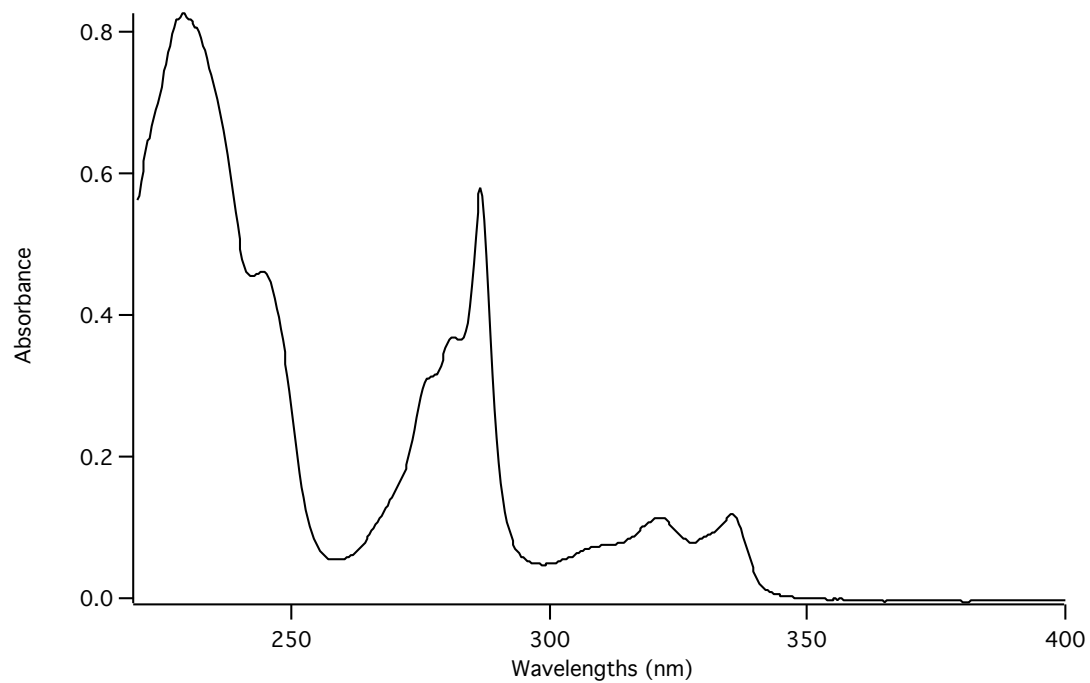
UV-Vis of compound 2C in pentane.



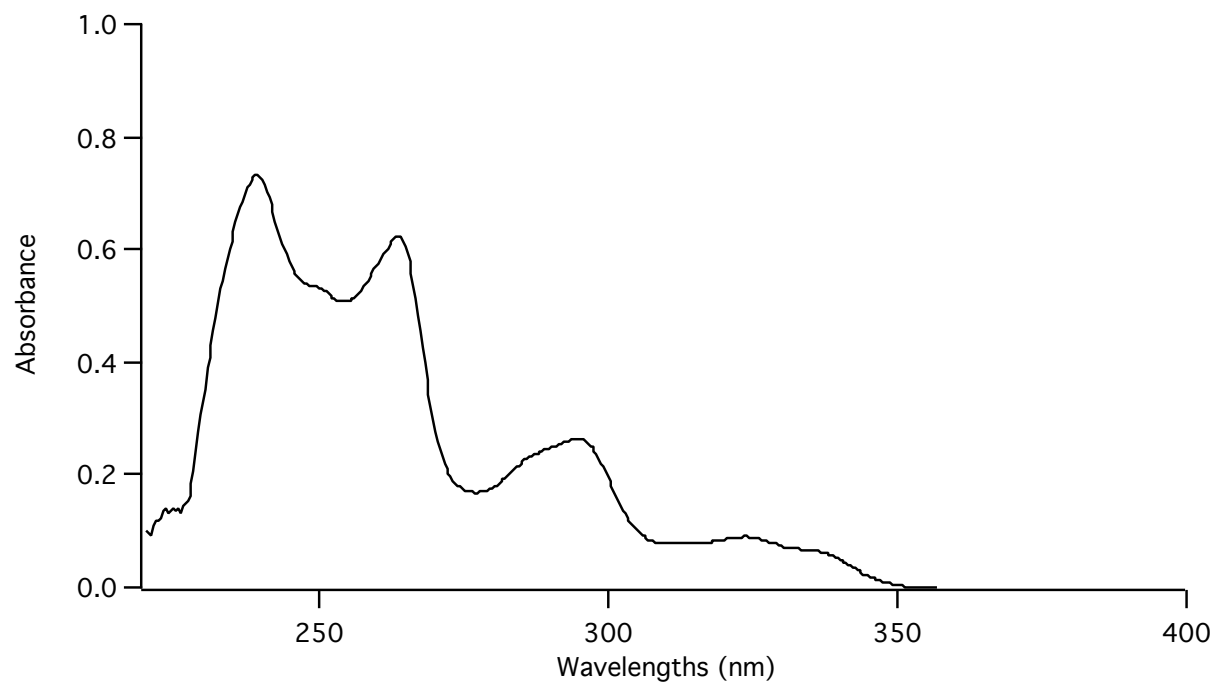
UV-Vis of compound 2D in pentane.



UV-Vis of compound 2E in pentane.

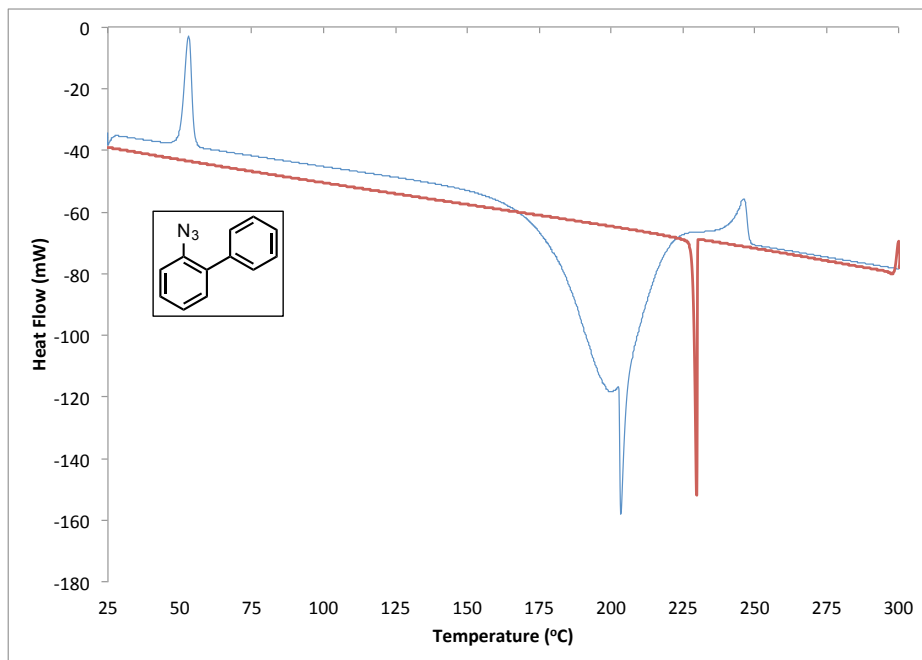


UV-Vis of compound 2F in pentane.

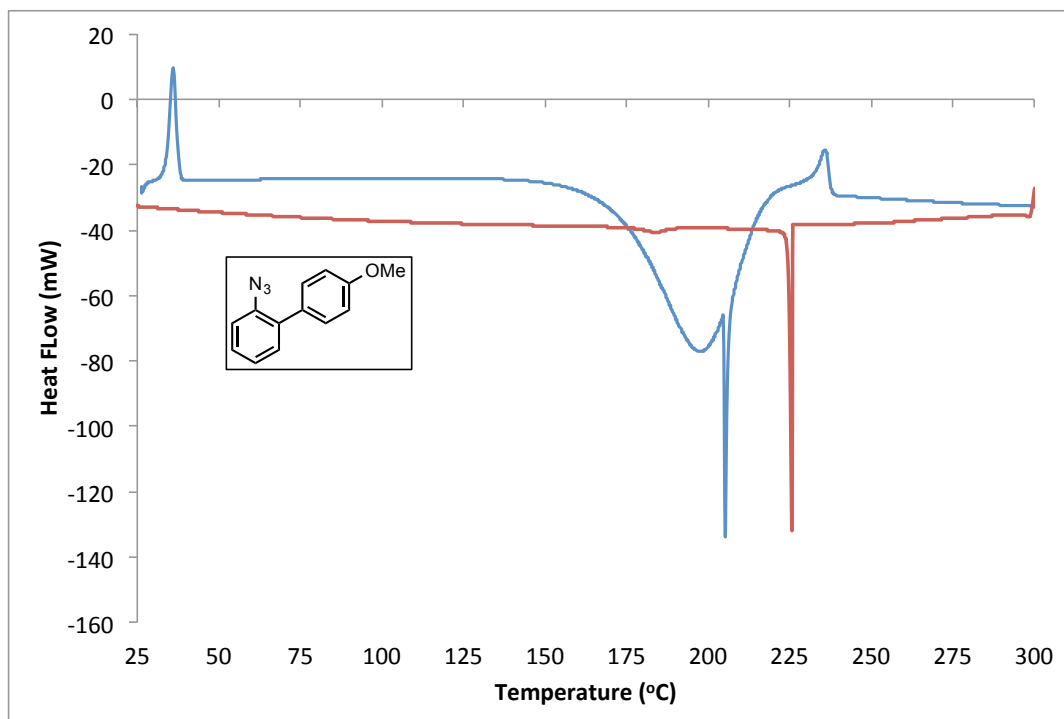


5.5.3 Thermal Analysis

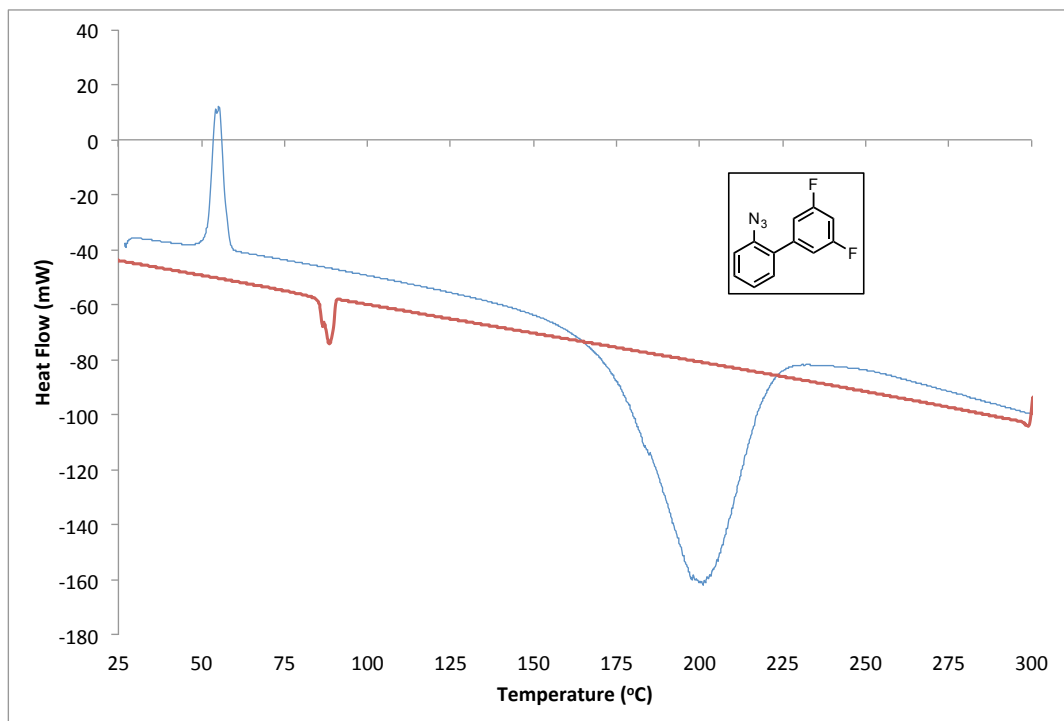
Differential Scanning Calorimetry of compound 1A.



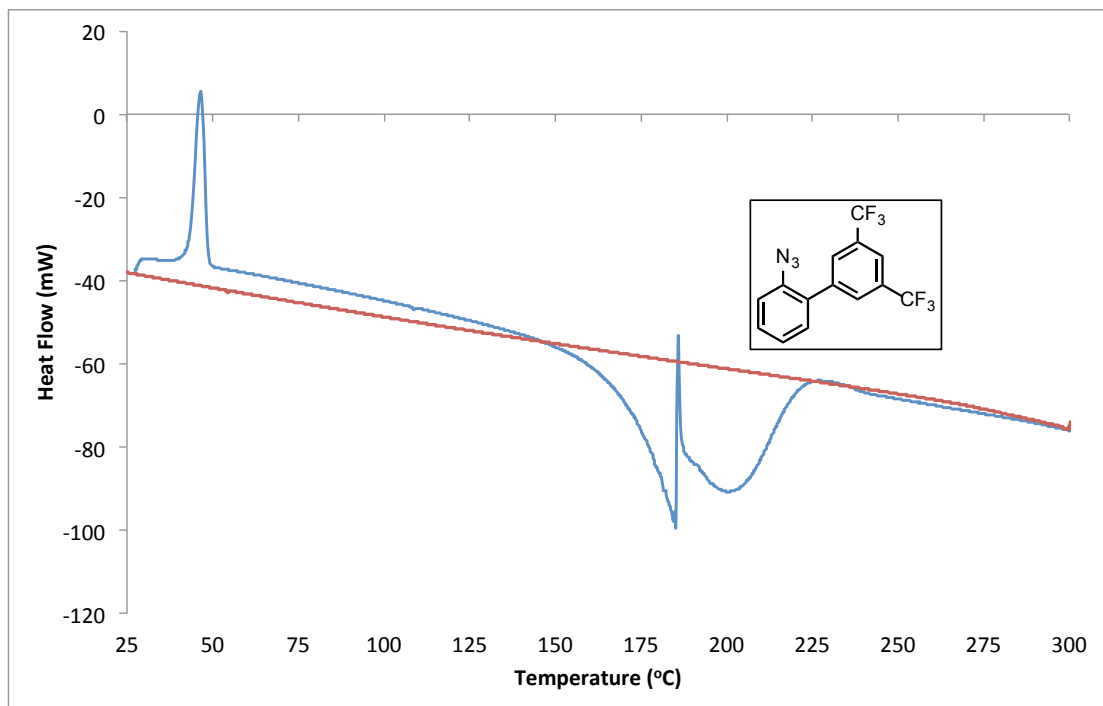
Differential Scanning Calorimetry of compound 1B.



Differential Scanning Calorimetry of compound 1E.



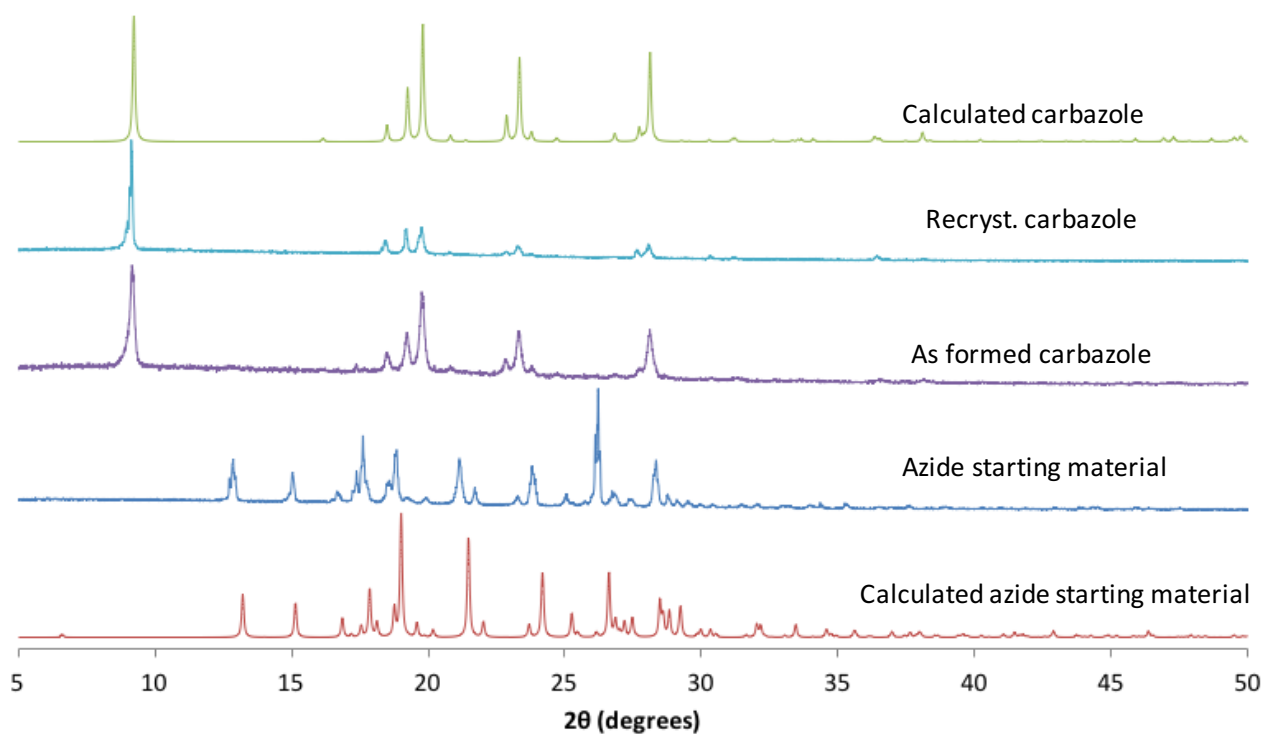
Differential Scanning Calorimetry of compound 1F



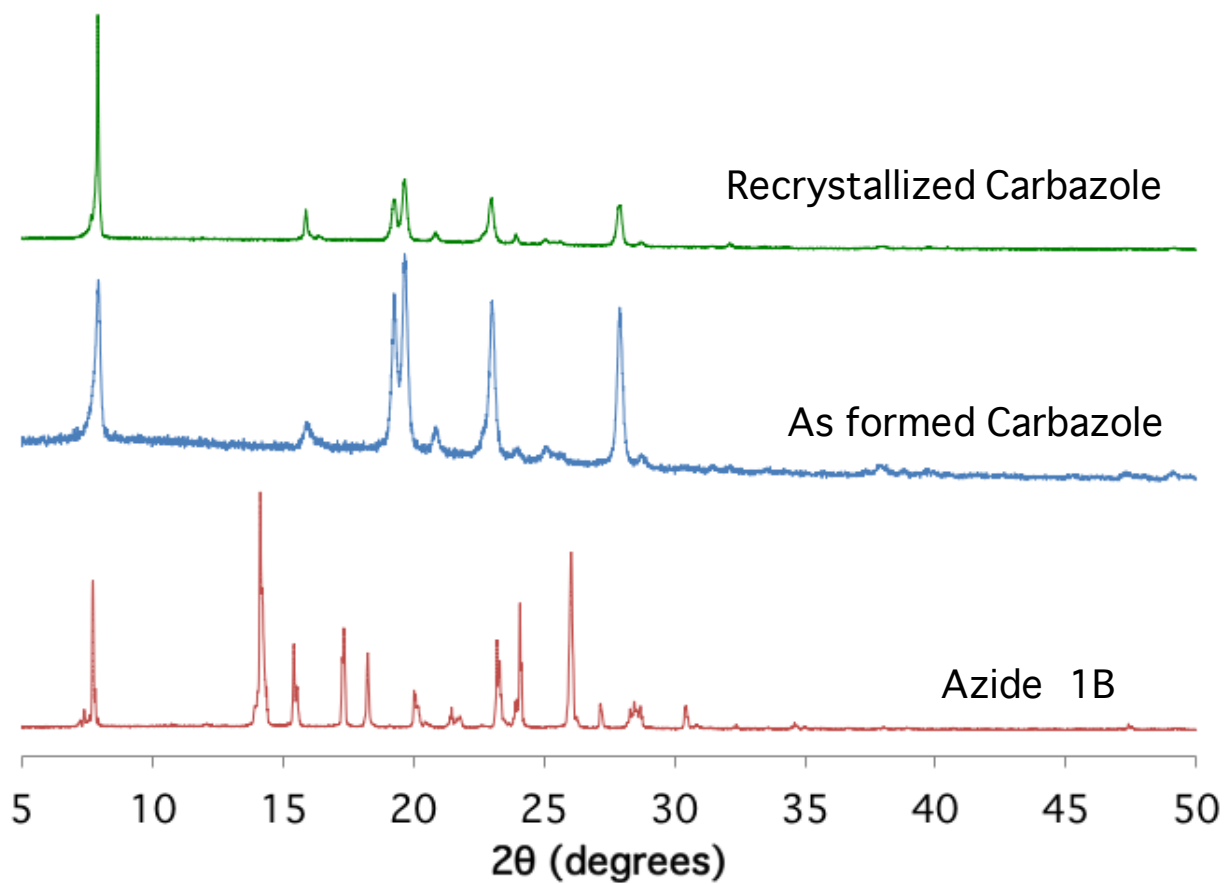
5.5.4 PXRD Analysis

Azide 1C had a melting point which was too close to room temperature and the solid melted onto zero diffraction plate during sample preparation. Thus Azide 1C by PXRD analysis is not reported. Azide 1D was a liquid at room temperature and PXRD was not recorded. All other azide samples are reported here.

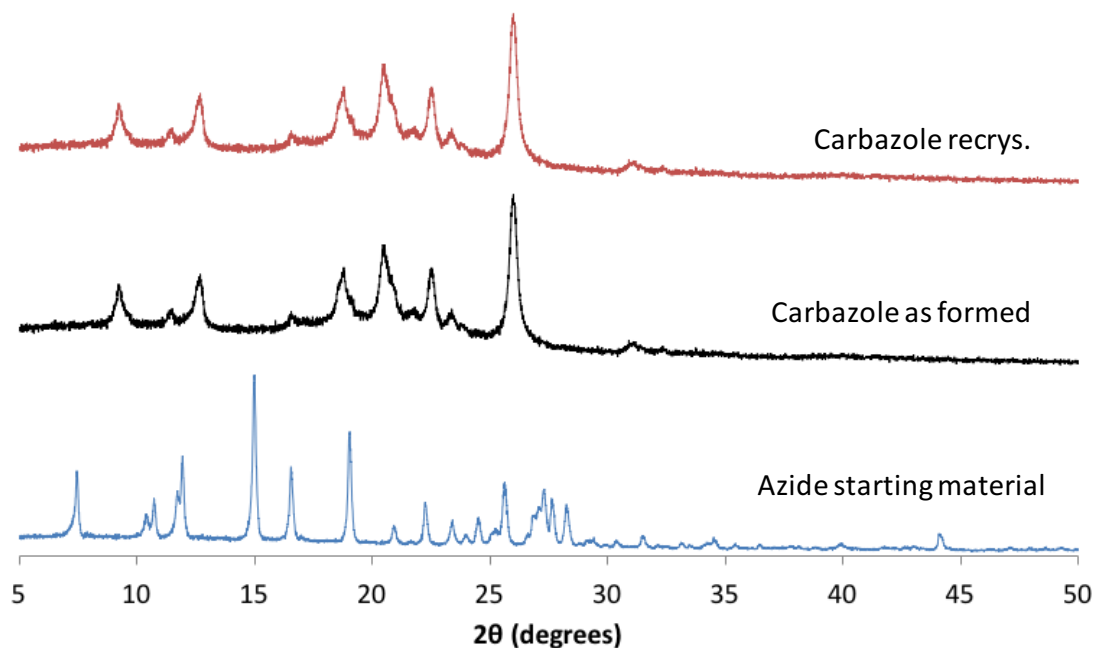
Powder X-Ray Diffraction analysis of azide 1A, product 2A as formed, and recrystallized product 2A in acetonitrile.



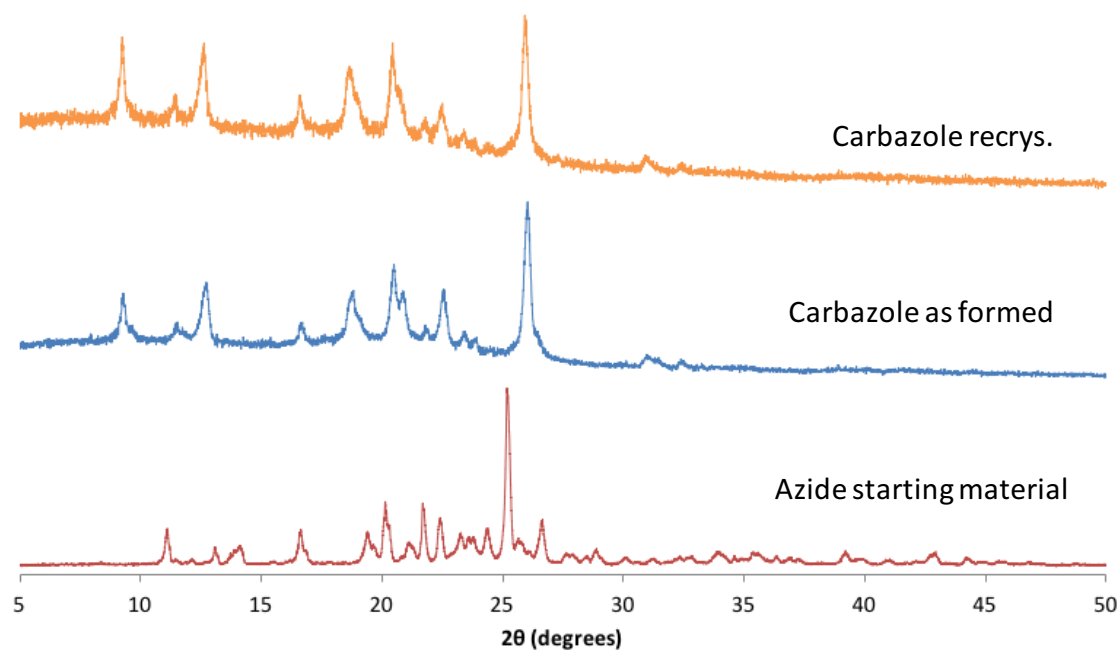
Powder X-Ray Diffraction analysis of azide 1B, product 2B as formed, and recrystallized product 2B in acetonitrile.



Powder X-Ray Diffraction analysis of azide 1E, product 2E as formed, and recrystallized product 2E in acetonitrile.



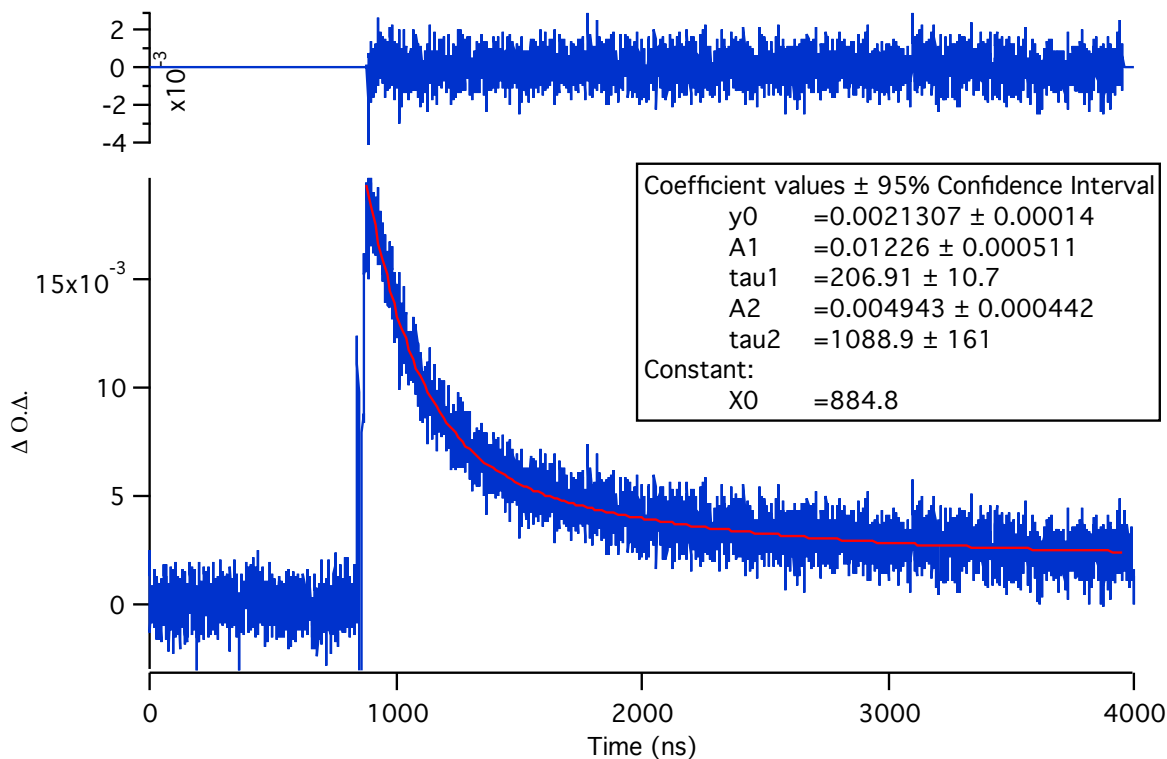
Powder X-Ray Diffraction analysis of azide 1F, product 2F as formed, and recrystallized product 2F in acetonitrile.



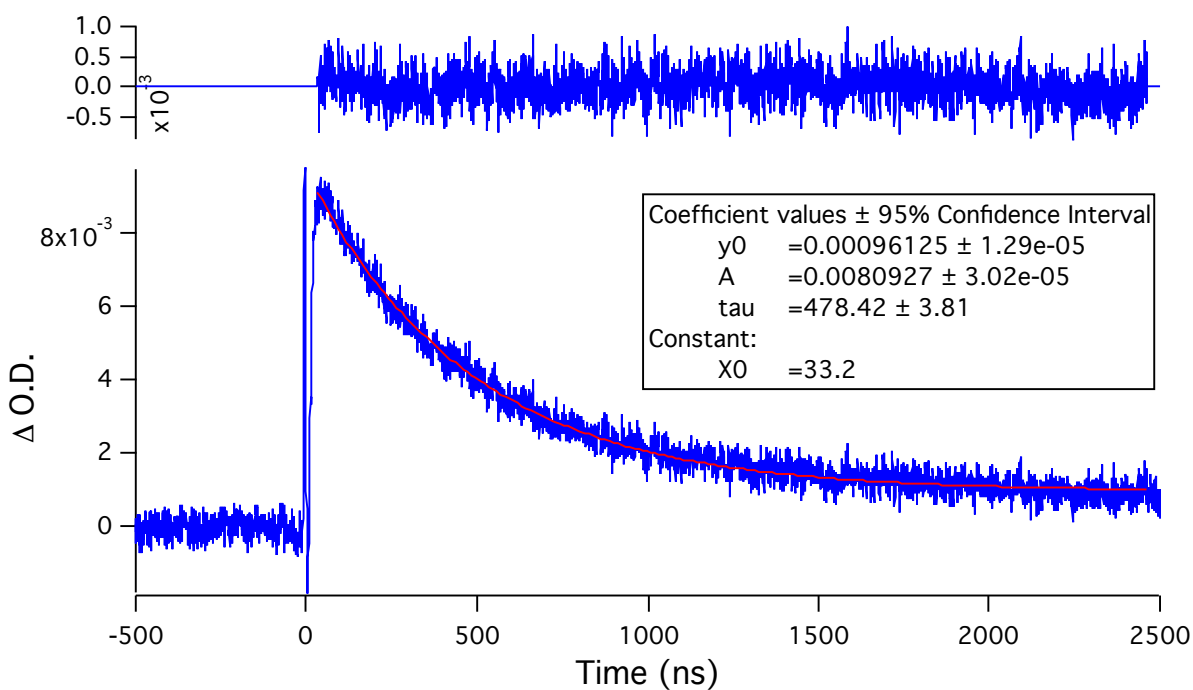
5.5.5 Laser Flash Photolysis

The laser flash photolysis experiments were performed with 1 cm quartz flow cell mounted on a home-built sample holder that is placed at the cross-section of the laser incident beam and the probe light. Continuously Argon gas purged acetonitrile solutions or crystalline suspensions of azides were flown through the quartz cell using a peristaltic pump (Masterflex L/S) at a rate of 2.5–4 mL/min. Lifetimes at λ_{\max} for end-of-pulse spectra were reproducible and doubly verified/processed with Edinburgh Instruments L900 and lifetimes were plotted on Igor Pro (version 6.34A, Wavemetrics) software. All measurements were performed on sample concentrations of azides having an O.D. of ca. 0.3 at 266nm.

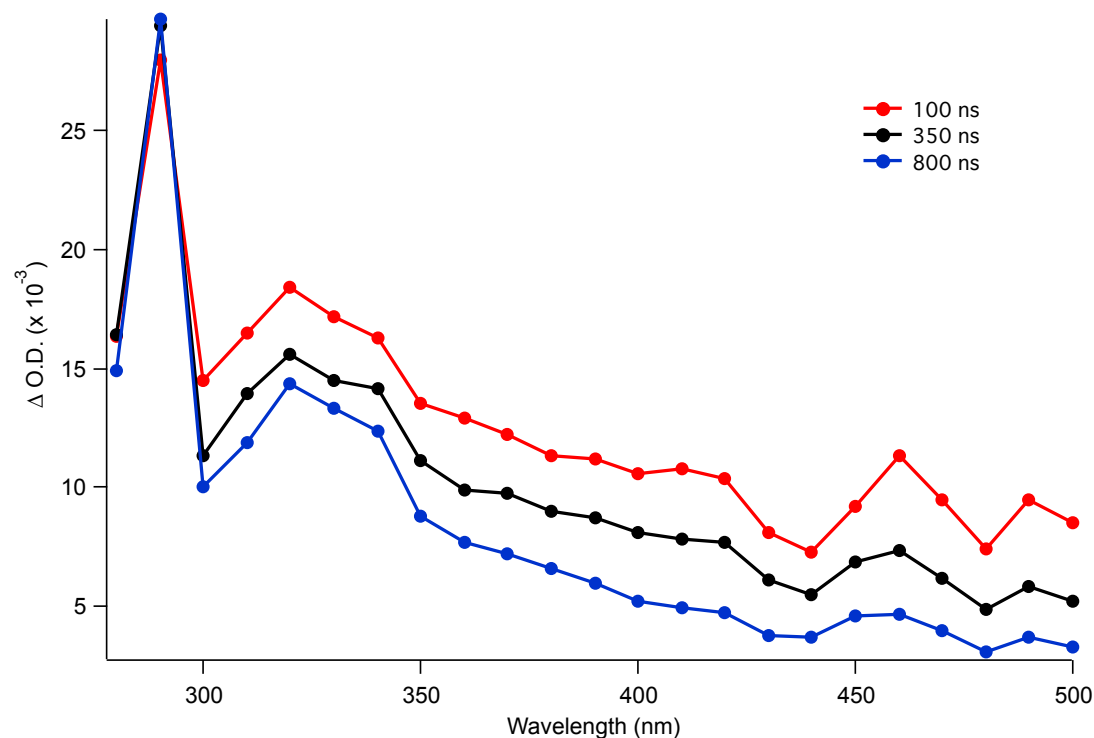
Azide 1A in pentane probed at 430 nm.



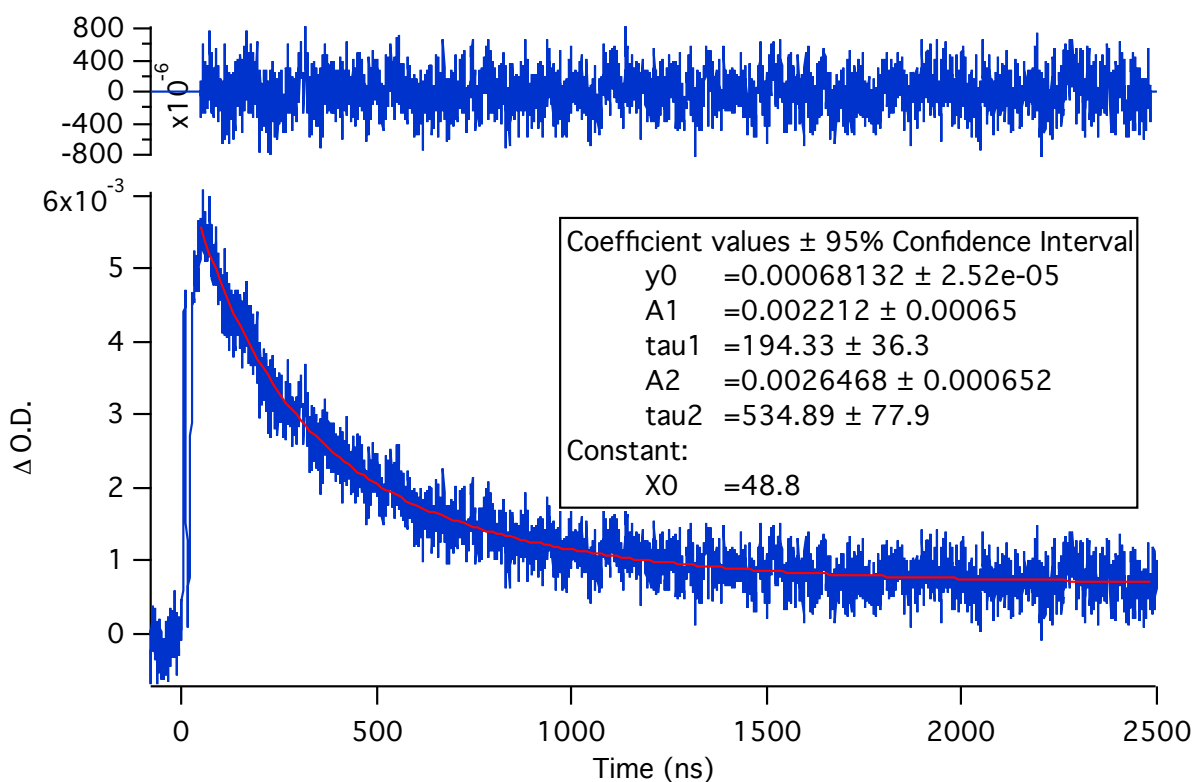
Azide 1A in nanocrystalline suspensions probed at 460 nm.



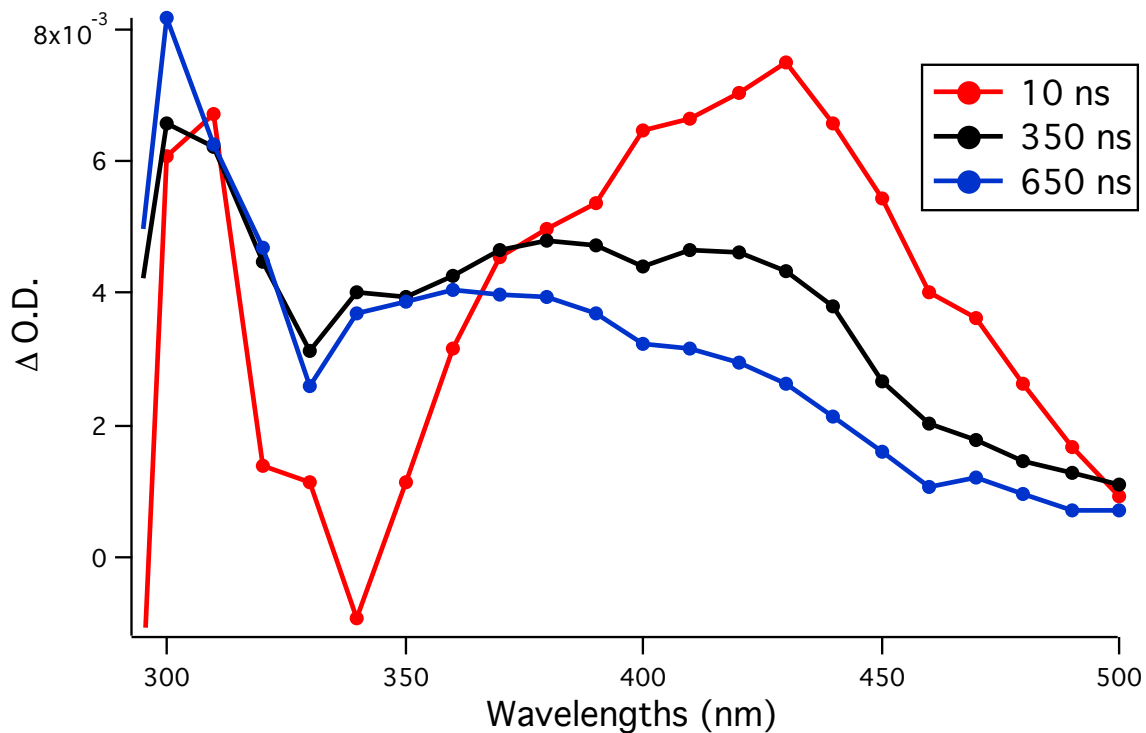
Sliced transient absorption spectra at different time points shown below of Azide 1A in nanocrystalline suspensions.



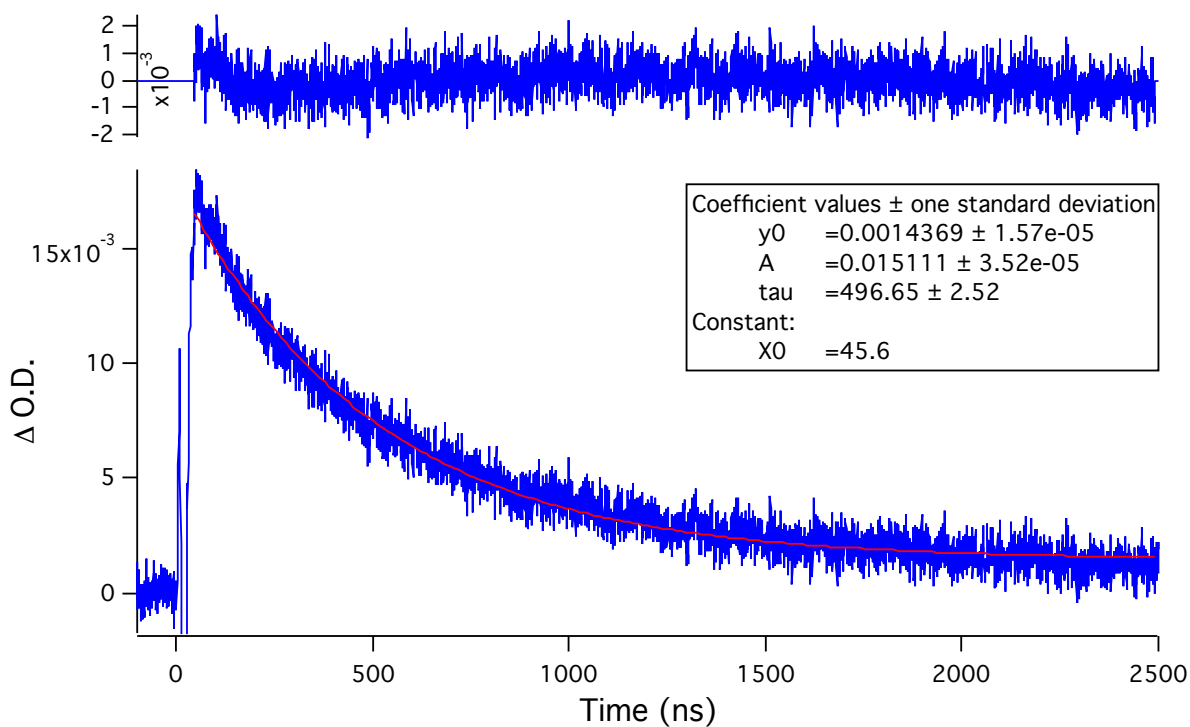
Azide 1B in pentane probed at 430 nm.



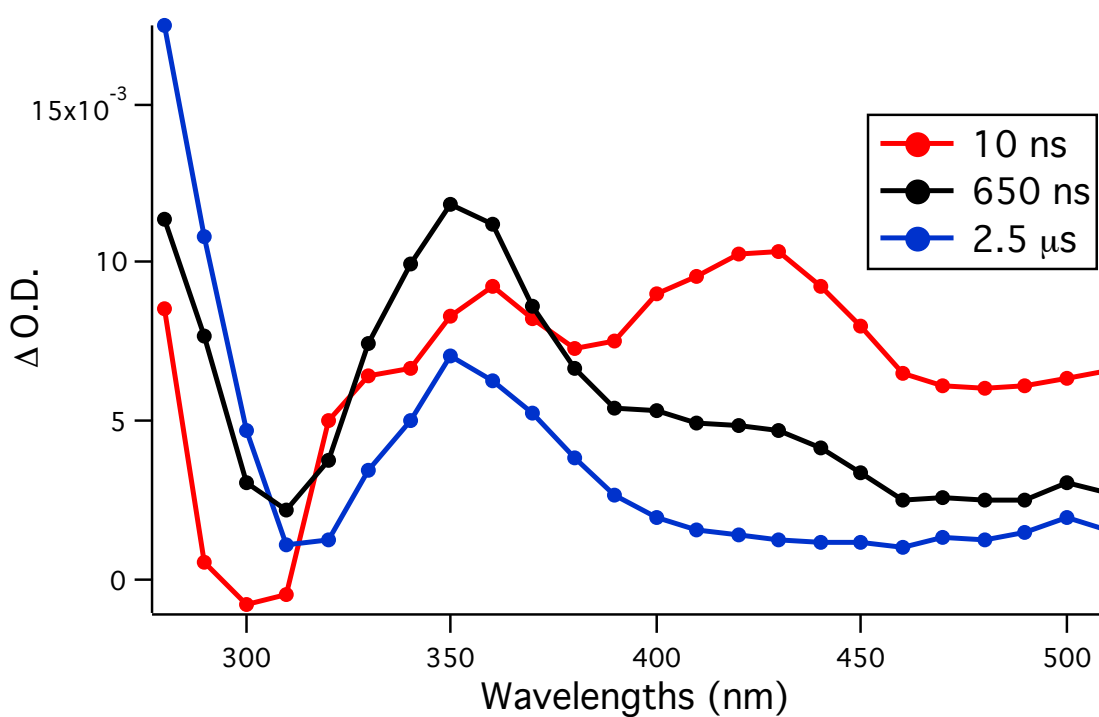
Sliced transient absorption spectra at different time points shown below of Azide 1B in pentane.



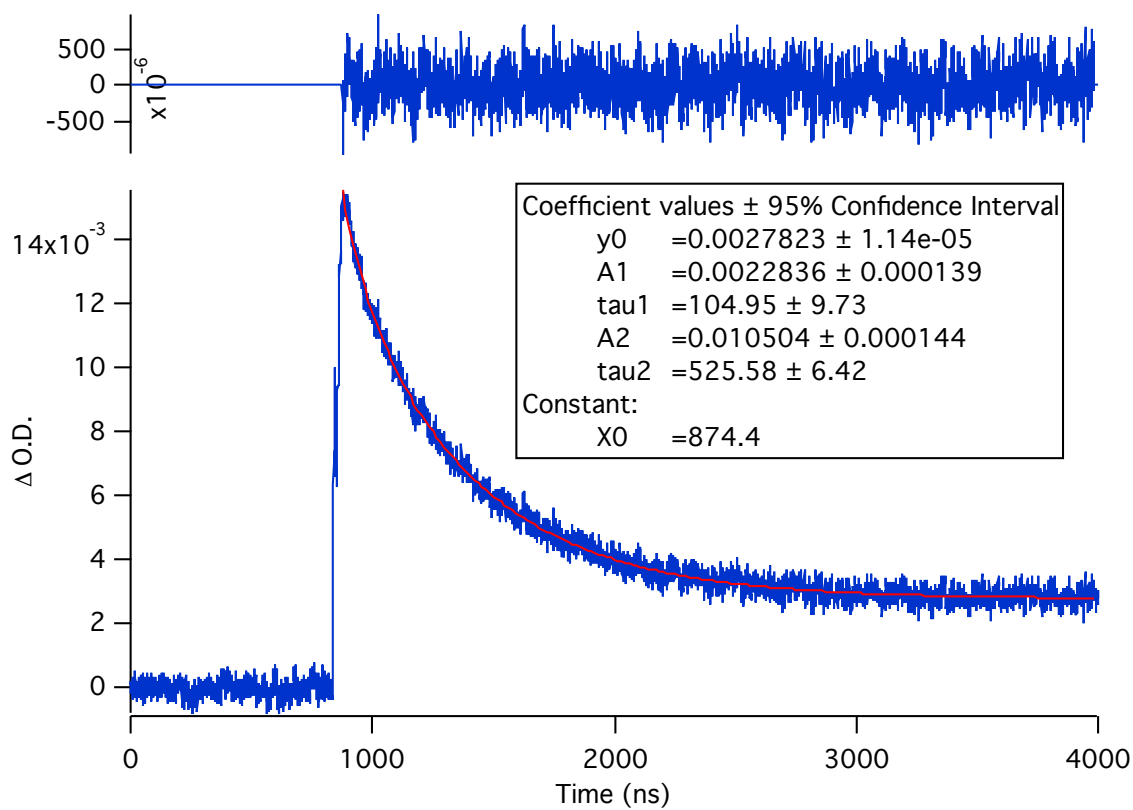
Azide 1B in nanocrystalline suspensions probed at 430 nm.



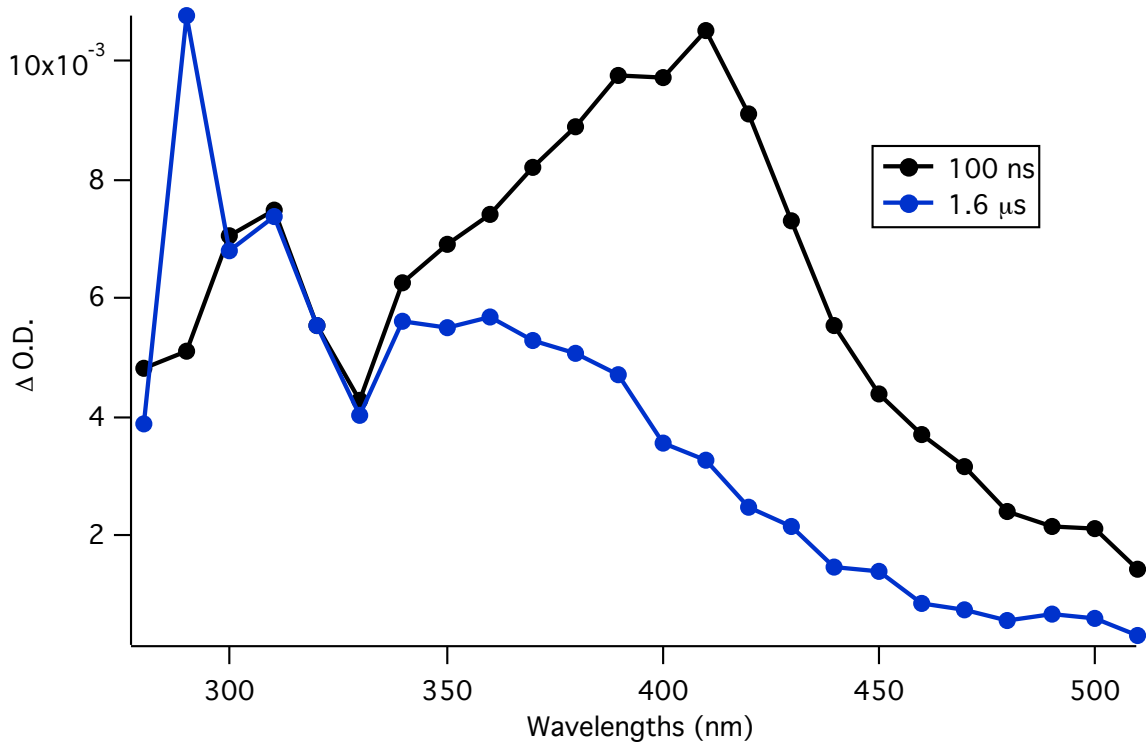
Sliced transient absorption spectra at different time points shown below of Azide 1B in nanocrystalline suspensions.



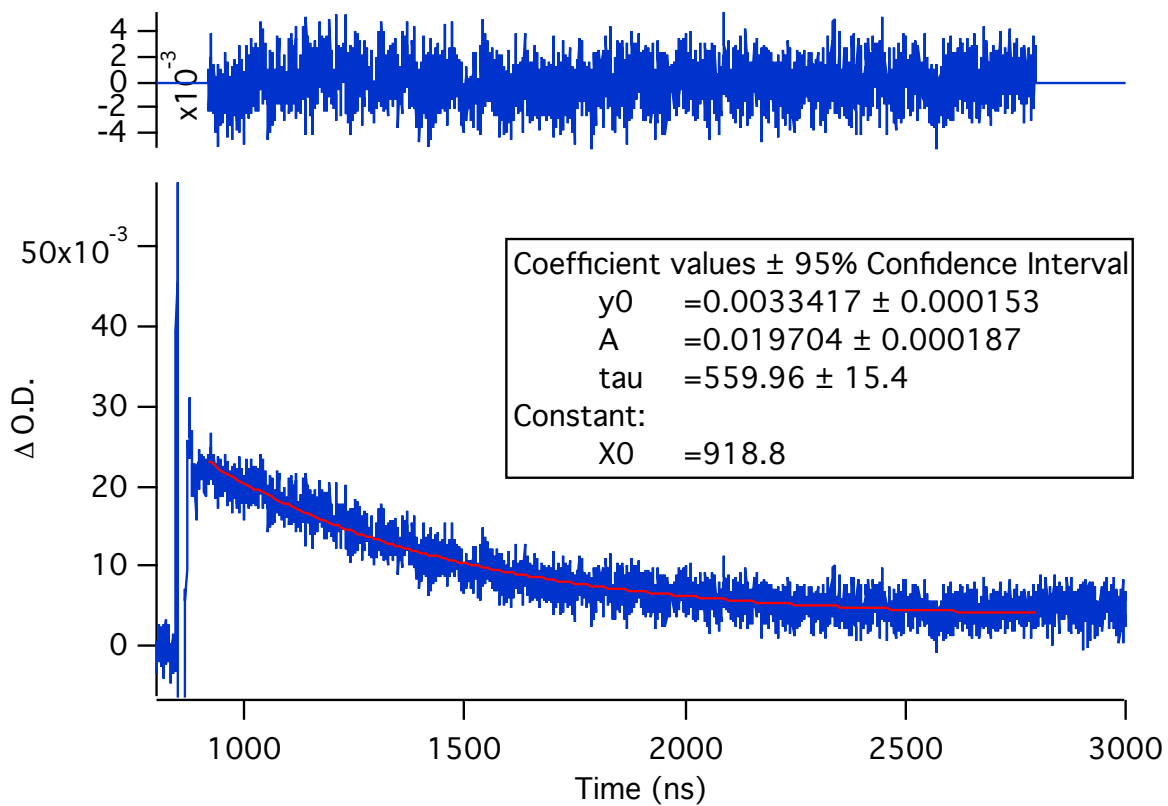
Azide 1C in pentane probed at 410 nm.



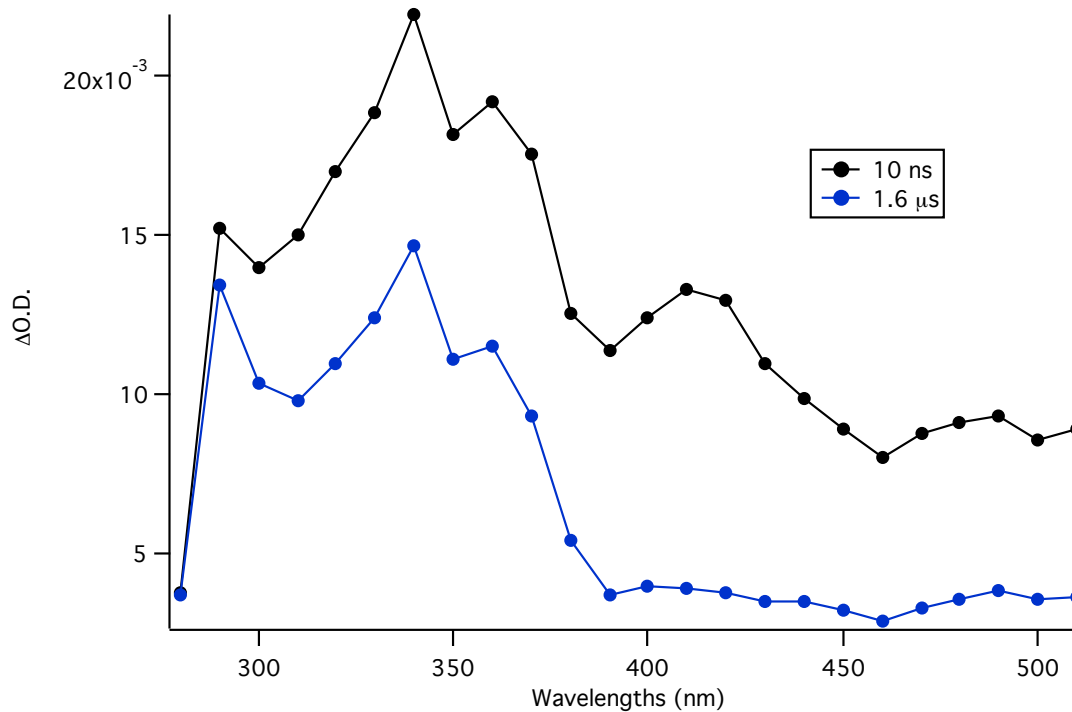
Sliced transient absorption spectra at different time points shown below of Azide 1C in pentane.



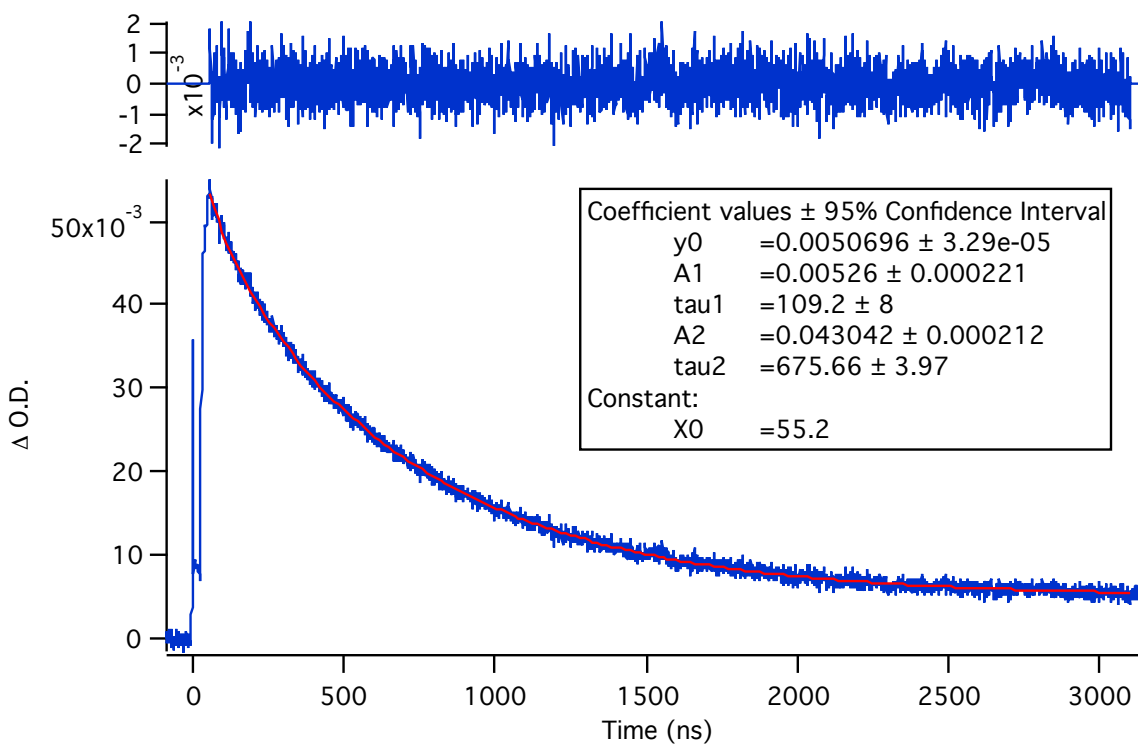
Azide 1C in nanocrystalline suspensions probed at 420 nm.



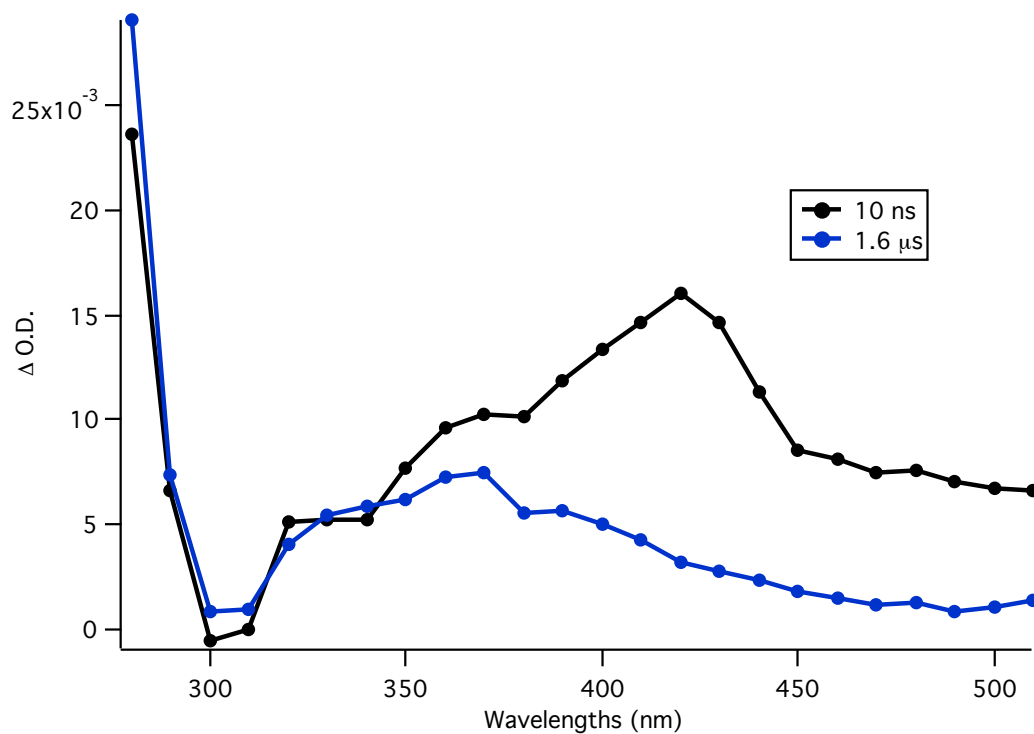
Sliced transient absorption spectra at different time points shown below of Azide 1C in nanocrystalline suspensions.



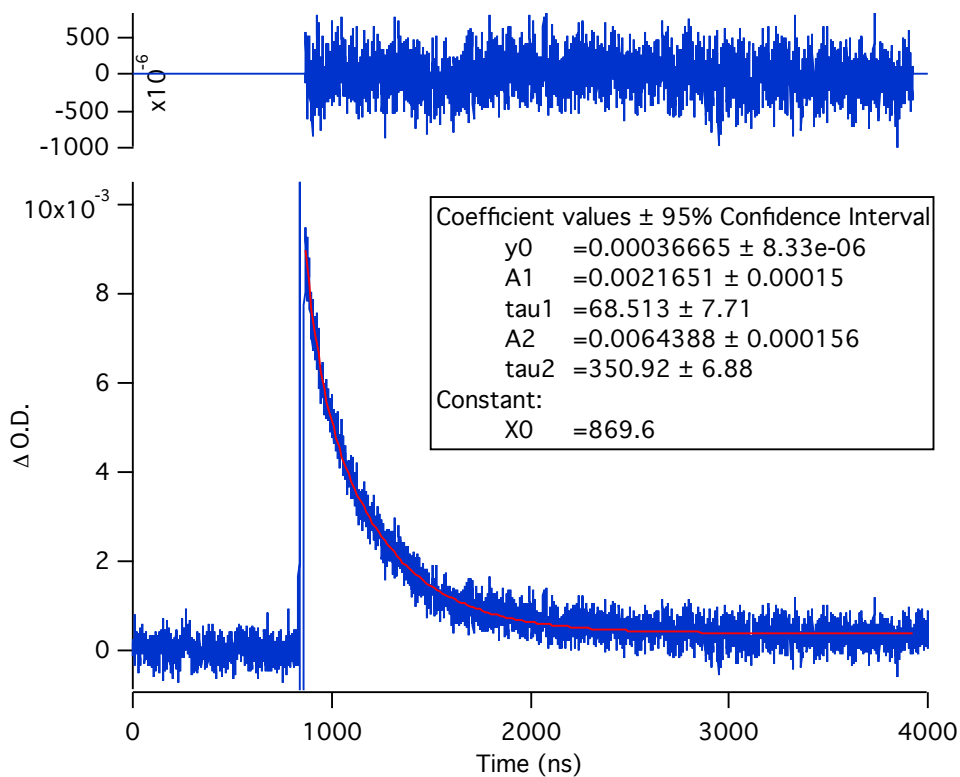
Azide 1D in pentane probed at 420 nm.



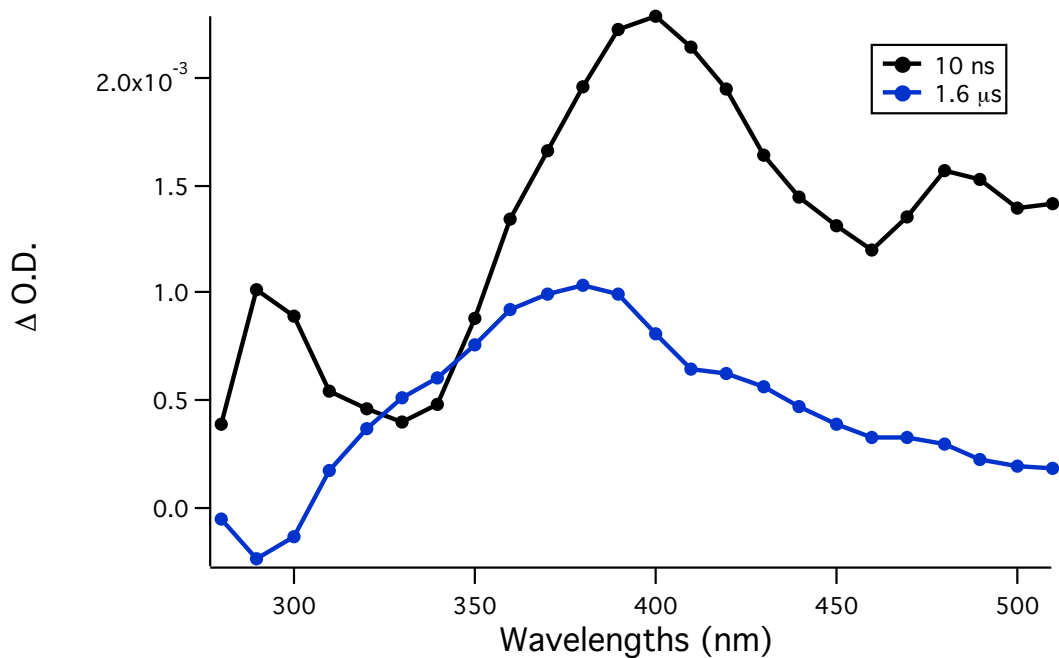
Sliced transient absorption spectra at different time points shown below of Azide 1D in pentane



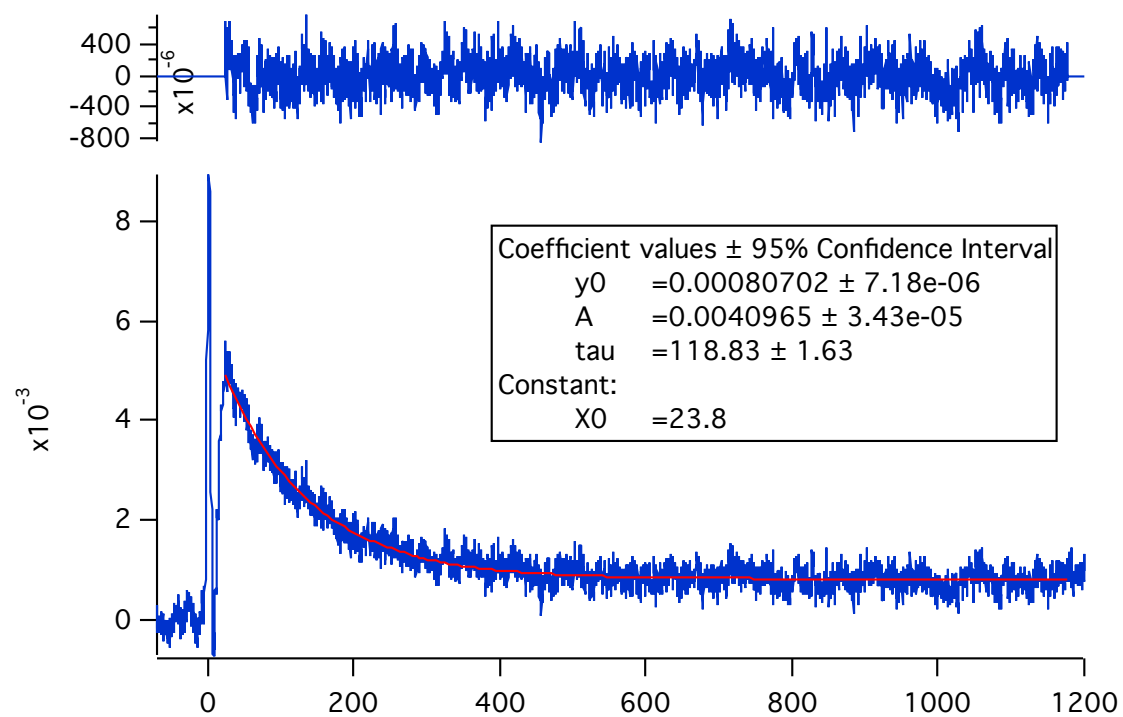
Azide 1E in pentane probed at 420 nm.



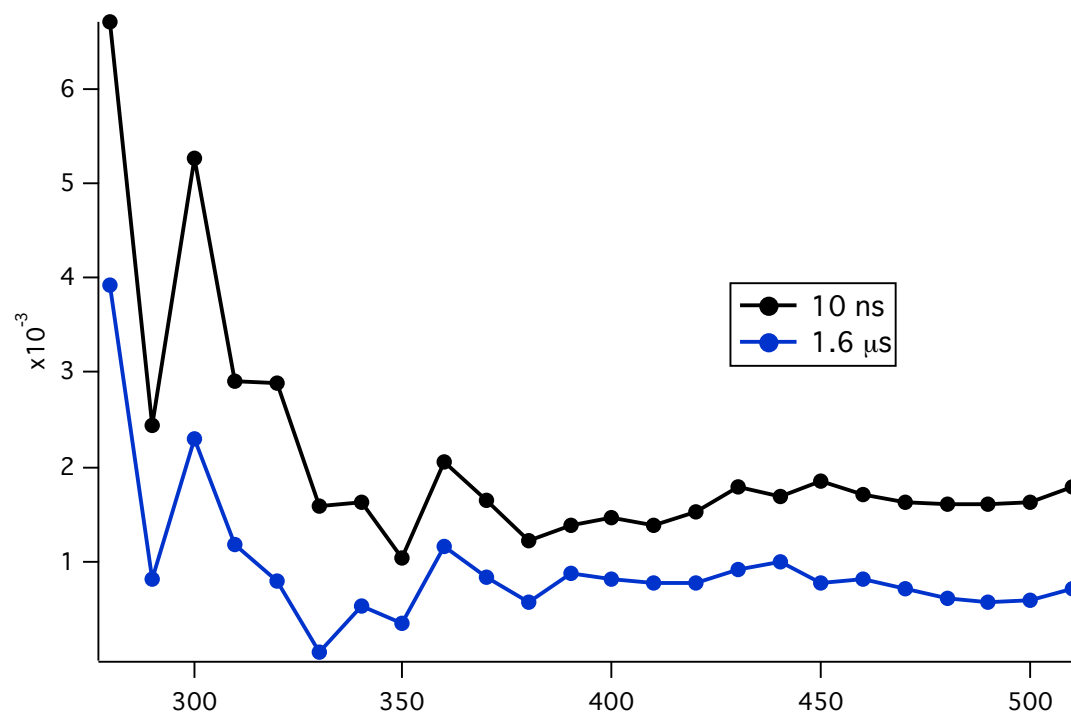
Sliced transient absorption spectra at different time points shown below of Azide 1E in pentane.



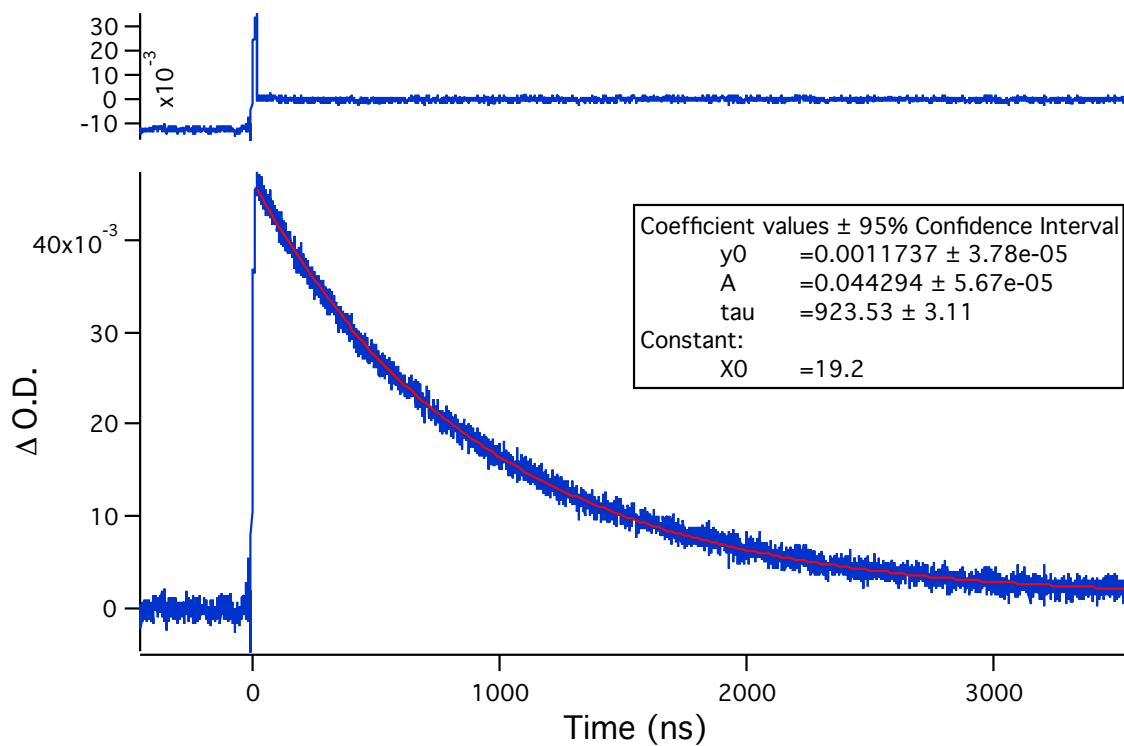
Azide 1E in nanocrystalline suspensions probed at 450 nm.



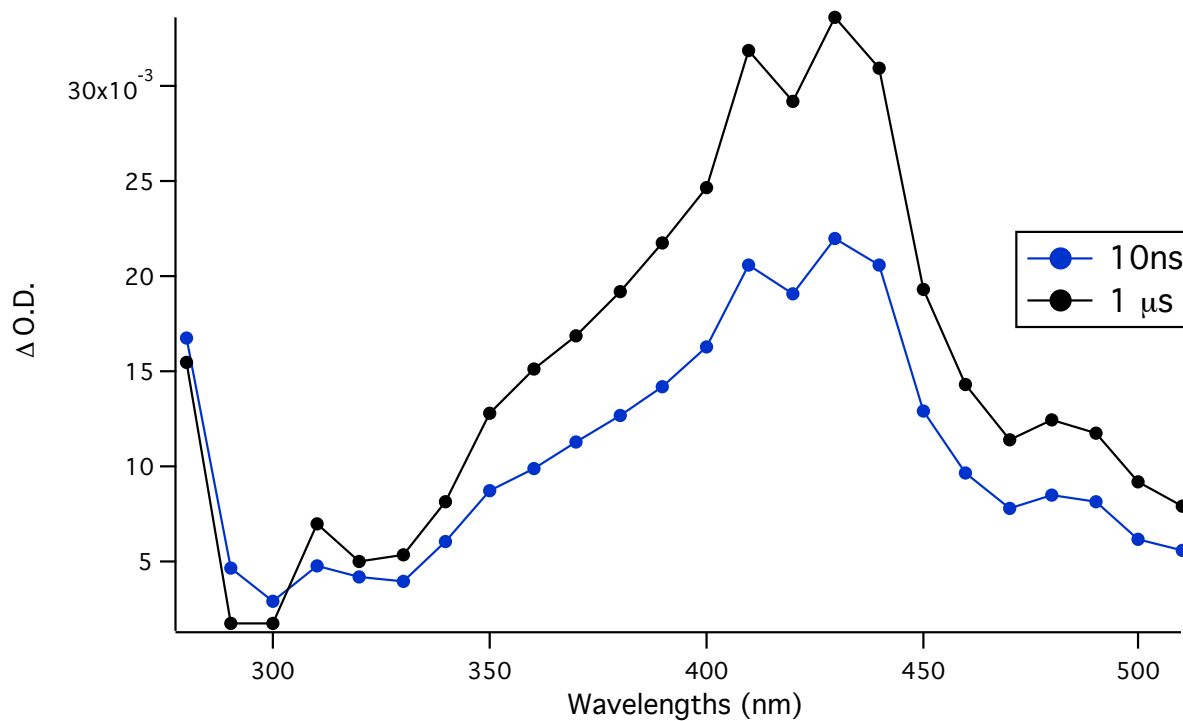
Sliced transient absorption spectra at different time points shown below of Azide 1E in nanocrystalline suspensions.



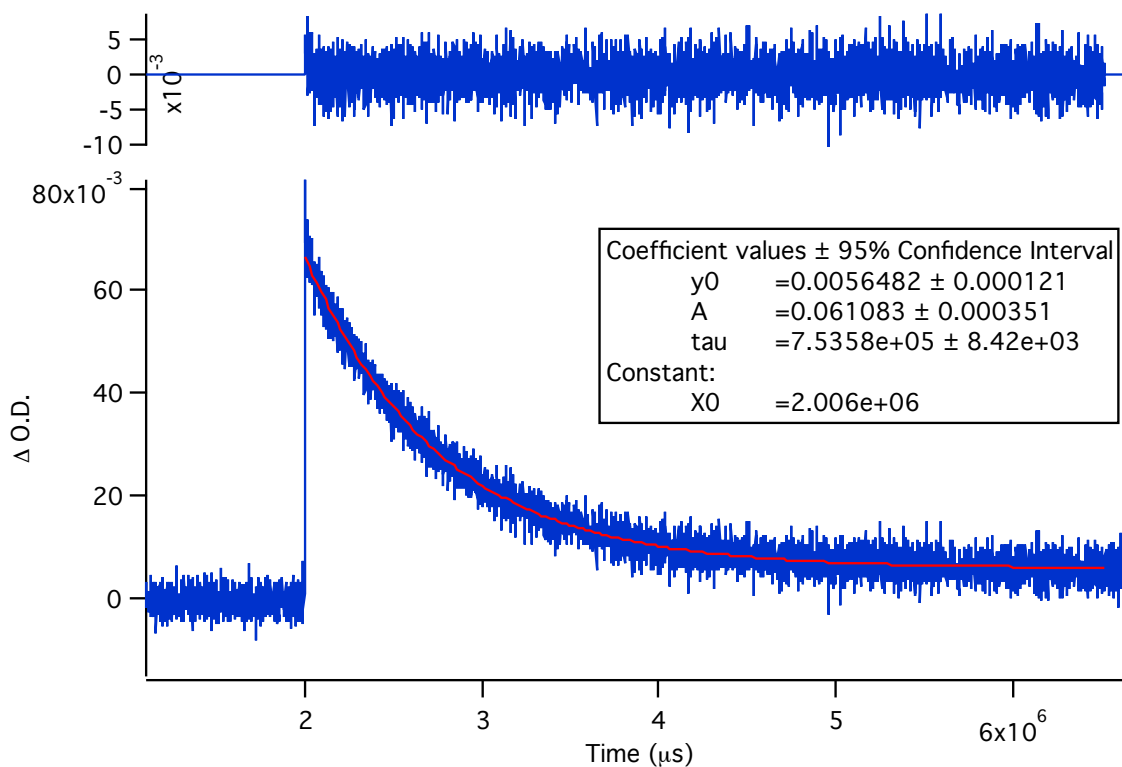
Azide 1F in pentane probed at 440 nm.



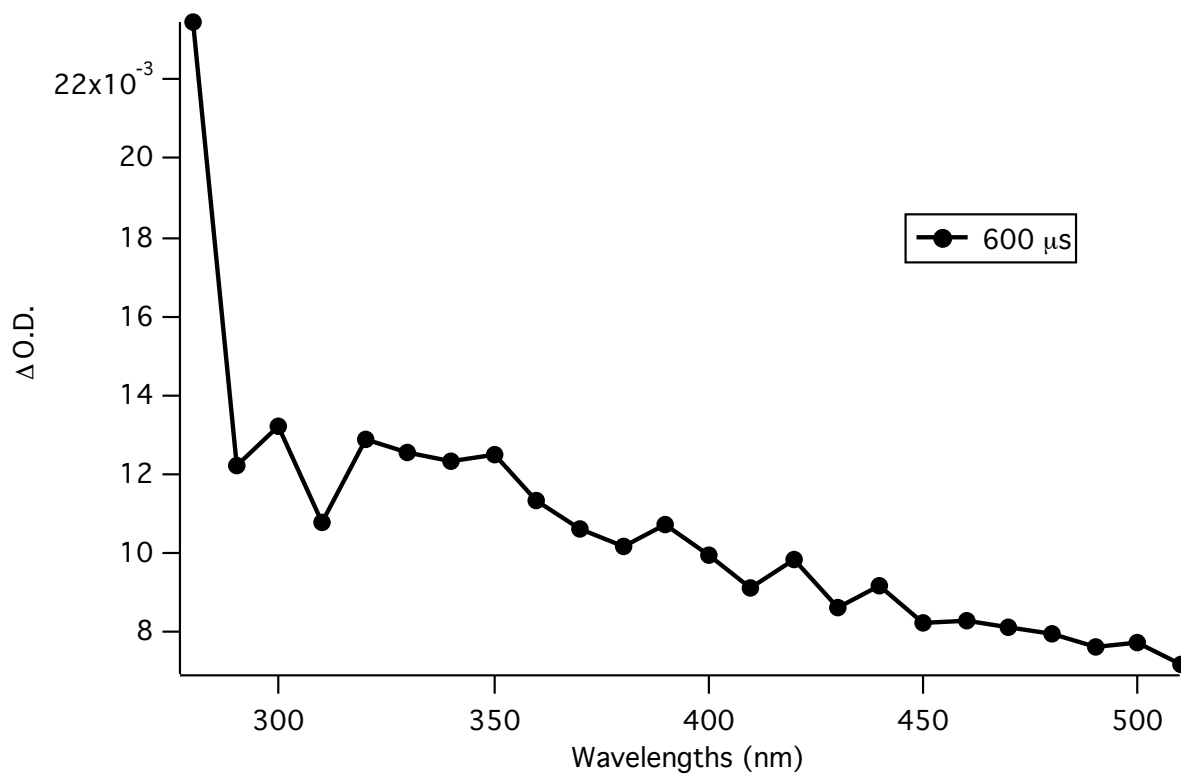
Sliced transient absorption spectra at different time points shown below of Azide 1F in pentane.



Azide 1F in nanocrystalline suspensions probed at 440 nm.



Sliced transient absorption spectra at different time points shown below of Azide 1F in nanocrystalline suspensions.



5.6 References

(1) (a) McGillivray, L. R.; Papaefstathiou, G. S.; Friscim T.; Hamilton, T. D.; Bucar, D.-K.; Chu, Q.; Varshney, D. B.; Georgiev, I. G. Supramolecular Control of Reactivity in the Solid State: From Templates to Ladderanes to Metal–Organic Frameworks *Acc. Chem. Res.*, **2008**, *41*, 280-291. (b) Hernández-Linares, M. G.; Guerrero-Luna, G.; Pérez-Estrada, S.; Ellison, M.; Ortin, M.-M.; Garcia-Garibay, M. A. Large-Scale Green Chemical Synthesis of Adjacent Quaternary Chiral Centers by Continuous Flow Photodecarbonylation of Aqueous Suspensions of Nanocrystalline Ketones *J. Am. Chem. Soc.* **2015**, *137*, 1679-1684. (c) Sakamoto, M.; Kato, M.; Aida, Y.; Fujita, K.; Mino, T.; Fujita, T. Photosensitized 2 + 2 Cycloaddition Reaction Using Homochirality Generated by Spontaneous Crystallization *J. Am. Chem. Soc.* **2008**, *130*, 1132-1133.

(2) (a) Cole, J. M.; Irie, M.; Solid State Photochemistry, *CrystEngComm*, **2016**, *18*, 7175-7179.

(3) (a) Campos, L. M.; Garcia-Garibay, M. A. Reactive Intermediates in Crystals: Form and Function, in *Reactive Intermediates*; Platz, M.S., Jones, M., Moss, R., Eds.; Hoboken, NJ, 2007. (b) Scheffer, J. R.; Scott, C. in *CRC Handbook of Organic Photochemistry and Photobiology*, Second Edition, Lenci, F.; Horspool, W. Eds. Volumes 1 & 2, Ch. 54, CRC Press, Boca Raton FL, 2003

(4) (a) Karch, N. J.; Koh, E. T.; Whitsel, B. L.; McBride, J. M. An X-ray and electron paramagnetic resonance structural investigation of oxygen discrimination during the collapse of methyl-benzoyloxy radical pairs in crystalline acetyl benzoyl peroxide. *J. Am. Chem. Soc.*, **1975**, *97*, 6729-6743. (b) McBride, J. M.; L. Pate, K. L. FTIR Study of Short Range Mobility in Some Crystalline Peroxides: Solid-State Rotational Isomerism of CO₂. *Turning Points in Solid-State, Materials and Surface Science: A Book in Celebration of the Life and Work of Sir John Meurig*

Thomas *Roy. Soc. Chem. London*, **2008**, 362-381. (c) Vary, M. W.; McBride, J. M. Single-crystal EPR studies of radical pairs in dibenzoyl peroxide. *Mol. Cryst. Liq. Cryst.* **1979**, *52*, 133-144.

(5) (a) Hollingsworth, M. D.; McBride, J. M. Photochemical mechanism in single crystals: FTIR studies of diacyl peroxides. *Adv. Photochem.* **1990**, *15*, 279-379. (b) Sarkar, S. K.; Sawai, A.; Kanahara, K.; Wentrup, C.; Abe, M.; Gudmundsdottir, A. D. Direct Detection of a Triplet Vinylnitrene, 1,4-Naphthoquinone-2-yl nitrene, in Solution and Cryogenic Matrices. *J. Am. Chem. Soc.*, **2015**, *137*, 4207–4214.

(6) (a) Hallmann, J. R.; Morgenroth, W.; Paulmann, C.; Davaasambuu, J.; Kong, Q.; Wulff, M.; Techert, S. Time-resolved x-ray diffraction of the photochromic alpha-styrylpyrylium Trifluoromethanesulfonate crystal films reveals ultrafast structural switching. *J. Am. Chem. Soc.* **2009**, *131*, 15018–15025. (b) Techert, S. Current Developments in Time-resolved X-ray. *Crystallogr. Rev.* **2006**, *12*, 25-45. (c) Makal, A.; Benedict, J. B.; Trzop, E.; Sokolow, J.; Fournier, B.; Chen, Y.; Kalinowski, J. A.; Graber, T.; Henning, R.; Coppens, P. Restricted photochemistry in the molecular solid state: structural changes on photoexcitation of Cu(I) phenanthroline metal-to-ligand charge transfer (MLCT) complexes by time-resolved diffraction. *J. Phys. Chem. A* **2012**, *116*, 3359-3365. (d) Coppens, P.; Zheng, S.-L. *Supramolecular Photochemistry*; Ramamurthy, V., Inoue, Y., Eds., John Wiley & Sons: Hoboken, NJ, 2011.

(7) (a) Chin, K. K.; Natarajan, A.; Gard, M. N.; Campos, L. M.; Johansson, E.; Shepherd, H.; Garcia-Garibay, M. A. Pump–probe spectroscopy and circular dichroism of nanocrystalline benzophenone—towards absolute kinetic measurements in solid state photochemical reactions. *Chem. Commun.* **2007**, *41*, 4266-4268. (b) Kuzmanich, G.; Simoncelli, S.; Gard, M.N.; Spänig, F.; Hoekstra, R.; Guldi, D. M.; Garcia-Garibay, M. A. Excited State Kinetics in Crystalline Solids:

Self-Quenching in Nanocrystals of 4,4'-Disubstituted Benzophenone Triplets Occurs by a Reductive Quenching Mechanism. *J. Am. Chem. Soc.*, **2011**, *133*, 17296-17306. (c) Doan, S. C.; Kuzmanich, G.; Gard, M. N.; Garcia-Garibay, M. A.; Schwarts, B. J. Ultrafast Spectroscopic Observation of a Quantum Chain Reaction: The Photodecarbonylation of Nanocrystalline Diphenylcyclopropenone. *J. Phys. Chem. Lett.*, **2012**, *3*, 81-86. (d) Kuzmanich, G.; Vogelsberg C. S.; Maverick, E. F.; Netto-Ferreira, J. C.; Scaiano, J. C.; Garcia-Garibay, M. A. Reaction Mechanism in Crystalline Solids: Kinetics and Conformational Dynamics of the Norrish Type II Biradicals from α -Adamantyl-*p*-Methoxyacetophenone. *J. Am. Chem. Soc.*, **2012**, *134*, 1115-1123. (e) Ayitou, A. J.-L.; Flynn, K.; Jockusch, S.; Khan, S. I.; Garcia-Garibay, M. A. Structure–Kinetics Correlations in Isostructural Crystals of α -(*ortho*-Tolyl)-acetophenones: Pinning Down Electronic Effects Using Laser-Flash Photolysis in the Solid State. *J. Am. Chem. Soc.*, **2016**, *138*, 2644-2648.

(8) Takayama, T., Mitsumori, T., Kawano, M., Sekine, A., Uekusa, H., Ohashi, Y. & Sugawara, T. Direct observation of aryl nitrene formation in the photoreaction of aryl azide crystals (2010). *Acta Cryst.* B66, 639–646.

(9) Burdzinski, G.; Hackett, J.C.; Wang, J.; Gustafson, T. L.; Hadad, C. M.; Platz, M. S. Early Events in the Photochemistry of Aryl Azides from Femtosecond UV/Vis Spectroscopy and Quantum Chemical Calculations. *J. Am. Chem. Soc.*, **2006**, *128*, 13402-13411.

(10) Tsao, M.-L.; Gritsan, N.; James, T. R.; Platz, M. S.; Hrovat, D. A.; Borden, W. T. Study of the Chemistry of *ortho*- and *para*-Biphenylnitrenes by Laser Flash Photolysis and Time-Resolved IR Experiments and by B3LYP and CASPT2 Calculations. *J. Am. Chem. Soc.* **2003**, *125*, 9343-9358.

- (11) Burdzinski, G.; Gustafson, T. L.; Hackett, J. C.; Hadad, C. M.; Platz, M. S. The Direct Detection of an Aryl Azide Excited State: An Ultrafast Study of the Photochemistry of para- and ortho-Biphenyl Azide. *J. Am. Chem. Soc.* **2005**, *127*, 13764–13765.
- (12) Sasaki, A., Mahe', L., Izuoka, A. & Sugawara, T. Chemical consequences of aryl nitrenes in the crystalline environment. *Bull. Chem. Soc. Jpn.*, **1998**, *71*, 1259–1275.
- (13) Stokes, B. J.; Jovanovic, B.; Dong, H.; Richert, K. J.; Riell, R. D.; Driver, T. G. Rh₂(II)-Catalyzed synthesis of carbazoles from biaryl azides. *J. Org. Chem.* **2009**, *74*, 3225-3228.
- (14) Kasai, H.; Nalwa, H. S.; Oikawa, H.; Okada, S.; Matsuda, H.; Minami, N.; Kuakuta, A.; Ono, K.; Mukoh, A.; Nakanishi, H. A novel preparation method of organic microcrystals. *Jpn. J. Appl. Phys.*, **1992**, *31*, 1132-1134.
- (15) Smith, P. A. S.; Brown, B. B. The reaction of aryl azides with hydrogen halides *J. Am. Chem. Soc.* **1951**, *73*, 2438-2441.
- (16) Sundberg, R. J.; Heintzelman, R. W. Reactivity of aryl nitrenes. Competition between carbazole formation and internal bond reorganization in biphenylnitrenes. *J. Org. Chem.* **1974**, *39*, 2546-2552.
- (17) (a) de Loera, D.; Stopin, A.; Garcia-Garibay, M. A. Photoinduced and thermal denitrogenation of bulky triazoline crystals: Insight into solid-to-solid transformations, *J. Am. Chem. Soc.* **2013**, *135*, 6626–6632. (b) Keating, A.E.; Garcia-Garibay, M. A. Photochemical Solid-To-Solid Reactions, in *Organic and Inorganic Photochemistry*; Ramamurthy, V., Schanze, K., Eds.; Marcel Dekker: New York, 1998, Vol. 2, pp. 195-248.